GENESIS OF MAFIC-ULTRAMAFIC INCLUSIONS IN SUBLAYER AND INCLUSION QUARTZ DIORITE AND IMPLICATIONS FOR THE FORMATION OF ASSOCIATED NI-CU-PGE MINERALIZATION IN THE SUDBURY IGNEOUS COMPLEX

by

Yujian Wang

A thesis submitted in partial fulfillment
of the requirements for the degree of
Doctor of Philosophy (Ph.D.)
in Mineral Deposits and Precambrian Geology

The Faculty of Graduate Studies
Laurentian University
Sudbury, Ontario, Canada

THESIS DEFENCE COMMITTEE/COMITÉ DE SOUTENANCE DE THÈSE
Laurentian Université/Université Laurentienne
Faculty of Graduate Studies/Faculté des études supérieures

Title of Thesis
Titre de la thèse: GENESIS OF MAFIC-ULTRAMAFIC INCLUSIONS IN SUBLAYER AND INCLUSION QUARTZ DIORITE AND IMPLICATIONS FOR THE FORMATION OF ASSOCIATED NI-CU-PGE MINERALIZATION IN THE SUDBURY IGNEOUS COMPLEX

Name of Candidate
Nom du candidat: Wang, Yujian

Degree
Diplôme: Doctor of Philosophy

Department/Program
Département/Programme: Mineral Deposits and Precambrian Geology

Date of Defence
Date de la soutenance: October 30, 2019

APPROVED/APPROUVÉ

Thesis Examiners/Examinateurs de thèse:

Dr. Michael Lesher
(Supervisor/Directeur de thèse)

Dr. Pedro Jugo
(Committee member/Membre du comité)

Dr. Edward Pattison
(Committee member/Membre du comité)

Dr. Peter Lightfoot
(Committee member/Membre du comité)

Dr. Steven Prevec
(External Examiner/Examinateur externe)

Dr. Eugene Ben-Awuah
(Internal Examiner/Examinateur interne)

Approved for the Faculty of Graduate Studies
Approuvé pour la Faculté des études supérieures
Dr. David Lesbarrères
Monsieur David Lesbarrères
Dean, Faculty of Graduate Studies
Doyen, Faculté des études supérieures

ACCESSIBILITY CLAUSE AND PERMISSION TO USE

ABSTRACT

The lowermost, discontinuous units of the impact-generated Sudbury Igneous Complex (SIC), Sublayer, Footwall Breccia (FWBX), and Inclusion Quartz Diorite (IQD), are distinguished from overlying Main Mass norite rocks by the presence of abundant inclusions and Ni-Cu-PGE (PGE – platinum group element) mineralization. The majority of the felsic-mafic inclusions appear to be derived from exposed country rocks, but volumetrically important mafic-ultramafic inclusions have only rare equivalents in the surrounding country rocks and appear to be preferentially associated with sulfide mineralization. Establishing the petrogenesis of the mafic-ultramafic inclusions and the nature of their association with the Ni-Cu-PGE mineralization are therefore critical to understand the evolution of the impact melt, genesis of Sublayer, FWBX, and IQD, and the formation of one of the world's largest accumulations of Ni-Cu-PGE mineralization.

Petrographic, mineralogical, geochemical, and Sm-Nd and Re-Os isotopic data indicate three origins for the olivine-bearing mafic-ultramafic inclusions:

(1) Anteliths, comprising olivine melanorites and olivine melagabbronorites in the Whistle and Levack embayments on the North Range, which are characterized by igneous textures, Zr/Y, Zr/Nb, Nb/U, and Zr/Hf ratios similar to igneous-textured Sublayer matrix (ITSM), unradiogenic $\varepsilon Nd_{1850\ Ma}$ values (-8 to -5), and slightly unradiogenic to radiogenic $\gamma Os_{1850\ Ma}$ values (-8 to +94). They likely crystallized from a local mixture of SIC impact melt and a more mafic melt derived by melting of the widespread Huronian volcanic and subvolcanic units in the region.

(2) Local xenoliths, comprising wehrlites and olivine clinopyroxenites in the Levack embayment and olivine melanorites in the Foy Offset on the North Range, which are characterized by shock mosaic and recrystallized textures, and trace element patterns (e.g., negative Th-U, Nb-Ta-(Ti),

Sr, and Zr-Hf anomalies) similar to and Nb/U ratios overlapping with a layered mafic-ultramafic intrusion in the footwall of the Levack and Fraser deposits. They were likely derived from local mafic-ultramafic protoliths that were petrogenetically-related to the layered mafic-ultramafic intrusion in the footwall of the Levack and Fraser deposits.

(3) Exotic xenoliths, comprising phlogopite/feldspar lherzolites in the Trill, Levack, and Bowell embayments and the Foy Offset dike on the North Range, which are characterized by variably igneous, tectonic-metamorphic, and shock-metamorphic textures, and orthopyroxene reaction rims against igneous-textured Sublayer matrix (ITSM), indicating disequilibrium with the impact melt. One composite inclusion exhibits igneous layering of feldspar lherzolite and olivine gabbro, suggesting derivation from an unexposed older layered mafic-ultramafic intrusion. The calculated parental magma for one particularly well-preserved feldspar lherzolite inclusion is similar to continental arc basalt formed by up to 5% partial melting of garnet peridotite. Ol-Cpx-Pl thermobarometry of several exotic inclusions indicate equilibration at 900^{o}C – 1120^{o}C and 210 – 300 MPa, suggesting emplacement into upper-middle crust (7.7 – 10.9 km), prior to being incorporated into the lower parts of the proto-SIC during impact excavation and/or thermomechanical erosion of target rocks.

Most analyzed inclusions, ITSM, and Main Mass lithologies are enriched in highly incompatible elements with negative Nb-Ta-Ti anomalies, unradiogenic Nd, and radiogenic Os isotopic signatures. These features suggest that the impact sampled rocks that were derived from subduction-metasomatized mantle, including the widespread Huronian volcanic and intrusive rocks adjacent to the SIC. Melting of these volcanic and intrusive rocks and the underlying Neoarchean Superior Province upper-middle crustal rocks would produce the observed geochemical characteristics of the SIC lithologies and inclusions.

The Main Mass has a very homogeneous Hf isotopic composition, indicating that the impact melt sheet was well mixed. However, Sublayer, IQD, and overlying basal Main Mass norites vary widely in terms of Pb-S-(Os) isotopic compositions. Most mafic-ultramafic inclusions, except for anteliths, contain no sulfides and exhibit no signatures of Ni-Cu-PGE depletion caused by prior sulfide saturation, which suggest that the association between mafic-ultramafic inclusions and Ni-Cu-PGE sulfide mineralization is attributable to the hydrodynamic equivalence of less dense but larger silicate inclusions and denser but smaller sulfide melt droplets during transport and/or settling. Anteliths, locally-derived inclusions, and local variations in Pb-S-(Os) isotopes must have been generated in situ, requiring significant degrees of assimilation of footwall rocks via thermomechanical erosion, whereas most exotic inclusions other than shocked feldspar lherzolite were derived from deeper mafic-ultramafic protoliths, generated during impact excavation and/or thermomechanical erosion, and physically transported into their current locations. Thus, thermomechanical erosion played an important role in the generation of embayments, incorporation of xenoliths and sulfide xenomelts from the mineralized country rocks (e.g., EBLI-Nipissing-Huronian), and formation of isotopic heterogeneity in the basal parts of the SIC. Convective- and gravity-driven mass flow contributed to the horizontal transportation of inclusions and sulfide xenomelts into the embayment when the impact melt contained <45% inclusions, but became less significant as proto-Sublayer incorporated more inclusions.

Keywords: Sudbury Igneous Complex, Sublayer, offset dikes, mafic-ultramafic inclusions, anteliths, local xenoliths, exotic xenoliths, thermomechanical erosion

CO-AUTHORSHIP STATEMENT

The research presented in this thesis was done as a collaboration between Laurentian University and Vale Ltd. The project design, general goals, and focus were developed by Prof. C.M. Lesher and Dr. P.C. Lightfoot. The thesis comprises one peer-reviewed journal (*Geology*) paper and two manuscripts intended for peer-review journal publication that have been co-authored with Prof. Lesher, Dr. Lightfoot, Mr. E.F. Pattison, and Dr. J.P. Golightly. An initial suite of 100 samples was provided by Dr. Lightfoot and the candidate collected 65 additional samples. The candidate performed all of the petrographic work, scanning electron microscopy (SEM) and electron probe microanalysis (EPMA), laser Raman spectrometry, selection and submittal of samples for whole-rock geochemical analysis, and LA-ICP-MS, with assistance from Dr. William Zhe and Ms. Sandra Clarke (SEM), Ms. Mary-Jane Walzak (Raman), Mr. Dave Crabtree (EPMA), and Drs. J. Petrus and M. Leybourne (LA-ICP-MS). Initial interpretation of the data was done by the candidate under the supervision of the co-authors. Mr. Pattison and Prof. Lesher provided summaries and tables of the various breccia types. The first drafts of the thesis, including the published journal paper, were completed by the candidate and edited and improved by scientific input and discussions with the co-authors.

ACKNOWLEDGEMENTS

I would like to express my sincere appreciation to my supervisor Prof. Michael Lesher for the continuous support of my PhD study and related research with his patience, motivation, and immense knowledge. His guidance and compliments helped me gain self-confidence in my study and research and make a commitment to academia as my future career.

I thank the rest of my thesis committee, Dr. Peter Lightfoot, Mr. Edward Pattison, Dr. Pedro Jugo, and Dr. Paul Golightly, for their insightful comments, guidance, and encouragement, as well as challenging and difficult questions that induced me to expand my way of thinking from various perspectives.

Vale is thanked for providing diamond drill cores, access to their thin section labs, and geological maps. Although numerous Vale personnel have contributed to the success of the project, I would like to extend a special thanks to Ms. Lisa Gibson and Noëlle Shriver for allowing me the opportunity to do this project and kindly providing needed information.

My sincere appreciation goes to Dr. Douglas Tinkham, Prof. Andrew McDonald, Prof. Daniel Kontak, Dr. Michael Schindler, Dr. Phillips Thurston, and Prof. Elizabeth Turner, who provided me with valuable suggestions and discussions, and excellent lectures that widened my scientific knowledge. Without their support it would not have been possible to complete this research.

I thank Mr. Willard Desjardins, Dr. William Zhe, Dr. Joseph Petrus, and Dr. Matthew Leybourne (Laurentian University) for assistance with sample preparation, SEM, and LA-ICP-MS work, Mr. David Crabtree and Ms. Sandra Clarke (Ontario Geoscience Laboratory) for assistance with the SEM and EPMA work, Ms. Mary-Jane Walzak (University of Western Ontario) for assistance

with the laser Raman analytical work, and Dr. Luca Ziberna (University of Bristol) for helpful discussions on the application of the Ol-Cpx-Pl geobarometer.

Special thanks go to Ms. Roxane Mehes and Edda Bozzato, who with warm hearts and friendly ears were always there to help me and my colleagues order supplies, take care of our files, and help us solve other issues in our lives.

Last, but not the least, I would like to appreciate my family and my friends for supporting me spiritually throughout my PhD study and my life in general. They offer me invaluable support, company and encouragement, and we shared a lot of happiness, sorrow, stress, and all other sensitive feelings in life.

TABLE OF CONTENTS

List of Figures

List of Tables

List of Supporting Information

CHAPTER 1

INTRODUCTION TO THE THESIS

1.1 Introduction

The Sudbury Structure (ca. 1.85 Ga) is one of the oldest, largest, and best-preserved terrestrial impact structures (Dietz, 1964; Grieve and Therriault, 2000), and contains one of the world's largest accumulations of magmatic Ni-Cu-PGE sulfide mineralization (Naldrett, 2004; Lightfoot, 2016). It is the erosional relic of an elliptically deformed multi-ring impact basin with an apparent crater diameter of approximately 260 km (Spray et al., 2004). The crater straddles the unconformable contact between felsic-mafic gneisses, granitoids, and greenstones of the Neo-Archean Superior Province along the western, northern, and eastern margins, and metabasalts, metasediments, and granites of the Paleoproterozoic Huronian Supergroup (Long, 2004), 2.4 Ga East Bull Lake Suite mafic-ultramafic intrusive rocks (James et al., 2002), and 2.2 Ga Nipissing Suite mafic intrusive rocks (Corfu and Andrews, 1986; Lightfoot and Noble, 1992) along the southern margin (e.g., Dressler, 1984; Naldrett, 2004; Lightfoot, 2016).

The Sudbury Structure comprises the Sudbury Igneous Complex (SIC), overlying fallback material and post-impact sediments of the Whitewater Group, and underlying brecciated, contact metamorphosed, and partially-melted breccias. The SIC includes a Main Mass, lower discontinuous inclusion- and sulfide-rich Sublayer and Footwall Breccia (FWBX) units, and associated concentric and radial Offset dikes. The Main Mass is presently exposed as a 60 km long × 27 km wide × 1.5 – 5.0 km thick differentiated body, comprising – from bottom-to-top – norite, quartz gabbro, and granophyre. Sublayer and FWBX occur in discontinuous trough-like depressions along the basal contact between Main Mass and underlying country rocks, and

contain abundant mafic-ultramafic and lesser felsic-intermediate inclusions and Fe-Ni-Cu-(PGE) sulfides in an igneous-textured dioritic-gabbroic-noritic (Sublayer) or felsic-intermediate-mafic (FWBX) matrix. The Offset dikes, extending up to 20 km from the periphery of the Main Mass, have aphanitic to fine-grained, inclusions-free, unmineralized quartz dioritic (QD) margins and locally-mineralized, inclusion-bearing quartz diorite (IQD) cores.

The abundant inclusions in Sublayer, FWBX, and IQD range from a few millimetres to more than 100m (Hewins, 1971; Naldrett et al., 1972) in diameter, and comprise felsic to mafic gneisses, mafic metavolcanic rocks, metagabbros, and metasedimentary rocks, and mafic-ultramafic lithologies (e.g., Naldrett et al., 1984). Although most of the inclusions appear to be derived from local country rocks, the mafic-ultramafic inclusions have only rare equivalents in the country rocks and have at least three origins:

1) Cognate: Anteliths derived from remnants of unexposed parts of the SIC (Naldrett et al., 1984) or earlier Sublayer cumulates (Lightfoot et al., 1997a, b; Farrell, 1997). Crystallization of any known SIC magma would not produce comparable olivine-orthopyroxene assemblages (Prevec, 2000), which has been interpreted to require contributions from i) mantle-derived magmas (e.g., Lightfoot et al., 1997a, b; Farrell, 1997), ii) unspecified more primitive magmas (Corfu and Lightfoot, 1996; Zhou et al., 1997), and/or iii) melted mafic country rocks (Prevec, 2000; Prevec et al., 2000).

2) Local: Xenoliths derived from local country rocks, including Nipissing diabase intrusions (Card and Pattison, 1973), East Bull Lake suite intrusions (Pattison, 1979), and ultramafic bodies in the Levack Gneiss (Pattison 1979; Moore et al., 1993, 1994, 1995). However, no systematic comparison of petrography and geochemistry has been conducted of the inclusions and these target rocks.

3) Exotic: Xenoliths derived from unexposed mafic-ultramafic intrusions (e.g., Rae, 1975; Kuo and Crocket, 1979; Scribbins, 1978; Scribbins et al., 1984; Wang et al., 2018). Rae (1975) suggested that exotic inclusions in the Strathcona mine represented disrupted fragments of a layered intrusion similar to the Muskox or Skaergaard on the basis of petrographic observations (e.g., modal variations, cumulus and poikilitic textures, and layering features). Scribbins (1978) suggested that exotic inclusions in various South Range localities also represented fragments of a hidden layered intrusion on the basis of mineral chemistry. The significant lithological differences between North Range and South Range inclusions were attributed to sampling different parts of the hidden intrusion (Scribbins, 1978).

Because Ni-Cu-PGE mineralization is so closely associated with Sublayer, FWBX, and IQD, in particular parts containing mafic-ultramafic inclusions (Naldrett and Kullerud, 1967; Pattison, 1979; Naldrett et al., 1984; Lightfoot et al., 1997a, b), understanding the origin of the mafic-ultramafic inclusions and the association between these inclusions and Ni-Cu-PGE mineralization are therefore critical to understanding the evolution of the impact melt, genesis of Sublayer, FWBX, and IQD, and the ore-formation process of the world's largest accumulation of Ni-Cu-PGE mineralization.

1.2 Research Problem and Objectives

Although several studies have focused on the petrography, geochemistry, and origin of the mafic-ultramafic inclusions in Sublayer and IQD (e.g., Souch et al., 1969; Rae, 1975; Kuo and Crocket, 1979; Naldrett et al., 1984; Scribbins, 1984; Morrison et al., 1994; Cohen et al., 2000; Prevec, 2000; Prevec et al., 2000), there is no consensus of their origin and mechanism of incorporation.

One reason is that their petrographic and geochemical characteristics vary from location to location, which makes it impossible to systematically investigate the whole inclusion population.

Similarly, although mafic-ultramafic inclusions are closely associated with mineralized Sublayer and IQD, their genetic relationship to the Ni-Cu-PGE mineralization has been rarely addressed. Naldrett and Kullerud (1967) noted that heavily disseminated sulfides in Sublayer norite matrix preferentially encircled ultramafic inclusions, but rarely occured in appreciable amounts within the inclusions. Davis (1984) noted that the ultramafic inclusions (pyroxenite and peridotite) in the Little Stobie mine were barren, but that some gabbroic inclusions contained fine disseminated and fracture-filling sulfides. Melanorite and olivine melanorite inclusions in the Whistle embayment, however, contain up to 75% disseminated or net-textured sulfides (Lightfoot et al., 1997a, b; Farrell, 1997), but no peridotite inclusions like those in other embayments have been reported in the Whistle embayment. The mineralization in many magmatic Ni-Cu-PGE deposits (e.g., Aguablanca: Tornos et al. 2001; Duluth: Ripley and Alawi, 1986; Noril'sk: Lightfoot and Zotov, 2007; Platreef: Kinnaird et al., 2005; Voisey's Bay: Li and Naldrett, 2000) is associated with inclusions, so characterising the relationship between the mafic-ultramafic inclusions and the Ni-Cu-PGE sulfide mineralization has wider implications and applications.

As one of the most important ore-bearing units, there is no consensus on the mechanism(s) of formation of Sublayer, with some authors suggesting that it represents splash-emplaced impact melt driven up the walls of the crater (Pattison, 1979), and some suggesting that it crystallized from a hybrid melt formed either by mixing between the impact melt and a mantle-derived high-Mg magma (Naldrett and Kullerud, 1967; Naldrett et al., 1984; Zhou et al., 1997) or mixing between the impact melt and a basaltic melt derived by melting mafic footwall rocks (Golightly, 1994; Lightfoot et al., 1997a; Prevec, 2000; Prevec et al., 2000; Prevec and Cawthorn, 2002).

The main research objective of this thesis has been to characterize the lithologies, textures (igneous, metamorphic, shock metamorphic), mineralogy, mineral chemistry, whole-rock geochemistry of the mafic-ultramafic inclusions in currently available occurences of Sublayer and representative occurrences of IQD, and to apply this to understanding the genesis of these lithologies and their role in the ore-forming process.

1.3 Outline of Methodology

In order to accomplish these objectives, the following methodologies were employed:

1) 165 representative mafic-ultramafic inclusions in Sublayer (n = 157) and IQD (n = 8) were collected from 20 diamond drill cores.

2) All 165 inclusions were examined using a compound polarizing microscope to establish their mineralogy and textures.

3) The structures of 3 shocked plagioclase grains and 2 undeformed plagioclase grains were assessed by Laser Raman spectroscopy.

4) Major and minor elements in olivine, orthopyroxene, clinopyroxene, chromite, and amphibole in 45 inclusions were analyzed by wavelength-dispersive X-ray emission spectrometry using an electron probe microanalyer (EPMA).

5) Trace elements in olivine, orthopyroxene, and amphibole in one phlogopite lherzolite inclusion (#373552 in the Foy offset) and one feldspar lherzolite inclusion (#4920 in the Trill embayment) were analyzed by laser ablation inductively-coupled plasma mass spectrometry.

6) Whole-rock major and minor elements in 83 inclusions were analyzed on fused glass discs by wavelength-dispersive X-ray fluorescence spectrometry.

7) Whole-rock trace elements in 83 inclusions were analyzed by inductively coupled plasma mass spectrometry.

1.4 Structure of Thesis

This thesis comprises an introductory chapter (Chapter 1), three journal manuscripts (Chapters 2-4), and a concluding chapter (Chapter 5). Chapters 2 – 4 repeat some information because they are intended for publication as individual stand-alone manuscripts.

Chapter 1 (this chapter) provides background information on the project, research problems and objectives, and the methodologies applied to solve the research problems.

Chapter 2, entitled "SHOCK METAMORPHIC FEATURES IN MAFIC AND ULTRAMAFIC INCLUSIONS IN THE SUDBURY IGNEOUS COMPLEX: IMPLICATIONS FOR THEIR ORIGIN AND IMPACT EXCAVATION", record the discovery of abundant shock metamorphic features (e.g., mosaicism of olivine; strong fracturing and partial isotropization of plagioclase) in the mafic and ultramafic inclusions consistent with a shock pressure of 20 – 30 GPa. Abundant plagioclase, the absence of garnet or Mg-spinel, and calculated low pressures (< 500 MPa) provide evidence for derivation of the inclusions from unexposed mafic-ultramafic intrusions in the upper to middle crust that were disrupted during formation of the transient crater, incorporated into the impact melt sheet, and preserved because of their relatively refractory compositions. These observations support models involving intermediate rather than very deep or very shallow excavation for the Sudbury impact event.

Chapter 3, entitled “GEOCHEMISTRY AND PETROGENESIS OF MAFIC AND ULTRAMAFIC INCLUSIONS IN SUBLAYER AND OFFSET DIKES, SUDBURY IGNEOUS COMPLEX, CANADA”, characterizes the petrography and geochemistry of the mafic-ultramafic inclusions, and addresses three different origins for the inclusions in this study. Anteliths comprise igneous-textured olivine melanorites and olivine melagabbronorites in the Whistle and Levack (Dowling and Onaping Depth) embayments on the North Range. They exhibit similar Zr/Y, Zr/Nb, Nb/U, and Zr/Hf ratios to igneous-textured Sublayer matrix (ITSM). Local xenoliths comprise shock metamorphosed and recrystallized wehrlites and olivine clinopyroxenites in the Levack embayment and shock metamorphosed olivine melanorites in the Foy Offset on the North Range. They have similar trace element patterns (e.g., negative Th-U, Nb-Ta-(Ti), Sr, and Zr-Hf anomalies) and overlapping Nb/U ratios as a layered mafic-ultramafic intrusion in the footwall of the Levack and Fraser deposits. Exotic xenoliths comprise phlogopite/feldspar lherzolites, orthopyroxenite, and olivine gabbro with igneous, recrystallized, and shock-metamorphic textures in the Trill, Levack, and Bowell embayments and the Foy Offset dike on the North Range. They have no equivalents in the exposed country rocks. Calculated parental magma composition and geobarometer constraints suggest that these inclusions could be derived from continental arc basalt magma formed by ~5% partial melting of garnet peridotite, equilibrated at 7.7 – 10.9 km depth, excavated during impact, and incorporated into the SIC.

Chapter 4, entitled “GENESIS OF SUBLAYER IN THE SUDBURY IGNEOUS COMPLEX”, addresses the formation mechanism of Sublayer and relationship between the Sublayer/mafic-ultramafic inclusions and the Ni-Cu-PGE mineralization. Overlying Main Mass norite is very homogeneous in terms of Hf isotopes, indicating that the impact melt sheet was well mixed. However, Sublayer, IQD, and overlying basal Main Mass norites vary widely in terms of S-Pb-

(Os) isotopic compositions. Shocked feldspar lherzolite inclusions were derived from shallow depths, but most others were derived from deeper mafic-ultramafic protoliths and must have been generated during impact excavation and transported into their current locations, requiring some degree of convective and/or gravity-driven mass flow, and preserved because of their refractory compositions. However, anteliths, locally-derived inclusions, and local variations in S-Pb-(Os) isotopes must have been generated in situ, requiring some degree of subsequent local thermomechanical erosion.

Chapter 5 presents the overall conclusions of the project and possible future work.

1.5 Statement of Original Contributions

The following is a summary of the original contributions made by this study:

1) This is the first study to describe the igneous (e.g., cumulate, poikilitic, and interstitial), tectonic metamorphic (e.g., granoblastic, hornfelsic, and recrystallized), and shock metamorphic (e.g., shock mosaicism, planar deformation features, and partial isotropization) textures of mafic-ultramafic inclusions on both the North and South Ranges. This is the first study to report shock metamorphic textures.
2) This thesis contains the most complete compilation of geochemical data from this study and previous published data, and is the first to make systematic comparisons between the mafic-ultramafic inclusions, ITSM, and mafic-ultramafic intrusions in the country rocks to address any potential petrogenetic relationships.
3) This is the first study to estimate P-T conditions of the mafic-ultramafic inclusions using the Ol-Cpx-Pl geobarometer and to provide better constraints on the depth of the impact excavation.

4) This is the first study to classify the origins of the mafic-ultramafic inclusions on the basis of their textures, mineralogy, and geochemistry.
5) This is the first study to compiled all available S, Pb-Pb, Sm-Nd, Re-Os, and Lu-Hf isotopic data to determine that the impact melt sheet was well mixed and obtained local variations during later thermomechanical erosion.
6) This is the first study to perform MELTS assimilation models and to evaluate the roles of convective currents, gravity currents, and thermomechanical erosion in the generation of Sublayer.

Reference Cited

Card, K.D., and Pattison, E.F., 1973. Nipissing diabase of the Southern province, Ontario. In Huronian Stratigraphy and Sedimentation (G.M. Young, ed.) Geological Association of Canada, special paper, v. 12, p. 7 - 30.

Cohen, L., Burnham, O.M., Hawkesworth, C.J., and Lightfoot, P.C., 2000. Pre-emplacement Re-Os ages from ultramafic inclusions in the sublayer of the Sudbury Igneous Complex, Ontario. Chemical Geology, v. 165, p. 37 - 46.

Corfu, F., and Andrew, A.J., 1986. A U-Pb age for mineralized Nipissing diabase. Gowganda, Ontario. Canadian Journal of Earth Science, v. 27, p. 107 – 109.

Corfu, F., and Lightfoot, P.C., 1996, U-Pb geochronology of the Sublayer environment, Sudbury Igneous Complex, Ontario: Economic Geology, v. 91, p. 1263 – 1269.

Davis, G.C., 1984. Little Stobie Mine: A South Range contact deposit. In Pye, E.G., Naldrett, A.J., and Giblin, P.E. (eds), The Geology and Ore Deposits of the Sudbury Structure, Ontario Geological Survey Special Volume 1, p. 361 – 369.

Dietz, R.S., 1964. Sudbury structure as an astrobleme. Journal of Geology, v.72, p. 412 – 434.

Dressler, B.O., 1984. General geology of the Sudbury area. In Pye, E.G. et al. (eds) The Geology and Ore Deposits of the Sudbury Structure. Ontario Geological Survey, Special Volume 1, p. 57 – 82.

Farrell, K., 1997, Mafic to ultramafic inclusions in the Sublayer of the Sudbury Igneous Complex at Whistle Mine, Sudbury, Ontario, Canada. Master thesis, Laurentian University, Sudbury, Ontario.

Golightly, J.P., 1994, The Sudbury Igneous Complex as an impact melt: Evolution and ore genesis, in Lightfoot, P.C., and Naldrett, A.J., eds., Proceedings of the Sudbury Noril'sk Symposium: Ontario Geological Survey Special Volume 5, p. 105 – 117.

Grieve, R.A.F., and Therriault, A., 2000, Vredefort, Sudbury, Chicxulub: Three of a Kind?: Annual Review of Earth and Planetary Sciences, v. 28, p. 305 – 338, https://doi.org/10.1146/annurev.earth.28.1.305.

Hewins, R.H., 1971. The petrology and some marginal mafic rocks along the North Range of the Sudbury Irruptive. PhD Thesis, University of Toronto.

James, R.S., Easton, R.M., Peck, D.C., Hrominchuk, J.L., 2002. The East Bull Lake Intrusive Suite: Remnants of a ~ 2.48 Ga large igneous and metallogenic province in the Sudbury area of the Canadian shield. Economic Geology, v. 97, p. 1577 – 1606.

Kinnaird, J.A., Hutchinson, D., Schurmann, L., Nex, P.A.M., de Lange, R., 2005. Petrology and mineralization of the Southern Platree: northern limb of the Bushveld Complex, South Africa. Mineralium Deposita, v. 40, p. 576 – 597.

Kuo, H.Y., Crocket, J.H., 1979, Rare earth elements in the Sudbury Nickel Irruptive: comparison with layered gabbro and implications for Nickel Irruptive petrogenesis. Economic Geology, v. 79, p. 590 – 605.

Li, C., Naldrett, A.J., 2000. Melting reactions of gneissic inclusions with enclosing magma at Voisey's Bay, Labrador, Canada: Implications with respect to ore genesis. Economic Geology, v. 95. p. 801 – 814.

Lightfoot, P. C., Zotov, I.A., 2007. Ni-Cu-PGE sulfide deposits at Noril'sk, Russia. Short Course; International Polar Year; Prospectors and Developers Association of Canada. Short Course Notes.

Lightfoot, P.C., 2016, Nickel sulfide ores and impact melts: Origin of the Sudbury Igneous Complex: Amsterdam, Netherlands, Elsevier

Lightfoot, P.C., Doherty, W., Farrell, K., Keays, R.R., Moore, M., and Pekeski, D., 1997a. Geochemistry of the main mass, sublayer, offsets, and inclusions from the Sudbury Igneous Complex, Ontario; Ontario Geological Survey, Open File Report, 5959, 231pp.

Lightfoot, P.C., Keays, R.R., Morrison, G.G., Bite, A., and Farrell, K.P., 1997b, Geologic and geochemical relationships between the contact sublayer, inclusions, and the main mass of the Sudbury Igneous Complex: A case study of the Whistle Mine Embayment: Economic Geology and the Bulletin of the Society of Economic Geologists, v. 92, p. 647 – 673, https:// doi.org /10 .2113/gsecongeo .92 .6 .647.

Lightfoot, P.C., Noble, S.R., 1992. U-Pb baddeleyite ages of the Kerns and Triangle Mountain Intrusions, Nipissing Diabase, Ontario. Canadian Journal of Earth Science, v. 29, p. 1424 – 1429.

Long, D.G.F., 2004. The tectonostratigraphic evolution of the Huronian basement and the subsequent basin fill: geological constraints on impact models of the Sudbury event. Precambrian Research, v. 129, p. 203 – 223.

Moore, M., Lightfoot, P.C., Keays, R.R, 1993, Project Unit 93-08, Geology and geochemistry of footwall ultramafic rocks, Sudbury Igneous Complex, Fraser Mine, Sudbury, Ontario. In: Baker, C.L., Dressler, B.O., De Souza, H.A.F., Fenwick, K.G., Newsome, J.W., Owsiacki, L. (Eds), Summary of field work and other activities 1993. Ontario Geological Survey Miscellaneous Paper 162, p. 85 – 86.

Moore, M., Lightfoot, P.C., Keays, R.R, 1994, Geology and geochemistry of footwall ultramafic rocks, Fraser mine and Levack West mine, Sudbury Igneous Complex, Sudbury, Ontario. In: Summary of Field Work and Other Activities, Ontario Geological Survey, Miscellaneous Paper 163, p. 91 – 94.

Moore, M., Lightfoot, P.C., Keays, R.R, 1995, Geology and geochemistry of footwall ultramafic rocks, Sudbury Igneous Complex, Sudbury, Ontario. In: Summary of Field Work, Other Activities, Ontario Geological Survey, Miscellaneous Paper 164, p. 122 – 123.

Naldrett, A.J., 2004. Magmatic sulfide deposits: Geology, geochemistry, and exploration. Springer, 727pp.

Naldrett, A.J., and Kullerud, G., 1967, A study of the Strathcona mine and its bearing on the origin of the Nickel-Copper ores of the Sudbury district, Ontario: Journal of Petrology, v. 8, p. 453 – 531.

Naldrett, A.J., Greenman, L., and Hewins, R.H., 1972. The Main Irruptive and the Sublayer at Sudbury, Ontario. International Geological Congress, 24th, Montreal, Proceedings Section 4, p. 206 – 214.

Naldrett, A.J., Hewins, R.H., Dressler, B.O., Rao, B.V., 1984, The Contact Sublayer of the Sudbury Igneous Complex, in Pye, E.G., Naldrett, A.J., and Giblin, P.E., The Geology and Ore Deposits of the Sudbury Structure, Ontario Geological Survey Special Volume 1, p. 253 – 274.

Pattison, E.F., 1979, The Sudbury Sublayer: Canadian Mineralogist, v. 17, p. 257 – 274.

Prevec, S., Lightfoot, P.C., and Keays, R.R., 2000. Evolution of the sublayer of the Sudbury Igneous Complex: Geochemical, Sm-Nd isotopic and petrologic evidence. Lithos, v. 51, p. 271 – 292.

Prevec, S.A. and Cawthorn, R.G., 2002. Thermal evolution and interaction between impact melt sheet and footwall: A genetic model for the contact sublayer of the Sudbury Igneous Complex, Canada. Journal of Geophysical Research, v. 107, p. 5-1 – 5-14.

Prevec, S.A., 2000. An examination of modal variation mechanisms in the contact sublayer of the Sudbury Igneous Complex, Canada: Mineralogy and Petrology, v. 68, p. 141 – 157.

Rae, D. R., 1975. Inclusions in the Sublayer from Strathcona Mine, Sudbury, and their significance. Department of Geology, University of Toronto. Degree of Master of Science.

Ripley, E.M., and Alawi, J.A., 1986. Sulfide mineralogy and chemical evolution of the Babbitt Cu-Ni deposit, Duluth Complex, Minnesota. Canadian Mineralogist, v. 24, p. 347 – 368.

Scribbins, B.T., Rae, D.R., and Naldrett, A.J., 1984. Mafic and ultramafic inclusions in the Sublayer of the Sudbury Igneous Complex. Canadian Mineralogist, v. 22, p. 67 – 75.

Souch, B.E., Podolsky, T., 1969. The sulfide ores of Sudbury: their particular relationship to a distinctive inclusion-bearing facies of the Nickel Irruptive. In Magmatic Ore Deposits (H.D.B. Wilson, ed.), Economic Geology, v. 4, p. 252 – 261.

Spray, J.G., Butler, H.R., and Thompson, L.M., 2004, Tectonic influences on the morphometry of the Sudbury impact structure: Implications for terrestrial cratering and modelling: Meteoritics & Planetary Science, v. 39, p. 287 – 301.

Tornos, F., Casquct, C., Galindo, C., Velasco, F., Canales, A., 2001. A new style of Ni-Cu mineralization related to magmatic breccia pipes in a transpressional magmatic arc, Aguablanca, Spain. Mineralium Deposita, v. 36, p. 700 – 706.

Wang, Y., Lesher, C.M., Lightfoot, P.C., Pattison, E.F., and Golightly, J.P., 2018, Shock metamorphic features in mafic and ultramafic inclusions in the Sudbury Igneous Complex: Implications for their origin and impact excavation. Geology, v. 46, p. 443 – 446.

Zhou, M.-F., Lightfoot, P.C., Keays, R.R., et al. 1997. Petrogenetic significance of chromian spinels from the Sudbury Igneous Complex, Ontario, Canada. Canadian Journal of Earth Science, v. 34, p. 1405 – 1419.

CHAPTER 2

SHOCK METAMORPHIC FEATURES IN MAFIC AND ULTRAMAFIC INCLUSIONS IN THE SUDBURY IGNEOUS COMPLEX: IMPLICATIONS FOR THEIR ORIGIN AND IMPACT EXCAVATION

Yujian Wang, C. Michael Lesher*, Peter C. Lightfoot, Edward F. Pattison, and J. Paul Golightly

Mineral Exploration Research Centre, Harquail School of Earth Sciences, Goodman School of Mines, Laurentian University, Sudbury P3E 2C6, Canada

*Corresponding Author E-mail: mlesher@laurentian.ca

2.1 Abstract

The lowermost, discontinuous parts of the impact-generated Sudbury Igneous Complex (Canada), comprising the Sublayer and Offset dikes, are distinguished from overlying Main Mass norite rocks by the presence of abundant inclusions and Ni-Cu-PGE (PGE = platinum group element) sulfide mineralization. The majority of the felsic to mafic inclusions appear to be derived from the exposed country rocks, but the volumetrically important olivine-bearing mafic and ultramafic inclusions have only very rare equivalents in the surrounding country rocks. We record the discovery of abundant shock metamorphic features (e.g., mosaicism of olivine; strong fracturing and partial isotropization of plagioclase) in the olivine-bearing mafic and ultramafic inclusions consistent with a shock pressure of 20 – 30 GPa. Olivine compositional data are inconsistent with a local country rock or mantle origin for these inclusions. Abundant plagioclase, the absence of garnet or Mg-spinel, and calculated low pressures (< 500 MPa) provide evidence for derivation

of the inclusions from unexposed mafic-ultramafic intrusions in the upper to middle crust that were disrupted during formation of the transient crater, incorporated into the impact melt sheet, and preserved because of their relatively refractory compositions. These observations support models involving intermediate rather than very deep or very shallow excavation for the Sudbury impact event.

2.2 Introduction

The Sudbury Igneous Complex is located at the boundary between the Archean Superior Province and the Paleoproterozoic Southern Province in northeastern Ontario. It is one of the world's oldest, largest, and best-exposed meteorite impact structures (e.g., Grieve and Therriault, 2000) and contains some of the world's largest magmatic Ni-Cu-PGE (PGE – platinum group element) sulfide deposits (e.g., Lightfoot, 2016). Although there is evidence that the country rocks have been deformed by hypervelocity impact (e.g., French, 1967), the proposed depth of impact has ranged from deep (as much as 40 km; e.g., Mungall et al., 2004) to shallow (<12 km; e.g., Darling et al., 2010). A better estimation of excavation depth is important in establishing the evolution of the Sudbury impact crater, the contributions of different rock units to the impact melt sheet, and the sources of metals in the associated world-class Ni-Cu-PGE sulfide deposits. Previous studies focused on geochemical and/or isotopic analyses of the impact melt sheet itself (Offset dike margins, averaged Main Mass lithologies, or glass shards contained in the overlying Onaping Formation breccias). All of these studies invoke significant degrees of impact homogenization of and post-impact modification by the country rocks. The approach taken here is new. We have studied the shock metamorphic record in the refractory olivine-bearing mafic and ultramafic inclusions from the Sublayer and the Offset dikes, which we argue are direct samples of the target rocks and provide better constraints on the depth of the impact process.

2.3 Background

The Sublayer occurs discontinuously within embayments and troughs along the basal contact of the Sudbury Igneous Complex and contains a similar inclusion population to the Offset dikes, which occur as concentric and radial dikes that extend as much as 20 km into the country rocks (e.g., Pattison, 1979; Lightfoot, 2016). The Sublayer and the Offset dikes host, or are directly associated with, most of the contact and offset Ni-Cu-PGE ores in the Sudbury structure. As a result, they are important not only from a petrogenetic perspective, but also from an economic perspective.

The Sublayer and the Offset dikes contain abundant inclusions, including felsic to mafic inclusions derived from local country rocks (Huronian metabasalts and metasediments, East Bull Lake mafic to anorthositic intrusions, and Nipissing mafic intrusions), and also abundant olivine-bearing mafic and ultramafic inclusions with only rare, poorly described potential equivalents in the surrounding country rocks (Naldrett et al., 1984). Some olivine melanorite inclusions have well-preserved igneous textures and are believed to have cognate origins involving contributions from (1) unspecified more primitive magmas (Corfu and Lightfoot, 1996), (2) mantle-derived magmas (e.g., Lightfoot et al., 1997), and/or (3) melted mantle-derived mafic country rocks (e.g., Prevec et al., 2000); however, most of the ultramafic inclusions have been proposed to be exotic (e.g., Pattison, 1979; Golightly, 1994). The olivine-bearing mafic and ultramafic inclusions range in size from centimeters to tens of meters, are typically rounded to subrounded, and are dominated by cumulate and poikilitic igneous textures. The lithologies include dunite and feldspar peridotite, pyroxenite, amphibole pyroxenite, olivine melanorite, and olivine gabbro, most of which contain 1% – 10% phlogopite. The inclusions can be divided into four lithological, textural, and geochemical groups (see Fig. S2.1).

2.4 Shock Metamorphic Features

Shock metamorphic features are recognized in multiple samples in all four groups. Four group I feldspar peridotite inclusions are characterized by undulose extinction and partial isotropization of plagioclase. All 14 samples of group II wehrlite inclusions are characterized by dynamic recrystallization or shock mosaicism of olivine. Three group III olivine- and amphibole-bearing orthopyroxenite contain kink-banded phlogopite. Two group IV olivine melanorite inclusions display mosaicism of olivine and potentially "decorated" planar deformation features (PDFs) in orthopyroxene. This paper focuses mainly on mosaicism of olivine and partial isotropization of plagioclase.

2.4.1 Shock Mosaicism of Olivine

Olivine in heavily shocked rocks (20 – 30 GPa) is commonly characterized by mosaic texture, where olivine grains have been deformed into aggregates of small domains having 1° – 5° (sometimes up to 20°) disorientations (Carter et al., 1968). The precise mechanism of mosaicism has not been established, but may be a result of intense fracturing and plastic flow on the scale of the crystal structure (Carter et al., 1968). The subequant to irregular domains of impact mosaicism differ from plastic polygonization, which is characterized by slip bands, deformation lamellae, and kink bands (e.g., Raleigh, 1968); from dynamic recrystallization, which is characterized by subgrain rotation and dislocation glide (e.g., Falus et al., 2011); and from static recrystallization, which is characterized by more uniform grain sizes with 120° angles (e.g., Ragan, 1969).

Mosaicism is present in olivine in group II and IV inclusions. Sample #373555, a group IV inclusion from the Foy Offset, is a representative example where olivine occurs as 1 – 2 mm

elliptical aggregates that exhibit smooth margins against the surrounding recrystallized plagioclase groundmass (Figs. 2.1A and 2.1B). The absence of any preferred orientation of the recrystallized olivine grains, or evidence of boundary migration of the elliptical olivine assemblages, precludes a strain-dependent (dynamic) recrystallization process. Although a few olivine subgrains exhibit 120° triple junctions, the wide range in sizes (10 – 200 μm) and wide variety of irregular grain shapes and contacts are unlikely to have been generated solely by static recrystallization. As a result, we suggest that primary olivine underwent shock mosaicism, which gave rise to variably small distortions of the crystal lattice, and was then thermally recrystallized during post-shock recovery and/or during incorporation into the Sublayer magma.

In addition, orthopyroxene also contains potential PDFs, which occur as pervasive parallel fractures (1 – 2 μm wide, 3 – 5 μm spaced) that are partially decorated by aligned fluid inclusions (Wang et al., 2016).

Shock mosaicism and PDFs usually form at a pressure of 20 – 30 GPa (Stöffler et al., 1991).

2.4.2 Shock Metamorphism of Plagioclase

Plagioclase is a common intercumulus phase in most ultramafic inclusions. Plagioclase in group I inclusions displays undulose extinction, pervasive fractures, and partial isotropization (Figs. 2.1C and 2.1D). The fractures are narrow (typically < 3 μm wide), but variably spaced (typically 5 – 30 μm), occur in multiple orientations, and generally cut through plagioclase grains. Most are filled with unidentified Mg- and Fe-rich phases. Although different from the closed planar fractures and PDFs in typical shocked plagioclase (e.g., Chao 1967), the complex and open fracture networks observed in the plagioclase in Sublayer inclusions have been reported in shocked plagioclase in the Stannern meteorite (Czech Republic) and Peace River meteorite

(Alberta, Canada) (Chen and Gorsey, 2000). The inhomogeneity on a micron scale, where glass and crystalline materials both occur, is common in shocked terrestrial rocks and meteorites (e.g., Kitamura et al., 1977).

We investigated unshocked and shocked plagioclase in a representative ultramafic inclusion (sample 373582) using micro-Raman spectroscopy. The analyses were performed using a Renishaw inVia Reflex Raman spectrometer at Surface Science Western in London, Ontario (Canada) using analytical procedures described by Fritz et al. (2005). Unshocked plagioclase (An_{50}) in a reference quartz gabbro sample from the Main Mass of the SIC exhibits characteristic Raman bands at 188.9, 480.0, and 508.3 cm^{-1}, and a minor band at 797.0 cm^{-1}. Full widths at half maximum (FWHM) of the key 480.0 and 508.3 cm^{-1} bands are 25.5 and 19.0 cm^{-1}, respectively (Fig. 2.2).

Shocked plagioclase is stoichiometric $An_{35–53}$ with no obvious zoning, and is characterized by pronounced short-frequency (< 450 cm^{-1}) Raman bands peaking at 182.9 and 281.7 cm^{-1} (spectrum 373582–1 in Fig. 2.2) and 186.6, 282.3, and 405 cm^{-1} (spectrum 373582–2 in Fig. 2.2). The 405 cm^{-1} band displays pronounced shoulders on both sides. The medium-frequency bands (450 – 520 cm^{-1}) exhibit decreasing width around 480 cm^{-1} (FWHM = 20.8 cm^{-1} in 373582–1, and 10.5 cm^{-1} in 373582–2) and merge into the major band at 506.3 cm^{-1} (373582–1) or 504.4 cm^{-1} (373582–2). This phenomenon has been recorded in the Raman spectra of plagioclase in Martian meteorites (Fritz et al., 2005). Bands in the 450 – 520 cm^{-1} range are attributed to the motion of bridging oxygens atoms in the “ring-breathing” modes of symmetric stretching in *T*-O-*T* linkages (T = Si^{4+}, Al^{3+}) (e.g., Matson et al., 1986; Freeman et al., 2008). Therefore, variations in *T*-O-*T* bond angles (i.e., disorder of TO_4 tetrahedra) will affect the positions of medium-range bands. The observed variations in short and intermediate frequencies cannot be regarded as

diagnostic of shock metamorphism because variations in composition and crystal orientation may also cause artificial variations in band properties (i.e., band broadening or reduced intensities). However, a longer-frequency band around 580 cm^{-1} (580.8 cm^{-1} in 373582–1, 584.4 cm^{-1} in 373582–2) emerges as a shoulder on the band near 500 cm^{-1}. This shoulder is assigned to symmetric stretching vibrations of three-membered Al-O ring structure, indicating the increased portion of this ring structure in pressure-induced amorphous $CaAl_2Si_2O_8$ (Daniel et al., 1997). This band appeared in synthetic anorthite after being experimentally shocked to 30 GPa (Velder et al., 1989). Additionally, both shocked plagioclases analyzed in this study exhibit a pronounced broad band at 999.6 cm^{-1} (373582–1) or 993.6 cm^{-1} (373582–2), which has been observed in shocked anorthite (An_{96}) in lunar meteorite NWA773 (Freeman et al., 2008). The occurrence of this broad, medium-intensity band around 1000 cm^{-1} in the spectra is diagnostic of the presence of $CaAl_2Si_2O_8$ glass (Daniel et al, 1995, Daniel et al., 1997). Thus, the Raman spectra indicate shock-induced partial isotropization of plagioclase at a pressure of 26–29 GPa (Stöffler et al., 1986).

2.5 Mineral Composition

Olivine is commonly the first silicate mineral to crystallize from mafic-ultramafic magmas and therefore provides insights into deciphering the early crystallization history of the magmas and the characteristics of the magma source. Wavelength-dispersive X-ray emission spectrometric analyses of olivine in 56 olivine-bearing mafic and ultramafic inclusions (using an electron probe microanalyzer) reveals that the olivines display a wide range of composition (i.e., $Fo_{86–68}$ and 3992 – 621 ppm Ni). This is distinctly different from olivine in residual mantle peridotite ($Fo_{93–89}$ and 3000 – 1500 ppm Ni; Pearson et al., 2004). Notably, some individual samples contain olivine that is characterized by very high Ni contents (3992 – 3010 ppm), up to 1500 ppm higher than the

dominant olivines with similar Fo contents (Fig. 2.3), and similar to the high-values in olivine in basalts derived from pyroxenitic sources (e.g., Ni-rich olivines from CMVB in Fig. 2.3). The dominant olivines commonly form clusters defined by individual samples and/or samples from the same locations, but vary greatly between different samples and locations (Fig. 2.3). The variations in olivine compositions are not consistent with fractional crystallization or magma mixing, which would generate systematic trends, suggesting that the olivine-bearing mafic and ultramafic inclusions are derived from multiple crustal target sources with different compositions.

2.6 Geobarometry

The absence of garnet or Mg-spinel and the universal presence of plagioclase in the inclusion assemblages imply a depth < 30 km (Green and Hibberson 1970). In order to more precisely estimate the depth of derivation, we selected several olivine-bearing mafic and ultramafic inclusions from multiple localities that exhibited textural and mineral-chemical evidence of being in chemical equilibrium, and applied the olivine-clinopyroxene-plagioclase (Ol-Cpx-Pl) barometer of Ziberna et al. (2017) (see Table 3-8 for the input data). The results (Table S2.1) suggest that all of the inclusions equilibrated between 210 ± 166 and 300 ± 178 MPa at depths between 7.7 ± 6.0 and 10.9 ± 6.5 km, assuming a geobarometric gradient of 27.5 MPa/km (equivalent to an average crustal density of 2800 kg m^{-3}, consistent with the abundance of mafic intrusive rocks in the Huronian and Archean sequences). Given the widely accepted crustal thickness of 37-38 km in the Sudbury region (Winardhi and Mereu, 1997) and the overwhelming upper crustal signature (after allowance for the great abundance of mafic intrusions in the Sudbury region) in the impact melt (Lightfoot, 2016), this suggests an upper to middle crustal origin for the inclusions; not a very shallow (e.g., Darling et al., 2010) or very deep (e.g.,

Mungall et al., 2004) excavation depth. The absence of any higher-pressure inclusions militates against an interpretation of deep impact.

2.7 Conclusion

Shock mosaicism of olivine and partial isotropization of plagioclase in olivine-bearing mafic and ultramafic inclusions in the Sublayer and the Offset dikes provide near-unequivocal evidence for shock metamorphism at 20–30 GPa and therefore an exotic origin of the inclusions. The dominant cumulate and poikilitic textures, and low forsterite contents of olivine in all inclusions preclude the inclusions being direct samples of the subcontinental lithospheric mantle. The estimated low to moderate pressure of all samples and the absence of any higher pressure samples support an upper to middle crust origin for these inclusions and therefore a shallow to intermediate rather than deep impact depth.

Acknowledgement

We thank Drs. K. Schulz, J. Mungall, and J. Darling for very constructive and helpful reviews, and Dr. J.B. Murphy for editorial assistance. Vale Canada Ltd. kindly provided access to their drill core samples and thin section library. We thank Drs. A. McDonald, W. Zhe, J. Petrus, M. Leybourne, D. Crabtree, S. Clarke, and M.-J. Walzak for assistance with the analytical work, and Dr. L. Ziberna for helpful discussions of the application of the Ol-Cpx-Pl geobarometer. This research was supported by a Natural Sciences and Engineering Research Council of Canada Discovery grant (203171–2012) to Lesher and a China Scholarship Council award to Wang.

Reference Cited

Carter, N.L., Raleigh, C.B., and Decarli, P.S., 1968, Deformation of olivine in stony meteorites: Journal of Geophysical Research, v. 73, p. 5439–5461, https://doi.org/10.1029/JB073i016p05439.

Chao, E.C.T., 1967, Shock effects of certain rock-forming minerals: Science, v. 156, p. 192–202, https://doi.org/10.1126/science.156.3772.192.

Chen, M., and Gorsey, A.E., 2000, The nature of maskelynite in shocked meteorites: Not diaplectic glass but a glass quenched from shock-induced dense melt at high pressures: Earth and Planetary Science Letters, v. 179, p. 489–502, https://doi.org/10.1016/S0012-821X(00)00130-8.

Corfu, F., and Lightfoot, P.C., 1996, U-Pb geochronology of the Sublayer environment, Sudbury Igneous Complex, Ontario: Economic Geology and the Bulletin of the Society of Economic Geologists, v. 91, p. 1263–1269, https://doi.org/10.2113/gsecongeo.91.7.1263.

Daniel, I., Gillet, P., McMillan, P.F., Wolf, G., and Verhelst, M.A., 1997, High-pressure behavior of anorthite: Compression and amorphization: Journal of Geophysical Research, v. 102, p. 10313–10325, https://doi.org/10.1029/97JB00398.

Daniel, I., Gillet, P., McMillian, P.F., and Richet, P., 1995, An in-situ high-temperature structural study of stable and metastable $CaAl_2Si_2O_8$ polymorphs: Mineralogical Magazine, v. 59, p. 25–33, https://doi.org/10.1180/minmag.1995.59.394.03.

Darling, J.R., Hawkesworth, C.J., Storey, C.D., and Lightfoot, P.C., 2010, Shallow impact: Isotopic insights into crustal contributions to the Sudbury impact melt sheet: Geochimica et Cosmochimica Acta, v. 74, p. 5680–5696, https://doi.org/10.1016/j.gca.2010.06.021.

Falus, G., Tommasi, A., and Soustelle, V., 2011, The effect of dynamic recrystallization on olivine crystal preferred orientations in mantle xenoliths deformed under varied stress conditions: Journal of Structural Geology, v. 33, p. 1528–1540, https://doi.org/10.1016/j.jsg.2011.09.010.

Freeman, J.J., Wang, A., Kuebler, K.E., Jolliff, B.L., and Haskin, L.A., 2008, Characterization of natural feldspars by Raman spectroscopy for future planetary exploration: Canadian Mineralogist, v. 46, p. 1477–1500, https://doi.org/10.3749/canmin.46.6.1477.

French, B.M., 1967, Sudbury Structure, Ontario: Some petrographic evidence for origin by meteorite impact: Science, v. 156, p. 1094–1098, https://doi.org/10.1126/science.156.3778.1094.

Fritz, J., Greshake, A., and Stöffler, D., 2005, Micro-Raman spectroscopy of plagioclase and maskelynite in Martian meteorites: Evidence of progressive shock metamorphism: Antarctic Meteorite Research, v. 18, p. 96–116.

Golightly, J.P., 1994, The Sudbury Igneous Complex as an impact melt: Evolution and ore genesis, in Lightfoot, P.C., and Naldrett, A.J., eds., Proceedings of the Sudbury Noril'sk Symposium: Ontario Geological Survey Special Volume 5, p. 105–117.

Green, D.H., and Hibberson, W., 1970, The instability of plagioclase in peridotite at high pressure: Lithos, v. 3, p. 209 – 221.

Grieve, R.A.F., and Therriault, A., 2000, Vredefort, Sudbury, Chicxulub: Three of a Kind?: Annual Review of Earth and Planetary Sciences, v. 28, p. 305–338, https://doi.org/10.1146/annurev.earth.28.1.305.

Kitamura, M., Goto, T., and Syono, Y., 1977, Intergrowth textures of diaplectic glass and crystal in shock-loaded P-anorthite: Contributions to Mineralogy and Petrology, v. 61, p. 299–304, https://doi.org/10.1007/BF00376703.

Lightfoot, P.C., Keays, R.R., Morrison, G.G., Bite, A., and Farrell, K.P., 1997, Geologic and geochemical relationships between the Contact Sublayer, inclusions, and the Main Mass of the Sudbury Igneous Complex: A case study of the Whistle Mine Embayment: Economic Geology and the Bulletin of the Society of Economic Geologists, v. 92, p. 647–673, https://doi.org/10.2113/gsecongeo.92.6.647.

Lightfoot, P.C., 2016, Nickel sulfide ores and impact melts: Origin of the Sudbury Igneous Complex: Amsterdam, Netherlands, Elsevier, p. 4.

Matson, D.W., Sharma, S.K., and Philpotts, J.A., 1986, Raman spectra of some tectosilicates and of glasses along the orthoclase-anorthite and nepheline-anorthite joins: The American Mineralogist, v. 71, p. 694–704.

Mungall, J.M., Ames, D.E., and Hanley, J.J., 2004, Geochemical evidence from the Sudbury structure for crustal redistribution by large bolide impacts: Nature, v. 429, p. 546–548, https://doi.org/10.1038/nature025777.

McDonough, W.F., Sun, S.-S., Ringwood, A.E., Jagoutz, E., and Hofmann, A.W., 1992, Potassium, rubidium, and cesium in the Earth and Moon and the evolution of the mantle of the Earth: Geochimica et Cosmochimica Acta, v. 56, p. 1001 – 1012, http://doi.org/10.1016/0016-7037(92)90043-I.

Naldrett, A.J., Hewins, R.H., Dressler, B.O., Rao, B.V., 1984, The Contact Sublayer of the Sudbury Igneous Complex, *in* Pye, E.G., Naldrett, A.J., and Giblin, P.E., The Geology and Ore Deposits of the Sudbury Structure, Ontario Geological Survey Special Volume 1, p. 253-274.

Pattison, E.F., 1979, The Sudbury Sublayer: Canadian Mineralogist, v. 17, p. 257–274.

Pearson, D.G., Canil, D., and Shirey, S.B., 2004, Mantle samples included in volcanic rocks: Xenoliths and diamonds, *in* Carlson, R.W., ed., The Mantle and Core: Oxford, UK, Elsevier-Pergamon, p. 171 – 275.

Prevec, S., Lightfoot, P.C., and Keays, R.R., 2000, Evolution of the Sublayer of the Sudbury Igneous Complex: Geochemical, Sm–Nd isotopic and petrologic evidence: Lithos, v. 51, p. 271–292, https://doi.org/10.1016/S0024-4937(00)00005-0.

Raleigh, C.B., 1968, Mechanisms of plastic deformation of olivine: Journal of Geophysical Research, v. 73, p. 5391–5406, https://doi.org/10.1029/JB073i016p05391.

Ragan, D.M., 1969, Olivine recrystallization textures: Mineralogical Magazine, v. 37, p. 238–240, https://doi.org/10.1180/minmag.1969.037.286.11.

Stöffler, D., Ostertag, R., Jammes, C., Pfannschmidt, G., Sen Gupta, P.R., Simon, S.B., Papike, J.J., and Beauchamp, R.H., 1986, Shock metamorphism and petrography of the Shergotty achondrite: Geochimica et Cosmochimica Acta, v. 50, p. 889–903, https://doi.org/10.1016/0016-7037(86)90371-6.

Stöffler, D., Keil, K., and Scott, E.R.D., 1991, Shock metamorphism of ordinary chondrites: Geochimica et Cosmochimica Acta, v. 55, p. 3845–3867, https://doi.org/10.1016/0016-7037(91)90078-J.

Straub, S.M., LaGatta, A.B., Martin-Del Pozzo, A.L., Langmuir, C.H., 2008, Evidence from high-Ni olivines for a hybridized peridotite/pyroxenite source for orogenic andesites from the central Mexican Volcanic Belt: Geochemistry Geophysics Geosystems, v. 9, no. 3, p. 1 – 33, http://doi:10.1029/2007GC001583

Velder, B., Syono, Y., Kikuchi, M., and Boyer, H., 1989, Raman microprobe study of synthetic diaplectic plagioclase feldspars: Physics and Chemistry of Minerals, v. 16, p. 436–441.

Wang, Yujian, Lesher, C.M., Lightfoot, P.C., Pattison, E.F., and Golightly, J.P., 2016, Shock metamorphic features of olivine, orthopyroxene, and plagioclase in phlogopite-bearing ultramafic-mafic inclusions in Sublayer, Sudbury Igneous Complex, Sudbury, Canada: Abstract 5082 presented at the 35th International Geological Congress, Cape Town, South Africa, 27 August – 4 September.

Winardhi, S., and Mereu, R.F., 1997, Crustal velocity structure of the Superior and Grenville provinces of the Southeastern Canadian Shield: Canadian Journal of Earth Science, v. 34, p. 1167 – 1184, doi: 10.1139/e17-094.

Ziberna, L., Green, E.C.R., and Blundy, J.D., 2017, Multiple-reaction geobarometry for olivine-bearing igneous rocks: American Mineralogist, v. 102, p. 2349 – 2366.

Figure Captions

Figure 2.1 Photomicrographs of the shock metamorphic features of the olivine-bearing mafic and ultramafic inclusions in the Sublayer and the Offset dikes of Sudbury Igneous Complex (Canada). A: Shocked mosaic olivine preserves the origin euhedral shape, but now comprises small subgrains (plane-polarized light) (sample 373555). B: Same field of view as A shows olivine subgrains with distinct interference colors (cross-polarized light). C: Shocked plagioclase shows pervasive, multi-oriented fractures (plane-polarized light) (sample 373582). D: Same field of view as C shows partial isotropization (cross-polarized light). Mineral abbreviations: Ol-olivine; Opx-orthopyroxene; Pl-plagioclase; Phl-phlogopite.

Figure 2.2 Raman spectra of shocked plagioclase (Pl) in an ultramafic inclusion (sample 373582) and unshocked plagioclase in quartz gabbro from Main Mass of Sudbury Igneous Complex (Canada).

Figure 2.3 Plot of forsterite (Fo) content (mole%) vs Ni concentration (ppm) of olivine in the olivine-bearing mafic and ultramafic inclusions in Sublayer and Offset dikes of Sudbury Igneous Complex (Canada). Light green and beige fields indicate serial melting up to 20% of peridotite and pyroxenite mantle sources, respectively. Lines of olivine fractionation in equilibrium with either peridotite- or pyroxenite-derived melts are referred to Straub et al. (2008). Stars and circles on the fractionation lines represent every 10% fractionation. Sample 373577 has higher Fo and Ni contents compared to the other samples. CMVB - olivines from central Mexican volcanic belt formed by mixing between peridotite- and pyroxenite-derived melts in Subduction environment (Straub et al., 2008); Ol – olivine; Pl – plagioclase; Phl – phlogopite; LHZT-lherzolite; GBBR-gabbro; NORT- norite; Recry-WHTE-recrystallized wehrlite – olivine clinopyroxenite.

Figure S2.1 The inclusions can be divided into four lithological, textural, and geochemical groups. Group I (~54% of sampled inclusions) includes serpentinized dunites, weakly serpentinized feldspar peridotites, pyroxenites, olivine melanorites, and olivine gabbros that have trace element geochemical patterns broadly similar to the igneous-textured Sublayer matrix (ITSM: Lightfoot et al., 1997), but with variably lower absolute abundances, especially heavy rare-earth elements (HREE), and more pronounced negative Sr-Ti anomalies. Group II (~27%) includes wehrlites and olivine clinopyroxenites that have lower abundances of all incompatible trace elements than the ITSM, especially highly incompatible lithospheric elements (HILE), and most have more pronounced negative Sr-Al anomalies. Group III (~11%) includes olivine- and amphibole-bearing orthopyroxenites and is characterized by interstitial olivine. Most are geochemically similar to Group II, but have no negative Sr-Al anomalies. One (#373577) is very strongly depleted in HILE and most moderately incompatible lithosphile elements (MILE), closer to primitive mantle values with positive U-K-Zr-Hf and negative Sr-Sc anomalies. The olivine in

the latter sample is characterized by significantly higher Fo and Ni compared to the other Group III samples (Fig. 3). Group IV (~4%) includes olivine melanorites that are distinguished from Group I olivine melanorites by low HILE-MILE abundances and unfractionated mantle-normalized patterns, similar to sample #373577 in Group III, but display moderately negative Nb-Ta and slightly positive Sr anomalies. Primitive mantle values from McDonough et al. (1992).

Table S2.1 Results of P calculations for the representative olivine-bearing mafic and ultramafic inclusions in Sublayer at several locations in the Sudbury Igneous Complex using the model of Ziberna et al. (2017).

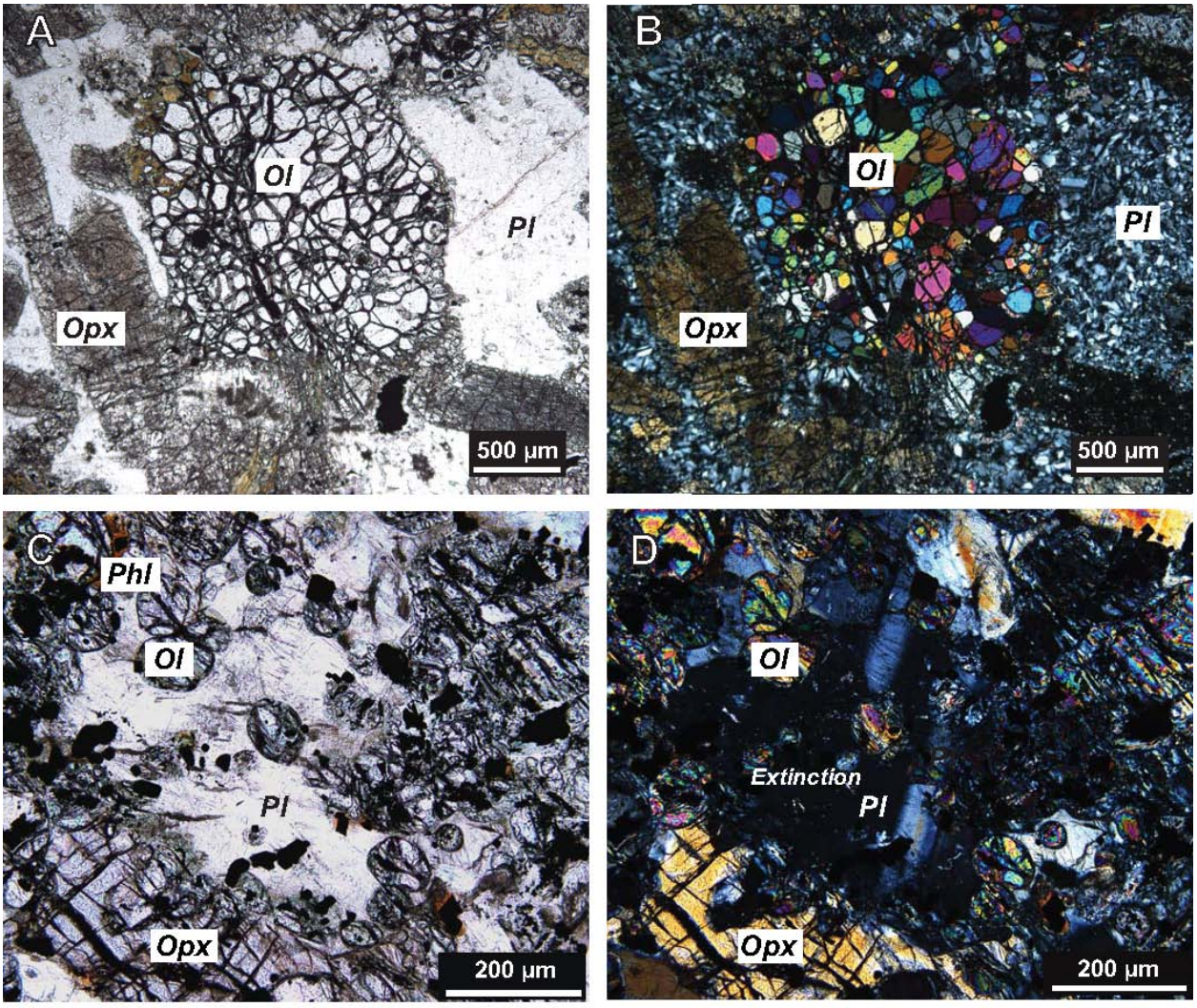

Figure 2.1 Photomicrographs of the shock metamorphic features of the olivine-bearing mafic and ultramafic inclusions in Sublayer and Offset dikes of Sudbury Igneous Complex (Canada)

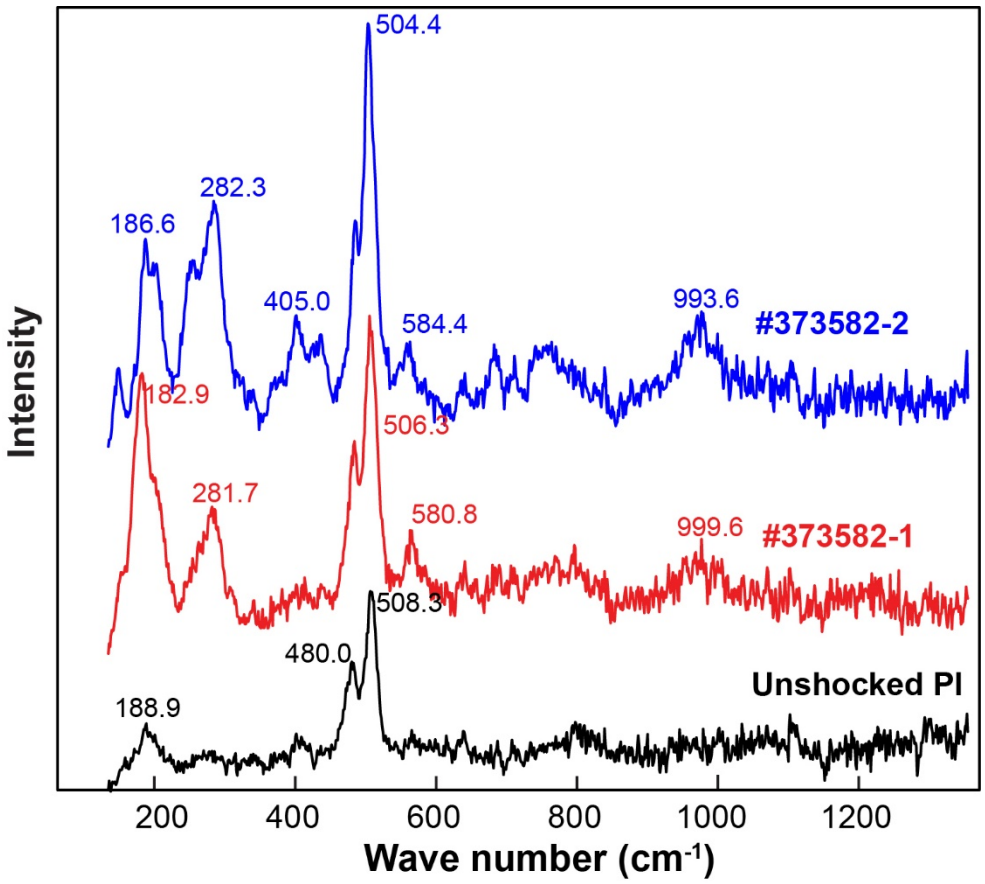

Figure 2.2 Raman spectra of shocked plagioclase (Pl) in an ultramafic inclusion (sample 373582) and unshocked plagioclase in quartz gabbro from Main Mass of Sudbury Igneous Complex (Canada)

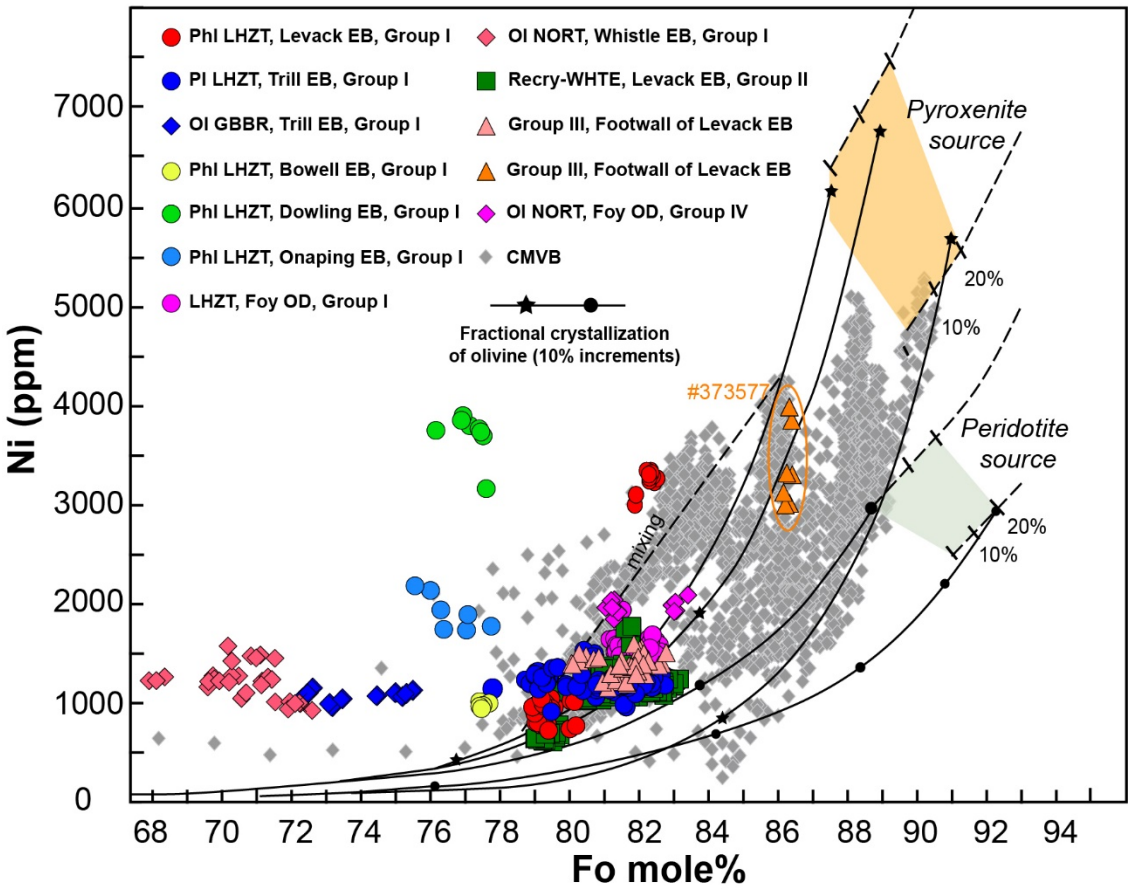

Figure 2.3 Plot of forsterite (Fo) content (mole%) vs Ni concentration (ppm) of olivine in the olivine-bearing mafic and ultramafic inclusions in Sublayer and Offset dikes of Sudbury Igneous Complex (Canada)

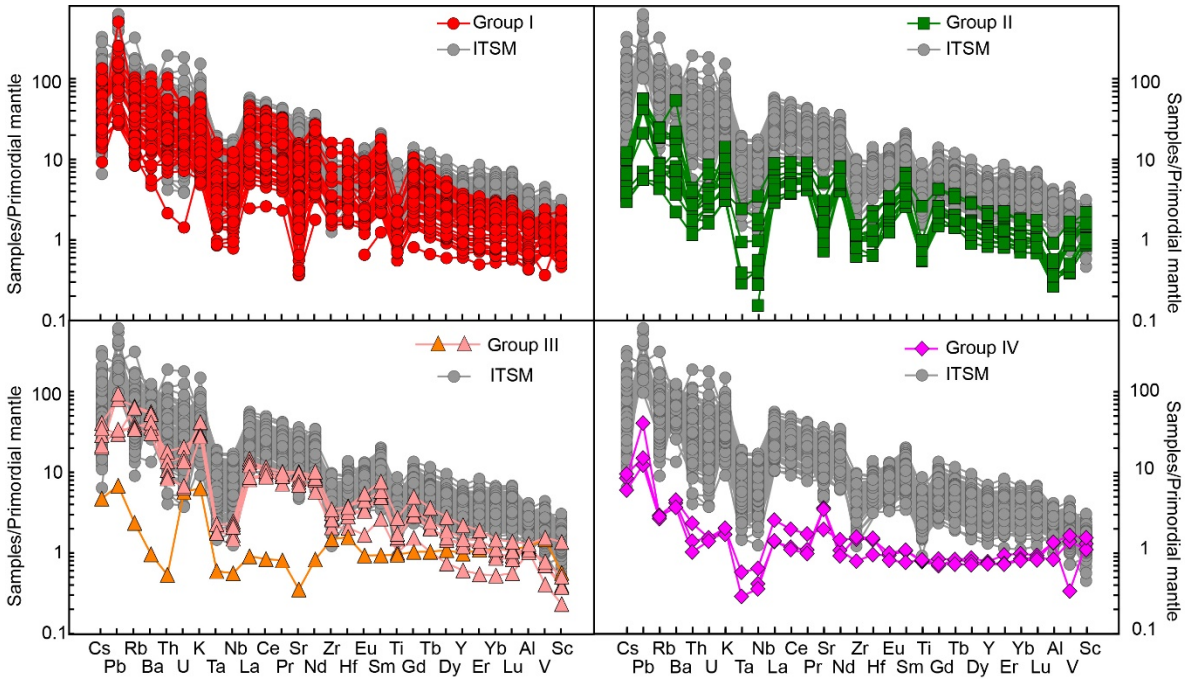

Figure S2.1 Group division of mafic-ultramafic inclusions on the basis of lithologic, textural, and geochemical characteristics

Table S2.1 Results of P calculations for the representative olivine-bearing mafic and ultramafic inclusions in Sublayer at several locations in the Sudbury Igneous Complex using the model of Ziberna et al. (2017).

Sample	Lithology	Location	$T\sigma_{fit}$°C	P MPa	σ_P MPa	σ_{fit}	Depth km
358091	Phl LHZT	Levack	900	300.0	178.0	0.7	10.9 ± 6.5
372980	Pl LHZT	Trill	1050	240.0	109.0	1.5	8.7 ± 4.0
4920B	Pl LHZT	Trill	1120	210.0	166.0	1.9	7.7 ± 6.0
4920A	Ol GBBR	Trill	1100	220.0	183.0	1.6	8 ± 6.7

Note: P_o = 4.0 kbar and $T_o = T_{\sigma fit}$ (see discussion by Ziberna et al., 2017) for all calculations. The effect of changing P_o on calculated P is neglible, but the effect of changing T_o on calculated P can be significant, so $T_{\sigma fit}$ has been selected by minimizing σ_{fit} across the temperature interval 700 - 1300°C. Because igneous spinel is not present in our assemblages, we have used the COlP (Cpx - Ol - Pl) calibration, which may overestimate P by ≤ 100 MPa at P < 500 MPa. All P calculations passed the $\chi 2$ test (σ_{fit} < 1.73), except for sample 4920B (within 20% of cut-off value - 1.73). Depth has been calculated assuming a geobarometric gradient of 27.5 MPa/km.

CHAPTER 3

GEOCHEMISTRY AND PETROGENESIS OF MAFIC AND ULTRAMAFIC INCLUSIONS IN SUBLAYER AND OFFSET DIKES, SUDBURY IGNEOUS COMPLEX, CANADA

Yujian Wang[1], **C. Michael Lesher***[1], **Peter C. Lightfoot**[2], **Edward F. Pattison**[1], and **J. Paul Golightly**

[1] Mineral Exploration Research Centre, Harquail School of Earth Sciences, Goodman School of Mines, Laurentian University, Sudbury P3E 2C6, Canada

[2] Hutchinson Visiting Industry Professor, University of Western Ontario, 1151 Richmond Street, London N6A3K7, Canada

*Corresponding Author e-mail: mlesher@laurentian.ca

3.1 Abstract

The ca. 1.85 Ga Sudbury Igneous Complex (SIC) is the igneous remnant of one of the oldest, largest, and best-preserved impact structures on Earth and contains some of the world's largest magmatic Ni-Cu-PGE sulfide deposits. Most of the mineralization occurs in Sublayer, Footwall Breccia (FWBX), and inclusion-bearing quartz diorite (IQD), which occur discontinuously in embayments/troughs along and in radial/concentric dikes emanating from the basal contact of the Main Mass of SIC into the underlying country rocks. All contain significant (Sublayer and IQD) to minor (FWBX) amounts of olivine-bearing mafic-ultramafic inclusions that have only rare equivalents in the country rocks and are closely associated with the Ni-Cu-PGE sulfide

mineralization. They can be divided into three groups on the basis of textures, mineralogy, and geochemical characteristics, especially trace element signatures. Group I (n = 47) includes igneous-textured olivine melanorite and olivine melagabbronorite inclusions in the Whistle and Levack (Dowling and Onaping Depth) embayments on the North Range. They exhibit similar Zr/Y, Zr/Nb, Nb/U, and Zr/Hf ratios to igneous-textured Sublayer matrix (ITSM) and olivine melanorite inclusions in the Whistle embayment have unradiogenic $\varepsilon Nd_{1850\ Ma}$ values (-8 to -5), and radiogenic to moderately unradiogenic $\gamma Os_{1850\ Ma}$ values (-8 to 94), indicating a contribution from older crustal rocks with low Re/Os ratios and unradiogenic Os isotope composition. These data indicate that Group I inclusions are anteliths that crystallized from a mixture of impact melt and a more mafic melt, probably derived by melting of the widespread Huronian volcanic and subvolcanic units in the region. Group II includes Group IIA (n = 17) shock metamorphosed and recrystallized wehrlite and olivine clinopyroxenite inclusions in the Levack embayment and Group IIB (n = 2) shock metamorphosed olivine melanorite inclusions in the Foy Offset on the North Range. Group IIA inclusions have similar trace element patterns (e.g., negative Th-U, Nb-Ta-(Ti), Sr, and Zr-Hf anomalies) as well as overlapping Nb/U ratios with a layered mafic-ultramafic intrusion in the footwall of the Levack and Fraser deposits, which together with their limited distribution suggests that Group IIA inclusions are locally-derived xenoliths. Group IIA inclusions have low Zr and Zr/Y ratios, variable Zr/Nb ratios, subchondritic Zr/Hf ratios, and superchondritic Nb/Ta ratios, which indicate that they crystallized from a melt derived from a heterogeneous source that had been metasomatized by slab-derived fluids/melts. The petrogenesis of Group IIB inclusions is the least clear because of the strong shock and thermal metamorphism and limited number of samples. They display overlapping Zr/Y, Zr/Nb, and Nb/U variations with and plot on the same trend as Group IIA inclusions in a plot of Ta/Yb vs Th/Yb, indicating that they are petrogenetically related to Group IIA inclusions. Group III (n = 21) includes

phlogopite/feldspar lherzolite inclusions with igneous, recrystallized, and shock-metamorphic textures in the Trill, Levack, and Bowell embayments and the Foy Offset dike on the North Range. They have no equivalents in the exposed country rocks. Feldspar lherzolite inclusions in the Trill embayment exhibit orthopyroxene reaction rims against ITSM, indicating disequilibrium with the impact melt, and one composite inclusion exhibits igneous layering of feldspar lherzolite and olivine gabbro, implying derivation from an unexposed layered mafic-ultramafic intrusion. The calculated parental magma is similar to continental arc basalt formed by approximately 5% partial melting of garnet peridotite. Ol-Cpx-Pl thermobarometry of several Group III inclusions indicate equilibration at 900^{o}C to 1120^{o}C and 210 ± 166 kbar to 300 ± 178 MPa, suggesting emplacement into upper-middle crust (7.7 ± 6.6 to 10.9 ± 6.5 km), prior to being incorporated into the lower parts of the proto-SIC during impact excavation.

Key words: Sudbury Igneous Complex, Sublayer, mafic-ultramafic inclusions, Ni-Cu-PGE sulfide mineralization, geochemistry

3.2 Introduction

The 1.85 Ga Sudbury Structure is the erosional remnant of one of the oldest, largest, and best-preserved impact structures on Earth (e.g., Dietz 1964; Grieve, 1991; Spray et al., 2004) and contains some of the world's largest magmatic Ni-Cu-PGE sulfide deposits (e.g., Naldrett, 2004; Lightfoot, 2016). The Sudbury Structure includes the Sudbury Igneous Complex (SIC), overlying fall-back breccias, suevites, and basin-fill sediments of the Whitewater Group, and underlying pseudotachylitic, anatectic, and contact-metamorphosed breccias. The SIC is divided into two domains: a South Range underlain by Huronian Supergroup mafic-felsic volcanic, felsic plutonic, and sedimentary rocks, 2.4 Ga East Bull Lake Suite mafic intrusive rocks, and 2.2 Ga Nipissing

Suite mafic rocks; and a North Range underlain by Archean felsic-mafic gneisses, granitoids, and mafic-ultramafic intrusions (Fig. 3.1A). The SIC comprises (from base to top) (1) radial and concentric Offset dikes that extend up to 20 km into the country rocks and comprise a marginal/distal phase of inclusion- and sulfide-poor quartz diorite (QD) and an interior/proximal phase of inclusion- and sulfide-rich quartz diorite (IQD); (2) a discontinuous inclusion- and sulfide-rich Sublayer unit with an igneous-textured norite-leuconorite matrix (ITSM; Fig. 3.1B) and an underlying Footwall Breccia unit that occurs in embayments or troughs along the base of the SIC; and (3) a 1.5 km- (parts of North Range) to 5 km- (parts of South Range) thick Main Mass that comprises (from base to top): norite, quartz gabbro, and granophyre.

The abundant inclusions in Sublayer and IQD range from a few millimetres to approximately 100 m (Hewins, 1971; Naldrett et al., 1972) in diameter, and comprise felsic to mafic gneisses, mafic metavolcanic rocks, metagabbros, and metasedimentary rocks, and mafic-ultramafic lithologies (e.g., Naldrett et al., 1984). Although most of the inclusions appear to be derived from local country rocks, the mafic-ultramafic inclusions have only rare equivalents in the country rocks and have at least three origins:

(1) **Cognate**: Anteliths derived from remnants of unexposed parts of the SIC (Naldrett et al., 1984) or earlier Sublayer cumulates (Lightfoot et al., 1997a, b; Farrell, 1997). Crystallization of any known SIC magma would not produce comparable olivine-orthopyroxene assemblages (Prevec, 2000), which has been interpreted to require contributions from i) mantle-derived magmas (e.g., Lightfoot et al., 1997a, b; Farrell, 1997), ii) unspecified more primitive magmas (Corfu and Lightfoot, 1996; Zhou et al., 1997), and/or iii) melted pre-existing mafic country rocks (Prevec, 2000; Prevec et al., 2000).

(2) **Local**: Xenoliths derived from local country rocks, including Nipissing diabase intrusions (Card and Pattison 1973), East Bull Lake suite intrusions (Pattison, 1979), and ultramafic bodies in the Levack Gneiss (Pattison 1979; Moore et al., 1993, 1994, 1995). However, no systematic comparison of petrography and geochemistry has been conducted for the inclusions and these target rocks.

(3) **Exotic**: Xenoliths derived from unexposed mafic-ultramafic intrusions (e.g., Rae, 1975; Kuo and Crocket, 1979; Scribbins, 1978; Scribbins et al., 1984; Wang et al., 2018).

Mafic-ultramafic inclusions are spatially associated with Ni-Cu-PGE sulfide mineralization (e.g., Naldrett and Kullerud, 1967; Pattison, 1979; Naldrett et al., 1984; Lightfoot et al., 1997a, b). Therefore, understanding the origin of the mafic-ultramafic inclusions is important not only in establishing the evolution of the SIC, but also in constraining the genesis of the world's largest accumulation of Ni-Cu-PGE sulfide mineralization. The purpose of this paper is to (1) review the occurrence of the mafic and ultramafic inclusions in Sublayer and IQD; (2) establish the petrography, whole-rock geochemistry, and mineral chemistry of the inclusions, ITSM, and rare mafic-ultramafic bodies in the country rocks; (3) determine the petrogenesis of the inclusions; and 4) constrain the evolution of the Sublayer and IQD.

3.3 Sampling and Analytical Methods

One hundred sixty-five samples of mafic and ultramafic inclusions from 20 localities around the SIC were sampled for this study, representing all locations where mafic-ultramafic inclusions could be obtained. These samples were supplemented with published and unpublished data for olivine chemistry for 28 ultramafic inclusions in the Craig mine (North Range) and Gertrude embayment (South Range) (M. Moore, unpubl.), whole-rock major and trace elements for 39

olivine melanorite inclusions in the Whistle embayment (Lightfoot et al., 1997a), whole-rock major elements for 16 mafic and ultramafic inclusions in the Murray, Creighton, Gertrude, and Little Stobie embayments and Frood offset on the South Range (Scribbins, 1978 and M. Moore, unpubl.), and whole-rock major and trace elements for 210 samples of ITSM in the Whistle, Fraser, Levack, and McCreedy West embayments on the North Range and Little Stobie, Creighton, and Crean Hill embayments on the South Range (Lightfoot et al., 1997a). Considering the variability of the inclusion-bearing lithologies and the paucity of trace element data for many previously-studied inclusions, we do not consider the database to be as comprehensive as desirable for olivine-bearing mafic inclusions, but we believe that it is representative of ultramafic inclusions.

All samples in this study were examined in transmitted and reflected light to derive textural and mineralogical information relevant to their petrogenesis. Best-preserved and most representative inclusions in the Levack, Trill, Dowling, Onaping Depth, and Bowell embayments, and Foy offset on the North Range (Fig. 3.1A) were selected for mineral (n = 45) and whole-rock (n = 83) geochemical analysis at the Ontario Geoscience Laboratories (OGL) in the Willet Green Miller Centre on the Laurentian University Campus in Sudbury.

Major and minor elements in olivine, orthopyroxene, clinopyroxene, chromite, and amphibole were analyzed by wavelength dispersive X-ray emission spectrometry using a 5-spectrometer Cameca SX-100 electron probe microanalyzer (EPMA). Analytical procedures are given in Crabtree (2011). Analytical conditions were: 20 kV accelerating voltage, 20 nA beam current, and count rates below 20000 counts per second. Raw data were corrected using the Cameca PAP correction routine. Lower limits of detection were maintained under 0.01 weight% for most major elements. Analytical precision of most elements is better than ±2%.

Major and minor elements in whole-rock powders were analyzed on fused glass discs by wavelength dispersive X-ray fluorescence spectrometry using a PANalytical Axios Advanced spectrometer. Analytical procedures are given in Keating and Burnham (2012). Fifty-two certified reference materials were used to calibrate the spectrometer. Analytical accuracy is better than ±0.5% (2 sigma, relative) for most elements. Analytical precision is better than ±1% for Si-Ti-Fe-Ca-Ba-K-P and better than ±2% for Al-Cr-Mn-Mg-Na (2 sigma, relative). Sulfur was analyzed by inductive combustion and infrared absorption using a LECO CS844 sulfur analyzer. Analytical precision is ±3%. Loss-on-ignition (LOI) was determined gravimetrically after heating at 1000°C under an oxygen atmosphere. Trace elements were analyzed by inductively-coupled plasma mass spectrometry (ICP-MS) using a Perkin-Elmer Sciex ELAN 9000 quadrupole spectrometer following a 10-day dissolution with HF-$HClO_4$-HCl-HNO in closed Teflon beakers. Dissolution details are given in Burnham et al. (2002) and analytical procedures are given in Burnham (2008). Calibration was against a set of three well-characterized reference materials (AC-E, AGV-1, and BE-N). Analytical accuracy is generally better than ±10%, however, several elements (e.g., Er, Hf, Lu, Pr, Tb, U and Y) are no better than ±10-15%. Analytical precisions for most elements range from ±10% close to the limits of quantification to ±2-8% at moderate to high concentrations.

Trace elements in olivine, orthopyroxene, and amphibole in two representative inclusions (#373552 in the Foy offset and #4920 in the Trill embayment) were determined by laser ablation inductively-coupled plasma mass spectrometry using a Resonetics RESOlution M-50 193 nm ArF excimer laser coupled to a Thermo X-Series II ICP-MS in the Harquail School of Earth Sciences at Laurentian University. Analytical conditions were: 20 ns pulse duration, 5-7 Hz repetition rate, 40-80 μm beam diameter, 3-18 μm sec^{-1} ablation rate (typically 1/3 to 1/2 beam

diameter), 4-5 J cm^{-2} energy density, 650 ml min^{-1} gas (He) rate. Data reduction was carried out using the Iolite software (Paton et al. 2011) in Igor Pro with NIST 610 and Fe^{56} acting as the external and internal references, respectively. Precision and accuracy were assessed from repeated analysis of BCR-2. The traverse data applies a time-slice technique, which equates to a single analysis collected each 0.35 s based on the analytical procedures used in this study, and is hence a proxy for a spot analysis. The limits of detection for integrated data were calculated according to Longerich et al. (1996) and were typically 0.01 to 1 ppm for trace elements, depending primarily on beam diameter and the analytic background signal.

3.4 Petrography

3.4.1 Sublayer and IQD Matrices

ITSM is typically fine- to medium-grained and igneous-textured, but may exhibit partial melting textures where transitional to Footwall Breccia. It is typically a fine-grained subophitic (Fig. 3.2A) to locally porphyritic (Fig. 3.2B) norite, gabbronorite, or leuconorite (Naldrett and Kullerud, 1967). It is composed of 30 – 50% cumulus orthopyroxene (or amphibole after pyroxene) and 30 – 40% plagioclase laths, with variable amounts of interstitial augite, phlogopite, granophyric intergrowths of K-feldspar and quartz, iron oxides, and trace to ~ 60% blebby, disseminated, semi-massive, massive, and stringer sulfides (Naldrett et al., 1984). Only rare replacement of silicate by sulfide has been reported (Naldrett and Kullerud, 1967; Coats and Snajdr, 1984).

IQD matrix is a fine- to medium-grained rock with a quartz dioritic composition. It is composed of variable amounts of plagioclase, ortho- and clinopyroxene (or amphibole after pyroxene), quartz, and biotite, minor amounts of granophyre (Figs. 3.2C and 3.2D), and accessory apatite and titanite. There is no evidence of accumulation of orthopyroxene and/or plagioclase in IQD.

Ni-Cu-PGE mineralization is generally associated with medium-grained IQD and often occurs in the core of the dikes or at jogs and discontinuities in the dikes. The silicate-sulfide textures in IQD range from disseminations and blebs of sulfide in a QD matrix to disseminations and blebs of QD in a sulfide matrix (Hawley, 1962).

3.4.2 Mafic-Ultramafic Inclusions in Sublayer and IQD

Mafic-ultramafic inclusions in Sublayer and IQD have been described by Souch et al. (1969), Hewins (1971), Rae (1975), Scribbins (1978), Hanbury (1982), Scribbins et al. (1984), Naldrett et al. (1984), Farrell (1997), Lightfoot et al. (1997a), and Farrow and Lightfoot (2002). They vary widely in size from a few millimeters to tens of meters and generally have sharp margins. North Range inclusions comprise phlogopite lherzolite, feldspar lherzolite, wehrlite – olivine clinopyroxenite, (olivine) orthopyroxenite, olivine melagabbronorite, olivine melanorite, and olivine gabbro with igneous (e.g., cumulate, poikilitic, and interstitial), tectonic metamorphic (e.g., granoblastic, hornfelsic, and recrystallized), and shock metamorphic (e.g., shock mosaicism, planar deformation features, and partial isotropization) textures. South Range inclusions comprise dunite, harzburgite, olivine orthopyroxenite, orthopyroxenite, and olivine melanorite with well-developed cumulate to extensively granulated and recrystallized textures.

Key petrographic characteristics of the mafic-ultramafic inclusions on the North Range (Lightfoot et al., 1997a; this study) and South Range (Scribbins, 1978) are summarized in Table 3.1, and detailed descriptions of inclusions types on the North Range are provided below.

Phlogopite lherzolite inclusions (n = 5) occur in the Foy offset (this study). They comprise 50 – 60% olivine, 15 – 25% orthopyroxene, 10 – 15% clinopyroxene, 10 – 15% phlogopite, and <5% plagioclase. They are characterized by intensive tectonic or impact-induced thermal

metamorphism (e.g., granoblastic olivine and hornfelsic clinopyroxene) and infiltration veins with contrasting compositions. No visible sulfide is present. The inclusions display sharp contacts with the matrix, occasionally with chlorite coatings.

Feldspar lherzolite inclusions (n = 12) occur in the Levack, Trill, and Bowell embayments on the North Range (this study). They comprise 45 – 65% olivine, 20 – 45% ortho- and clinopyroxene, 5 – 15% interstitial plagioclase, <5% interstitial phlogopite, and occasionally <5% interstitial amphibole. They are characterized by well-preserved orthocumulate, poikilitic, and interstitial textures. There are two types of olivines: i) coarse-grained (1 – 2 mm) cumulus grains, and ii) fine-grained (0.1 – 0.3 mm) chadacrysts enclosed by coarse-grained (1 – 3 mm) pyroxene and plagioclase oikocrysts (Fig. 3.3A). One composite inclusion in the Trill embayment displays parallel layering of feldspar lherzolite and olivine gabbro (described below). No visible sulfide is present in these inclusions. The contact between feldspar lherzolites and ITSM is commonly marked by a 5 – 7 mm (olivine) orthopyroxenite reaction zone, which comprises predominantly adcumulate coarse-grained (1 – 2 mm) orthopyroxene (Fig. 3.3B). One shocked feldspar lherzolite inclusion from the Levack embayment comprises 40 – 45% medium-grained (0.5 – 1 mm) cumulus pyroxene, ~ 40% fine-grained (0.1 – 0.2 mm) olivine chadacrysts, 20 – 25% interstitial plagioclase, and <2% interstitial phlogopite. Plagioclase displays undulose extinction, pervasive fractures (typically <3 μm wide), and partial isotropization, where glass and crystalline materials both occur (Figs. 2.1C and 2.1D in Wang et al., 2018; Wang et al., Ch2). No sulfide is present.

Wehrlite – Olivine clinopyroxenite inclusions (n = 17) occur in the Levack embayment (this study). They comprise variable proportions of olivine and clinopyroxene. Olivine occurs as

fluidal and/or sheared clusters containing olivine neoblasts with variable shapes (e.g., subrounded, subangular, angular, elongate) and sizes (0.1 – 1 mm). Some olivine neoblasts exhibit identical orientations, suggesting that they were originally part of larger single grains, but most have different optical orientations due to recrystallization. The mosaic nature is attributed to shock mosaicism and thermal recrystallization (Wang et al., 2018; Wang et al., Ch2). Clinopyroxene occurs as large polygonal clusters (2 – 5 mm) comprising fine-grained (0.1 – 0.2 mm) clinopyroxene neoblasts with 120° grain-boundary intersections (Fig. 3.3C). Several wehrlite inclusions contain coarse-grained primary orthopyroxene in sharp contact with recrystallized clinopyroxene. They generally display sharp contacts with the matrix, occasionally with chlorite and carbonate coatings. Rare cm-scale felsic clots and streaks and random wisps veins are present. Some samples contain 1 – 3% pyrrhotite and chalcopyrite, but most contain no sulfide minerals.

Olivine melanorite inclusions (n = 42) occur in the Whistle embayment (Lightfoot et al., 1997a). They comprise 15 – 35% fine- to medium-grained (0.5 – 2 mm) cumulus orthopyroxene, 7 – 17% fine to medium-grained (0.5 – 1.5 mm) clinopyroxene, 9 – 19% rounded to subrounded fine-grained (0.1 – 0.5 mm) olivine chadacrysts, 19 – 33% interstitial plagioclase, and 6 – 12% interstitial phlogopite (Farrell, 1997). These rocks show well-preserved orthocumulate, poikilitic, and interstitial textures. The contacts between these inclusions and ITSM are very indistinct, defined by a gradational (several mm to several cm) change from poikilitic texture (inclusion) to non-poikilitic texture (ITSM) and/or a change in grain sizes (Farrell, 1997). These inclusions contain blebby, patchy, and disseminated Fe-Ni-Cu sulfides (Farrell, 1997; Lightfoot et al., 1997b; Scribbins, 1978), and occasionally chalcopyrite-rich stringers that are associated with 2 – 4 mm grains of biotite and amphibole.

Shocked olivine melanorite inclusions (n = 2) occur in the Foy offset dike (this study). They comprise 15 – 25% olivine, 50 – 70% orthopyroxene, and 15 – 30% plagioclase, and are characterized by strong shock metamorphic textures (i.e., shock mosaicism in olivine and planar deformation features in orthopyroxene) and recrystallization in plagioclase. Sample #373555 contains coarse (1 – 2 mm) elliptical aggregates of olivine that exhibit smooth margins against the surrounding recrystallized plagioclase groundmass (figs. 2.1A and 2.1B in Wang et al., Ch2). There is no preferred orientation of the recrystallized olivine subgrains or evidence of boundary migration of the olivine aggregates. Olivine aggregates comprise abundant olivine subgrains that have widely variable sizes (10 – 200 μm) and many different irregular grain shapes. Orthopyroxene is characterized by pervasive, thin (1 – 2 μm wide, 3 – 5 μm spacing), parallel fractures that are partially decorated by aligned fluid inclusions (Wang et al., Ch2). Plagioclase occurs as recrystallized neoblasts and exhibits fluidal foliations. The inclusions display sharp contacts with ITSM, and occasionally have chlorite and carbonate coatings. They are barren of sulfide.

Olivine melagabbronorite inclusions (n = 2) occur in the Levack embayment (Dowling and Onaping Depth) on the North Range (this study). They comprise 40 – 65% ortho- and clinopyroxene, 10 – 25% olivine chadacrysts, 15 – 30% interstitial plagioclase, and 5 – 7% interstitial phlogopite (Fig. 3.3D). They are characterized by orthocumulate, poikilitic, and interstitial textures. Pyroxenes in the Onaping Depth inclusion occur as two forms: i) sub-euhedral 1 – 3 mm cumulus grains, and ii) euhedral fine-grained (0.2 – 0.5 mm) chadacrysts enclosed by plagioclase and phlogopite, while pyroxenes in the Dowling inclusion occur as coarse-grained (2 – 4 mm) cumulus grains. Olivines in both inclusions occur as chadacrysts (0.3

– 0.5 mm) enclosed by plagioclase and/or phlogopite. The Onaping Depth inclusion contains 1 – 3% disseminated sulfides, whereas the Dowling inclusion contains no sulfides.

One **composite feldspar lherzolite - olivine gabbro** inclusion occurs in the Trill embayment (this study). The feldspar lherzolite portion of this inclusion is similar to the above feldspar lherzolite in the same embayment. The olivine gabbro portion of this inclusion comprises 60 – 70% euhedral plagioclase laths, 10 – 18% anhedral – subhedral olivine, 10 – 15% anhedral clinopyroxene, and < 3% biotite. It has a trachytic texture (Fig. 3.3E), where euhedral tabular plagioclase displays a flow foliation, and anhedral olivine and clinopyroxene are interstitial to and/or enclose plagioclase. The contact between the two lithologies is planar and sharp with no disequilibrium reaction textures (Fig. 3.3F).

3.4.3 Mafic-Ultramafic Bodies in the Footwall

The numerous Nipissing and East Bull Lake Intrusive (EBLI) suite intrusions that have intruded Archean Superior and Huronian Southern Province rocks are well characterized (e.g., Jambor, 1971; Peck et al., 1995; Lightfoot and Naldrett, 1996; Vogel et al., 1998, 1999; James et al., 2002, Prevec and Baadsgaard, 2005), but contain only minor olivine-bearing lithologies. The numerous small to large boudins and layers of mafic-ultramafic rocks in the Levack Gneiss contain more olivine (e.g., Coats and Snadjr, 1984; Moore et al., 1993, 1994, 1995), but are less well described.

3.4.3.1 Boudins of olivine amphibole pyroxenite in Levack Gneiss

Olivine-bearing amphibole pyroxenites (n = 9) occur in the country rocks of the Levack embayment (this study). The freshest sample (#373577) comprises 45 – 50% fine-grained (0.3 – 0.5 mm) cumulus orthopyroxene, 45 – 50% fine-grained (0.3 – 0.5 mm) green amphibole, and 10 – 15% interstitial olivine.

3.4.3.2 Amy Lake ultramafic body

Wallbridge Mining has described a Ni-(Cu-PGE) mineralized ultramafic body within the Levack Gneiss Complex on the East Range of the Sudbury Structure ~1 km from the basal contact of the SIC near Amy Lake. The body is 800m long and 100m wide and is composed of variably altered and recrystallized olivine-amphibole pyroxenite with varying amounts of olivine, ortho- and clinopyroxene, and brown amphibole. MgO contents range from 12% to 25%, Ni from 200 to 600 ppm, and Cr from 300 to 725 ppm. Some of the preserved fresh olivine appears to exhibit mosaic texture.

3.4.3.3 Joe Lake (Wisner Township) intrusion and Podolsky Grey Gabbro

The Joe Lake intrusion in Wisner Township on the North Range had long been interpreted to be a member of the EBLI suite, but Bleeker et al. (2013) obtained a 2757 ± 9 Ma single-zircon TIMS age, indicating that it is Archean and therefore a component of the Levack Gneiss Complex. A similar body exposed in the Podolsky Mine in the Whistle offset was dated at ~2714 Ma by MacInnis (2019). Both are composed of medium- to coarse-grained equigranular gabbro containing ~55% altered pyroxene, ~45% plagioclase, and minor amounts of orthopyroxene, hornblende, biotite, ilmenite, zircon, apatite, and quartz (MacInnis, 2019). No olivine has been reported.

3.4.3.4 Layered mafic-ultramafic body in the footwall of the Levack and Fraser Mines

The 1 km-long layered mafic-ultramafic body in the footwall of Levack and Fraser Mine is up to 140 m thick (Coats and Snadjr, 1984). It is composed of fine- to medium-grained and rhythmically-layered dunite, peridotite, orthopyroxenite, clinopyroxenite, and websterite (Coats and Snadjr, 1984; Moore et al., 1993, 1994, 1995). U-Pb TIMS dating of zircons yielded a

discordant array with an upper intercept age of ~2640 Ma and a lower intercept age of ~1860 Ma (M. Moore et al., unpubl. data).

3.4.3.5 Olivine gabbronorite zone in the EBLI Suite

Intrusions of the East Bull Lake Intrusive suite, including the well-studied East Bull Lake (2480 Ma: Krogh et al., 1984), Agnew Lake (2491 Ma: Krogh et al., 1984), and River Valley (2475 Ma: Easton and Hrominchuk, 1999) intrusions, typically contain olivine gabbronorite zones and inclusion-bearing zones with rare pyroxenite and peridotite autoliths/anteliths. The East Bull Lake intrusion contains a 50-70 m thick Olivine Gabbronorite Zone at the base of the Upper Series (James et al., 2002). In this zone, variations in olivine and plagioclase generate rhythmically layering of olivine gabbronorites, gabbronorites, and leucogabbronorites, containing up to 25% olivine. Olivine is weakly zoned from Fo_{65-59} to Fo_{72-65} (Peck et al., 1995; Vogel et al., 1998). Unaltered pyroxene primocrysts in the Olivine Gabbronorite Zone are hypersthene ($En_{70}Fs_{26}Wo_4$ – $En_{67}Fs_{29}Wo_4$), whereas interstitial pyroxene is augite ($En_{43}Fs_{14}Wo_{43}$ – $En_{41}Fs_{15}Wo_{44}$: Vogel et al., 1998). The Agnew Lake intrusion is a 200-300-m-wide composite body with a strike length of approximately 10 km. It contains an Olivine Gabbronorite Zone with plagioclase (An_{78-56}) – olivine (Fo_{76-72}) – orthopyroxene (En_{76-56}) primocrysts above the Marginal Zone. The River Valley intrusion contains an Olivine Gabbronorite Zone that is normally 50 to 150 m thick, with olivine (Fo_{72-76}) – orthopyroxene (En_{70-76}) – plagioclase (An_{72-76}), and clinopyroxene as interstitial anhedral crystals.

3.4.3.6 Olivine gabbronorites in Nipissing Suite Intrusions

The 2.21 Ga (Corfu and Andrews, 1986; Noble and Lightfoot, 1992) Nipissing diabase suite extends in an arcuate area from Sault Saint Marie in the west, through the Sudbury Structure, and northeastwards to the Cobalt-Gowganda area. It intrudes and is regionally coextensive with

supracrustal rocks of the 2.45 – 2.2 Ga Paleoproterozoic Southern Province, and also intrudes underlying granitoid and supracrustal lithologies of the Archean Superior Province. Most of the intrusions consist of undifferentiated quartz diabase, but some are more differentiated, varying upwards from quartz diabase through hypersthene diabase, vari-textured diabase, and granophyric diabase to aplite (Lightfoot et al., 1993). Several intrusions in the Cobalt-Gowganda area contain trace to 4% olivine with compositions between Fo_{60-69} (Conrod, 1989; Lightfoot et al., 1993). Olivine appears to be restricted to intrusions in the Cobalt-Gowganda area and has not been reported in intrusions within the area of the Sudbury impact structure. It is therefore unlikely that these rocks could contribute to the particular suite of mafic-ultramafic inclusions which are the subject of this paper, but a suite of two-pyroxene gabbronorites with textural similarities to Nipissing diabase are a common component of the inclusion suite within South Range Sublayer.

3.4.3.7 South Range Sudbury Gabbro

A spatially restricted subfacies of the Nipissing intrusive suite, locally known as Sudbury Gabbro, occurs south of the SIC. It comprises dominantly melagabbronorites and feldspathic pyroxenites, the most mafic parts of which average 16% MgO. Olivine has not been identified as a component of these rocks. Hanbury (1982) and Farrow & Lightfoot (2002) compared the compositions of Sudbury Gabbro with olivine-absent mafic inclusions in contact Sublayer at several locations along the South Range (Hanbury, 1982) and inclusions hosted by IQD at the Totten mine in the Worthington Offset (Farrow & Lightfoot, 2002). Lithochemical and textural similarities led both to conclude that these inclusions are derived from bodies of Sudbury Gabbro.

3.5 Mineral Chemistry

3.5.1 Olivine

Olivine compositions are shown in Figure 3.4, summarized in Table 3.2, and given in detail in Table S3.1.

Olivines in South Range inclusions, mainly harzburgites and orthopyroxenites, range from Fo_{85} to Fo_{73} (Scribbins et al., 1984), whereas olivines in North Range inclusions range from Fo_{86} to Fo_{68}. Olivines in all inclusions are slightly to highly enriched in Ni and slightly depleted in Mn (except for one group of Mn-enriched wehrlitic olivines) compared to the modelled compositions of olivine crystallized from peridotite-derived melts, and they vary widely in composition from locality to locality, lithology to lithology, and sample to sample.

Olivines in feldspar lherzolite inclusions exhibit broad correlations between Ni-Mn and Fo contents, especially those in the composite inclusion containing layered feldspar lherzolite and olivine gabbro that exhibit a positive correlation between Ni and Fo content and a negative correlation between Mn and Fo content. Olivines in shocked feldspar lherzolite inclusions are strongly enriched in Ni compared to those in unshocked counterparts with similar Fo contents. Olivines in phlogopite lherzolite inclusions exhibit slightly higher Ni and Mn within similar range of Fo content compared to feldspar lherzolitic olivines. Olivines in the majority of wehrlite inclusions overlap with the trend of olivines in feldspar lherzolite inclusions, except for some Ni-enriched olivines and some Ni-depleted olivines. Wehrlite inclusions containing higher abundances of olivine tend to have more Ni-enriched olivine. Notably, wehrlitic olivines have variable Mn contents within a very narrow range of Fo contents. Olivines in igneous-textured olivine melanorite inclusions have lower Fo but slightly higher Ni than the broad Ni trend generated by olivines in feldspar lherzolite inclusions, and are also characterized by negative

correlations between Ni and Fo content, and widely variable Mn. However, olivines in shocked olivine melanorite have higher Fo and Ni contents than igneous-textured counterparts. Olivines in olivine melagabbronorite inclusions in the Levack embayment (Onaping Depth and Dowling) are moderately to highly enriched in Ni relative to the majority of peridotitic inclusions, and they also exhibit negative correlations between Ni and Fo contents.

Olivines in olivine amphibole pyroxenites in the country rocks of the Levack embayment have slightly higher Fo and significantly higher Ni contents than the majority of the olivines in all inclusions. Olivines in the layered mafic-ultramafic body in the footwall of the Levack and Fraser deposits have widely variable Ni-Mn and Fo contents, overlapping with most olivines in the Sublayer/IQD inclusions, and they also have extremely high Mn contents over a restricted range of Fo that are similar to some wehrlitic olivines. Olivines in EBLI olivine leucogabbronorites and gabbronorites overlap the compositions of igneous-textured olivine melanorite inclusions.

3.5.2 Orthopyroxene

Orthopyroxene compositions are shown in Figures 3.5 and 3.6, summarized in Table 3.3, and given in detail in Table S3.2.

Orthopyroxenes in ITSM are hypersthenes characterized by decreasing Al and Cr, and relatively constant Ca and Ti with decreasing Mg#. Orthopyroxenes in orthopyroxenite reaction rims between feldspar lherzolites and ITSM are also hypersthenes, and display similar chemical variations within a wider range of Mg#, except Ti increases in the range of Mg# value between 82 and 76, and is roughly constant at lower Mg#.

Orthopyroxenes in feldspar lherzolite (including the layered composite inclusion), phlogopite lherzolite, and wehrlite inclusions are bronzites – hypersthenes with wide ranges of Al-Ca-Ti-Cr contents over a similar narrow range of Mg#. Orthopyroxenes in unshocked olivine melanorite

and olivine gabbronorite inclusions are also bronzites – hypersthenes, but they have lower Mg# than those in peridotite inclusions, and have significantly lower Al-Cr contents than those in orthopyroxenite inclusions with similar Mg#. Orthopyroxenes in shocked feldspar lherzolite are also bronzites – hypersthenes, and have similar composition to the unshocked counterparts except for significant Ti enrichment. In contrast, orthopyroxenes in shocked olivine melanorite inclusions are bronzites characterized by higher Mg# and significantly higher Cr than unshocked equivalents.

3.5.3 Clinopyroxene

Clinopyroxene compositions are shown in Figures 3.5 and 3.7, summarized in Table 3.4, and given in detail in Table S3.3.

Clinopyroxenes in ITSM are augites with significantly lower Mg# and Cr than those in mafic-ultramafic inclusions. Clinopyroxenes in orthopyroxenite reaction rim between feldspar lherzolites and ITSM are also augites and range from high Mg# and Cr (close to clinopyroxenes in feldspar lherzolites) to low Mg# and Cr (close to clinopyroxenes in ITSM).

Clinopyroxenes in phlogopite lherzolite, feldspar lherzolite, and wehrlite inclusions are diopsides – endiopsides, in which Al increases with decreasing Mg#, but Cr contents are widely variable. Clinopyroxenes in unshocked olivine melanorite and olivine gabbronorite inclusions have lower Mg# than those in the majority of peridotites. In contrast, clinopyroxenes in shocked olivine melanorite inclusions have higher Mg# and Cr contents than unshocked counterparts. Clinopyroxenes in all of the rocks plot outside of the high-pressure field, indicating that they equilibrated at low-moderate pressures.

3.5.4 Chromite

Chromite compositions are shown in Figure 3.8 and given in detail in Table S3.4. All chromite grains are unzoned.

Three different trends/clusters are evident: (1) a Fe-Ti trend, including chromites in the majority of igneous-textured feldspar lherzolite and olivine melanorite, wehrlite – olivine clinopyroxenite, and olivine melagabbronorite inclusions; (2) a Cr-Al trend, including chromites in a few individual samples #373576 (phlogopite lherzolite), #372980 (feldspar lherzolite), and #373555 (shocked olivine melanorite); (3) a high-Cr cluster with distinctive Fe^{3+}-depletion, consisting of chromites in harzburgite and olivine orthopyroxenite inclusions on the South Range (Fig. 3.8A).

Chromites in the Fe-Ti trend are euhedral grains characterized by increasing Fe3# (atomic Fe^{3+}/(Fe^{3+}+Cr+Al)) and Fe2# (atomic Fe^{2+}/(Mg+Fe^{2+})) at relatively constant Cr# (atomic Cr/(Cr+Al)) (Figs. 3.8B and 3.8C). The Fe-Ti trend is attributed to variations in the degree of fractional crystallization of olivine or pyroxene from the host magma (Barnes & Roeder, 2001). Chromites in feldspar lherzolite inclusions in the Trill embayment and wehrlite inclusions in the Levack embayment have much lower Ti contents than chromites in feldspar lherzolite inclusions in the Levack embayment and unshocked olivine melanorite inclusions in the Whistle embayment (Fig. 3.8D).

Chromites in the Cr-Al trend form rod-like intergrowths with plagioclase and are characterized by widely variable Cr# at low Fe2#, and sharply increasing Ti within a narrow range of Fe3# (Figs. 3.8B and 3.8D). Contacts between chromite and plagioclase matrix are sometimes curved, sometimes fairly straight, and sometimes square angled, probably representing relict grain

boundaries. The formation of this texture may involve remelting and remobilization of cumulus chromite.

Chromites in the high Cr cluster are characterized by intermediate Cr# and Fe2#, and distinctly low Fe3# and Fe^{3+} contents (Figs. 3.8B, 3.8D; Fig. 3.9B). Aluminum decreases with increasing Cr in these chromites, whereas Al increases with increasing Cr in other North Range chromites (Fig. 3.9A).

3.5.5 Amphibole

Oikocrystic brown amphiboles in feldspathic lherzolite inclusions poikilitically enclose cumulus olivine chadacrysts. The compositions of brown amphibole in Sublayer inclusions are compared with amphiboles in the SIC and country rocks in Figure 3.10, summarized in Table 3.5, and given in detail in Table S3.5, including green and brown amphiboles in the Main Mass norite at Garson Mine (Mukwakwami et al., 2012), green amphiboles in metagabbro country rocks at Garson Mine (Mukwakwami et al., 2012), green cumulus amphiboles in olivine amphibole pyroxenite inclusions in the footwall at Levack Mine (this study), and brown amphiboles in the layered mafic and ultramafic body in the footwall at the Levack and Fraser deposits (M. Moore, unpubl. data).

Brown amphiboles in feldspar lherzolite inclusions in the Levack embayment have relatively high Mg# and Cr-Al-Ti contents and fall in the magmatic amphibole field. Titanium content in amphibole increases with increasing temperature (e.g., Raase, 1974; Fleet and Bernett, 1978), indicating that the brown amphibole in feldspar lherzolite inclusions crystallized at relatively high temperatures (~900°C: Ernst and Liu, 1998).

Brown amphiboles in the layered mafic-ultramafic intrusion in the footwall at the Levack and Fraser deposits vary widely in composition: some overlap with brown amphibole in feldspar lherzolite inclusions; some have lower Mg# and Cr-Al-Ti contents. Green and brown amphiboles in Main Mass norite have lower Mg# and Cr contents than brown amphiboles in feldspar lherzolite inclusions, but brown amphiboles fall in the magmatic field and have obviously higher temperature (700 – 750°C: Ernst and Liu, 1998), whereas green amphiboles fall in the low-pressure metamorphic field and have lower temperature (~ 600°C: Ernst and Liu, 1998). Similarly, green amphibole in metagabbros in the country rocks fall in the low-pressure metamorphic field and have very low Mg#, Cr-Al-Ti contents, and low temperature (~ 600°C: Ernst and Liu, 1998). Green amphibole in olivine amphibole pyroxenite in the footwall at Levack and Fraser deposits is distinguished from other green amphiboles by falling in the magmatic field, relatively high Mg# and Al contents, but widely variable Cr-Ti contents and wide range of temperature (700 – 800°C: Ernst and Liu, 1998).

A few brown amphiboles in the layered mafic-ultramafic intrusion in the footwall at Levack Mine are similar to the brown amphibole in feldspar lherzolite inclusions in the Levack embayment.

3.6 Whole-Rock Geochemistry

3.6.1 Major and Minor Element Geochemistry

The whole-rock geochemical data for ITSM, mafic-ultramafic inclusions, and comparative mafic-ultramafic bodies in the surrounding country rocks are plotted in Figure 3.11 and shown in Table S3.6, together with the compositions of major mineral phases above.

ITSM is relatively constant within individual embayments, but varies from embayment to embayment (Lightfoot, 1997a). It ranges between 4 and 17% MgO with the more Mg-rich samples representing an orthopyroxene-porphyritic phase at Creighton (Lightfoot et al., 1997a). Iron generally increases and Al-Na-(Ti) generally decrease with increasing Mg. Calcium exhibits two intersecting/overlapping trends: one in which Ca increases with increasing Mg (North and South Ranges) and one in which Ca decreases with increasing Mg (North Range only). These trends suggest that ITSM has accumulated orthopyroxene (North Range and Creighton) and/or clinopyroxene (North and South Ranges).

Harzburgite inclusions contain 38–26% MgO and display negative correlations between Ca-Al and Mg and no correlations between Fe-Ti and Mg. Phlogopite lherzolite inclusions contain 29–28% MgO, and have significantly higher P-K (not shown) and slightly higher Ca relative to harzburgites at similar Mg contents. Feldspar lherzolites and orthopyroxenite inclusions contain 32–23% MgO, with no well-defined correlations between all elements and Mg. They have slightly higher Ca and lower Al than harzburgites possibly due to the lower proportion of orthopyroxene. Wehrlites – olivine clinopyroxenite inclusions contain 32–23% MgO, with well-defined arrays between the average compositions of olivine and clinopyroxene within these inclusions. Several orthopyroxene-rich rocks with lower Mg contents appear to deviate away from the olivine-clinopyroxene defined arrays with lower Ca but higher Fe-Al-Ti. Olivine melanorite (except for shocked olivine melanorites) and olivine melagabbronorite inclusions contain 28–15% MgO and wide range of Fe-Ca-P contents. They have low Al-Na when MgO > 21%, reflecting the absence of plagioclase, whereas they have higher Al-Na when MgO < 21%, reflecting the presence of plagioclase. Titanium decreases with increasing Mg, suggesting olivine and/or orthopyroxene accumulation in these rocks. Two shocked olivine melanorite inclusions

have higher MgO (30% and 25%) and significantly lower Ti-P contents than the majority of unshocked olivine melanorite inclusions.

Olivine amphibole pyroxenites in the footwall rocks at Levack have widely variable compositions and are obviously different from the mafic-ultramafic inclusions. The layered mafic-ultramafic body in the footwall at Levack-Fraser Mine exhibits two clusters: one with approximately 33–24% MgO and one with approximately 21–15% MgO. Iron broadly increases and Ca-Na-Al (possibly two trends in Al) broadly decrease with increasing Mg, and they both vary widely in terms of Ti-P concentrations. Olivine leucogabbronorites and gabbronorites within the EBLI Suite contain 20– 13% MgO with Fe increasing, Ca-Al-Na decreasing, and Ti-P staying constant with increasing Mg.

The mafic rocks in the country rocks, including the EBLI suite (Prevec, 1993; Peck et al., 1995; Vogel et al., 1999; James et al., 2002; Prevec et al., 2005), Nipissing suite (Buchan et al., 1988; Lightfoot and Naldrett, 1996; James et al., 2002), and Huronian Supergroup mafic volcanic rocks (Ketchum et al., 2013) are plotted for reference. They have broadly overlapping to slightly lower Mg, higher Ca-Al, and lower Ti-P contents than ITSM.

3.6.2 Trace Element Geochemistry

Trace element geochemical characteristics of ITSM, mafic-ultramafic inclusions in Sublayer and IQD, and mafic-ultramafic intrusions in the country rocks are shown in Figures 3.12 to 3.15, and relevant ratios for all rock units are summarized in Table 3.6 and shown in detail in Table S3.1. The mafic-ultramafic inclusions can be divided into three groups on the basis of trace element geochemical characteristics (Table 3.6). Key trace element geochemical characteristics of ITSM and inclusions are described below.

All ITSM samples are significantly enriched in highly incompatible lithophile elements (HILE: Cs-Rb-Ba-Pb-LREE) relative to moderate incompatible lithophile elements (MILE: MREE-Zr-Hf-HREE) with pronounced negative Nb-Ta-(Ti) anomalies, minor negative Zr-Hf anomalies, and a wide range of Th-U and Sr concentrations (Fig. 3.12). They exhibit widely fractionated REE, especially LREE (Fig. 3.13), variable Zr/Y ratios, broadly constant Nb/U that are approximate to the values of continental crust (Fig. 3.14), and slightly subchondritic Nb/Ta ratios (Fig. 3.15). The Zr/Nb and Zr/Hf ratios of ITSM on the North Range are slightly higher than those on the South Range (Fig. 3.15).

Group I olivine-bearing mafic-ultramafic inclusions include igneous-textured olivine melanorites and olivine melagabbronorites in the Whistle and Levack (Onaping Depth and Dowling) embayments. Compared to ITSM they are similarly enriched in HILE relative to MILE and exhibit pronounced negative Nb-Ta-(Ti) anomalies, a similar range of Th-U but a wider range of Sr concentrations (Fig. 3.12), and similar Zr/Y, Zr/Nb, and Nb/U ratios (Fig. 3.14), but exhibit a wider range of fractionated REE (Fig. 3.13).

Group IIA comprises wehrlite to olivine clinopyroxenite inclusions with shock metamorphosed and recrystallized textures in the Levack embayment. Compared to ITSM they have more pronounced negative Th-U and Zr-Hf anomalies, more variable negative Nb-Ta-(Ti) and Sr anomalies, and smaller negative Al anomalies (Fig. 3.12). They exhibit distinctively lower LREE contents and La/Yb_N but higher Gd/Yb_N (Fig. 3.13), lower Zr/Y ratios, more variable Zr/Nb and Nb/U ratios (Fig. 3.14), and more variable subchondritic Zr/Hf ratios and superchondritic Nb/Ta ratios (Fig. 3.15).

Group IIB comprises shock metamorphosed olivine melanorite inclusions in the Foy offset dike. Compared to ITSM they have much lower abundances of trace elements, insignificant HILE enrichment, moderate Nb-Ta depletion, no Th-U, Zr-Hf, or Ti anomalies (Fig. 3.12), and much less REE fractionation (Fig. 3.13). They have similar Zr/Y and Zr/Nb ratios to Group IIA inclusions, and appear to follow the positive trend defined by Group IIA inclusions (Fig. 3.14).

Group III comprises phlogopite/feldspar lherzolite, orthopyroxenite, and olivine gabbro inclusions in the Trill, Levack, Bowell embayments and Foy offset dike on the North Range. Compared to ITSM phlogopite lherzolite inclusions are similarly enriched in HILE relative to MILE with pronounced negative Nb-Ta-(Ti) anomalies and minor negative Zr-Hf anomalies, but exhibit distinctively less absolute trace element abundances, more negative Sr anomalies (Fig. 3.12), and significantly lower Nb/U ratios (Fig. 3.14). Compared to ITSM feldspar lherzolite and orthopyroxenite inclusions are similarly enriched in HILE relative to MILE with negative Nb-Ta-(Ti) anomalies, and minor negative Zr-Hf and Sr anomalies, but in lower absolute abundances (Fig. 3.12), and they exhibit significantly lower Nb/U ratios (Fig. 3.14). The shocked feldspar lherzolite inclusions are distinguished from ITSM and other feldspar lherzolites by insignificant HREE fractionation (Fig. 3.13).

Olivine amphibole pyroxenite in the footwall at Levack embayment is enriched in Cs-Pb-U-K, slightly depleted in Sr, and uniformly depleted in most other HILE-MILE elements with small positive Zr-Hf anomalies (Fig. 3.12). The overall trace element features of olivine amphibole pyroxenite appear to be different from all of the mafic-ultramafic inclusions.

The layered peridotite-pyroxenite body in the footwall at Levack and Fraser mines is characterized by slight enrichment of HILE relative to MILE with pronounced negative Nb-Ta-Ti

and Sr-Al anomalies, and moderately negative Th-U-Zr-Hf anomalies (Fig. 3.12). It exhibits comparable Zr/Y and Zr/Nb ratios as Group III inclusions, and widely variable Nb/U ratios, overlapping with Group II inclusions (Fig. 3.14).

Olivine leucogabbronorites and gabbronorites in EBLI have low absolute concentrations of most trace elements, particularly LREE-MREE. They display insignificant Nb-Ta-Ti depletion relative to other incompatible elements and minor positive Sr-Al anomalies (Fig. 3.12), similar Zr/Y and Zr/Nb ratios to but lower Nb/U ratios than ITSM on the South Range (Fig. 3.14). The overall trace element features of EBLI mafic suites appear to be different from all the mafic-ultramafic inclusions.

3.7 Discussion

Before discussing the petrogenesis and tectonic settings of the inclusion types and their relationships to the Ni-Cu-PGE mineralization, it is necessary to evaluate the influences of partial melt loss and/or SIC melt infiltration.

3.7.1 Role of Partial Melt Loss

Jørgensen (2017) and Jørgensen et al. (2018, 2019) have shown that metabasalts within the 250m-thick two-pyroxene hornfels contact metamorphic zone on the South Range lost up to 65% of Cs-Rb-K-U-Th-LREE and Zr-Hf relative to Nb-Ta and MREE-Y-HREE. They attributed the changes to loss of 10-20% partial melt at temperatures approaching ~ 925°C at ~ 1–3 kbar.

The inclusions in this study would have been subjected to similar pressures and variably higher temperatures. Temperatures were ~ 1700^{o}C immediately after impact (Ivanov and Deutsch, 1999) and ~ 1180^{o}C immediately prior to crystallization of the Sublayer (estimated using MELTS) and

would have declined to ~ 1000^{o}C over a period ~ 11,000 years (Prevec and Cawthorn, 2002). Exposure would have been longer for those incorporated earliest (exotic inclusions) and shorter for those incorporated latest (anteliths), but all would have been exposed to subliquidus temperatures for the same period of time. Although the major phases in the inclusions (olivine, orthopyroxene, clinopyroxene, plagioclase) might have been stable at the lower temperatures, they and late-crystallizing accessory phases would have been partially melted – most likely incongruently – at the higher temperatures. Extracted melts would end up in the Sublayer matrix and any residual melts would be preserved as veinlets in the inclusions. Although there is some evidence of these (see below), the mafic-ultramafic inclusions generally do not exhibit any textural or geochemical evidence of partial melting. This contrasts with widespread evidence of partial melting of inclusions derived from mafic and felsic footwall lithologies (e.g., Coats and Snadjr, 1984; Boast and Spray, 2006; Jørgensen, 2017; Jørgensen et al., 2018, 2019).

Some of the inclusions (e.g., Group IIB olivine melanorites) are depleted in Cs-Rb-Th-U-LREE relative to MREE-Y-HREE, but remain depleted in Nb-Ta relative to other HILE and are not significantly depleted in Zr-Hf relative to other MILE. Although the original trace element contents are not well enough known to permit an unequivocal evaluation, these do not appear to be the signatures of melt loss.

3.7.2 Role of Silicate Melt Infiltration

The abundances of incompatible trace elements in mafic-ultramafic xenoliths may be modified by infiltration of host melts or diffusion across grain boundaries (e.g., Nielson-Pike and Noller, 1987). Such metasomatism is commonly recognizable by the presence of replacement textures and/or secondary hydrous minerals (e.g., phlogopite and hornblende: Dawson, 1984; Franz and

Romer, 2010), dissolution of primary phases (e.g., pyroxenes and garnet: Griffin et al., 1999), and strongly contrasting compositions of veins (Franz and Romer, 2010).

The great similarity in the trace element signatures of Group I olivine melanorite and olivine melagabbronorite inclusions, Group III phlogopite lherzolite inclusions, and ITSM (Fig. 3.12) raises the possibility that SIC melt infiltrated into these inclusions during incorporation into the Sublayer. However, Group I olivine melanorite and olivine melagabbronorite inclusions exhibit well-preserved poikilitic and interstitial textures with no evidence of replacement textures or veins of melt infiltration, and the abundant hydrous minerals are unambiguously primary. In contrast, Group III phlogopite lherzolite inclusions contain pyroxene replaced by hornblende, abundant phlogopite (both primary and secondary), and veins of contrasting composition, suggesting that these inclusions may have been modified by SIC melt infiltration.

In order to evaluate the amount of infiltration and its contribution to the trace element signatures in modified Group III phlogopite lherzolite inclusions, we have performed least-squares mixing calculations using (1) the whole-rock composition of a representative modified inclusion (#373552), (2) mineral (olivine and orthopyroxene) compositions analyzed by LA-ICP-MS, (3) a calculated trapped liquid composition based on analyzed orthopyroxene compositions and published partition coefficients between orthopyroxene and coexisting melt (Table S3.7: Bédard, 2007), and 4) the average composition of QD on North Range offset dikes (Lightfoot et al., 1997a), which is regarded as a reasonable estimate of the original impact melt composition. The mass balance calculations were performed using the non-linear generalized reduced gradient least-squares multiple regression method implemented in the Solver optimization tool in Microsoft Excel version 2010. The calculated amount of infiltrated SIC melt in #373552 is ~21% (Table S3.7), suggesting significant SIC melt infiltration in phlogopite lherzolites. Initial

composition by removal of this melt fraction is characterized by lower La/Yb_N, Zr/Y, and Zr/Nb ratios, similar to unaltered, unmodified Group III feldspar lherzolite inclusions.

3.7.3 Constraints from Olivine Compositions

There are several possible explanations for elevated Ni concentrations of olivine in the inclusions: (1) derivation of the parental magma from a pyroxenitic source (e.g., Sobolev et al., 2005, 2007; Herzberg, 2011), (2) higher-than-normal $D_{Ni}^{Ol/melt}$ (partition coefficient for Ni between olivine and silicate melt = Ni_{Ol}/Ni_{melt}) caused by elevated temperatures and pressures of melting of a peridotite source (e.g., Li and Ripley, 2010; Niu et al., 2011; Putirka et al., 2011; Matzen et al., 2013), (3) Fe/Ni ratios modified by equilibration with sulfide (e.g., Clark and Naldrett, 1972; Fleet and McRae, 1983, 1987; Li and Naldrett, 1999; Brenan, 2003; Barnes et al., 2013), and/or (4) diffusion of Ni from sulfide into olivine. Each of these will be discussed below.

3.7.3.1 Pyroxenitic source

Olivine that crystallizes from magmas formed by melting mantle pyroxenite (or hybrids of pyroxenite and peridotite) are characteristically enriched in Si-Ni but depleted in Mg-Ca-Mn compared to olivines crystallizing from magmas formed by melting mantle peridotite (e.g., Sobolev et al., 2005, 2007).

The compositions of olivines in feldspar lherzolite and phlogopite lherzolite inclusions overall do not show obvious enrichment in Ni or depletion in Mn, indicating that the role of pyroxenite-derived melt, if any, is insignificant in the formation of these inclusions. The shallower slope of the correlation between Ni and Fo content in feldspar lherzolite, especially in the layered feldspar lherzolite – olivine gabbro inclusion, is attributed to the trapped liquid shift (Barnes et al., 1986). Olivines in shocked feldspar lherzolite inclusion and some layered mafic-ultramafic intrusion

rocks in the footwall of Levack-Fraser deposit are enriched in Ni compared to other olivine grains with similar Fo contents. These Ni-enriched olivines could crystallize from derivative liquids that mix with primary melts of a pyroxenitic source, as shown by the dash line in Figure 3.4 (Straub et al., 2008; Herzberg et al., 2016). Olivines in wehrlite inclusions have similar Ni concentrations to those in feldspar lherzolite inclusions and mysterious Mn enrichment, which can not be explained by contribution from a pyroxenitic melt. Differently, olivines in the igneous-textured olivine melanorite inclusions in the Whistle embayment have higher Ni content than olivines crystallizing from the primary melt from a peridotite source, and their Mn contents are widely varied between the olivine fractionation lines calculated from a peridotitic melt and a pyroxenitic melt. Similar Ni-enrichment and Mn-depletion can be seen in olivines in shocked olivine melanorite inclusions, although at higher Fo contents relative to the igneous-textured counterparts. The characteristic olivine composition in both igneous-textured and shocked olivine melanorite inclusions is strongly indicative that a pyroxenitic melt has contributed to the formation of the Ni-rich and Mn-poor olivines in the igneous-textured olivine melanorite inclusions. However, olivines in olivine melagabbronorite inclusions are characterized by extremely enriched Ni at low Fo content, which have surpassed the maximum Ni contents that olivines from a pyroxenitic melt can have at similar Fo contents. Thus, another mechanism is required to generate the high Ni olivines in these olivine melagabbronorite inclusions.

3.7.3.2 Elevated partition coefficient for Ni

The partition coefficient between olivine and silicate melt is defined as

$$D_{Ni}^{Ol/melt} = X_{Ni}^{Ol}/X_{Ni}^{melt} \quad [1]$$

where X_{Ni}^{Ol} is the atomic/mass fraction of Ni in olivine and X_{Ni}^{melt} is the atomic/mass fraction of Ni in the silicate melt.

$D_{Ni}^{Ol/melt}$ varies with liquid composition, temperature, and/or pressure (Leeman and Lindstrom, 1978; Mysen and Kushiro, 1979; Li and Ripley, 2010; Putrika et al., 2011; Matzen et al., 2013). Herzberg (2011) calculated the Ni contents of olivine crystallizing from primary magmas with 20 – 30% MgO that were derived from a peridotite source (see Fig. 3.16). The compositions of olivines in the harzburgite, feldspar lherzolite, phlogopite lherzolite, and wehrlite inclusions and many layered mafic-ultramafic intrusive rocks in the footwall of the Levack-Fraser deposits in this study are consistent with having crystallized from peridotite-derived melts with different Mg contents. However, olivines in the shocked feldspar lherzolite inclusions, some layered mafic-ultramafic intrusive rocks in the footwall of Levack and Fraser deposits, and olivine-bearing amphibole orthopyroxenite in the footwall of Levack embayment have Ni contents that are up to 0.15% higher than the maximum olivines expected to crystallize from primary peridotitic magmas, which might indicate a pyroxenite contribution (similar to olivines in Hawaii basalts: see e.g., Sobolev et al., 2005, 2007). Olivines in the olivine melagabbronorite inclusions have extremely high Ni contents at low Fo contents, indicating the operation of additional processes, such as interaction with sulfides (see Barnes et al., 2013).

3.7.3.3 Sulfide-olivine Fe-Ni exchange model

High-Ni olivines can also be generated by equilibration with sulfides (e.g., Clark and Naldrett, 1972; Fleet and McRae, 1983, 1987; Li and Naldrett, 1999; Brenan, 2003; Barnes et al., 2013). The equilibrium between sulfide liquid and olivine is expressed in terms of the exchange coefficient for Fe and Ni (e.g., Boctor, 1982; Fleet and MacRae, 1983, 1987; Brenan and Caciagli, 2000):

$$K_D = (X_{NiS}/X_{FeS})_{Sul}/(X_{NiSi_{0.5}O_2}/X_{FeSi_{0.5}O_2})_{Ol} \quad [2]$$

Brenan (2003) experimentally measured the equilibrium exchange of Fe and Ni between coexisting olivine and sulfide liquid at controlled temperature, oxygen and sulfide fugacities as shown in Figure 3.17, and showed that there is a positive dependence between K_D and Ni content in the sulfide liquid. The range of NiO (0.08 – 0.51%) observed in the mafic-ultramafic inclusions can be produced by equilibrium exchange of Fe and Ni at sulfide liquids with Ni contents of approximately 5 – 10%, consistent with the average composition of sulfide liquid in the SIC (~5 wt% Ni_{100} and ~5 wt% Cu_{100}: Keays and Lightfoot, 2004). Furthermore, Ni-upgrading via sulfide-olivine exchange causes Ni content to increase with increasing Fe but decrease with increasing Mg (Fleet et al., 1981, 1987; Barnes and Naldrett, 1985; Li and Naldrett, 1999). Olivines in olivine melanorite inclusions in the Whistle and olivine melagabbronorite inclusions in the Onaping Depth and Dowling exhibit mild negative correlation between Ni and Fo contents. As a result, sulfide-olivine Fe-Ni exchange can adequately explain Ni-enriched olivines in olivine melanorite inclusions in the Whistle and olivine melagabbronorite inclusions in the Onaping Depth and Dowling.

3.7.3.4 Diffusion of Ni from sulfide into olivine

Diffusion of Ni from sulfide liquid into olivine could contribute to the enrichment of Ni in the mafic-ultramafic inclusions. We have estimated the amount of time required to diffuse Ni from a sulfide liquid into the core of olivine grains ranging between 0.1 mm to 2 mm in diameter. We use a modified one-dimensional (1-D) analytical solution to Fick's second law of diffusion (equation 2.45 in Crank, 1975) to allow for the diffusion of Ni into an olivine containing 1000 ppm Ni from an impact melt containing 60 ppm Ni and a sulfide liquid containing 5% Ni_{100}:

$$\frac{C_x - C_{ol}}{C_{interf} - C_{ol}} = erfc\,\frac{x}{2\sqrt{Dt}} \qquad [3]$$

Where C_x is the concentration of Ni in the olivine grain at distance *x* from the rim, C_{ol} is the initial concentration of Ni in the olivine, C_{interf} is the advectively maintained concentration in the silicate melt or sulfide liquid, and D is the diffusion constant, which has been experimentally investigated at 1 atmosphere and over a temperature range of 900 – 1445°C (Petry et al., 2004). A least-squares regression of all experimental data defines a good correlation between log D_{Ni} and 10000/T, suggesting that we can safely extrapolate D_{Ni} to 1700°C.

The results (Fig. 3.18) indicate that 0.1 – 2 mm olivine grains achieve uniformly lower Ni concentrations when immersed in silicate melt in 10^{11} to 10^{13} million years, which is much longer than the duration of cooling of the SIC to 1180°C (45,000 years: Prevec and Cawthorn, 2002) and achieve uniformly higher Ni concentrations when immersed in sulfide melt for 10^{11} to 10^{12} years (Fig. 3.18). The olivines in the mafic-ultramafic inclusions are unzoned and vary widely from locality to locality and individual to individual sample, suggesting that the olivines never equilibrated with the impact melt or sulfide melt.

3.7.4 Petrogenesis of Mafic-Ultramafic Inclusions in the North Range

3.7.4.1 Group I inclusions

Group I olivine melanorites and olivine gabbronorites are petrographically similar to olivine gabbronorites and gabbronorites in the EBLI suite, which led Pattison (1979) and Lightfoot (2016) to suggest a local xenolithic origin. However, EBLI olivine gabbronorites and gabbronorites are geochemically quite different, exhibiting: (1) well-defined orthopyroxene accumulation trends with lower Mg# (Fig. 3.11), (2) insignificant Nb-Ta-Ti depletion (Fig. 3.12), (3) conspicuously lower La/Yb_N and Gd/Yb_N ratios (Fig. 3.13), and (4) systematically lower Zr/Y, Zr/Nb, and Nb/U ratios (Fig. 3.14), which negate the possibility of them being derived from EBLI-related sources.

In contrast to the sharp contacts or reaction zones between the other inclusions and ITSM, some of the contacts between Group I inclusions in the Whistle embayment and ITSM are gradational in terms of grain size, texture, and/or composition (Farrell, 1997; Lightfoot et al., 1997a). Gradational contacts could indicate cognate origin for Group I inclusions or they could indicate resorption and partial assimilation. Based on their primary igneous textures and geochemical similarity to ITSM, Farrell (1997) and Lightfoot et al. (1997b) suggested that Group I inclusions are "cognate xenoliths" (referred to hereafter as anteliths). This study confirms that Group I inclusions and ITSM have very similar incompatible trace element patterns (Fig. 3.12) with indistinguishable Zr/Y, Zr/Nb, Nb/U, and Zr/Hf ratios (Figs. 3.14 and 3.15). They exhibit no evidence of replacement textures or veins of melt infiltration, and the abundant phlogopite and amphibole are unambiguously primary. Hence, infiltrating contamination by the hosting magma (as suggested below for some Group III inclusions) can be excluded as a mechanism to account for the trace element similarity between Group I inclusions and ITSM. The well-preserved igneous textures, geochemical similarities to ITSM, and gradational contacts with ITSM suggest that they are anteliths that crystallized from the impact melt at an early stage.

Group I inclusions contain significant amounts of olivine (10 – 34%), whereas ITSM only rarely contains minor olivine (e.g., Whistle: Pattison, 1979), suggesting a contribution from (1) an early unspecified more primitive magma (e.g., Corfu and Lightfoot, 1996; Zhou et al., 1997), (2) a mantle-derived magma (e.g., Lightfoot et al., 1997a, b; Farrell, 1997), and/or (3) an assimilated mafic crustal component (e.g., Prevec, 2000; Prevec et al., 2000). The slightly unradiogenic to radiogenic $\gamma Os_{1850\ Ma}$ values (-8 to 94: Cohen et al., 2000) of analyzed Group I inclusions in the Whistle embayment are compatible with derivation from subduction-related metasomatized mantle (Marques et al., 2003) or from older crustal rocks

with low Re/Os ratios and unradiogenic Os isotope compositions (see Cohen et al., 2000). However, their highly unradiogenic $\varepsilon Nd_{1850\ Ma}$ values (-8 to -5: Prevec et al., 2000; Prevec and Baadsgaard, 2005) require derivation from older crustal rocks (Cohen et al., 2000).

It seems most likely that the older mafic component in Group I inclusions was generated by melting Archean volcanic and intrusive rocks, such as those present in the footwall on the North Range, which have been considered to be derived from a subduction-metasomatized lithospheric mantle (Jolly, 1987; Jolly et al., 1992; Ketchum et al., 2013), facilitated by the high temperature of the SIC magma, and incorporated into an early marginal phase of the SIC (Prevec et al., 2000). Bowen (1922) and Kelemen & Hart (1996) have shown that assimilation of an ultramafic rock by a mafic melt with orthopyroxene on the liquidus would crystallize an olivine-bearing assemblage and that it would be more alkalic, explaining the high phlogopite content of Group I inclusions. The more-mafic melt component may also be preserved in North Range Mafic Norite, which occurs only in association with Sublayer (Naldrett, 2004; Lightfoot, 2016), and which contains significantly less radiogenic Pb than overlying Felsic Norite and Quartz Gabbro (McNamara et al., 2017). Thus, Group I inclusions and Mafic Norite both provide evidence of *local* thermomechanical erosion of footwall rocks in the ore-localizing embayments. Prevec (2000) suggested that the more-mafic melt was generated by post-impact melting of basaltic footwall rocks (as preserved on the South Range and inferred by McNamara et al. (2015) to have been present on the North Range) that mixed with the liquid that formed overlying Main Mass norite to form a hybrid that was saturated in olivine. It is not clear why the SIC was able to subsequently remelt the olivine melanoritic protolith of the anteliths, although Lesher et al. (2016) suggested that some of the geochemical reversals in the lower parts of the stratigraphy on the

South Range may reflect influxes from other parts of the multi-ring impact basin. These influxes may have resulted in remelting of the protolith of the anteliths.

In summary, Group I inclusions appear to be anteliths that crystallized from a mixture of impact melt and melted mafic country rocks, and that were subsequently incorporated into Sublayer.

3.7.4.2 Group II inclusions

The presence of shock metamorphism in Group IIA inclusions precludes a cognate origin. They are petrographically, mineralogically, and geochemically very similar to a rhythmically layered peridotite-orthopyroxenite-clinopyroxenite-websterite body in the footwall of the Levack and Fraser deposits. They are characterized by (1) a very narrow range of Mg# (81 – 83, one sample with 78), suggesting that fractional crystallization played a minimal role, (2) arrays linking the average composition of olivine and clinopyroxene, suggesting that they are mainly controlled by variable degrees of accumulation of olivine and clinopyroxene, (3) extreme Mn enrichment in olivine, and 4) similar trace element signatures, including enrichment in HILE relative to MILE with pronounced negative Th-U, Nb-Ta-(Ti), Sr, and Zr-Hf anomalies, similar Zr/Hf ratios, and broadly increasing Nb/U with increasing Nb, to the layered mafic-ultramafic body. These features suggest a genetic affinity between Group IIA inclusions and the layered mafic-ultramafic body.

However, there are several inconsistencies in the trace element signatures. For example, Group IIA inclusions have lower Zr contents and Zr/Y ratios, a wider range of Zr/Nb ratios (Fig. 3.14), variably lower Zr/Hf ratios, and distinctively higher Nb/Ta ratios (Fig. 3.15), compared to the layered mafic-ultramafic body. Zirconium is more incompatible than Y during partial melting (Pearce and Norry, 1979), indicating that Group IIA inclusions are derived from a more depleted

source. Niobium is only slightly more incompatible than Zr (Pearce and Norry, 1979), suggesting that the variations in Zr/Nb may reflect multiple genetically-unrelated intrusions (less likely because of the progressive mineralogical variations and consistency in geochemical compositions) or a single intrusion formed from a heterogeneous source(s) (more likely). Variable Zr/Hf ratios can be produced by fractional crystallization of clinopyroxene, as Hf is more compatible in clinopyroxene than Zr ($D_{Hf}^{Cpx/Melt} = 0.20 – 0.25$, $D_{Zr}^{Cpx/Melt} = 0.10 – 0.14$: Green, 1994), but Group IIA inclusions do not exhibit the expected negative correlation between Sc (index of clinopyroxene fractionation: David et al., 2000) and Zr/Hf (Fig. 3.19). For the same reason, variable Zr/Hf ratios can also be produced by variations in the degree of partial melting (David et al., 2000), but Group IIA inclusions do not exhibit the expected positive correlation between Zr (index of partial melting: Rollinson et al., 1993) and Zr/Hf. Hence, the highly variable Zr/Hf is most likely inherited from heterogeneous sources (see Fábio et al., 2002). Niobium and Ta have the same Nb/Ta ratio of 17.6 (± 2) in carbonaceous chondrites, MORB, and OIB (Jochum et al., 1986). However, superchondritic Nb/Ta ratios are a common feature of subduction-related basalts (Stolz et al., 1996; Münker, 1998), as refractory sphene and rutile will fractionate Nb and Ta ($D_{Nb}/D_{Ta} \sim 0.3 – 0.4$ for sphene, 0.6 – 0.7 for rutile: Wolff, 1984). The wide variations in Zr/Y, Zr/Nb, and Zr/Hf could be attributed to source heterogeneity produced during metasomatism of mantle by the slab-derived fluids/melts (Ionov and Hofmann, 1995; Stolz et al., 1996).

In summary, considering the local distribution of Group IIA, and closely spatial relationship and close similarities in the trace element signatures of Group IIA and the layered mafic-ultramafic intrusion in the footwall of Levack-Fraser Mine, Group IIA inclusions appear to be locally derived xenoliths that were sampled from a mafic-ultramafic intrusion petrogenetically-related to the above layered mafic-ultramafic intrusion.

Group IIB includes only two samples, and their petrogenesis is the least clear because of the strong shock and thermal metamorphism that have obscured most primary textures. The shock mosaicism of olivine and planar deformation features of orthopyroxene in sample 373555 imply a shock regime of 20 – 30 GPa and an exotic origin (Wang et al., 2018). As indicated, Group IIB inclusions are distinguished from their mineralogical equivalents in Group I by very distinctive trace element features, but they have overlapping Zr/Y, Zr/Nb, and Nb/U ratios and define a similar Ta/Yb vs Th/Yb trend (Fig. 3.23, as discussed below) as Group IIA inclusions. The complete recrystallization and incipiently melted morphology of plagioclase and chromite in Group IIB inclusions suggest that they have experienced intensive melting and recrystallization, and the very low trace element abundance in Group IIB may be due to loss of partial melt. However, as noted above, partial melting of inclusions should occur in the form of melting of the matrix and incongruent melting along grain boundaries, forming selvedges and veinlets. Although the plagioclase groundmass is highly recrystallized, olivine and orthopyroxene experienced no boundary migration or reaction, and there are no selvedges and veinlets with contrasting composition in the groundmass. As a result, given the similarities in trace element geochemistry with Group IIA inclusions, Group IIB are most likely also local xenoliths derived from a now-consumed or now-hidden source.

3.7.4.3 Group III inclusions

The orthopyroxenite selvedges between Group III inclusions and ITSM suggest that they are reaction products between the inclusions and ITSM. The reaction of olivine to orthopyroxene has been well documented in experiments (e.g., Hirschmann et al. 2006; Sobolev et al. 2006), and commonly occurs as narrow reaction zones between mantle peridotitic xenoliths and percolating

fluids in natural rocks (e.g., Liu et al. 2005; Porrera et al. 2006). This indicates that the feldspar lherzolites are out of equilibrium with ITSM.

The well-preserved igneous textures (e.g., cumulus, poikilitic textures) and well-defined layering in the composite feldspar lherzolite – olivine gabbro inclusion imply that the Group III inclusions are derived from a layered mafic-ultramafic intrusion. The parental magma composition of Group III inclusions can be estimated by mass balance using the following equation, assuming that the whole-rock composition represents mixtures of cumulus minerals (olivine and orthopyroxene) and evolved interstitial melt (clinopyroxene, plagioclase, and accessory phases) in a closed system (e.g., Cawthorn et al., 1991; see also Godel et al., 2011):

$$X_i^{WR} = F^{Opx} * X_i^{Opx} + F^{Ol} * X_i^{Ol} + F^{Liq} * X_i^{Liq}) \quad [4]$$

with $X_i^{Opx} = D^{Opx/Liq} * X_i^{Liq}$ and $X_i^{Ol} = D^{Ol/Liq} * X_i^{Liq}$, where X_i^{WR} is the concentration of the element *i* in the whole rock, F^{Opx} is the mass fraction of cumulus orthopyroxene prior to post-cumulus overgrowth (assumed to be equal to the amount of clinopyroxene), F^{Ol} and F^{Liq} are the mass fractions of olivine and trapped liquid, $D^{\frac{Opx}{Liq}}$ and $D^{\frac{Ol}{Liq}}$ are the partition coefficients of the element *i* between the orthopyroxene or olivine and the liquid.

Group III inclusions, except for shocked feldspar lherzolites, exhibit well-defined cumulate and interstitial textures and show no evidence of significant melt migration or significant interaction with Sublayer magma, so are amenable to this method. The parameters, including the whole rock composition and partition coefficients between olivine or orthopyroxene and the liquid (Bédard, 2005, 2007) used in the calculation are summarized in Table 3.7. The estimated parental magma (Table 3.7) is enriched in HILE relative to MILE with pronounced negative Nb-Ta-Ti anomalies

and intermediate negative Zr-Hf anomalies (Fig. 3.20), similar to continental arc basalts and quite different (as expected) from ocean island basalts (OIB) or mid-ocean ridge basalts (MORB). The fractionations of La/Sm and Sm/Yb are sensitive indicators of the degree of partial melting because the incompatibility of REE during melting decreases from La to Yb (Willbold et al., 2006). The $[La/Sm]_N$ ratio of the inferred parental magma (2.7) is lower but within the lower range of OIB (3.0 ± 0.3: Willbold et al., 2006), suggesting similar or somewhat higher degree of partial melting than OIB (3 – 5%: Hofmann and Feigenson, 1983; Ormerod et al., 1991). The $[Sm/Yb]_N$ ratios of partial melts produced by a range of different degrees of batch melting of garnet peridotite (Ol:Opx:Cpx:Grt = 55:25:15:5) and spinel peridotite (Ol:Opx:Cpx:Sp = 55:25:15:5) have been calculated using the batch melting equation (Shaw, 1970):

$$\frac{C_L}{C_o} = \frac{1}{D_o + F(1-D_o)} \quad [5]$$

and the fractional melting equation (Shaw, 1970):

$$\frac{C_L}{C_o} = \frac{1}{D_o} * (1 - F)^{(\frac{1}{D_o}-1)} \quad [6]$$

where F = weight fraction of melt produced, C_o = original bulk rock composition, C_L = final concentration in the liquid, and D = bulk distribution coefficient. The bulk partition coefficients between minerals and melts are from Salters and Stracke (2004). The calculated results at variable degrees of batch melting and fractional melting is shown in Table 3.8, which demonstrate that Group III inclusions could be generated from continental arc basalts formed by approximately 5% batch melting or 1 – 5% fractional melting of garnet peridotite.

Several Group III mafic and ultramafic inclusions that exhibit textural, mineral, and chemical evidence of being in equilibrium have been selected to apply the Ol – Cpx – Pl barometer

(discussed below in detail) (Ziberna et al., 2017). Four Group III inclusions in the Trill embayment appear to have equilibrated at low P (210 – 240 MPa) but relatively high T (1050 – 1120°C), whereas one Group III inclusion in the Levack embayment appears to have equilibrated at higher P (300 ± 180 MPa) but lower T (900°C). The results suggest that these inclusions equilibrated at depths between 7.7 ± 6.0 and 10.9 ± 6.5 km, assuming a geobarometric gradient of 27.5 MPa/km (Wang et al., 2018).

In summary, Group III inclusions are exotic fragments of one or more layered mafic-ultramafic intrusions that could be derived from continental arc basalt magma formed by up to 5% partial melting of garnet peridotite, equilibrated at 7.7 – 10.9 km depth, excavated during impact, and incorporated into the SIC.

3.7.5 Petrogenesis of Mafic-Ultramafic Inclusions in the South Range

The petrogenesis of olivine-bearing mafic-ultramafic inclusions on the South Range is less clear, as no samples were available for this study, they are generally more altered, and previous studies reported mainly major element with limited mineral chemical and no trace element data.

Scribbins et al. (1984) compared the lithologies between mafic-ultramafic inclusions on the North and South Ranges. The abundances of rock types are statistically imprecise as most samples were collected from available localities in the mine and were insufficient to span the diversity of rock types, but the results are informative. A characteristic feature of South Range mafic-ultramafic inclusions is the lack of clinopyroxene-dominant rock types (lherzolites, wehrlites, and clinopyroxenites). Hydrous arc basalts will stabilize olivine and clinopyroxene over a substantial temperature interval (e.g., Gaetani et al., 1994; Pichavant and Macdonald,

2007), consistent with the presence of igneous phlogopite and amphibole in North Range inclusions, but not in South Range inclusions.

The available major element dataset of South Range inclusions exhibits well-defined negative correlations between Ca-Al-Na-Ti and Mg that extrapolate to ~ Fo_{85-73}, suggesting olivine accumulation in South Range inclusions, compared to the orthopyroxene accumulation inferred for North Range inclusions. South Range inclusions also contain lower Ca but higher Al than North Range inclusions, which is attributed to the higher abundance of orthopyroxene in South Range inclusions. Chromites in South Range and North Range inclusions are compositionally different (Fig. 3.8A). Zhou et al. (1997) suggested it was an arbitrary break that would be filled in as more samples become available, but our work reveals significant compositional distinctions between South and North Range chromites, including lower Fe^{3+}# (15 – 19 vs 29 – 85: Fig. 3.8C), higher Cr_2O_3 and Al_2O_3 (30 – 51% and 10 – 22% vs 16 – 37% and 3 – 13%: Fig. 3.9), and negatively-correlated Cr-Al vs positively-correlated Cr-Al (Fig. 3.9). The Fe^{3+} will be affected by the fO_2 in the liquid (see Barnes, 1998) and post-cumulus Fe-Mg exchange between chromite and olivine (Scowen et al., 1991). The negatively correlated trend of Cr-Al in the South Range chromites is parallel to the mantle array, whereas the positively correlated Cr-Al in the North Range chromites appear to follow the field of arc cumulate spinels (Fig. 3.9). This suggests that the chromites in South Range inclusions may have crystallized at higher temperatures (Franz and Wirth, 2000), whereas the chromites in North Range inclusions may have crystallized under lower temperatures and/or have been influenced by post-cumulus effects (Irvine, 1967).

3.7.6 Tectonic Settings

A common geochemical characteristic of all inclusions and ITSM is the enrichment in HILE relative to MILE with pronounced negative Nb-Ta-(Ti) and minor negative Zr-Hf anomalies (Fig.

3.12). These geochemical characteristics indicate that the magma from which they crystallized was of subduction-related arc affinity (e.g., Pearce and Norry 1979; Perfit et al. 1980; Pearce, 1982) or that it was contaminated by continental crust (e.g., Wilson 1989; Thompson et al. 1984). Figure 3.19 compares the incompatible element patterns of mafic-ultramafic inclusions and arc basalts formed by addition of various subduction components (shallow/deep slab melts) into peridotitic mantle (Pearce et al., 2005) and upper continental crust (Taylor and McLennan, 1995). Upper continental crust exhibits less pronounced negative Nb-Ta-(Ti) anomalies and no Zr-Hf depletion, whereas the mafic-ultramafic inclusions and arc basalts exhibit different degrees of Th-U and Zr-Hf depletion.

The Th/Yb vs Nb/Yb or Ta/Yb diagram (Fig. 3.22) is used to constrain the influence of crustal contamination (Pearce, 1983, 2008), where Yb is used as a normalizing factor to minimize the effects of fractional crystallization and crystal accumulation (Pearce, 1983). Crustal contamination is normally variable, affecting some magma batches more than other magma batches, producing an array trending toward the composition of the crustal contaminant (Pearce, 1983, 2008). However, subduction affects the entire source and enriches Th relative to Nb-Ta (Pearce et al., 2005; Pearce, 2008).

There are three trends – one stronger and two weaker – defined by mafic-ultramafic inclusions and ITSM:

Trend 1 is defined by the majority of the inclusions, particularly the abundant Group I inclusions, and the majority of ITSM samples. They are uniformly enriched in Th relative to Nb-Ta and form a trend subparallel to the mantle array with some samples following along a trajectory to the

upper continental crust, implying a subduction-related origin for the magmas with contamination by upper continental crust that formed the precursors to the inclusions.

Trend 2 is very weak and is defined by Group II inclusions. The trend is shallower than the mantle array. It may be a spurious trend, but all of the inclusions are enriched in Th relative to Nb-Ta, consistent with crystallization from magmas derived from subduction-influenced sources.

Trend 3 is weak and defined by Group III inclusions. It is subparallel to Trend 2 with higher Ta/Yb and Th/Yb ratios. It may also be a spurious trend, but is also consistent with crystallization from magmas derived from subduction-influenced sources.

A trend similar to Trend 2 and 3 with variable Nb/Yb or Ta/Yb over a narrower range of Th/Yb can be generated by constant subduction component added to a variable mantle source (Pearce et al., 1995). Because the subduction component will have a greater effect on Th/Yb than on Nb/Yb or Ta/Yb, the resulting trend will therefore have a negative slope (Pearce et al., 1995). Thus, Trends 2 and 3 might have formed by addition of subduction component into a variable mantle source.

Ratios of elements with different compatibilities (e.g., Zr/Y, Ta/Yb, Nb/Yb) are indicative of mantle source variations and/or degrees of partial melting (Pearce et al., 2005). Group I and III inclusions have overall higher Zr/Y and Ta/Yb ratios than Group II inclusions, suggesting that they are derived from melts derived from a more fertile source and/or at lower degrees of partial melting compared to that of Group II. The layered mafic-ultramafic rocks in the footwall of Levack-Fraser Mine – the probable source of Group II inclusions – scatter widely but overlap with the majority of the mafic-ultramafic inclusions.

Ketchum et al. (2013) suggested that the SCLM beneath the southern Superior Province during the formation of the Huronian basalts and EBLI at ~2450 Ma and Nipissing Suite intrusions at ~2210 Ma was "likely heterogeneous, potentially consisting of ancient peridotite with a chondrite-like composition, remnants of subducted oceanic lithosphere including sediments, trapped portions of Archean arc magmas that did not ascend to the crust, and peridotite metasomatized by the release of fluids from a subducting slab." It is not clear to us why chondritic mantle would be preserved, given that the core and continental crust had already segregated (Polat and Kerrich, 2001). The widespread Huronian volcanic and intrusive rocks are considered to be derived from the subduction-metasomatized mantle (Jolly, 1987; Jolly et al., 1992; Ketchum et al., 2013), that likely occurred at 2750 – 2690Ma under the Abitibi-Wawa terrane (Bédard and Harris, 2014). Magma generated by melting of these volcanic and intrusive rocks and underlying Neoarchean Superior Province upper-middle crustal rocks would produce the enriched-LILE trace element geochemistry of the rocks, the variably-influenced sources to the trace element, and the Nd and Os isotopic compositions of Group I olivine melanorite inclusions.

3.7.7 Formation Conditions of Mafic-Ultramafic Inclusions and Constraints on their Extraction Depth

The absence of plagioclase compositional data for Group I inclusions precludes P-T calculations, but their petrographic and whole-rock geochemical similarities to ITSM indicate a shallow, cognate origin.

The recrystallized nature and absence of amenable mineral assemblages in Group II inclusions also precludes P-T calculations, but their petrographic and whole-rock geochemical similarities to local country rocks indicates a shallow-crustal depth of incorporation.

The pressures and temperatures of equilibration of several Group III feldspar lherzolite and olivine gabbro have been estimated using the olivine-clinopyroxene-plagioclase (Ol – Cpx – Pl) barometer of Ziberna et al. (2017), which can be applied to gabbroic, pyroxenitic, or peridotitic rocks that contain the appropriate igneous Ol + Cpx + Pl ± Sp (magnetite or Cr/Al-spinel) assemblage. Because igneous spinel is not present in our assemblages, we have conducted the COlP (Cpx - Ol - Pl) calibration using THERMOCALC (Powell and Holland, 1988) version 3.47i. The input data are originally derived from mineral composition determined by WD-XRES (EPMA) and the recalculated formula in terms of cations expressed as atoms per formula unit (apfu) (Table 3.9). Compositional variables in THERMOCALC are written in terms of site fractions, defined as follows:

$$x(cpx) = \frac{x_{Fe}^{M1} + x_{Fe}^{M2}}{x_{Fe}^{M1} + x_{Fe}^{M2} + x_{Mg}^{M1} + x_{Mg}^{M2}} = \frac{Fe^{2+}}{Fe^{2+} + Mg} \quad [7]$$

$$y(cpx) = 2x_{Al}^{T} = 2 - Si \quad [8]$$

$$f(cpx) = x_{Fe^{3+}}^{M1} = Fe^{3+} \quad [9]$$

$$z(cpx) = x_{Ca}^{M2} = Ca \quad [10]$$

$$j(cpx) = x_{Na}^{M2} = Na \quad [11]$$

$$x(ol) = \frac{x_{Fe}^{M1} + x_{Fe}^{M2}}{x_{Fe}^{M1} + x_{Fe}^{M2} + x_{Mg}^{M1} + x_{Mg}^{M2}} = \frac{Fe}{Fe + Mg} \quad [12]$$

$$ca(pl) = \frac{Ca}{Ca + Na + K} \quad [13]$$

$$k(pl) = \frac{K}{Ca + Na + K} \quad [14]$$

Because there is negligible effect of P_o (initial estimate of pressure), but a significant effect of T_o (initial estimate of temperature) on the calculated pressure (P), we ran the calculation every 10°C over a range of 700 – 1300°C and selected the T_o that produced the lowest standard deviation of fit (σ_{fit}). All average P calculations (Table 3.10) pass the χ^2 test ($\sigma_{fit} < 1.73$), except for sample 4920B ($\sigma_{fit} = 1.9$), and show low uncertainties (± 110 – 180 MPa). The calculations suggest that feldspar lherzolite and olivine gabbro in the Trill embayment equilibrated at 1050 – 1120^{o}C and 210 ± 166 MPa and 240 ± 109 MPa, which is equivalent to depths between 7.7 ± 6.0 and 8.7 ± 4.0 km, assuming a geobarometric gradient of 27.5 MPa/km and that one feldspar lherzolite in the Levack equilibrated at 900^{o}C and 300 ± 178 MPa, which is equivalent to a depth of 10.9 ± 6.5 km (Wang et al., 2018) (Fig. 3.23).

The inferred relatively low temperatures but high pressures of the inclusions may be related to a low liquidus temperature of the hydrous magma required to stabilize igneous phlogopite and amphibole. However, they may also reflect different cooling rates (e.g., Coogan et al., 2007): inclusions with lower calculated equilibration temperatures may have been derived from bodies intruded into deeper and hotter crust that cooled more slowly, resulting in lower closure temperatures, whereas inclusions with higher calculated equilibration temperatures may have been derived from bodies intruded into shallower and colder crust that cooled more rapidly, resulting in higher closure temperatures.

The relatively low pressures and shallow equilibration depth (7.7 – 10.9 km) of all inclusions are consistent with the absence of garnet or Al-spinel and the widespread presence of plagioclase in the inclusions, indicating a depth <30 km (Green and Hibberson, 1970). Given that the continental crust in the Sudbury region is widely accepted to be thin (37 – 38 km: Winardhi and Mereu, 1997; Mungall et al., 2004), the calculated depths for all inclusions correspond to upper –

middle crust. Given the overwhelming upper crustal signature in the impact melt (e.g., Faggart et al., 1985; Walker et al., 1991; Dickin et al., 1992, 1996, 1999; Lightfoot et al., 1997c; Prevec et al., 2000; Morgan et al., 2002; Lightfoot, 2016), this implies an intermediate (upper – middle crustal) (Wang et al., 2018), not very shallow (< 12 km; Darling et al., 2010) or very deep (> 40 km; e.g., Mungall et al., 2004; Petrus et al., 2016) excavation depth.

3.8 Implications for the Genesis of the Sublayer and IQD

The origin of Sublayer is discussed in more detail in Wang et al. (Ch 4), but the data in this study provide important constraints:

1) The presence of clinopyroxene-rich assemblages in North Range inclusions and their absence in South Ranges inclusions could reflect i) heterogeneities preserved from the initial impact and/or ii) heterogeneities produced by post-impact thermomechanical erosion. The S and Pb isotopic compositions of the ores vary significantly, which has been attributed to volatilization of S and Pb followed by thermomechanical erosion of footwall rocks (McNamara et al., 2017; Lesher, 2019). The Hf isotopic compositions of the Main Mass and offset dikes are much more homogeneous than the country rocks (Kenny et al., 2017), indicating that the impact melt was originally well mixed. This mixing should have removed any initial heterogeneities in inclusion populations, indicating a more significant role for post-impact thermomechanical erosion than previously suspected.

2) Group I olivine melanorites and Mafic Norite occur only on the North Range (thus far Group I inclusions have been identified only at Whistle and at Onaping Depth and Dowling in the Levack embyament, whereas Mafic Norite is present in most embayments on the North Range). This may indicate that i) the mafic component that was incorporated to generate them

was present only on the North Range, ii) the impact melt on the North Range was hotter and able to incorporate more mafic material than on the South Range, and/or iii) that the mafic component that was incorporated on the South Range was more completely assimilated. The Main Mass is up to 2x thicker on the South Range (Souch et al. 1969; Naldrett et al., 1984; Naldrett, 2004; Lightfoot, 2016), the two-pyroxene contact metamorphic zone is 10x wider on the South Range (Jørgensen, 2017; Jørgensen et al., 2019) than on the North Range (Dressler, 1984; Boast and Spray, 2006), and the amount of mafic material (Huronian metabasalt, EBLI, and Nipissing) is much greater on the South Range, so the degree of post-impact thermomechanical erosion of mafic rocks should have been significantly greater and the greater thickness would have facilitated greater degrees of assimilation. In contrast, the thinner Main Mass on the North Range would have had a lower capacity for thermomechanical erosion and assimilation, leading to the crystallization of a marginal layer as the impact melt had its liquidus raised by assimilation of less abundant but more mafic footwall rocks.

3) Group I anteliths, ITSM, and Mafic Norite contain abundant cumulus orthopyroxene and plagioclase, whereas QD and IQD contain only rapidly-crystallized non-cumulate orthopyroxene and plagioclase. This can be most likely attributed to QD and IQD being injected into the offset dikes where they crystallized more rapidly, whereas Group I inclusions, ITSM, and Mafic Norite formed at the base of the Main Mass, so crystallized much more slowly and in communication with a much larger mass of magma that was able to continually provide cumulus components and incorporate non-cumulus components.

4) Group II local inclusions and Group III exotic inclusions have only been identified on the North Range (Levack embayment and Foy offset, and Trill, Levack, and Bowell embayments,

respectively). Equivalent inclusions are likely also present on the South Range, but their shock textures would have been annealed by the much longer cooling time of the overlying much thicker Main Mass, as it conducted heat through the Sublayer into the footwall rocks. Finding a way to recognized Group III exotic inclusions on the South Range will be especially important to confirm that the impact melt sheet was well mixed.

5) All of the inclusions appear to exhibit subduction signatures, which is consistent with them having formed from materials that can reasonably be expected to be present in the crustal section at the time of impact. There is no evidence that they came directly from subcontinental lithospheric (cratonic) mantle or asthenospheric mantle, supporting the interpretation that the impact excavated upper-middle crust and did not reach the mantle. Ubide et al. (2017) suggested that green shards in the Onaping Formation require that the impact create pathways to tap a MORB-like reservoir at greater depths, but there is no evidence for this volcanism as dikes anywhere else in the system. On the other hand, the depletion of LREE>HREE that characterizes the green shards (Ubide et al., 2017) is similar to the higher-grade parts of the contact metamorphic aureole in the underlying Elsie Mountain Formation, which has lost HILE-Zr-Hf relative to Nb-Ta-MILE (Jørgensen, 2017; Jørgensen et al, 2019). The rate of conduction of heat from the superheated impact melt into the footwall rocks would have been much slower than the rate of thermomechanical erosion, but as the impact melt approached the liquidus the rate of erosion would have decreased and melts of devolatilized Huronian basalts may have formed and escaped along the crater margins to form the observed green shards. This possibility requires further testing.

3.9 Conclusions

Mafic-ultramafic inclusions are derived from multiple origins on the basis of significantly various lithologies, textures, and distinctive geochemical characteristics.

Anteliths comprise Group I olivine melanorite and olivine melagabbronorite inclusions. They show great similarities in the geochemical characteristics to ITSM, and are believed to crystallize from the impact melt with a contribution from a more mafic melt, which was probably derived by melting the widespread Huronian volcanic and subvolcanic in the region.

Local xenoliths comprise Group IIA wehrlite – olivine clinopyroxenite inclusions and Group IIB olivine melanorite inclusions. They are characterized by shock metamorphic features (e.g., shock mosaicism in olivine, planar deformation features in orthopyroxene) and strong thermal recrystallization (e.g., clinopyroxene and plagioclase). They occur in restricted locations (Group IIA in Levack embayment and Group IIB in Foy Offset) and show geochemical similarities to an exposed layered mafic-ultramafic intrusion in the footwall at Levack and Fraser deposits.

Exotic xenoliths comprise Group III phlogopite/feldspar lherzolite, orthopyroxenite, and olivine gabbro inclusions. They are interpreted as exotic fragments of one or more layered mafic-ultramafic intrusions that could be derived from continental arc basalt magma formed by up to 5% partial melting of garnet peridotite, equilibrated at 7.7 – 10.9 km depth, excavated during impact, and incorporated into the SIC.

Mafic-ultramafic inclusions and ITSM exhibit both unambiguous arc and upper continental crust signatures. The widespread Huronian volcanic and subvolcanic rocks are considered to be derived from the subduction-metasomatized mantle that likely occurred at 2750 – 2690 Ma

beneath the Abitibi-Wawa terrane. Melting of these volcanic and subvolcanic rocks and other upper continental material should have produced magma that shows consistent geochemical characteristics in the Main Mass rocks and the majority of inclusions, i.e., enriched-LILE trace element geochemistry of the rocks, the variably Ni-rich and Mn-poor olivines in Group I inclusions, and the significant contributions of subduction-influenced sources to Th/Yb vs Nb(Ta)/Yb, and the Nd and Os isotopic compositions of Group I olivine melanorite inclusions. Calculated low pressures (< 500 MPa) using Ol-Cpx-Pl geobarometer indicate derivations from multiple pre-existing mafic-ultramafic intrusions at the depth of upper-middle crustal area (7.7 – 10.9 km), and thus an intermediate excavation depth.

Acknowledgements

Vale Canada Ltd. provided access to drill core samples and their thin section library. We thank Andrew McDonald, William Zhe, Joseph Petrus, Matthew Leybourne, David Crabtree, and Sandra Clarke for assistance with the analytical work, and Luca Ziberna for helpful discussions of the application of the Ol-Cpx-Pl geobarometer. This research was supported by a Natural Sciences and Engineering Research Council (NSERC) of Canada Discovery grant (203171-2012) to CML, a China Scholarship Council (CSC) award to YW, and support from the Canada First Research Excellence Fund. Metal Earth contribution MERC-ME-2019.

References Cited

Barnes, S.J. and Naldrett, A.J., 1985. Geochemistry of the J-M (Howland) Reef of the Stillwater Complex, Minneapolis Adit Area. I. Sulfide chemistry and sulfide-olivine euilibrium. Economic Geology, v. 80, p. 627 – 645.

Barnes, S.J. and Roeder, P.L., 2001. The range of spinel compositions in terrestrial mafic and ultramafic rocks. Journal of Petrology: v. 42, p. 2279 – 2302.

Barnes, S.J., 1998. Chromite in komatiites, 1. Magmatic controls on crystallization and composition. Journal of Petrology, v. 39, p. 1689 – 1720.

Barnes, S.J., Godel, B.G., Gürer, D., Brenan, J.M., Robertson, J., and Paterson, D., 2013. Sulfide-olivine Fe-Ni exchange and the origin of anomalously Ni rich magmatic sulfides. Economic Geology, v. 108, p. 1971 – 1982.

Bédard, J.H. and Harris, L.B., 2014. Neoarchean disaggregation and reassembly of the Superior craton. Geology, v. 42, p. 951 – 954, doi:10.1130/G35770.1

Bédard, J.H., 2005. Partitioning coefficients between olivine and silicate melts. Lithos, v. 83, p. 394 – 419.

Bédard, J.H., 2007. Trace element partitioning coefficients between silicate melts and orthopyroxene: Parameterizations of D variations. Chemical Geology, v.244, p. 263 – 303.

Bleeker, W., Kamo, S.L., Ames, D.E., and Davis, D., 2015. New field observation and U-Pb ages in the Sudbury area: toward a detailed cross-section through the deformed Sudbury Structure, In: Targeted Geoscience Initiative 4: Canadian Nickel-Copper-Platinum Group Elements-Chromium Ore Systems - Fertility, Pathfinders, New and Revised Models, (ed.) D.E. Ames and M.G. Houlé; Geological Survey Of Canada, Open File 7856, p. 151 – 166.

Bleeker, W., Kamo, S.L., and Ames, D.E., 2013. New field observation and U-Pb age data for footwall (target) rocks at Sudbury: Towards a detailed cross-section through the Sudbury Structure. Meteorite Impacts and Planetary Evolution V, abstract, p. 3112.

Boast, M., and Spray, J.G., 2006. Superimposition of a thrust-transfer fault system on a large impact structure: Implications for Ni-Cu-PGE exploration at Sudbury. Economic Geology, v. 101, p.1583 – 1593.

Boctor, N.Z., 1982. The effect of fO_2, fS_2 and temperature on Ni partitioning between olivine and iron sulfide melt. Annual Report of the Director, Geophysical Laboratory, Carnegie Institute, Washington, v. 81, p. 366 – 369.

Bowen, N.L., 1922. The reaction principle in petrogenesis. Journal of Geology, v. 30, p. 177 – 198.

Brenan, J.M. and Caciagli, N.C., 2000. Fe-Ni exchange between olivine and sulfide liquid: Implications for oxygen barometry in sulfide-saturated magmas. Geochimica et Cosmochimica Acta, 64, p. 307 – 320.

Brenan, J., 2003. Effects of fO2, fS2, temperature, and melt composition on Fe-Ni exchange between olivine and sulfide liquid: Implications for natural olivine-sulfide assemblages. Geochimica et Cosmochimica Acta, v. 67, p. 2663 – 2681.

Burnham, O.M., 2008. Trace element analysis of geological samples by inductively coupled plasma mass spectrometry (ICP-MS) at the Geoscience Laboratories: Revised capabilities due to metod improvements. In Summary of Field Work and Other Activities, Ontario Geological Survey, Open File Report 6226, p. 38-1 to 38-10.

Burnham, O.M., Hechler, J.H., Semenyna, L., and Schweyer, J., 2002. Mineralogical controls on the determination of trace elements following mixed acid dissolution. In Summary of Field Work and Other Activities, Ontario Geological Survey, Open File Report 6100, p. 36-1 to 36-12.

Card, K.D. and Pattison, E.F., 1973. Nipissing diabase of the Southern Province, Ontario, p. 7 - 30 in Huronian Stratigraphy and Sedimentation, edited by G.M. Young, Geological Association of Canada. Special Paper Number 12.

Chakraborty, S., 2010. Diffusion coefficients in olivine, wadsleyite and ringwoodite. Reviews in Mineralogy and Geochemistry, v. 72, p. 603 – 639.

Clark, T. and Naldrett, A.J., 1972. The distribution of Fe and Ni between synthetic olivine and sulfide at 900°C. Economic Geology, v. 67, p. 939 – 952.

Coats, C.J. and Snajdr, P., 1984. Chapter 14 Ore deposits of the North Range, Onaping-Levack area, Sudbury. In The Geology and Ore Deposits of the Sudbury Structure. In E.G. Pye, A.J. Naldrett, and P.E. Giblin (eds), Ontario Geological Survey, Special Volume 1. 603pp.

Cohen, L., Burnham, O.M., Hawkesworth, C.J., and Lightfoot, P.C., 2000. Pre-emplacement Re-Os ages from ultramafic inclusions in the sublayer of the Sudbury Igneous Complex, Ontario. Chemical Geology, v. 165, p.37 – 46.

Conrod, D.M., 1989. The petrology and geochemistry of the Duncan Lake, Beaton Bay, Milner Lake, and Miller Lake Nipissing Intrusions within the Gowganda Area, District of Timiskaming. Ontario Geological Survey, Open File Report 5701, 210pp.

Coogan, L.A., Jenkin, C.R.T., and Wilson, R.N., 2007. Contrasting cooling rates in the lower oceanic crust at fast- and slow-spreading ridges revealed by geospeedometry. Journal of Petrology, v. 48, p. 2211 – 2231.

Corfu, F., and Andrews, A.J., 1986. A U-Pb age for mineralized Nipissing diabase. Gowganda, Ontario. Candian Journal of Earth Science, v.27, p. 107 – 109.

Corfu, F., and Lightfoot, P.C., 1996. U-Pb geochronology of the Sublayer environment, Sudbury Igneous Complex, Ontario: Economic Geology, v. 91, p. 1263 – 1269.

Crabtree, D.C., 2011. Analysis of garnets by electron probe micro-analyzer: optimizing analytical conditions to meet the needs of the diamond exploration community; in Summary of Field Work and Other Activities 2011, Ontario Geological Survey, Open File Report 6270, p. 35-1 to 35-5.

Darling, J.R., Hawkesworth, C.J., Storey, C.D., and Lightfoot, P.C., 2010. Shallow impact: Isotopic insights into crustal contributions to the Sudbury impact melt sheet. Geochimica et Cosmochimica Acta, v. 74, p. 5680 – 5696.

David, K., Schiano, P., and Allègre, C.J., 2000. Assessment of the Zr/Hf fractionation in oceanic basalts and continental materials during petrogenic processes. Earth and Planetary Science Letters, v. 178, p. 285 – 301.

Dawson, J.B., 1984. Contrasting types of upper mantle metasomatism? In Kornprobst, J. Ed, Kimberlites II: The mantle and crust-mantle relations. Developments in petrology, v. 11b, Elsevier, Amsterdam, p. 277 – 287.

Dickin, A.P., Artan, M.A., and Crocket, J.H., 1996. Isotopic evidence for distinct crustal sources of North and South Range ores, Sudbury Igneous Complex. Geochimica et Cosmochimica Acta, v. 60, p. 1605 – 1613.

Dickin, A.P., Nguyen, T. and Croket, J.H., 1999. Isotopic evidence for a single impact melting origin of the Sudbury Igneous Complex. In Dressler, B.O., and Sharpton, V.L., eds, Large Meteorite Impacts and Planetary Evolution II: Boulder, Colorado, Geological Society of America, Special Paper 339.

Dickin, A.P., Richardson, J.M., Crocket, J.H., McNutt, R.H., and Peredery, W.V., 1992. Osmium isotope evidence for a crustal origin of platinum group elements in the Sudbury nickel ore. Geochimica et Cosmochimica Acta, v. 56, p. 3531 – 3537.

Dietz, R.S., 1964. Sudbury structure as an astrobleme. Journal of Geology, v. 72, p. 412 – 434.

Dressler, B.O., 1984. General geology of the Sudbury area. In Pye, E.G. et al. (eds) The Geology and Ore Deposits of the Sudbury Structure. Ontario Geological Survey, Special Volume 1, p. 57 – 82.

Easton, R.M. and Hrominchuk, J.L., 1999. Geology and copper-platinum group element mineral potential of Dana and Crerar Township, River Valley area, Grenville Province. In Summary of Field Work and Other Activities 1999. Ontario Geological Survey, Open File Report 6000, p. 30-1 to 30-36.

Ernst, W.G. and Liu, J., 1998. Experimental phase-equilibrium study of Al- and Ti-contents of calcic amphibole in MORB-A semiquantitative thermobarometer. American Mineralogist, v. 83, p. 952 – 969.

Fábio, R.D. de A., Möller, P., Dulski, P., 2002. Zr-Hf in carbonatites and alkaline rocks: New data and a re-evaluation. Revista Brasileira de Geociencias, v. 32, p. 361 – 370.

Faggart, B.E., Basu, A.R. and Tatsumoto, M., 1985. Origin of the Sudbury Complex by meteoritic impact: Neodymium isotopic evidence. Science, New Series, v. 230, p. 436 – 439.

Farrell, K., 1997. Mafic to ultramafic inclusions in the Sublayer of the Sudbury Igneous Complex at Whistle Mine, Sudbury, Ontario, Canada. Master thesis, Laurentian University, Sudbury, Ontario.

Farrow, C.E.G. and Lightfoot, P.C., 2002. Sudbury PGE revisited: Toward and integrated model. In: Cabri, L.J. (Ed.), The Geology, Geochemistry, Mineralogy and Mineral Beneficiation of Platinum-Group Elements; Canadian Institute of Mining, Metallurgy and Petroleum, Special Volume 54, p. 273 – 297.

Fleet, M.E. and MacRae, N.D., 1983. Partition of Ni between olivine and sulfide and its application to Ni-Cu sulfide deposits. Contributions to Mineralogy and Petrology, v. 83, p. 75 – 81.

Fleet, M.E. and MacRae, N.D., 1987. Partition of Ni between olivine and sulfide: The effect of temperature, fO2 and fS2. Contributions to Mineralogy and Petrology, v. 95, p. 336 – 342.

Fleet, M.E., and Bernett, R.L., 1978. AlIV/AlVI partitioning in calciferous amphiboles from the Frood mine, Sudbury, Ontario. Canadian Mineralogist, v. 16, p. 527 – 532.

Fleet, M.E., MacRae, N.D., and Osborne, M.D., 1981. The partition of nickel between olivine, magma and immiscible sulfide liquid. Chemical Geology, v. 32, p. 119 – 127.

Franz, L. and Romer, R.L., 2010. Different styles of metasomatic veining in ultramafic xenoliths from the TUBAF Seamount (Bismarck Microplate, Papua New Guinea). Lithos, v. 114, p. 30 – 53.

Franz, L. and Wirth, R., 2000. Spinel inclusions in olivine of peridotite xenoliths from TUBAF seamount (Bismarck Archipelago/Papua New Guinea): evidence for the thermal and tectonic evolution of the oceanic lithosphere. Contributions to Mineralogy and Petrology, v. 140, p. 283 – 295.

Gaetani, G.A., Grove, T.L., Wilfred, B., 1994. Experimental phase relations of basaltic andesite from Hole 839B under hydrous and anhydrous conditions. In: Hawkins, J., Parson, L.,

Allan, J., et al. (eds), Proceedings of the Ocean Drilling Program, Scientific Results, College Station, TX (Ocean Drilling Program), v.135, p. 557 – 563.

Godel, B., Barnes, S.-J., and Maier, W.D., 2011. Parental magma composition inferred from trace elements in cumulus and intercumulus silicate minerals: An example from the Lower and Lower Critical Zones of the Bushveld Complex, South-Africa. Lithos, v. 125, p. 537 – 552.

Green, D.H., and Hibberson, W. 1970. The instability of plagioclase in peridotite at high pressure: Lithos, v. 3, p. 209 – 221.

Green, T.H., 1994. Experimental studies of trace-element partitioning applicable to igneous petrogenesis-Sedona 16 years later. Chemical Geology, v. 117, p. 1 – 36.

Grieve, R.A., 1991. The Sudbury Structure: Controversial or Misunderstood? Journal of Geophysical Research, v. 96, p. 22753 – 22764.

Griffin, W.L., Shee, S.R., Ryan, C.G., Win, T.T., Wyatt, B.A., 1999. Harzburgite to lherzolite and back again: metasomatic processes in ultramafic xenoliths from the Wesselton kimberlite, Kimberley, South Africa. Contributions to Mineralogy and Petrology, v. 134, p. 232 – 250.

Hanbury, P.M., 1982. A petrographic and petrochemical comparison of exotic gabbroic inclusions of the Sudbury Sublayer and Nipissing Diabase-Sudbury Gabbro. MSc thesis, Washinton State University.

Hawley, J.E., 1962. The Sudbury ores, their mineralogy and origin; Part 3, Interpretations: The history and origin of the Sudbury ores. The Canadian Mineralogist, v. 7(1): p. 146 – 207.

Herzberg, C. and O'Hara, M.J., 2002. Plume-associated ultramafic magmas of Phanerozoic age, Journal of Petrology: v. 43, p. 1857 – 1883.

Herzberg, C., Vidito, C., Starkey, N.A., 2016. Nickel-cobalt contents of olivine record origins of mantle peridotite and related rocks. American Mineralogist, v. 101, p. 1952 – 1966.

Herzberg, C., 2011. Identification of source lithology in the Hawaiian and Canary Islands: Implications for origins. Journal of Petrology, v. 52, p. 113 – 146.

Hewins, R.H., 1971. The petrology and some marginal mafic rocks along the North Range of the Sudbury Irruptive. PhD Thesis, University of Toronto.

Hirschmann, M., Kogiso, T., and Pertermann, M., 2006. Petrologic considerations of pyroxenite heterogeneities in basalt source regions, paper presented at Fifth GERM Workshop, Lamont-Doherty Earth Obs., The Earth Inst. at Columbia University, New York.

Hofmann, A.W. and Feigenson, M.D., 1983. Case studies on the origin of basalt: O. Theory and reassessment of Grenada basalts. Contributions to Mineralogy and Petrology, v. 84, p. 382 – 389.

Ionov, D.A., and Hofmann, A.W., 1995. Nb-Ta-rich mantle amphiboles and micas: Implications for subduction-related metasomatic trace element fractionations. Earth and Planetary Science Letter, v. 131, p. 341 – 356.

Irvine, T.N., 1967. Chromian spinel as a petrogenetic indicator. Part 2. Petrologic implications. Ibid, v. 4, p. 71 – 103.

Ivanov, B.A. and Deutsch, A., 1999. Sudbury impact event: Cratering mechanics and thermal history, in Dressler, B.O. and Sharpton, V.L., eds., Large Meteorite and Planetary Evolution II: Boulder, Colorado, Geological Society of America, Special Paper 339, p. 389 – 397.

Jambor, J.L., 1971. The Nipissing Diabase. The Canadian Mineralogist, v. 11, p. 34 – 75.

James, R.S., Easton, R.M., Peck, D.C., Hrominchuk, J.L., 2002. The East Bull Lake Intrusive Suite: Remnants of a ~ 2.48 Ga large igneous and metallogenic province in the Sudbury area of the Canadian shield. Economic Geology, v. 97, p. 1577 – 1606.

Jochum, K.P., Seufert, H.M., Spettel, B., and Palme, H., 1986. The solar-system abundances of Nb, Ta, and Y, and the relative abundances of refractory lithophile elements in differentiated planetary bodies. Geochimica et Cosmochimica Acta, v. 50, p. 1173 – 1183.

Jolly, W.T., 1987. Geology and geochemistry of Huronian rhyolites and low-Ti continental tholeiites from the Thessalon region, central Ontario. Canadian Journal of Earth Science, v. 24, p. 1360 – 1385.

Jolly, W.T., Dickin, A.P., and Wu, T.-W., 1992. Geochemical stratigraphy of the Huronian continental volcanics at Thessalon, Ontario: contributions of two-stage crustal fusion. Contributions to Mineralogy and Petrolgy, v. 110, p. 411 – 428.

Jørgensen, T.R., 2017. Evolution of the Sudbury Igneous Complex southern metamorphic aureole and controls on anatexis. PhD thesis, Laurentian University, Sudbury, Canada, 327pp.

Jørgensen, T.R., Tinkham, D.K., Lesher, C.M., 2019. Low-P and high-T metamorphism of basalts: Insights from the Sudbury impact melt sheet aureole and thermodynamic modelling. Journal of metamorphic geology, v. 37, p. 271 – 313.

Jørgensen, T.R., Tinkham, D.K., Lesher, C.M., and Petrus, J.A., 2018. Decoupling of Zr-Hf during contact metamorphic anatexis of metabasalts and timing of zircon growth, Sudbury, Canada. Geology, v. 46, p. 159 – 162.

Keating, G.L. and Burnham, O.M., 2012. Revision of the calibration for major element analysis of geological samples by wavelength dispersive X-Ray fluorescence at the Geoscience

Laboratories. Summary of Field Work and Other Activies, Ontario Geological Survey, Open Report 6280, p. 39-1 to 39-4.

Keays, R.R. and Lightfoot, P.C., 2004. Formation of Ni-Cu-Platinum Group Element sulfide mineralization in the Sudbury Impact Melt Sheet. Mineralogy and Petrology, v. 82, p. 217 – 258.

Kelemen, P.B. and Hart, S.R., 1996. Silica enrichment in the continental lithosphere via melt/rock reaction, V.M. Goldschmidt Conference Abstract, v.1, p. 308.

Kenny, Gavin G., Petrus, Joseph A., Whitehouse, Martin J., Daly, J. Stephen, Kamber, Balz S., 2017. Hf isotope evidence for effective impact melt homogenisation at the Sudbury impact crater, Ontario, Canada. Geochimica et Cosmochimica Acta, v. 215, p. 317 – 336.

Ketchum, K.Y., Heaman, L.M., Bennett, G., and Hughes, D.J., 2013. Age, petrogenesis and tectonic setting of the Thessalon volcanic rocks, Huronian Supergroup, Canada. Precambrian Research, v. 233, p. 144 – 172.

Krogh, T.E., Davis, D.W., and Corfu, F., 1984. Precise U-Pb xircon and baddeleyite ages for the Sudbury area, in Pye, E.G., Naldrett, A.J., and Giblin, P.E., The Geology and Ore Deposits of the Sudbury Structure, Ontario Geological Survey Special Volume 1, p. 431 – 447.

Kuo, H.Y., Crocket, J.H., 1979. Rare earth elements in the Sudbury Nickel Irruptive: comparison with layered gabbro and implications for Nickel Irruptive petrogenesis. Economic Geology, v. 79, p. 590 – 605.

Langmuir, C.H., Klein, E.M., and Plank, T., 1992. Petrological systematics of mid-ocean ridge basalts: Constraints on melt generation beneath ocean ridges, In J.P. Morgan, D.K.

Blackman, and J.M. Sinton (eds), Mantle Flow and Melt Generation at Mid-Ocean Ridges, Geophys. Monogr. Ser., v. 71, p. 183 – 280, AGU, Washington, D.C.

Leeman, W.P. and Lindstrom, D.J., 1978. Partitioning of Ni^{2+} between basaltic and synthetic melts and olivines – an experimental study. Geochimica et Cosmochimica Acta, v. 42, p. 801 – 816.

Lesher CM, Golightly JP, Pattison EF, Lightfoot PC, Strongman K, Walker J, Baird S, 2016, Two melts in the Sudbury Igneous Complex, 35th International Geological Congress, 27 Aug – 04 Sept, Capetown, South Africa, Extended Abstract Volume.

Li, C. and Naldrett, A.J., 1999. Geology and petrology of the Viosey's Bay intrusion: reaction of olivine with sulfide and silicate liquids. Lithos, v. 47, p. 1 – 31.

Li, C. and Ripley, E.M., 2010. The relative effects of composition and temperature on olivine-liquid Ni partitioning: Statistical deconvolution and implications for petrologic modelling. Chemical Geology, v. 275, p. 99 – 104.

Lightfoot, P.C. and Naldrett, A. J., 1996. Petrology and geochemistry of the Nipissing Gabbro: Exploration strategies for nickel, copper, and platinum group elements in a large igneous province. Ontario Geological Survey Study 58, 87pp.

Lightfoot, P.C., 2016. Nickel sulfide ores and impact melts: Origin of the Sudbury Igneous Complex: Amsterdam, Netherlands, Elsevier.

Lightfoot, P.C., de Souza, H., and Doherty, W., 1993. Differentiation and source of the Nipissing Diabase intrusion, Ontario, Canada. Canadian Journal of Earth Science, v. 30, p. 1123 – 1140.

Lightfoot, P.C., Doherty, W., Farrell, K., Keays, R.R., Moore, M., and Pekeski, D., 1997a. Geochemistry of the main mass, sublayer, offsets, and inclusions from the Sudbury Igneous Complex, Ontario; Ontario Geological Survey, Open File Report, 5959, 231pp.

Lightfoot, P.C., Keays, R.R., Morrison, G.G., Bite, A., and Farrell, K.P., 1997b. Geologic and geochemical relationships between the contact sublayer, inclusions, and the main mass of the Sudbury Igneous Complex: A case study of the Whistle Mine Embayment: Economic Geology and the Bulletin of the Society of Economic Geologists, v. 92, p. 647 – 673, https:// doi.org /10 .2113/gsecongeo .92 .6 .647.

Lightfoot, P.C., Keays, R.R., Morrison, G.G., Bite, A., and Farrell, K.P., 1997c. Geochemical relationships in the Sudbury Igneous Complex: Origin of the Main Mass and Offset dikes. Economic Geology, v. 92, p. 289 – 307.

Liu Y.S., Gao S., Lee C.-T., Hu S.H., Liu X.M., Yuan H.L., 2005. Melt-peridotite interactions: Links between garnet pyroxenite and high-Mg# signature of continental crust, Earth and Planetary Science Letters, v. 234, p. 39 – 57.

Longerich, H.P., Jackson, S.E., and Günther, D., 1996. Laser ablation inductively coupled plasma mass spectrometric transient signal data acquisition and analyte concentration calculation. Journal of Analytical Atomic Spectrometry, v. 11, p. 899 – 904.

MacInnis, L., 2016. Constraining alteration in the Footwall of the Sudbury Igneous Complex: A case study of the alteration footprint to the Podolsky Cu-(Ni)-PGE deposit, Sudbury. Master Thesis, Laurentian University.

Marques, J.C., Filho, C.F.F., Carlson, R.W., and Pimentel, M.M., 2003. Re-Os and Sm-Nd isotope and trace element constraints on the origin of the chromite deposit of the Ipueira-Medrado Sill, Bahia, Brazil. Journal of Petrology, v. 44, p. 659 – 678.

Matzen, A.K., Baker, M.B., Beckett, J.R., and Stopler, E.M., 2013. The temperature and pressure dependence of nickel partitioning between olivine and silicate melt. Journal of Petrology, v. 54, p. 2521 – 2545.

Matzen, A.K., Baker, M.B., Beckett, J.R., Wood, B.J., and Stopler, E.M., 2017. The effect of liquid composition on the partitioning of Ni between olivine and silicate melt. Contributions to Mineralogy and Petrology, v. 172, p. 1 – 18.

McDonough, W.F., Sun, S.-S., Ringwood, A.E., Jagoutz, E.J., and Hofmann, A.W., 1992. Potassium, rubidium, and cesium in the Earth and Moon and the evolution of the mantle of the Earth. Geochimica et Cosmochimica Acta, v. 56, p. 1001 – 1012.

McNamara, G.S., Lesher, C.M., and Kamber, B.S., 2017. New feldspar lead isotope and trace element evidence from the Sudbury Igneous Complex indicate a complex origin of associated Ni-Cu-PGE mineralization involving underlying country rocks. Economic Geology, v. 112, p. 569 – 590.

Moore, M., Lightfoot, P.C., Keays, R.R, 1993. Project Unit 93-08, Geology and geochemistry of footwall ultramafic rocks, Sudbury Igneous Complex, Fraser Mine, Sudbury, Ontario. In: Baker, C.L., Dressler, B.O., De Souza, H.A.F., Fenwick, K.G., Newsome, J.W., Owsiacki, L. (Eds), Summary of field work and other activities 1993. Ontario Geological Survey Miscellaneous Paper 162, p. 85 – 86.

Moore, M., Lightfoot, P.C., Keays, R.R, 1994. Geology and geochemistry of footwall ultramafic rocks, Fraser mine and Levack West mine, Sudbury Igneous Complex, Sudbury, Ontario. In: Summary of Field Work and Other Activities, Ontario Geological Survey, Miscellaneous Paper 163, p. 91 – 94.

Moore, M., Lightfoot, P.C., Keays, R.R, 1995. Geology and geochemistry of footwall ultramafic rocks, Sudbury Igneous Complex, Sudbury, Ontario. In: Summary of Field Work, Other Activities, Ontario Geological Survey, Miscellaneous Paper 164, p. 122 – 123.

Morgan, J.W., Walker, R.J., Horan, M., Beary, E.S., and Naldrett, A.J., 2002. 190Pt-186Os and 187Re-187Os systematics of the Sudbury Igneous Complex, Ontario. Geochimica et Cosmochimica Acta, v. 66, p. 273 – 290.

Morrison, G.G., Jago, B.C., Little, T.L., 1994. Footwall mineralization of the Sudbury Igneous Complex. In: Lightfoot, P.C., Naldrett, A.J. (Eds), Proceedings of the Sudbury-Noril'sk Symposium, Ontario Geological Survey Volume 5, p. 57 – 64.

Mukwakwami, J., Lafrance, B., Lesher, C.M., 2012. Back-thrusting and overturning of the southern margin of the 1.85 Ga Sudbury Igneous Complex at the Garson mine, Sudbury, Ontario. Precambrian Research, v. 196 – 197, p. 81 – 105.

Mungall, J.M., Ames, D.E., and Hanley, J.J., 2004. Geochemical evidence from the Sudbury structure for crustal redistribution by large bolide impacts. Nature, v. 429, p. 546 – 548.

Münker, C., 1998. Nb/Ta fractionation in a Cambrian arc/back arc system, New Zealand: Source constraints and application of refined ICPMS techniques. Chemical Geology, v. 144, p. 23 – 45.

Mysen, B.O., Kushiro, I., 1979. Pressure dependence of nickel partitioning between forsterite and aluminous silicate melts. Earth Planetary Science Letter, v. 42, p. 383 – 388.

Naldrett, A.J., 2004. Magmatic sulfide deposits: Geology, geochemistry, and exploration. Springer, 727pp.

Naldrett, A.J., and Kullerud, G., 1967. A study of the Strathcona mine and its bearing on the origin of the Nickel-Copper ores of the Sudbury district, Ontario: Journal of Petrology, v. 8, p. 453 – 531.

Naldrett, A.J., Greenman, L., and Hewins, R.H., 1972. The Main Irruptive and the Sublayer at Sudbury, Ontario. International Geological Congress, 24th, Montreal, Proceedings Section 4, p. 206 – 214.

Naldrett, A.J., Hewins, R.H., Dressler, B.O., Rao, B.V., 1984. The Sublayer of the Sudbury Igneous Complex, in Pye, E.G., Naldrett, A.J., and Giblin, P.E., The Geology and Ore Deposits of the Sudbury Structure, Ontario Geological Survey Special Volume 1, p. 253 – 274.

Nielson-Pike, J.E. and Noller, J.S., 1987. Processes of mantle metasomatism: Evidence from xenoliths and peridotite massifs, in Morris, E.M. and Pasteris, J.D., Eds, Mantle metasomatism and alkaline volcanism, Geological Society of America, Special Paper, 215, p. 62 – 78.

Noble, S.R., and Lightfoot, P.C., 1992. U-Pb baddeleyite ages of the Kerns and Triangle Mountain intrusions, Nipissing Diabase, Ontario. Candian Journal of Earth Science, v. 29, p. 1424 – 1429.

Ormerod, D.S., Rogers, N.W., and Hawkesworth, C.J., 1991. Melting in the lithospheric mantle. Inverse modelling of alkali olivine basalt from the Big Pine volcanic field, California. Contributions to Mineralogy and Petrology, v. 108, p. 305 – 317.

Paton, C., Hellstrom, J., Paul, B., Woodhead, J., and Hergt, J., 2011. Iolite: Freeware for the visualization and processing of mass spectrometric data. Journal of Analytical Atomic Spectroscopy, v. 26, p. 2508 – 2518.

Pattison, E.F., 1979, The Sudbury Sublayer: Canadian Mineralogist, v. 17, p. 257 – 274.

Pearce, J.A, 1982. Trace Element Characteristics of Lavas from Destructive Plate Boundaries. Orogenic Andesites, p. 525 – 548.

Pearce, J.A. and Norry, M.J., 1979. Petrogenetic implications of Ti, Zr, Y, and Yb variations in volcanic rocks. Contributions to Mineralogy and Petrology, v. 69, p. 33 – 47.

Pearce, J.A., 1983. Role of the subcontinental lithosphere in magma genesis at active continental margins. In: Hawkesworth, C.J. and Norry, M.J. eds., Continental basalts and mantle xenoliths. Shiva, Nantwich, p. 230 – 249.

Pearce, J.A., 2008. Geochemical fingerprinting of oceanic basalts with applications to ophiolite classification and the search for Archean oceanic crust. Lithos, v. 10, p. 14 – 48.

Pearce, J.A., Baker, P.E., Harvey, P.K., and Luff, I.W., 1995. Geochemical evidence for subduction fluxes, mantle melting and fractional crystallization beneath the South Sandwich island arc. Journal of Petrology, v. 36, p. 1073 – 1109.

Pearce, J.A., Stern, R.J., Bloomer, S.H., Fryer, P., 2005. Geochemical mapping of the Mariana arc-basin system: Implications for the nature and distribution of subduction components. Geochemistry Geophysics Geosystems, v. 6, p. 1 – 27.

Peck, D.C., James, R.S., Chubb, P.T., Prevec, S.A., and Keays, R.R., 1995. Geology, metallogeny and petrogenesis of the East Bull Lake Intrusion, Ontario. Ontario Geological Survey, Open File Report 5923, 149pp.

Perfit, M.R., Gust, D.A., Bence, A.E., Arculus, R.J., and Taylor, S.R., 1980. Chemical characteristics of island-arc basalts: Implications for mantle sources. Chemical Geology, v. 30, No. 3, p. 227 – 256.

Petrus, J.A., Kenny, G.G., Ayer, J.A., Lightfoot, P.C., and Kamber, B.S., 2016. Uranium-lead zircon systematics in the Sudbury impact crater-fill: implications for target lithologies and crater evolution. Journal of the Geological Society, v. 173, p. 59 – 75.

Petry, C., Chakraborty, S., and Palme, H., 2004. Experimental determination of Ni diffusion coefficients in olivine and their dependence on temperature, composition, oxygen fugacity, and crystallographic orientation. Geochimica et Cosmochimica Acta, v. 68, p. 4179 – 4188.

Pichavant, M. and Macdonald, R., 2007. Crystallization of primitive badaltic magmas at crustal pressures and genesis of the calc-alkaline igneous suite: experimental evidence from St Vincent, Lesser Antilles arc. Contributions to Mineralogy and Petrology, Springer Verlag, v. 154, p. 535 – 558.

Polat, A., and Kerrich, R., 2001. Geodynamic processes, continental growth, and mantle evolution recorded in late Archean greenstone belts of the southern Superior Province, Canada. Precambrian Research, v. 112, p. 5 – 25.

Porrera, C., Selverstone, J., and Samuels, K., 2006. Pyroxenite xenoliths from the Rio Puerco volcanic field, New Mexico: Melt metasomatism at the margin of the Rio Grande rift, Geosphere, v. 2, p. 333 – 351, doi:10.1130/GES00058.1.

Powell, R., and Holland, T.J.B., 1988. An internally consistent thermodynamic dataset with uncertainties and correlations: 3: application mothods, worked examples and a computer program. Journal of Metamorphic Geology, v. 6, p. 173 – 204.

Prevec, S., Lightfoot, P.C., and Keays, R.R., 2000. Evolution of the sublayer of the Sudbury Igneous Complex: Geochemical, Sm-Nd isotopic and petrologic evidence. Lithos, v. 51, p. 271 – 292.

Prevec, S.A. and Baadsgaard, H., 2005. Evolution of Paleoproterozoic mafic intrusions located within the thermal aureole of the Sudbury Igneous Complex, Canada: Isotopic, geochronological and geochemical evidence. Geochimica et Cosmochimica Acta, v. 69, p. 3653 – 3669.

Prevec, S.A. and Cawthorn, R.G., 2002. Thermal evolution and interaction between impact melt sheet and footwall: A genetic model for the contact sublayer of the Sudbury Igneous Complex, Canada. Journal of Geophysical Research, v. 107, p. 5-1 to 5-14.

Prevec, S.A., 1993. An isotopic, geochemical and petrographic investigation of the genesis of early Proterozoic mafic intrusions and associated volcanism near Sudbury, Ontario. PhD thesis, University of Alberta.

Prevec, S.A., 2000. An examination of modal variation mechanisms in the contact sublayer of the Sudbury Igneous Complex, Canada: Mineralogy and Petrology, v. 68, p. 141 – 157.

Putirka, K., Ryerson, F.J., Perfit, M., Ridley, W.I., 2011. Mineralogy and composition of the oceanic mantle. Journal of Petrology, v. 52, p. 279 – 313.

Raase, P., 1974. Al and Ti contents of hornblende, indicators of pressure and temperature of regional metamorphism. Contributions to Mineralogy and Petrology, v. 45, p. 231 – 236.

Rae, D. R., 1975. Inclusions in the Sublayer from Strathcona Mine, Sudbury, and their significance. Department of Geology, University of Toronto. Degree of Master of Science.

Rollinson, H.R., 1993. Using geochemical data: evolution, presentation, interpretation. London (Longman Scientific and Technical), 352pp.

Salters, V.J.M., and Stracke, A., 2004. Composition of the depleted mantle. Geochemistry Geophysics Geosystems, v. 5, p. 1 – 27.

Scowen, P.A.H., Roeder, P.L., and Heltz, R.T., 1991. Reequilibration of chromite within Kilauea Iki lava lake, Hawaii. Contributions to Mineralogy and Petrology, v. 107, p. 8 – 20.

Scribbins, B.T., 1978. Exotic inclusions from the South Range Sublayer, Sudbury. MSc thesis, University of Toronto.

Scribbins, B.T., Rae, D.R., and Naldrett, A.J., 1984. Mafic and ultramafic inclusions in the Sublayer of the Sudbury Igneous Complex. Canadian Mineralogist, v. 22, p. 67 – 75.

Shaw, D.M., 1970. Trace element fractionation during anatexis. Geochimica et Cosmochimica Acta, v. 34, p. 237 – 243.

Sobolev, A.V., Hofmann, A.W., Kuzmin, D., and Yaxley, D., 2006. Recycled crust in the source of mantle-derived melt: How much?, paper presented a Fifth GERM Workshop, Lamont-Doherty Earth Obs., The Earth Inst. at Columbia University, New York.

Sobolev, A.V., Hofmann, A.W., Kuzmin, D.V., et al., 2007. The amount of recycled crust in sources of mantle-derived melts, Science: v. 316, p. 412 – 417.

Sobolev, A.V., Hofmann, A.W., Sobolev, S.V., and Nikogosian, I.K., 2005. An olivine-free mantle source of Hawaiian shield basalts. Nature, v. 434, p. 590 – 597.

Souch, B.E., Podolsky, T., and Geological Staff of Inco Limited, 1969. The Sulfide Ores of Sudbury: Their particular relation to a distinctive inclusion-bearing facies of the Nickel Irruptive; Economic Geology Monograph 4. p. 252 – 261.

Spray, J.G., Butler, H.R., and Thompson, L.M., 2004. Tectonic influences on the morphometry of the Sudbury impact structure: Implications for terrestrial cratering and modelling: Meteoritics & Planetary Science, v. 39, p. 287 – 301.

Stolz, A.J., Jochum, K.P., Spettel, B., and Hofmann, A.W., 1996. Fluid- and melt-related enrichment in the subarc mantle: Evidence from Nb/Ta variations in island-arc basalts. Geology, v. 24, p. 587 – 590.

Straub, S.M., La Gatta, A.B., Pozzo, A.L., and Langmuir, C.H., 2008. Evidence from high-Ni olivines for a hybridized peridotite/pyroxenite source for orogenic andesites from the central Mexican Volcanic Belt, Geochemistry Geophysics Geosystems: v. 9, p. 1 – 33.

Sun, S.-S. and McDonough, W.F., 1989. Chemical and isotopic systematics of oceanic basalts: implications for mantle composition and processes. In Saunders, A.D. and Norry, M.J. (eds), 1989, Magmatism in the ocean basins, Geological Society Special Publication No. 42, p. 313 – 345.

Taylor, S.R., and McLennan, S.M., 1995. The geochemical evolution of the continental crust. Reviews of Geophysics, v. 33, p. 241 – 265.

Thompson, L.C., Mosley-Thompson, E., Grootes, P.M., Pourchet, M. and Hastenrath, S., 1984. Tropical glaciers: Potential for ice core paleoclimatic reconstructions. Journal of Geophysical Research 89: doi: 10.1029/JD089iD03p04638. issn: 0148-0227

Ubide, T., Guyett, P.C., Kenny, G.G., O'Sullivan, E.M., Ames, D.E., Petrus, J.A., Riggs, N., and Kamber, B.S., 2017. Protracted volcanism after large impacts: Evidence from the Sudbury impact basin. Journal of Geophysical Rsearch: Planets, v. 122, p. 701 – 728.

Vogel, D.C., James, R.S., and Keays, R.R., 1998. The early tectono-magmatic evolution of the Southern province: Implications from the Agnew intrusion, central Ontario, Canada: Canadiam Journal of Earth Sciences, v. 35, p. 854 – 870.

Vogel, D.C., Keays, R.R., James, R.S., and Reeves, S.J., 1999. The geochemistry and petrogenesis of the Agnew Intrusion, Canada: A product of S-undersaturated, high-Al and low-Ti tholeiitic magmas. Journal of Petrology, v. 40, p. 423 – 450.

Walker, R.J., Morgan, J.W., Naldrett, A.J., Li, C., and Fassett, J.D., 1991. Re-Os isotope systematics of Ni-Cu sulfide ores, Sudbury Igneous Complex, Ontario: evidence for a major crustal component. Earth and Planetary Science Letters, v. 105, p. 416 – 429.

Walter, M.J., 2003. Melt extraction and compositional variability in mantle lithosphere. In: Holland, H.D., Turekian, K.K. (eds.), Treatise on Geochemistry. The Mantle and Core. Elsevier-Pergamon, Oxford, p. 363 – 394.

Wang, Y., Lesher, C.M., Lightfoot, P.C., Pattison, E.F., and Golightly, J.P., 2018. Shock metamorphic features in mafic and ultramafic inclusions in the Sudbury Igneous Complex: Implications for their origin and impact excavation. Geology, v. 46, p. 443 – 446.

Weisberg, M.K., Connolly, H.C., Ebel, D.S., 2004. Petrology and origin of amoeboid olivine aggregates in CR chondrites, Meteoritics & Planetary Science, v. 39, p. 1741 – 1753.

Willbold, M. and Stracke, A., 2006. Trace element composition of mantle end-members: Implications for recycling of oceanic and upper and lower continental crust. Geochemistry Geophysics Geosystems, v.7. 7. 10.1029/2005GC001005.

Wilson, M., 1989. Review of igneous petrogenesis: A global tectonic approach. Terra Nova, 1: p. 218 – 222. doi:10.1111/j.1365-3121.1989.tb00357.x.

Winardhi, S., and Mereu, R.F., 1997. Crustal velocity structure of the Superior and Grenville provinces of the Southeastern Canadian Shield: Canadian Journal of Earth Science, v. 34, p. 1167 – 1184, doi: 10.1139/e17-094.

Wolff, J.A., 1984. Variation in Nb/Ta during differentiation of phonolitic magma, Tenerife, Canary Islands. Geochimica et Cosmochimica Acta, v. 48, p. 1345 – 1348.

Zhou, M.-F., Lightfoot, P.C., Keays, R.R., Moore, M.L., and Morrison, G.G., 1997. Petrogenetic significance of chromian spinels from the Sudbury Igneous Complex, Ontario, Canada. Canadian Journal of Earth Science, v. 34, p. 1405 – 1419.

Ziberna, L., Green, E.C.R., and Blundy, J., 2017. Multiple-reaction geobarometry for olivine-bearing igneous rocks: American Mineralogist, v. 102, p. 2349 – 2366.

Figure Captions

Figure 3.1 A: Geological map of the Sudbury Igneous Complex, Canada (after Lightfoot, 2016); B: Geological map of Whistle embayment and Whistle Offset dike (after Pattison, 1979)

Figure 3.2 Photomicrographs of petrographic features of ITSM and IQD. A: Ophitic-textured ITSM in the Whistle embayment in cross-polarized light; sample shows abundant plagioclase laths (Pl), and variable orthopyroxene (Opx) and clinopyroxene (Cpx) in ophitic texture; B: ITSM from Whistle embayment in cross-polarized light; sample shows abundant prismatic

cumulus orthopyroxene (Opx); C: QD in the Foy Offset shown in cross-polarized light; sample shows fresh laths of orthopyroxene (Opx) and plagioclase (Pl) in a groundmass of amphibole, quartz, graphic intergrowths of quartz + K-feldspar. D: IQD in the Worthington Offset in plane polarized light; sample shows secondary amphibole (Amph) and primary plagioclase (Pl) with interstitial mica (Mica) and magmatic Fe-Ni-Cu sulfide (Sul).

Figure 3.3 Photomicrographs of petrographic features of mafic and ultramafic inclusions in Sublayer and IQD. **A**: Coarse-grained, and orthocumulate olivine (Ol) coexisting with fine-grained olivine chadacrysts enclosed by interstitial plagioclase (Pl) in feldspar lherzolite inclusion in the Trill Embayment, cross-polarized light. **B**: Adcumulate orthopyroxene (Opx) in orthopyroxenite reaction zone between a feldspar lherzolite inclusion and ITSM in the Trill Embayment, cross-polarized light. **C**: Polygonal clinopyroxene (Cpx) aggregates comprising equigranular recrystallized clinopyroxene neoblast, and fluidal and/or sheared olivine (Ol) aggregates comprising shock mosaic and recrystallized olivine neoblasts in wehrlite inclusion in the Levack embayment, plane-polarized light. **D**: Euhedral olivine (Ol), orthopyroxene (Opx) and clinopyroxene (Cpx) chadacrysts enclosed by interstitial plagioclase (Pl) and phlogopite (Phl) in olivine melagabbronorite inclusion in the Onaping Depth, plane-polarized light. **E:** Trachytic texture in an olivine gabbro inclusion in the Trill Embayment, cross-polarized light. **F**: Sharp contact between layered feldspar lherzolite and olivine gabbro inclusion in the Trill Embayment, cross-polarized light.

Figure 3.4 Plots of olivine compositions in mafic-ultramafic inclusions and comparable mafic-ultramafic country rocks. A: NiO vs forsterite contents (Fo mole%), and B: MnO vs forsterite content (Fo mole%). Light green and beige fields in A with solid lines along their margins indicate peridotite- and pyroxenite-mantle sources that have lost up to 20% melt via sequential

melting (Straub et al., 2008). Black dash and solid lines are olivine fractional crystallization trajectories from peridotitic and pyroxenitic melts, respectively, calculated in 1% increment using the method of Herzberg and O'Hara (2002). The red dash line in (A) shows the mixing line between a derivative peridotitic melt and a pyroxenitic melt. The stars and circles with italic numbers represent the degree of olivine fractionation. The peridotite- and pyroxenite-derived melts in (A), from which olivine crystallized, are from Straub et al. (2008), and the peridotite- and pyroxenite-derived melts in (B) are from Sobolev et al. (2007). Reference data: CMVB: olivines in the Central Mexican volcanic belt crystallized from calc-alkaline basaltic andesites formed by mixing between peridotite- and pyroxenite-melts (Straub et al. 2008); MORB: olivine in mid-ocean ridge basalts that are derived from peridotite melts (Sobolev et al., 2007); WPM-THIN: olivine in within plate magmas emplaced over thin lithosphere that are derived from peridotite melts. WPM-THICK: olivine in within plate magmas emplaced over thick lithosphere that are derived from hybrid magma mixing between pyroxenite melts (amount to approximate 61 ± 16%) and peridotite melts (Sobolev et al., 2007). Lithological abbreviations (thereafter): HZBG – harzburgite; Phl LHZT – phlogopite lherzolite; Fsp LHZT-1 – igneous-textured feldspar lherzolite; OLGA – olivine gabbro; Fsp LHZT-2 – shocked feldspar lherzolite; ORPY – orthopyroxenite; WHTE – wehrlite; OLMN-1 – igneous-textured olivine melanorite; OLMN-2 – shocked olivine melanorite; OLGN – olivine melagabbronorite; OAPY, Levack FW – olivine-bearing amphibole pyroxenite in the footwall of Levack Mine; M-UM, Levack-Fraser FW – mafic-ultramafic intrusion in the footwall of Levack-Fraser Mine; OLMN, EBLI – olivine melanorite in the East Bull Lake intrusive suite.

Figure 3.5 Classification diagram of pyroxenes in the mafic-ultramafic inclusions, ITSM, and comparable mafic-ultramafic country rocks. Lithological abbreviations are in Figure 3.4.

Figure 3.6 Plots of Al_2O_3,CaO, TiO_2, and Cr_2O_3 vs Mg# (molar MgO/(MgO+FeO)) orthopyroxene compositions in mafic-ultramafic inclusions, ITSM, and comparable mafic-ultramafic country rocks. Lithological abbreviations are in Figure 3.4.

Figure 3.7 Plots of clinopyroxene compositions in mafic-ultramafic inclusions, ITSM, and comparable mafic-ultramafic country rocks. A: Al_2O_3 vs Mg#, and B: Cr_2O_3 vs Mg#; Fields of cratonic and non-cratonic peridotites in (A) are from Walter (2003); symbols as in Figure 3.6 and lithological abbreviations are in Figure 3.4.

Figure 3.8 Plots of chromite compositions in mafic-ultramafic inclusions and comparable mafic-ultramafic country rocks. A: Cr3+–Al3+–Fe3+, B: 100*Cr/(Cr+Al) vs 100*Fe2+/(Mg+Fe2+), C: 100*Fe3+/(Cr+Al+Fe3+) vs 100*Fe2+/(Mg+Fe2+), and D: TiO2 vs 100*Fe3+/(Cr+Al+Fe3+); The recrystallized nature and absence of amenable mineral assemblages in Group II inclusions also precludes P-T calculations, but their petrographic and whole-rock geochemical similarities to local country rocks indicates a shallow-crustal depth of incorporation trends and fields after Barnes and Roeder (2001). Lithological abbreviations are in Figure 3.4.

Figure 3.9 Plots of chromite compositions in mafic-ultramafic inclusions in the North and South Ranges. A: Al_2O_3 vs Cr_2O_3, and B: Fe_2O_3 vs Mg#; Fields of arc cumulate chromite and mantle array in (A) after Franz and Wirth (2000). Lithological abbreviations are in Figure 3.4.

Figure 3.10 Plots of amphibole compositions in mafic-ultramafic inclusions and various reference amphiboles in the literature (data sources in text). A: Cr_2O_3 vs Mg#, B: Al_2O_3 vs Mg#, C: Al^{IV} (apfu) vs Al^{VI} (apfu), and D: Ti (apfu) vs Al^{IV} (apfu); Field boundaries in (C) are from Fleet and Bernett (1978). Lithological abbreviations: Gr-MMN – green amphibole in Main Mass

Norite; Br-MMN – brown amphibole in Main Mass norite; MG – amphibole in melagabbro in the country rocks; the other abbreviations as in Figure 3.4.

Figure 3.11 Plots of whole-rock compositions for mafic and ultramafic inclusions, ITSM, and comparable mafic-ultramafic rocks country rocks, together with major cumulus mineral compositions determined by EPM. A: FeO vs MgO, B: CaO vs MgO, C: Al_2O_3 vs MgO, D: Na_2O vs MgO, E: TiO_2 vs MgO, and F: MnO vs MgO; Closed stars are average compositions of cumulus phases in the inclusions (same colours as their group), and solid lines show compositional ranges. Lithological abbreviations are in Figure 3.4.

Figure 3.12 Primitive mantle-normalized trace element patterns for mafic and ultramafic inclusions, ITSM, and comparable mafic-ultramafic rocks country rocks. Normalizing values from McDonough et al. (1992). Lithological abbreviations are in Figure 3.4.

Figure 3.13 Plots of whole-rock compositions for mafic-ultramafic inclusions, ITSM, and comparable mafic-ultramafic country rocks. A: La/Yb_N vs Mg#, and B: Gd/Yb_N vs Mg#; Normalizing values are from Sun and McDonough et al. (1989). Lithological abbreviations are in Figure 3.4.

Figure 3.14 Plots of whole-rock compositions for mafic-ultramafic inclusions, ITSM, and comparable mafic-ultramafic country rocks. A: Zr/Y vs Zr, B: Zr/Nb vs Zr, and C: Nb/U vs Nb; The arrowed line in (A) shows the directions of source enrichment/depletion. The star symbols show the value of C3 chondrite (Pearce and Norry 1979). Field reference in (A): IAB – island arc basalt; MORB – mid-ocean ridge basalt; WPB – within plate basalt

Figure 3.15 Box plots of whole-rock trace element ratios for mafic-ultramafic inclusions, ITSM, and comparable mafic-ultramafic country rocks. A: Zr/Hf and B: Nb/Ta

Figure 3.16 NiO and Fo contents of olivines in mafic-ultramafic inclusions and model olivines crystallizing from primary magmas at the surface. Pink lines are model olivine lines of descent for primary magmas having MgO contents of 20 to 30% derived from a peridotite source (Herzberg, 2011). Black star is olivine composition at the liquidus for near-total melting. Black lines are olivine compositions in equilibrium with accumulated fractional melts using the Beattie-Jones parameterization (Herzberg, 2011). Grey field is measured olivine compositions in Hawaii (Sobolev et al., 2007).

Figure 3.17 NiO contents of olivine and Ni content of sulfide liquid that have underwent equilibrium exchange of Fe-Ni in experiments at controlled temperature, oxygen, and sulfur fugacities. Data sources given in Brenan (2003).

Figure 3.18 Ni Diffusion between olivine and silicate melt and between olivine and sulfide liquid at 1700°C and 1180°C, respectively

Figure 3.19 Plots whole-rock trace element compositions for mafic-ultramafic inclusions and ITSM. A: Zr/Hf vs Sc and B: Zr/Hf vs Zr

Figure 3.20 Primitive mantle-normalized trace element patterns of the calculated parental magma of Group III inclusions. Primitive mantle values from McDonough et al. (1992). Reference data: N-MORB – normal mid-ocean ridge basalt from Sun and McDonough (1989); OIB – ocean island basalt from Sun and McDonough (1989); CAB – continental arc basalts from GEOROC (http://georoc.mpch-mainz.gwdg.de/georoc).

Figure 3.21 Incompatible trace element patterns (normalized to mid-ocean ridge basalt: Sun and McDonough, 1989) of the average composition of all groups of inclusions, various subduction components (shallow/deep) in arc basalts (Pearce et al., 2005), and upper continental crust (Taylor and McLennan, 1995)

Figure 3.22 Plot of Th/Yb vs Ta/Yb of mafic and ultramafic inclusions, ITSM, and comparable mafic-ultramafic rocks country rocks; Mantle array, values of N-MORB (normal MORB) and E-MORB are from Pearce (1983).

Figure 3.23 Calculated P-T diagram of selective mafic-ultramafic inclusions using Ol-Cpx-Pl geobarometer

Table 3.1 Petrographic characteristics of the mafic and ultramafic inclusions in Sublayer and IQD on the North Range

Table 3.2 Summary of compositions of olivine in mafic-ultramafic inclusions and comparable mafic-ultramafic country rocks

Table 3.3 Summary of compositions of orthopyroxene in the mafic-ultramafic inclusions and comparable mafic-ultramafic country rocks

Table 3.4 Summary of compositions of clinopyroxene in the mafic-ultramafic inclusions and comparable mafic-ultramafic country rocks

Table 3.5 Summary of compositions of amphibole in the mafic-ultramafic inclusions and comparable mafic-ultramafic country rocks

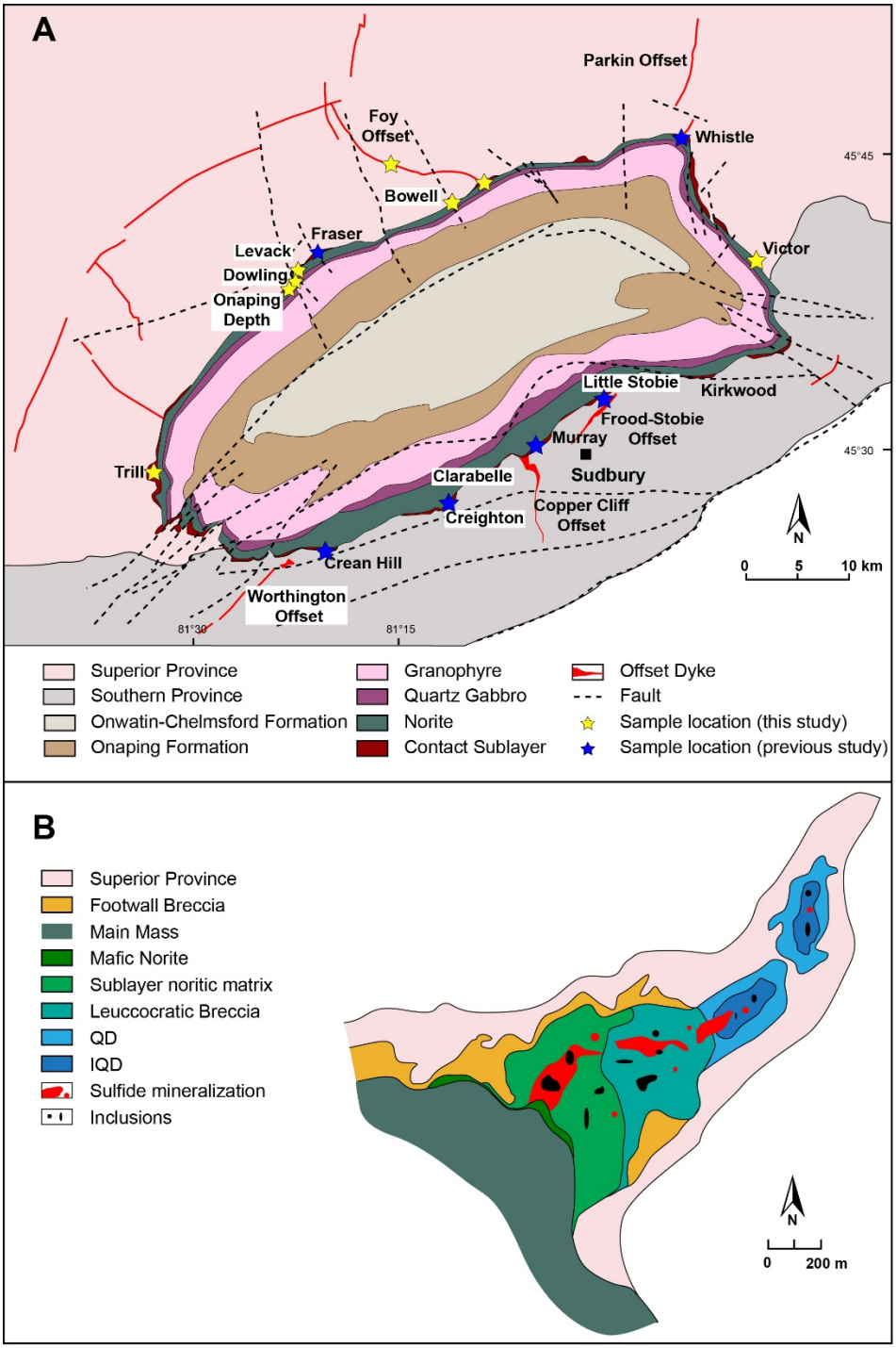

Figure 3.1 A: Geological map of the Sudbury Igneous Complex, Canada (after Lightfoot, 2016); B: Geological map of Whistle embayment and Whistle Offset dike (after Pattison, 1979)

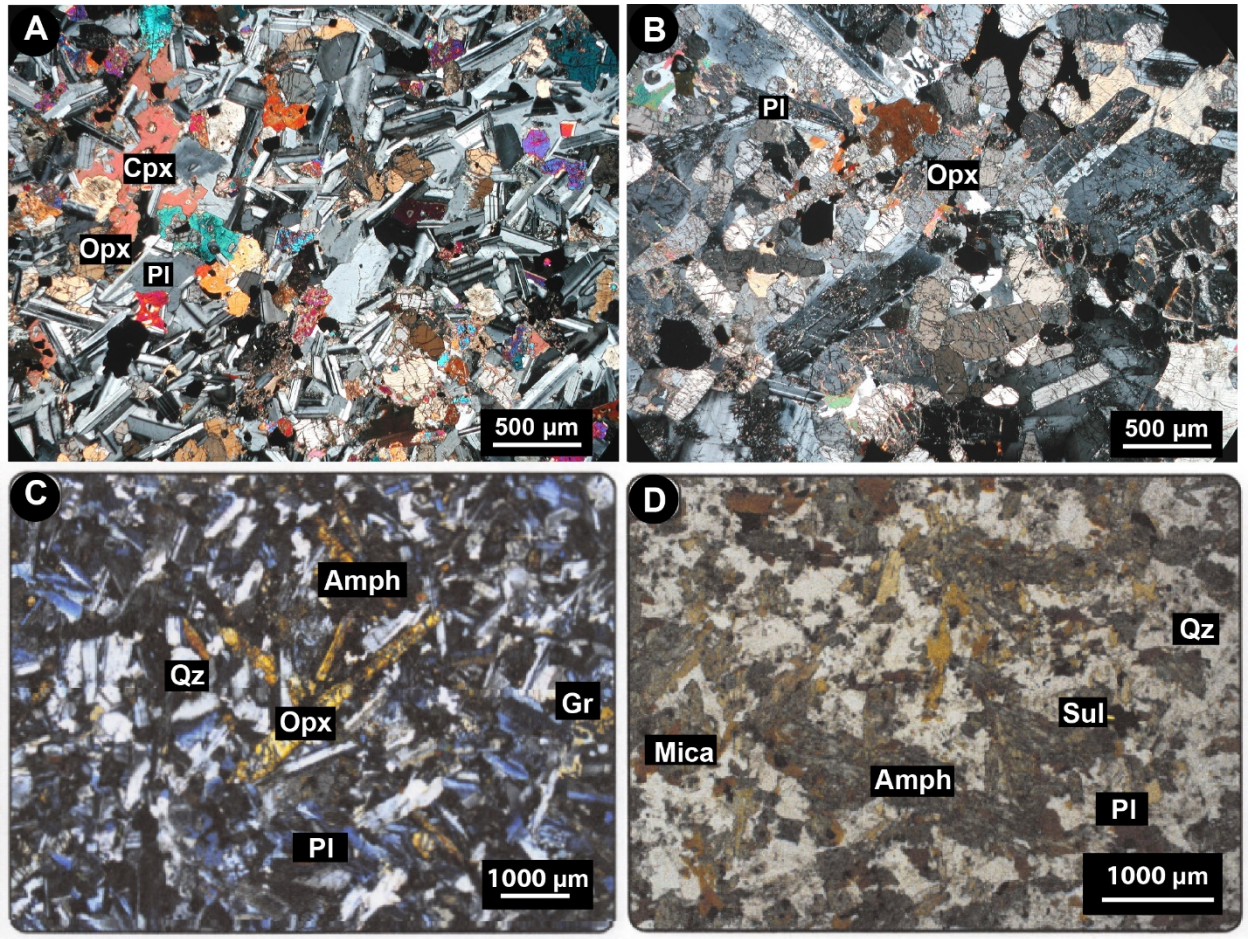

Figure 3.2 Photomicrographs of petrographic features of ITSM and IQD

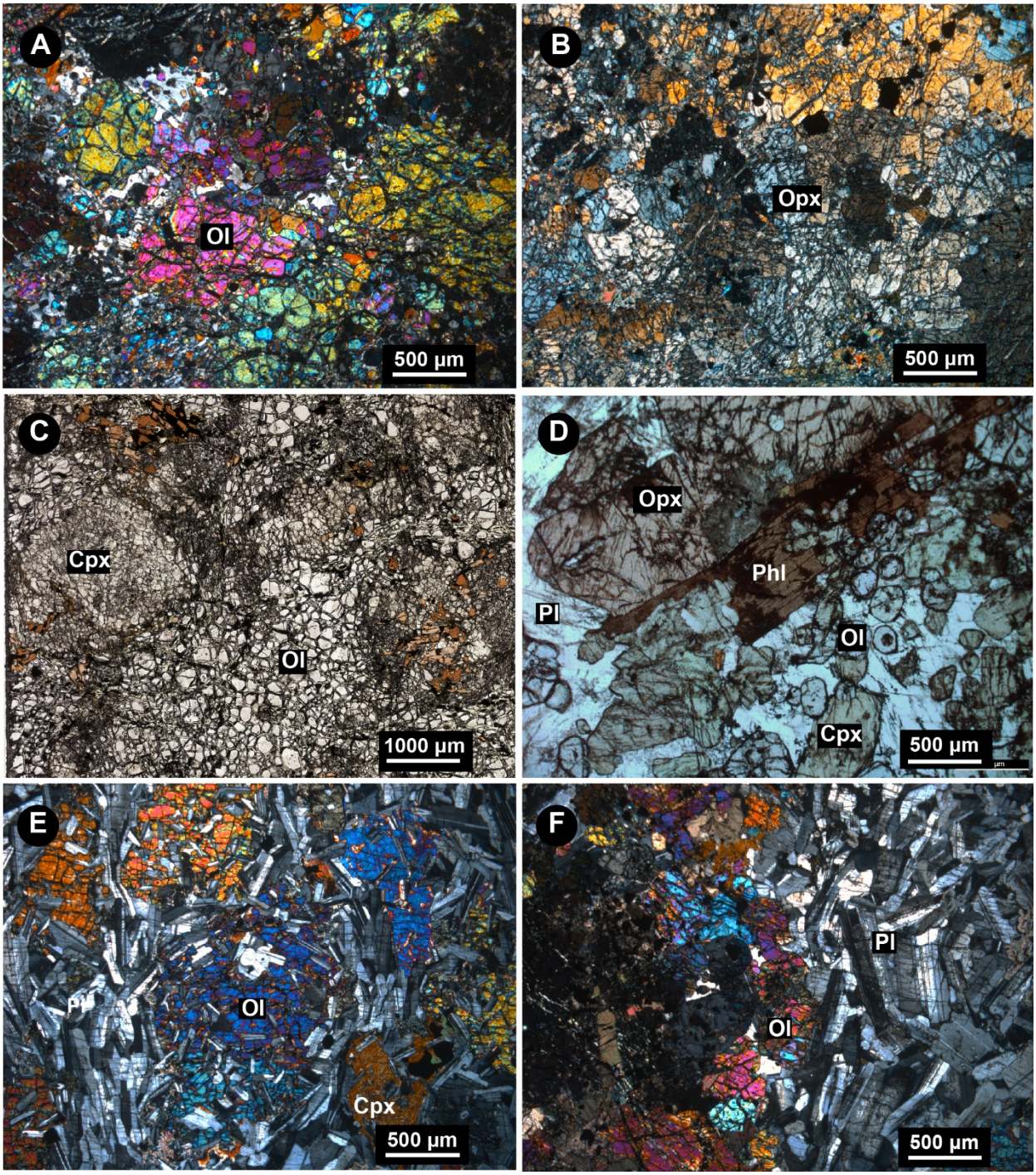

Figure 3.3 Photomicrographs of petrographic features of olivine-bearing mafic and ultramafic inclusions in Sublayer and IQD

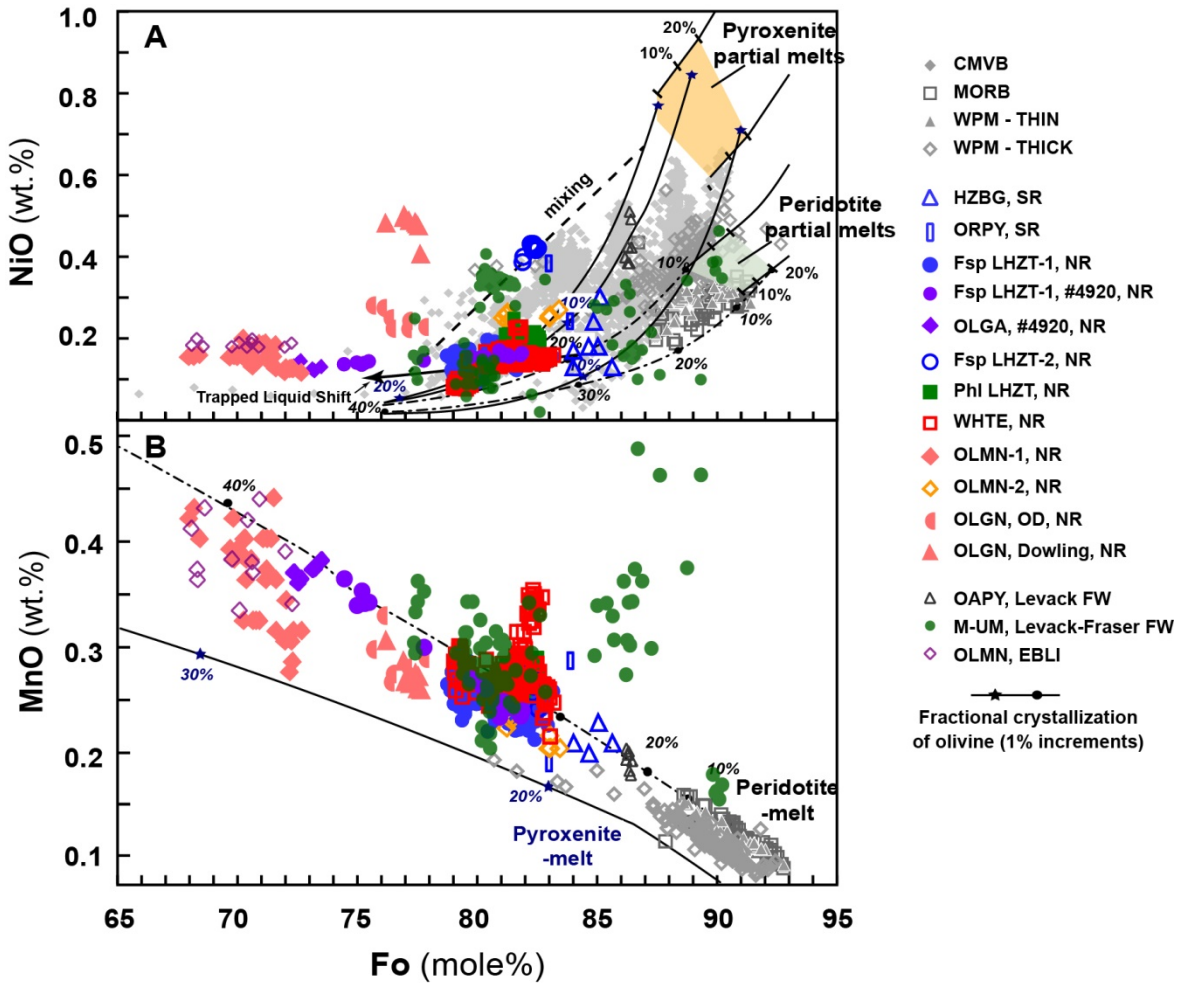

Figure 3.4 Plots of olivine compositions in mafic-ultramafic inclusions and comparable mafic-ultramafic country rocks. A: NiO vs forsterite contents (Fo mole%) and B: MnO vs forsterite content (Fo mole%)

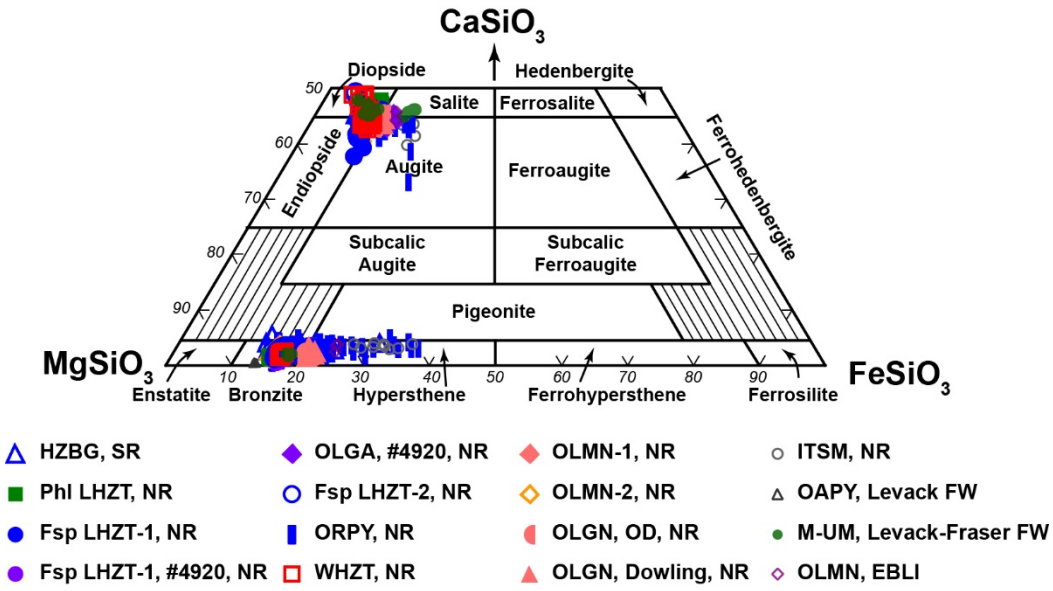

Figure 3.5 Classification diagram of pyroxenes in the mafic-ultramafic inclusions, ITSM, and comparable mafic-ultramafic country rocks

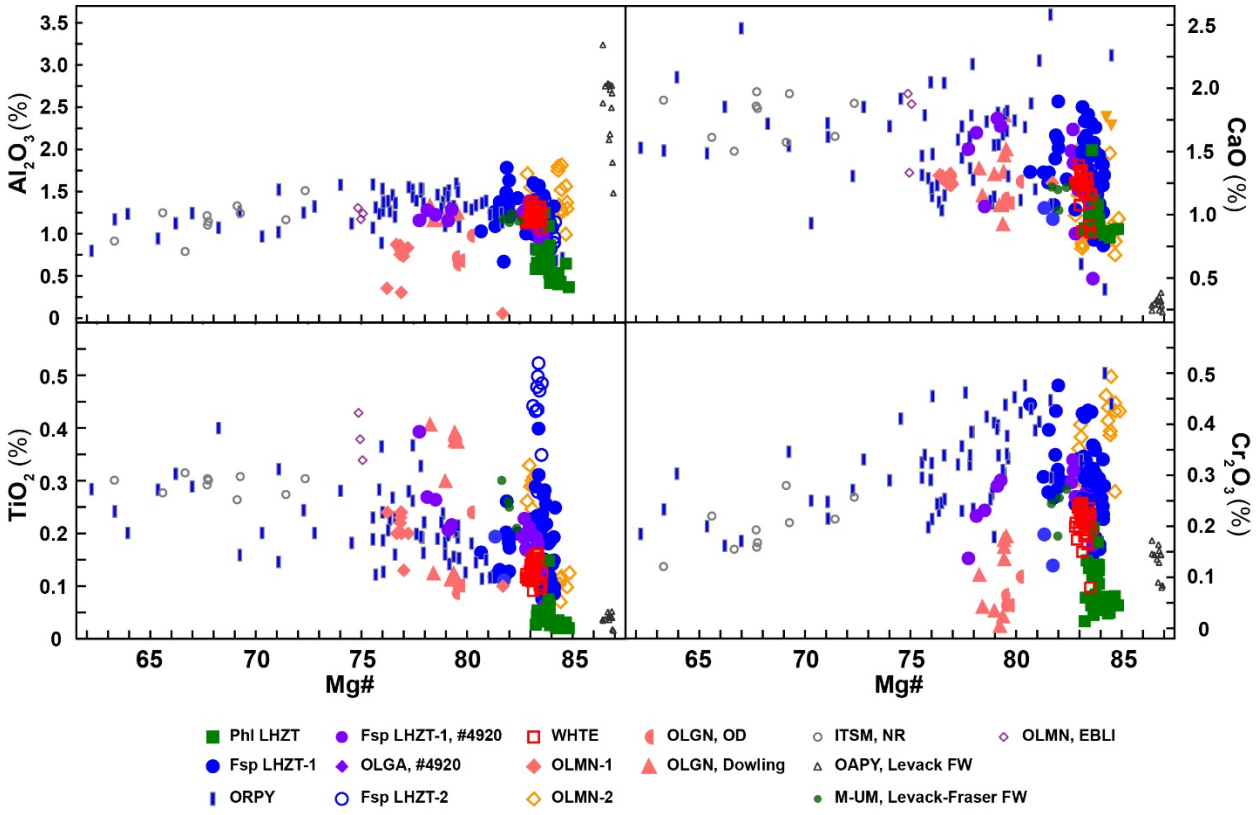

Figure 3.6 Plots of Al_2O_3, CaO, TiO_2, and Cr_2O_3 vs Mg# (molar MgO/(MgO+FeO)) orthopyroxene compositions in mafic-ultramafic inclusions, ITSM, and comparable mafic-ultramafic country rocks

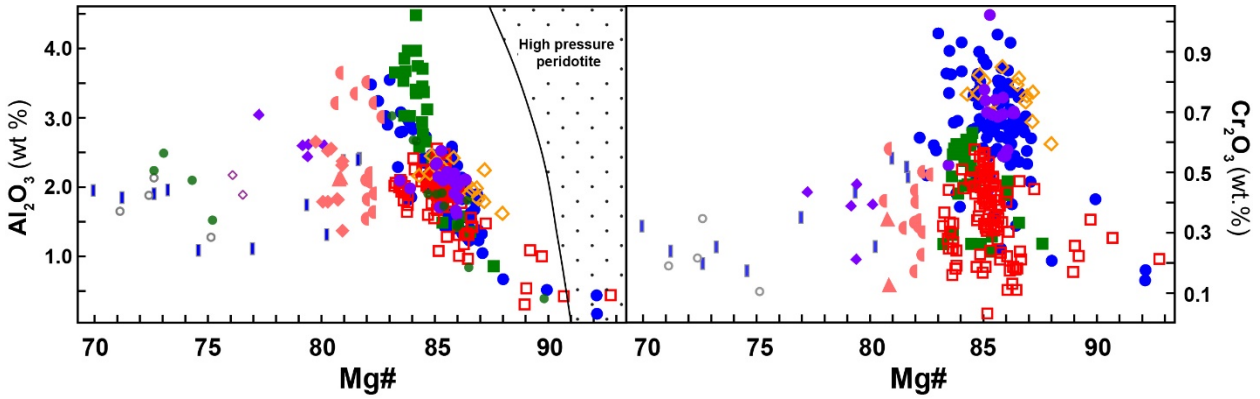

Figure 3.7 Plots of clinopyroxene compositions in mafic-ultramafic inclusions, ITSM, and comparable mafic-ultramafic country rocks. A: Al_2O_3 vs Mg#, and B: Cr_2O_3 vs Mg#

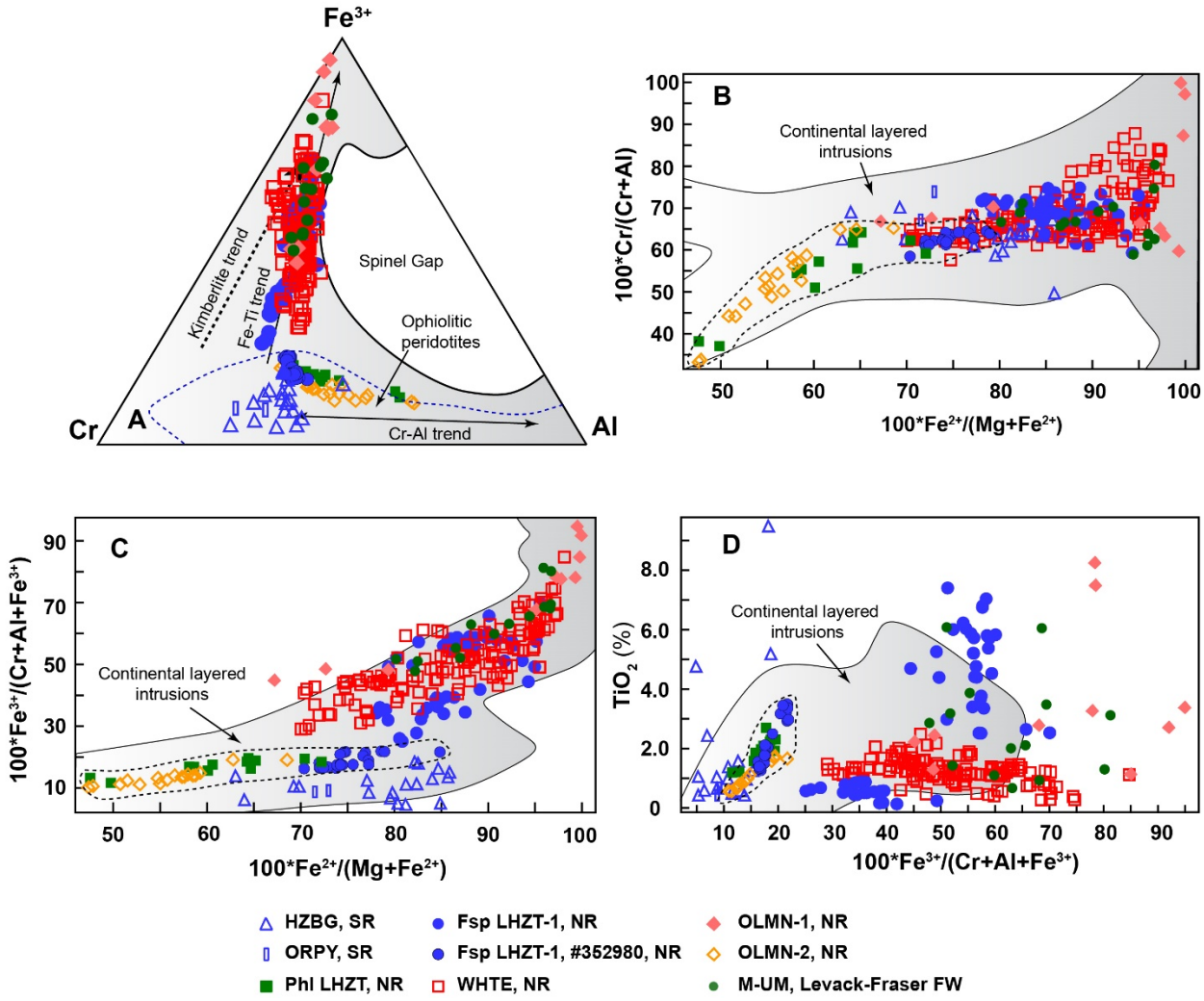

Figure 3.8 Plots of chromite compositions in mafic-ultramafic inclusions and comparable mafic-ultramafic country rocks. A: Cr^{3+}–Al^{3+}–Fe^{3+}, B: 100*Cr/(Cr+Al) vs 100*Fe^{2+}/(Mg+Fe^{2+}), C: 100*Fe^{3+}/(Cr+Al+Fe^{3+}) vs 100*Fe^{2+}/(Mg+Fe^{2+}), and D: TiO_2 vs 100*Fe^{3+}/(Cr+Al+Fe^{3+})

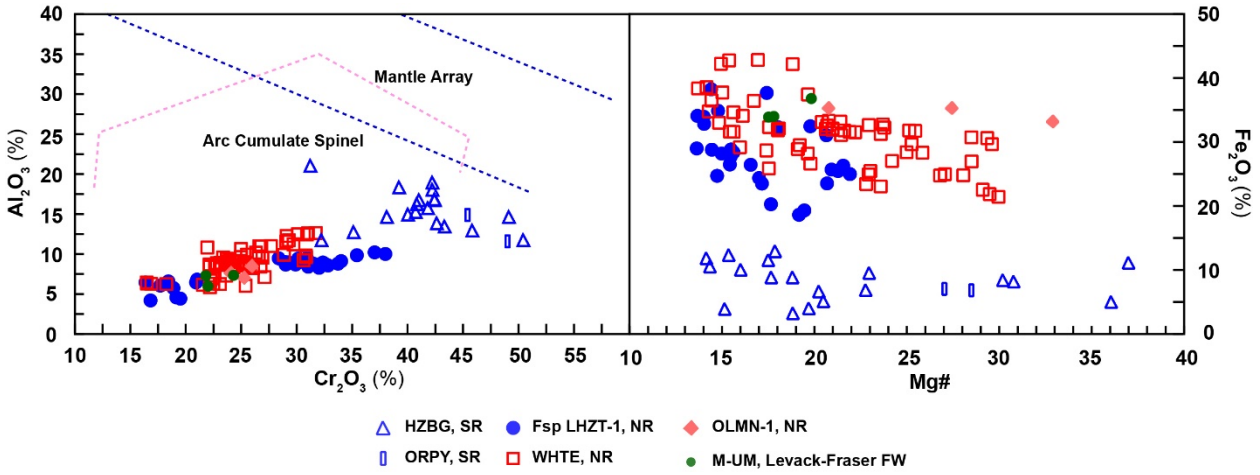

Figure 3.9 Plots of chromite compositions in mafic-ultramafic inclusions in the North and South Ranges. A: Al_2O_3 vs Cr_2O_3, and B: Fe_2O_3 vs Mg#

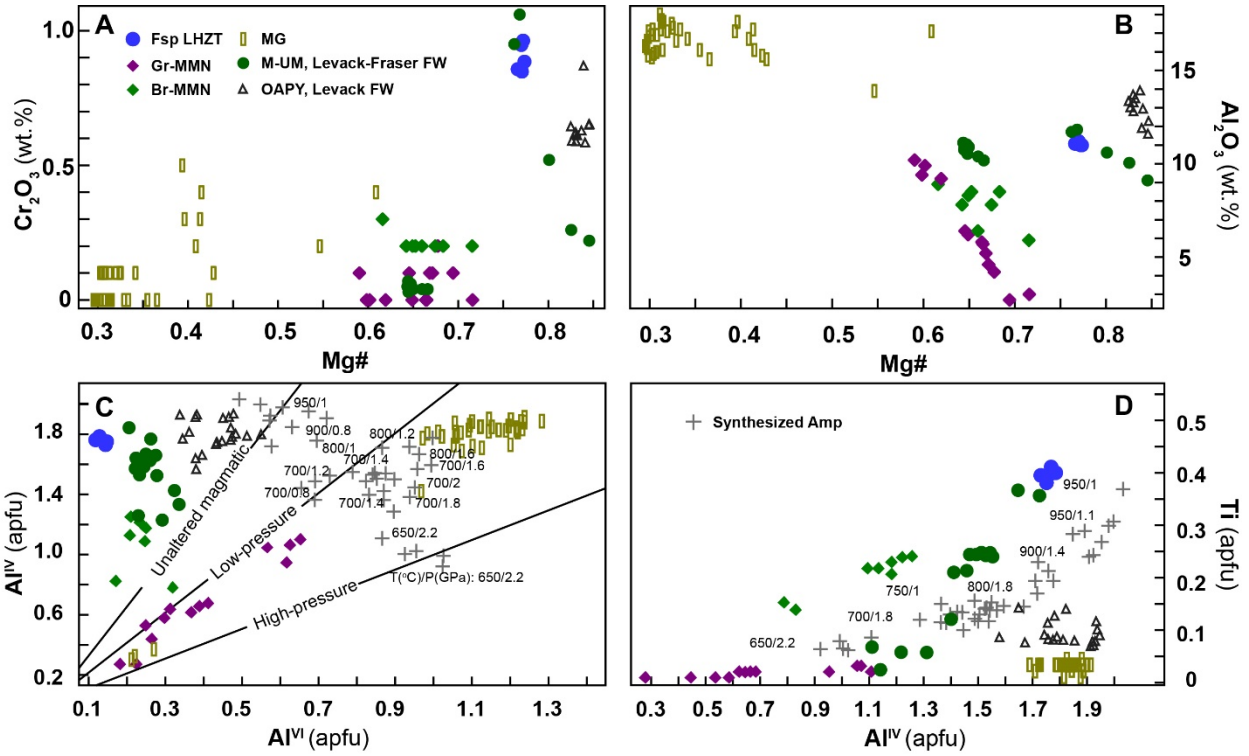

Figure 3.10 Plots of amphibole compositions in mafic-ultramafic inclusions and various reference amphiboles in the literature (data sources in text). A: Cr_2O_3 vs Mg#, B: Al_2O_3 vs Mg#, C: Al^{IV} (apfu) vs Al^{VI} (apfu), and D: Ti (apfu) vs Al^{IV} (apfu)

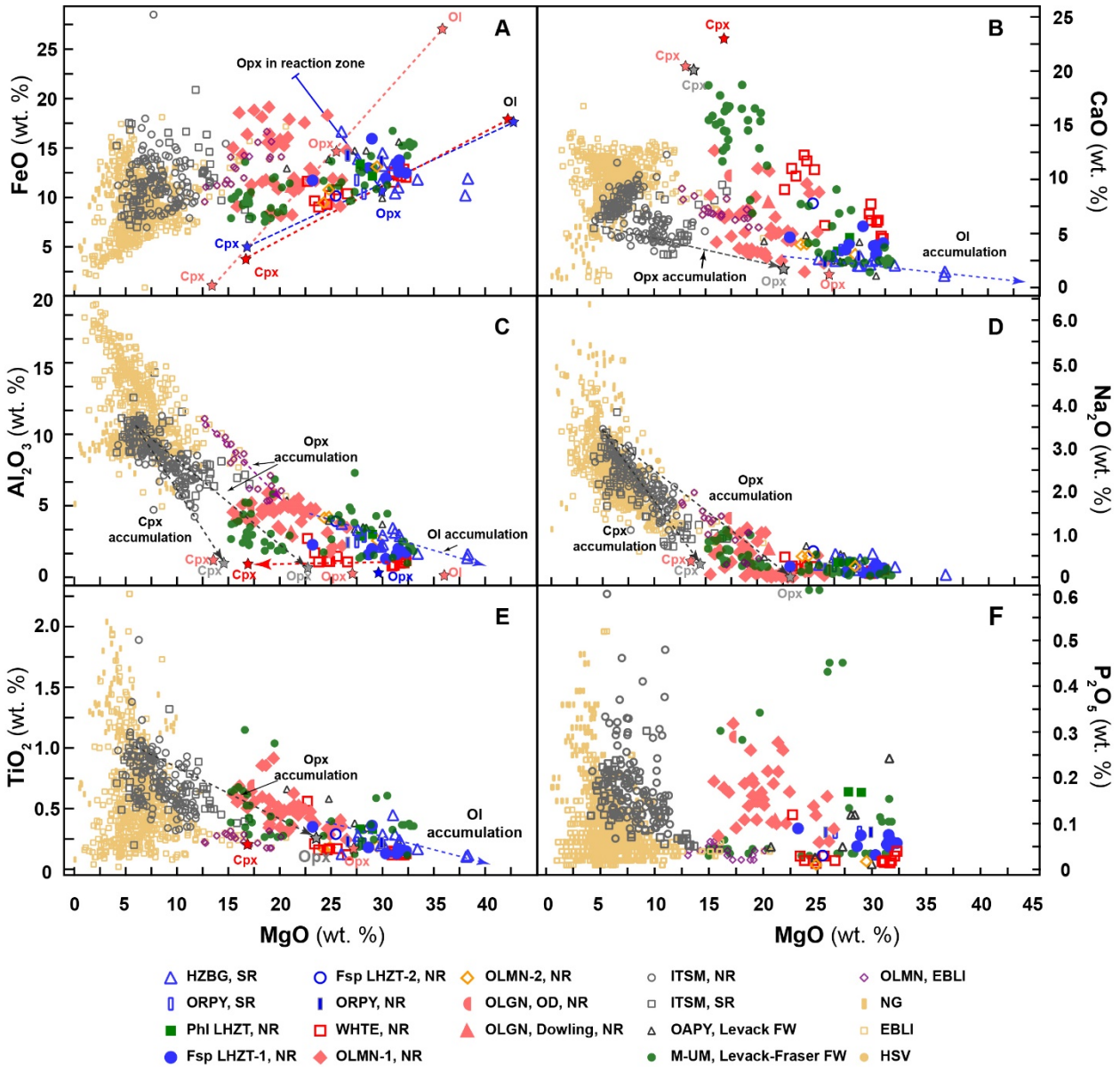

Figure 3.11 Plots of whole-rock compositions for mafic and ultramafic inclusions, ITSM, and comparable mafic-ultramafic rocks country rocks, together with major cumulus mineral compositions determined by EPM. A: FeO vs MgO, B: CaO vs MgO, C: Al_2O_3 vs MgO, D: Na_2O vs MgO, E: TiO_2 vs MgO, and F: MnO vs MgO

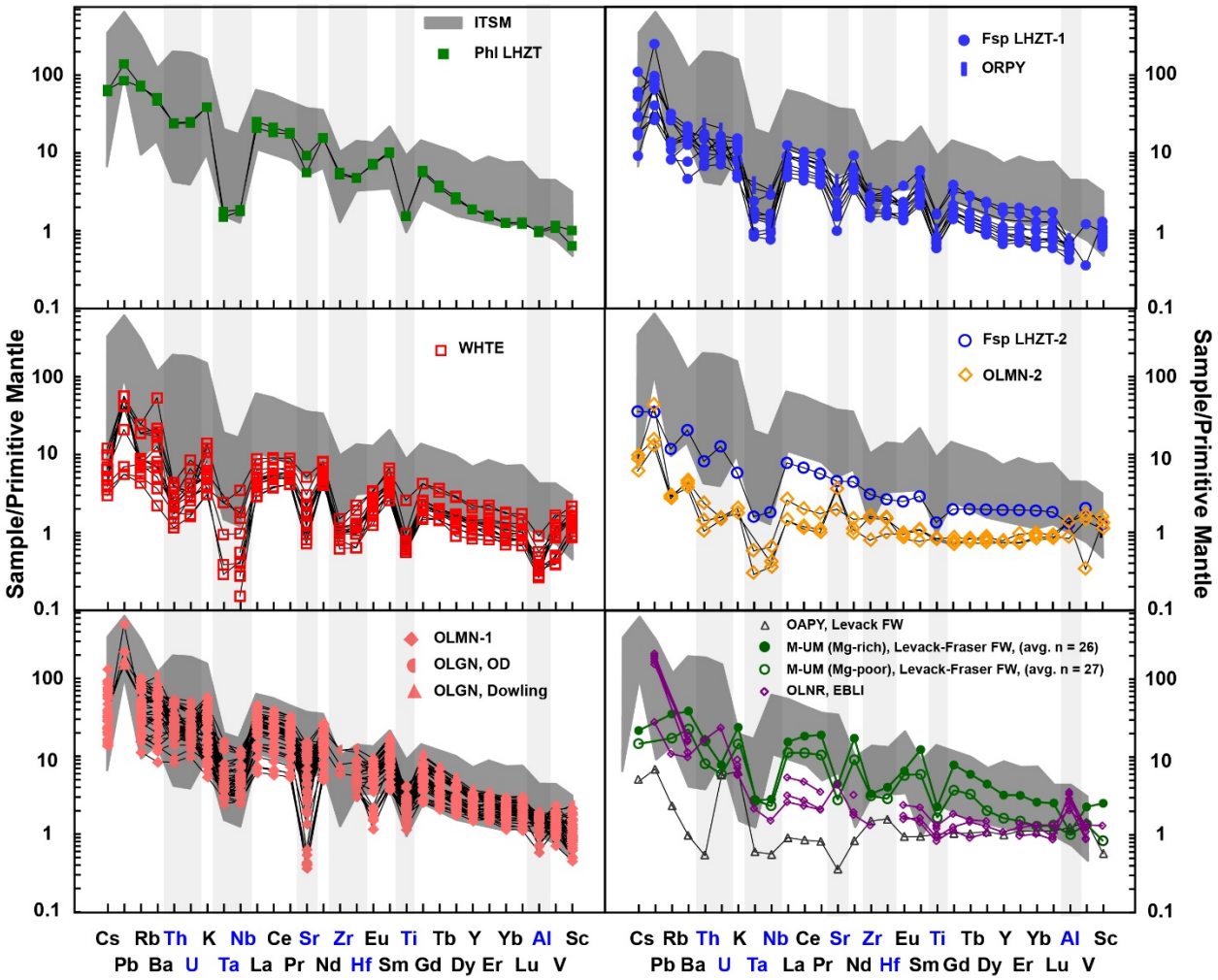

Figure 3.12 Primitive mantle-normalized trace element patterns for mafic and ultramafic inclusions, ITSM, and comparable mafic-ultramafic country rocks

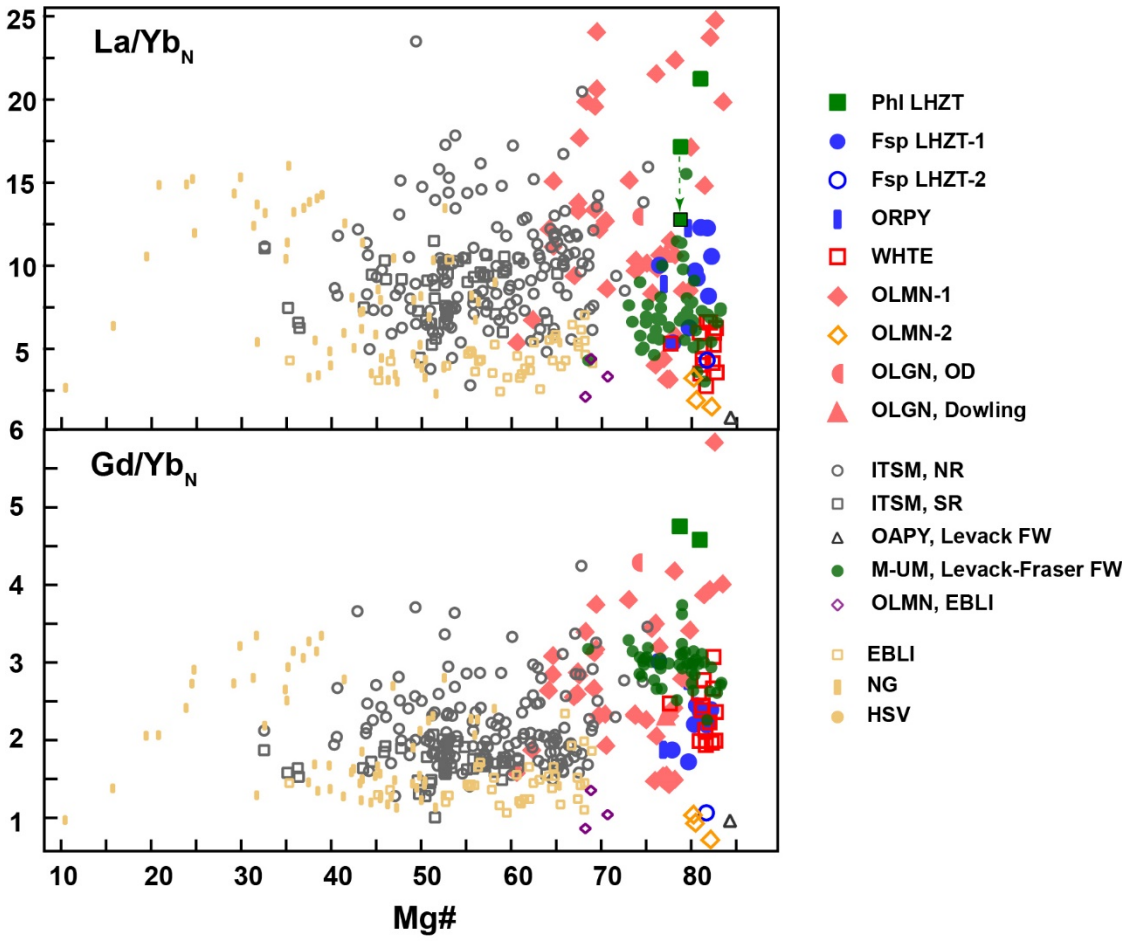

Figure 3.13 Plots of whole-rock compositions for mafic-ultramafic inclusions, ITSM, and comparable mafic-ultramafic country rocks. A: La/Yb_N vs Mg#, and B: Gd/Yb_N vs Mg#

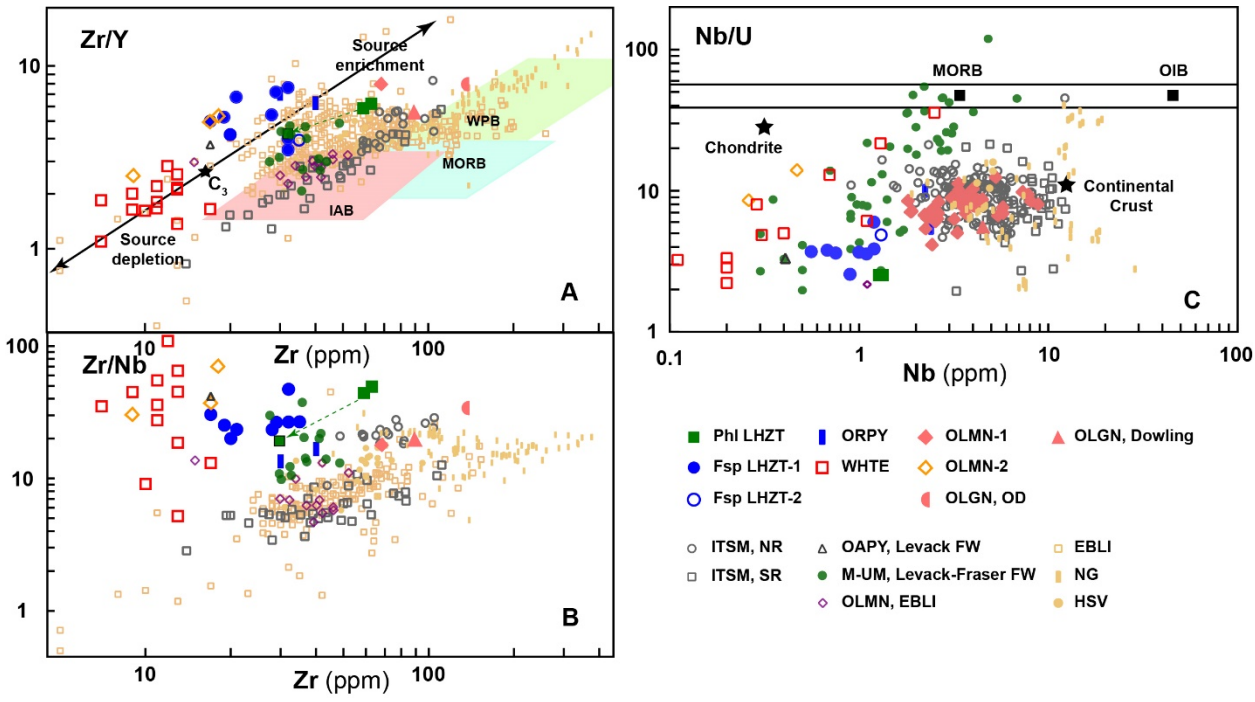

Figure 3.14 Plots of whole-rock compositions for mafic-ultramafic inclusions, ITSM, and comparable mafic-ultramafic country rocks. A: Zr/Y vs Zr, B: Zr/Nb vs Zr, and C: Nb/U vs Nb

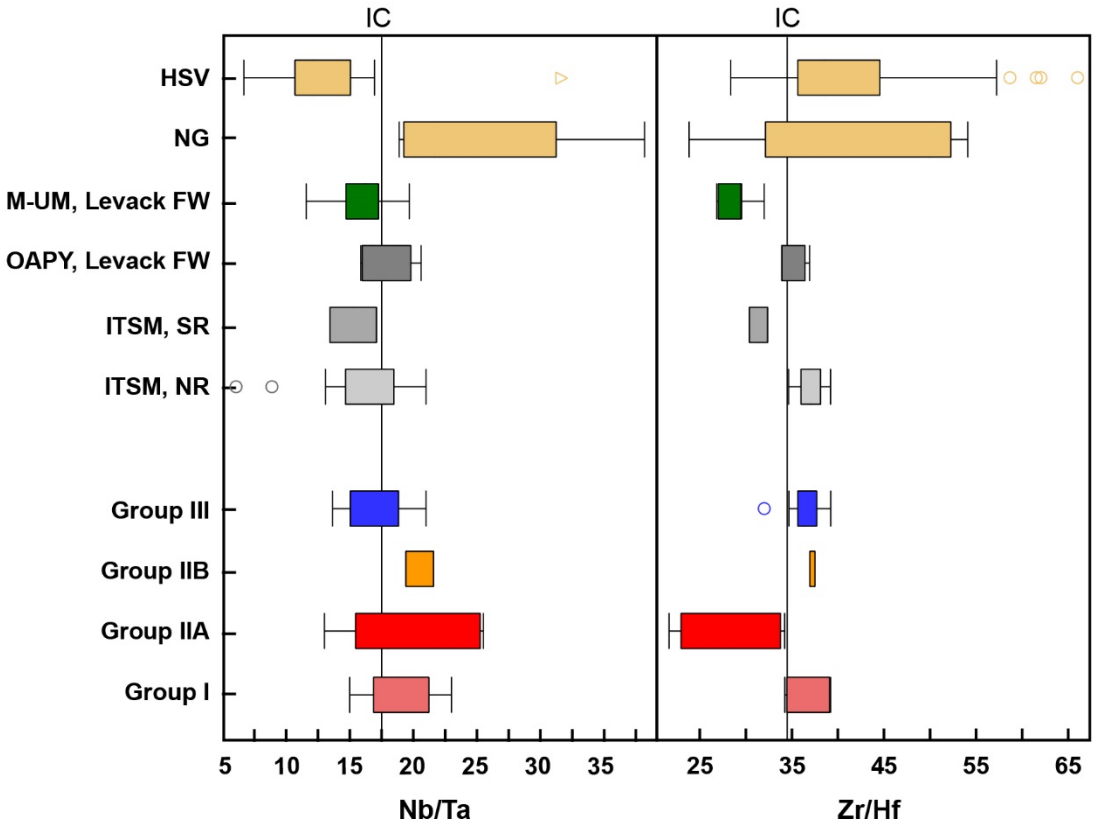

Figure 3.15 Box plots of whole-rock trace element ratios for mafic-ultramafic inclusions, ITSM, and comparable mafic-ultramafic country rocks. A: Zr/Hf and B: Nb/Ta

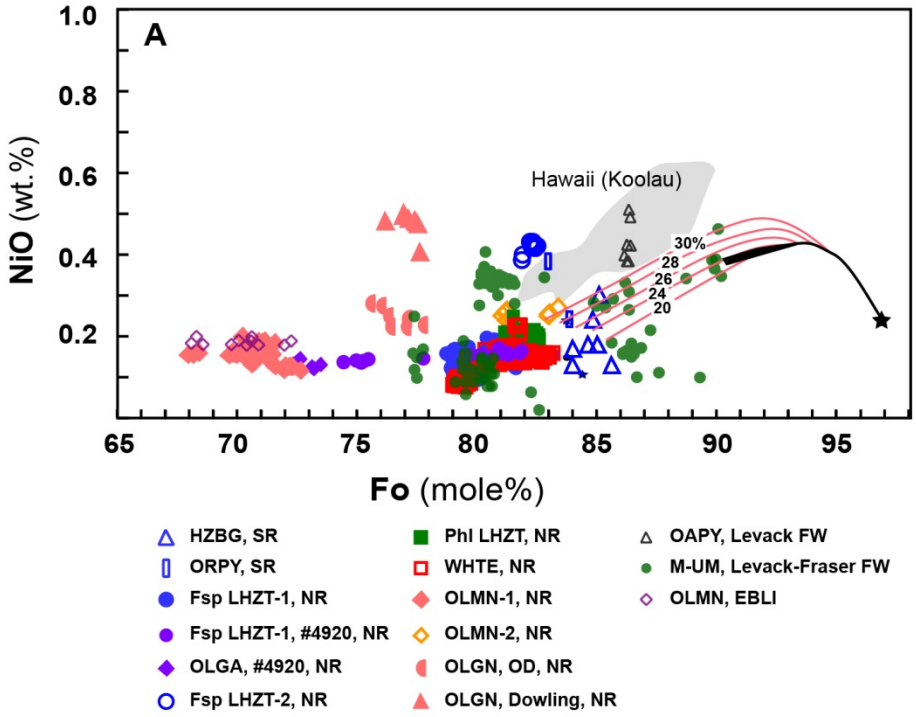

Figure 3.16 NiO and Fo contents of olivines in mafic-ultramafic inclusions and model olivines crystallizing from primary magmas at the surface.

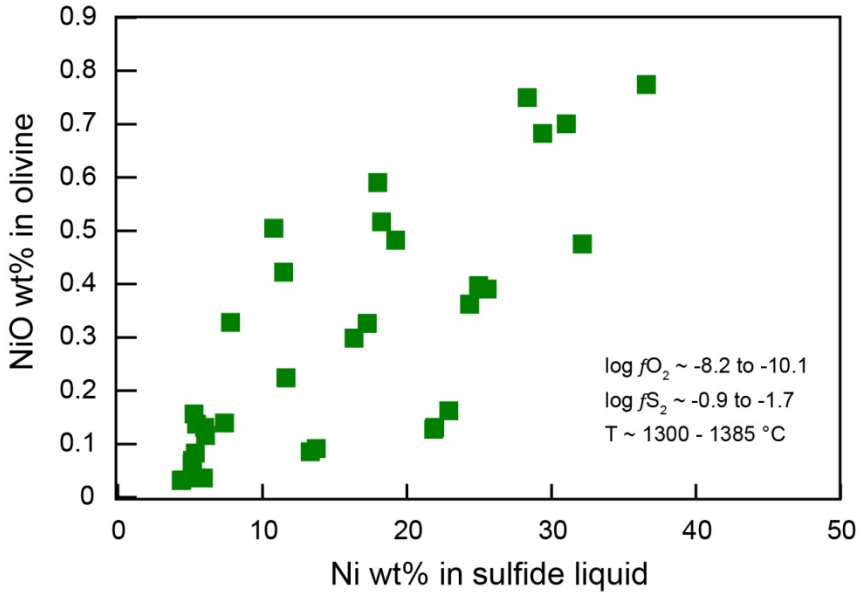

Figure 3.17 NiO contents of olivine and Ni content of sulfide liquid that have underwent equilibrium exchange of Fe-Ni in experiments at controlled temperature, oxygen, and sulfur fugacities. Data sources given in Brenan (2003).

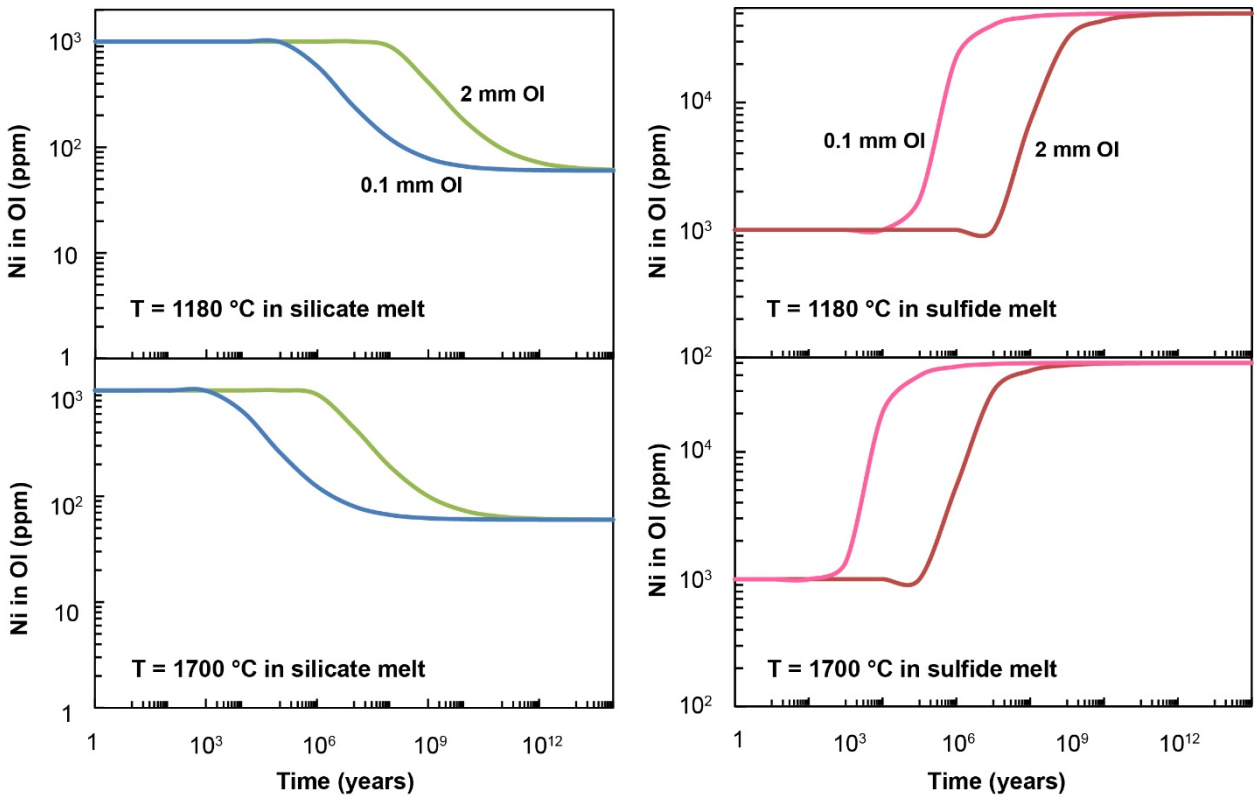

Figure 3.18 Ni Diffusion between olivine and silicate melt and between olivine and sulfide liquid at 1700°C and 1180°C, respectively

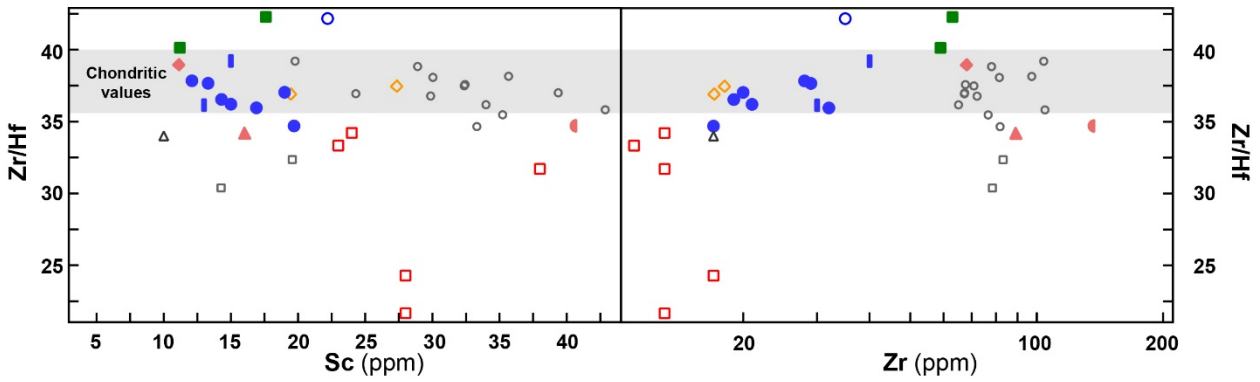

Figure 3.19 Plots whole-rock trace element compositions for mafic-ultramafic inclusions and ITSM. A: Zr/Hf vs Sc and B: Zr/Hf vs Zr

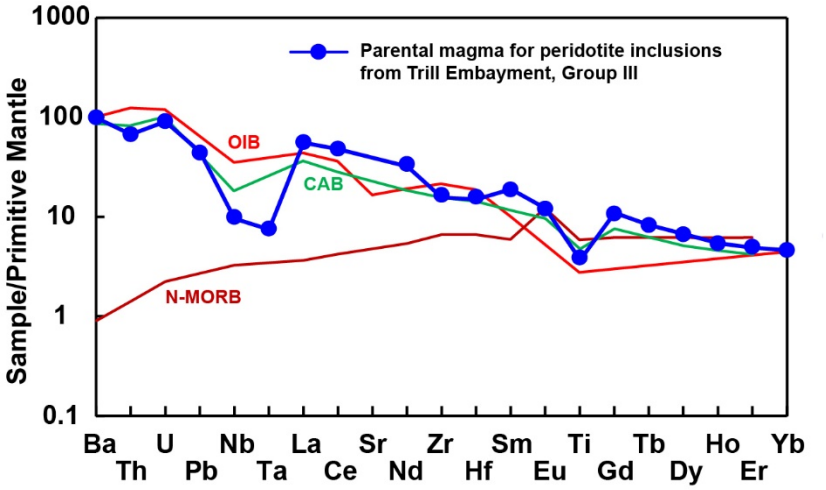

Figure 3.20 Primitive mantle-normalized trace element patterns of the calculated parental magma of Group III inclusions

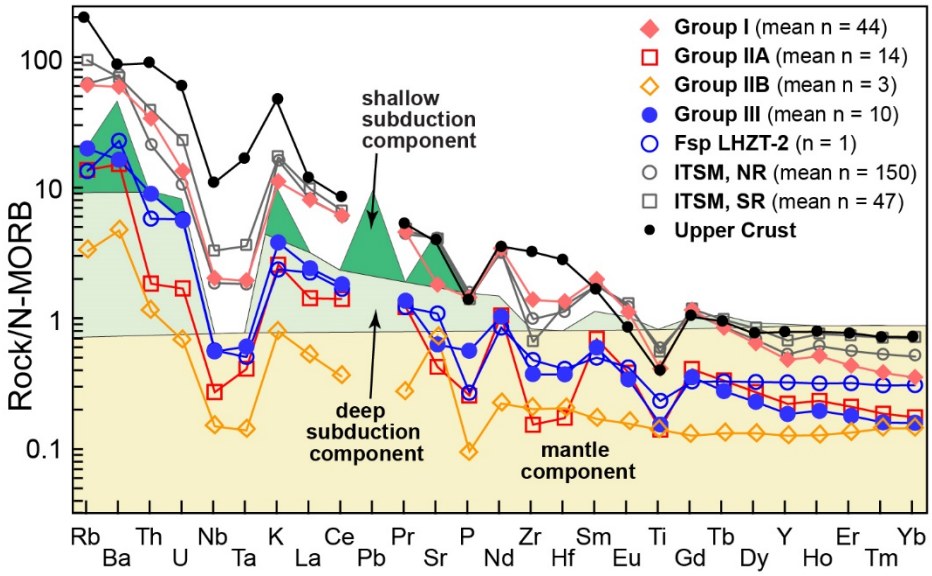

Figure 3.21 Incompatible trace element patterns (normalized to mid-ocean ridge basalt: Sun and McDonough, 1989) of the average composition of all groups of inclusions, various subduction components (shallow/deep) in arc basalts (Pearce et al., 2005), and upper continental crust (Taylor and McLennan, 1995)

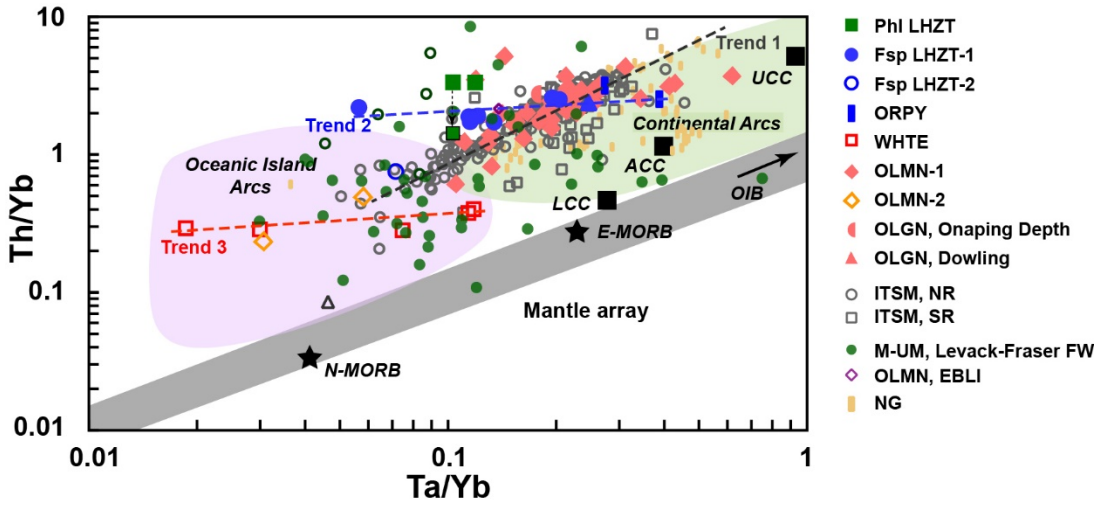

Figure 3.22 Plot of Th/Yb vs Ta/Yb of mafic and ultramafic inclusions, ITSM, and comparable mafic-ultramafic rocks country rocks

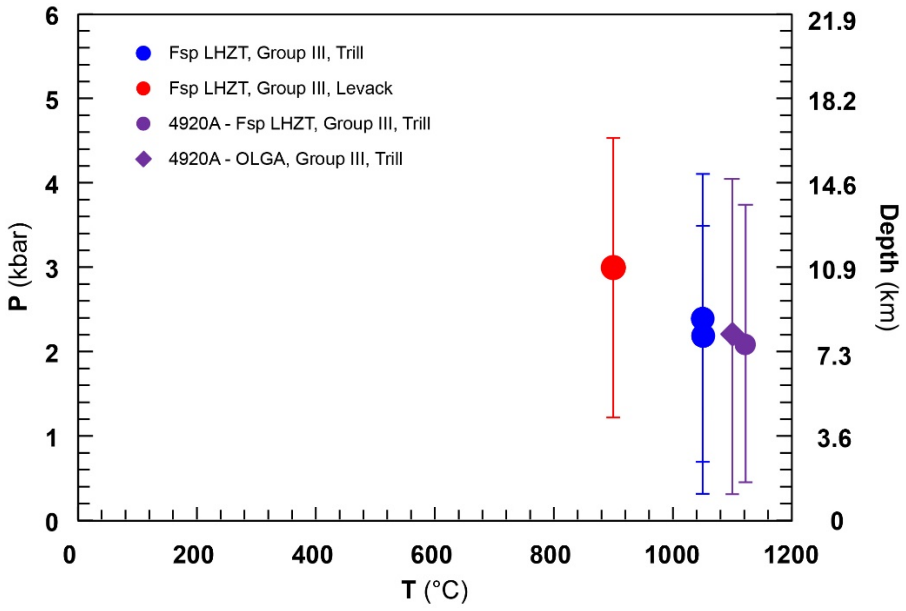

Figure 3.23 Calculated P-T diagram of selective mafic-ultramafic inclusions using Ol-Cpx-Pl geobarometer

Table 3.1 Petrographic characteristics of the mafic and ultramafic inclusions in Sublayer and IQD on the North Range

Lithologies (n)	**Localities**	**Contacts**	**Sulfides**	**Textures**
Mafic-Ultramafic Inclusions on the North Range				
Phl lherzolite (n = 5)	**Foy Offset**: Foy Offset	Sharp contacts with the matrix, occasionally with chlorite coatings	Barren	**Tectonic metamorphic**: porphyroclastic, granoclastic, hornfelsic, and recrystallized
Fsp lherzolite (n = 15)	**Sublayer**: Levack, Trill, Bowell	Sharp to reaction zone, comprising orthopyroxenite between peridotite and ITSM	Barren	**Igneous**: orthocumulate, poikilitic, and interstitial **Shock metamorphic**: partial isotropic Pl
Orthopyroxenite (n = 5)	**Sublayer**: Trill, Bowell	Reaction zone	Barren	**Igneous**: orthocumulate, poikilitic, and interstitial **Shock metamorphic**: partial isotropic Pl
Ol gabbro (n = 1)	**Sublayer**: Trill	No direct contact	Barren	**Igneous**: trachytic
Wehrlite - Ol clinopyroxenite (n = 17)	**Sublayer**: Levack	Sharp, occasionally with chlorite and carbonate coatings, and rare felsic clots and streaks and wisps breccia veins in cm scale	Disseminated to net-texture sulfides	**Shock metamorphic:** shock mosaic and recrystallized Ol **Thermal metamorphic:** recrystallized Cpx
Ol melanorite (n = 44)	**Sublayer**: Whistle	Sharp to gradational, with slickensides and/or a change in grain size and mineralogy percentage	Barren to weakly disseminated, 1 – 3%	**Igneous**: poikilitic and interstitial

Shocked Ol melanorite (n = 2)	**Offset dike**: Foy Offset	Sharp, with chlorite coatings	Barren to occasional blebs, <1%	**Shock metamorphic:** shock mosaic Ol; planar deformation features in Opx **Tectonic metamorphic:** recrystallized Ol, Opx, and Pl
Ol melagabbronorite (n = 2)	**Sublayer**: Levack (Dowling and Onaping Depth)	No information	**Onaping Depth**: disseminated, 1 – 3% **Dowling**: barren	**Igneous**: poikilitic and interstitial
Mafic-Ultramafic Inclusions on the South Range from Scribbins (1978)				
Harzburgite (n = 36)	**Sublayer**: Murray, Creighton, Little Stobie **Foy Offset**: Frood Offset	No information	No information	**Igneous**: orthocumulate, poikilitic, and interstitial **Tectonic metamorphic:** recrystallized
(Ol) Orthopyroxenite (n = 9)	**Sublayer**: Little Stobie	No information	Significant amount of sulfide	**Igneous**: poikilitic, interstitial **Tectonic metamorphic:** recrystallized
Clinopyroxenite (n = 2)	**Sublayer**: Creighton	No information	Significant amount of sulfide	**Igneous**: poikilitic, interstitial **Tectonic metamorphic**: hornfelsic
Ol melatroctolite (n = 2)	**Sublayer**: Little Stobie	No information	Significant amount of sulfide	**Igneous**: poikilitic, interstitial
Ol melanorite (n = 2)	**Sublayer**: Little Stobie, Creighton,	No information	Significant amount of sulfide	**Igneous**: poikilitic, interstitial, subophitic-ophitic **Tectonic metamorphic:** recrystallized
Ol norite (n = 1)	**Sublayer**: Creighton	No information	No information	**Igneous**: noritic **Tectonic metamorphic:** recrystallized

Note: Ol – olivine; Opx – orthopyroxene; Cpx – clinopyroxene; Phl – phlogopite; Fsp – feldspar; n – sample number

Table 3.2 Summary of compositions of olivine in the mafic-ultramafic inclusions and comparable mafic-ultramafic country rocks

Lithology	n	Subgroup	Localities	Ol		
				Fo	NiO (wt. %)	MnO (wt. %)
Fsp LHZT-1	160	Trill	Trill, NR	83 - 79	0.19 - 0.12	0.21 - 0.29
	10	Levack	Levack, NR	80 - 79	0.13 - 0.09	0.25 - 0.30
	5	Bowell	Bowell, NR	77	0.13 - 0.12	0.29 - 0.30
Layered Fsp LHZT-1 - OLGA	10	Fsp LHZT	Trill, NR	82 - 78	0.17 - 0.15	0.24 - 0.30
	5	Fsp LHZT close to OLGA		75 - 74	0.14	0.34 - 0.37
	6	OLGA		73 - 72	0.15 - 0.12	0.37 - 0.39
Phl LHZT	45		Foy Offset, NR	83 - 81	0.25 - 0.19	0.26 - 0.30
WHTE	6	High-Ni	Levack, NR	82	0.22 - 0.21	0.26 - 0.28
	136	Moderate-Ni		83 - 80	0.18 - 0.13	0.22 - 0.36
	28	Low-Ni		80 - 79	0.10 - 0.08	0.26 - 0.30
OLMN-1	32		Whistle, NR	73 - 68	0.20 - 0.12	0.28 - 0.45
Fsp LHZT-2	11		Trill, NR	83 - 82	0.43 - 0.38	0.24 - 0.28
OLMN-2	12		Foy Offset, NR	83 - 81	0.30 - 0.24	0.20 - 0.24
OLGN	8	Dowling	Levack, NR	78 - 76	0.50 - 0.40	0.26 - 0.31
	7	Onaping Depth	Levack, NR	78 - 76	0.28 - 0.22	0.27 - 0.33
OAPY, Levack FW	7		Footwall of Levack	86	0.51 - 0.38	0.18 - 0.20
M-UM, Levack-Fraser FW	58		Footwall of Levack-Fraser	82 - 69	0.36 - 0.06	0.20 - 0.49
OLMN, EBLI	6		EBLI	72 - 70	0.20 - 0.18	0.34 - 0.44

Note: Fsp LHZT-1 – igneous-textured feldspar lherzolite; OLGA – olivine gabbro; Phl LHZT – phlogopite lherzolite; WHTE – wehrlite; OLMN-1 – igneous-textured olivine melanorite; Fsp LHZT-2 – shocked feldspar lherzolite; OLMN-2 – shocked olivine melanorite; OLGN – olivine melagabbronorite; OAPY, Levack FW – olivine-bearing amphibole pyroxenite in the footwall of Levack Mine; M-UM, Levack-Fraser FW – mafic-ultramafic intrusion in the footwall of Levack and Fraser deposits; OLMN, EBLI – olivine melanorite in the East Bull Lake intrusive suite; NR – North Range; Ol – olivine; n – analysis number

Table 3.3 Summary of compositions of orthopyroxene in the mafic-ultramafic inclusions and comparable mafic-ultramafic country rocks

Lithology	n	Subgroup/Localities	Species	Mg#	Al_2O_3 (wt. %)	CaO (wt. %)	TiO_2 (wt. %)	Cr_2O_3 (wt. %)
ITSM	10	Trill, NR	Hyp	72 - 63	0.79 - 1.51	1.50 - 1.97	0.26 - 0.32	
ORPY	46	Trill, NR	Hyp	82 - 63	1.09 - 1.58	1.03 - 2.58	0.11 - 0.40	0.18 - 0.48
Fsp LHZT-1	84	Trill, Levack, Bowell, NR	Brz - Hyp	84 - 81	0.69 - 1.78	0.50 - 1.90	0.03 - 0.40	0.12 - 0.48
Phl LHZT	26	Foy Offset, NR	Brz	85 - 83	0.37 - 1.25	0.81 - 1.12	0.02 - 0.08	0.01 - 0.20
WHTE	29	Levack, NR	Brz	84 - 83	1.06 - 1.38	0.86 - 1.39	0.09 - 1.16	0.15 - 0.25
OLMN-1	10	Whistle, NR	Brz	76 - 75	0.05 - 0.87	1.24 - 1.32	0.10 - 0.24	
Fsp LHZT-2	10	Levack, NR	Brz	84 - 83	1.19 - 1.44	1.23 - 1.74	0.28 - 0.52	0.21 - 0.31
OLMN-2	22	Foy Offset, NR	Brz	85 - 83	0.98 - 1.81	0.69 - 1.78	0.08 - 0.33	0.27 - 0.49
OLGN	9	Dowling (Levack), NR	Brz - Hyp	79 - 78	1.16 - 1.34	0.93 - 1.79	0.11 - 0.41	0.14 - 0.18
	5	Onaping Depth (Levack), NR	Brz - Hyp	80 - 79	0.64 - 0.98	1.08 - 1.26	0.09 - 0.24	
OAPY, Levack FW	13	Levack FW	Brz	87 - 86	1.68 - 3.24	0.24 - 0.38	0.02 - 0.05	0.08 - 0.17
M-UM, Levack-Fraser FW	4	Levack-Fraser FW	Brz	82	1.12 - 1.24	1.03 - 1.22	0.21 - 0.30	0.18 - 0.27
OLMN, EBLI	4	EBLI	Hyp	75	1.17 - 1.30	1.33 - 1.95	0.34 - 0.43	

Note: ITSM – igneous-textured Sublayer matrix; ORPY – orthopyroxenite; Brz – Bronzite; Hyp – Hypersthene

Table 3.4 Summary of compositions of clinopyroxene in the mafic-ultramafic inclusions and comparable mafic-ultramafic country rocks

Lithology	n	Subgroup/Location	Species	Mg#	Al_2O_3 (wt. %)	Cr_2O_3 (wt. %)
ITSM	4	Trill, NR	Aug	75 - 71	1.28 - 2.13	0.11 - 0.35
Fsp LHZT-1	100	Trill, Levack, NR	Di - Edi	92 - 82	0.17 - 3.55	0.14 - 0.96
Layered Fsp LHZT-1	10	Trill, NR	Di - Edi	86 - 83	1.60 - 2.52	0.44 - 1.02
Layered OLGA	9	Trill, NR	Sa - Aug	80 - 77	2.45 - 3.05	0.21 - 0.46
Fsp LHZT-2	4	Levack, NR	Di - Edi	85 - 84	2.34 - 2.84	0.64 - 0.93
WHTE	107	Levack, NR	Di - Edi	93 - 83	0.30 - 2.56	0.03 - 0.58
OLMN-1	10	Whistle, NR	Sa - Aug	81 - 79	1.37 - 2.66	
OLMN-2	14	Foy Offset, NR	Di - Edi	88 -84	1.61 - 2.44	0.60 - 0.85
OLGN	2	Dowling (Levack), NR	Di - Edi - Sa - Aug	81	2.11 - 2.14	0.13 - 0.35
	13	Onaping Depth (Levack), NR	Di - Edi - Sa - Aug	83 - 81	1.54 - 3.65	0.17 - 0.58
ORPY	11	Trill, NR; Victor, SR	Aug	75 - 70	1.09 - 1.95	0.17 - 0.32
M-UM, Levack-Fraser FW	12	Footwall of Levack-Fraser	Di	90 - 83	0.40 - 3.03	
OLMN, EBLI	2	EBLI	Sa - Aug	77 - 76	2.05 - 2.36	0.26

Note: Di – Diopside; Sa – Salite; Edi – Endiopside; Aug – Augite

Table 3.5 Summary of amphibole (Amp) chemical composition of mafic-ultramafic inclusions and comparable mafic-ultramafic country rocks

Lithology	n	Subgroup/Location	Species	Mg#	Cr_2O_3 (wt. %)	Al_2O_3 (wt. %)
Fsp LHZT	5	Levack, NR	Prg	77	0.9 – 1.0	11.0 - 11.2
Br-MMN	8	Garson, SR	Hbl	72 - 61	0.2 - 0.3	5.9 - 8.9
Gr-MMN	10	Garson, SR	Hbl	72 - 59	0 - 0.2	2.7 - 10.2
MG	37	Footwall of Garson	Ts -Hbl	61 - 29	0 - 0.5	13.9 - 18
OAPY, Levack FW	12	Footwall of Levack	Prg	85 - 81	0 - 0.87	11.7 - 14.4
M-UM, Levack-Fraser FW	20	Footwall of Levack-Fraser	Hs-Prg-Hbl	85 - 64	0.0 - 1.1	9.1 - 11.7

Note: Br-Amp - brown amphibole; Gr-Amp - green amphibole; MG - metagabbro; Br-MMN - brown amphibole in Main Mass Norite; Gr-MMN - green amphibole Main Mass Norite; Prg – pargasite; Hbl – hornblende; Ts – tschermakite; Hs – hastingsite

Table 3.6 Geochemical characteristics of mafic-ultramafic inclusions, ITSM, and comparable mafic-ultramafic intrusions

Group	Lithologies (n)	Localities	La/Sm_N	Gd/Yb_N	Zr/Y	Zr/Nb	Nb/U	Zr/Hf	Nb/Ta
ITSM	GBBR - NORT (n = 197)	**NR Sublayer:** Whistle, Fraser, Levack, McCreedy West **SR Sublayer:** Little Stobie, Creighton, Crean Hill	**NR**: 1.8 – 7.0 **SR**: 4.2 – 6.2	**NR**: 1.3 – 4.2 **SR**: 1.0 – 2.1	**NR**: 2.5 – 8.3 **SR**: 0.8 – 5.8	**NR**: 8.8 – 28.7 **SR**: 2.8 – 12.6	**NR**: 4.7 – 45.3 **SR**: 1.9 – 21.3	**NR**: 34.7 –39.2 **SR**: 30.3 – 32.4	**NR**: 6.1 – 21 **SR**: 13.4 – 17.1
I	OLMN-1 (n = 44) OLGN (n = 2)	**Sublayer**: Whistle, Levack (Dowling and Onaping Depth)	2.3 – 5.4	1.4 – 5.8	5.6 – 8.0	18.1 – 34.0	4.2 – 12.6	34.2 – 39.0	15.0 – 18.8
IIA	WHTE (n = 17)	**NR Sublayer**: Levack	1.3 – 3.0	1.9 – 3.1	1.4 – 2.8	5.2 – 109.1	2.2 – 35.7	21.7 – 34.2	13.0 – 25.5
IIB	OLMN-2 (n = 2)	**Offset dike**: Foy Offset	2.1 – 3.8	0.7 – 1.0	2.5 – 5.3	30 – 69.5	8.6 – 14.1	37.0 – 37.5	19.4 – 21.6
III	Phl LHZT (n = 5) Fsp LHZT (n = 15) ORPY (n = 5) OLGA (n = 1)	**Sublayer**: Levack, Trill, Bowell **Foy Offset**: Foy Offset	2.9 – 5.0	1.1 – 4.8	3.5 – 11.5	13.4 – 49.3	2.5 – 10.0	32.0 – 42.3	13.6 – 23.0
OAPY, Levack FW	OAPY (n = 9)	Footwall of Levack embayment	1.5	1.0	3.7	41.7	3.3	34.0	16.3
M-UM, Levack-Fraser FW	M-UM (n = 53)	Footwall of Levack and Fraser deposits	0.7 – 4.4	2.3 – 3.8	2.1 – 5.2	10.3 – 36.9	2.0 – 119.8	26.5 – 32.0	4.2 – 22.8
OLMN, EBLI	OLMN (n = 18)	EBLI	1.6 – 2.5	1.0 – 1.4	2.3 – 3.3	4.8 – 13.6	2.2		

Note: GBBR – gabbro; NORT – norite

Table 3.7 Estimation of the composition of parental magma of Group III inclusions

	Ba	Th	U	Pb	Nb	Ta	La	Ce	Nd	Zr	Hf	Sm	Eu	Ti	Gd	Tb	Dy	Ho	Er	Yb
WR	111.0	0.9	0.3	2.0	1.1	0.1	6.3	13.9	7.0	29.0	0.8	1.4	0.3	939.0	1.1	0.2	0.8	0.2	0.4	0.4
$D^{Ol/L\ (1)}$	0.000	0.003	0.003	0.132	0.001	0.126	0.010	0.007	0.004	0.010	0.009	0.003	0.006	0.025	0.003	0.009	0.009	0.015	0.022	0.005
$D^{Opx/L\ (2)}$	0.012	0.006	0.004	0.033	0.015	0.000	0.003	0.007	0.014	0.014	0.027	0.024	0.022	0.238	0.019	0.044	0.046	0.048	0.098	0.132
Parental melt	688	5.7	1.9	8.3	6.8	0.3	38	84	43	173	4.6	8.3	2.0	4727	6.4	0.9	4.9	0.9	2.3	1.2

Note: The proportion of olivine and orthopyroxene was calculated using the lithogeochemical classification method by Stanley (2017) and point counting. WR = whole-rock composition; (1)-Bédard, J.H. (2005); (2)-Bédard, J.H. (2007)

Table 3.8 Calculated results of Sm/Yb_N at variable degrees of batch melting (BM) and fractional melting (FM) of spinel peridotite and garnet peridotite

	BM of Garnet Peridotite			**FM of Garnet Peridotite**		
	Sm	**Yb**	**Sm/Yb_N**	**Sm**	**Yb**	**Sm/Yb_N**
1%	20.3	2.9	7.9	19.7	2.9	7.7
5%	11.4	2.7	4.8	7.3	2.6	3.1
10%	7.4	2.4	3.3	2.0	2.4	0.9
	BM of Spinel Peridotite			**FM of Spinel Peridotite**		
	Sm	**Yb**	**Sm/Yb_N**	**Sm**	**Yb**	**Sm/Yb_N**
1%	16.7	9.3	2.0	16.4	9.3	2.0
5%	10.2	7.0	1.6	7.5	6.3	1.3
10%	6.9	5.3	1.4	2.7	3.9	0.8

Table 3.9 Mineral compositions determined by EPMA (wt%) and compositional variables calculated for COlP calibration in representative Group III mafic-ultramafic inclusions

Sample #		**372980**			**4919**			**4920B**			**4920A**			**358091**		
Lithology		**Fsp LHZT**			**Fsp LHZT**			**Fsp LHZT**			**OLGA**			**Fsp LHZT**		
Localities		**Trill**			**Trill**			**Trill**			**Trill**			**Levack**		
Phase		**Cpx**	**Ol**	**Pl**	**Cpx**	**Ol**	**Pl**	**Cpx**	**Ol**	**Pl**	**Cpx**	**Ol**	**Pl**	**Cpx**	**Ol**	**Pl**
Analysis spot (n)		5	13	3	4	19	6	11	17	9	5	6	8	5	10	7
Mineral composition (wt%)	**SiO_2**	52.6	39.2	48.3	53.0	39.3	53.9	52.9	39.2	56.0	51.6	37.8	54.7	52.0	39.2	47.3
	σ	0.156	0.197	0.331	0.225	0.180	0.458	0.307	0.177	0.724	0.544	0.220	1.057	0.842	0.165	0.268
	TiO_2	0.4	0.0	0.0	0.3	0.0	0.0	0.4	0.0	0.0	0.8	0.0	0.1	0.6	0.0	0.0
	σ	0.028	0.000	0.005	0.065	0.001	0.007	0.077	0.008	0.019	0.087	0.004	0.009	0.208	0.002	0.009
	Al_2O_3	2.2	0.0	32.4	2.0	0.2	28.8	2.0	0.0	27.4	2.7	0.0	27.9	2.7	0.3	33.2
	σ	0.120	0.002	0.308	0.092	0.349	0.281	0.230	0.002	0.333	0.203	0.001	0.600	0.709	0.451	0.169
	Cr_2O_3	0.6	0.0	ND	0.6	0.0	ND	0.6	0.0	ND	0.4	<0.008	ND	0.5	0.0	ND
	σ	0.005	0.009		0.026	0.018		0.080	0.018		0.087			0.089	0.002	
	FeO_T	5.2	19.0		4.8	17.5		5.0	17.4		7.2	24.4		5.7	19.1	
	σ	0.250	0.327		0.090	0.546		0.178	0.346		0.290	0.303		0.187	0.322	
	Fe_2O_3	1.1		0.5	1.2		0.4	1.3		0.3	1.2		0.4	1.8		0.4
	σ	0.234		0.038	0.145		0.080	0.322		0.033	0.466		0.048	0.296		0.148
	MnO	0.1	0.3	<0.027	0.1	0.2	<0.027	0.1	0.2	<0.027	0.2	0.4	<0.027	0.1	0.3	<0.027
	σ	0.007	0.008		0.006	0.016		0.010	0.007		0.008	0.007		0.008	0.010	
	MgO	16.5	41.4	0.0	16.8	42.7	0.0	16.7	42.7	0.0	15.3	36.7	0.0	15.8	41.3	0.0
	σ	0.069	0.233	0.008	0.098	0.505	0.005	0.211	0.198	0.003	0.466	0.362	0.009	0.329	0.313	0.019
	NiO	0.0	0.1	ND	0.0	0.2	ND	0.0	0.2	ND	0.0	0.1	ND	0.0	0.1	ND
	σ	0.003	0.007		0.009	0.013		0.005	0.005		0.010	0.008		0.004	0.004	
	CaO	21.8	0.1	16.0	21.9	0.0	11.7	21.8	0.1	10.0	21.1	0.1	10.8	21.9	0.0	16.8
	σ	0.229	0.012	0.228	0.183	0.007	0.346	0.280	0.032	0.448	0.481	0.006	0.776	0.196	0.010	0.116
	Na_2O	0.3	<0.005	2.5	0.4	0.0	4.8	0.4	<0.005	5.8	0.4	<0.005	5.2	0.5	<0.005	2.0
	σ	0.013		0.118	0.007	0.000	0.149	0.036		0.343	0.028		0.408	0.061		0.068
	K_2O	<0.005	<0.012	0.1	<0.005	0.0	0.3	<0.005	0.0	0.3	<0.005	<0.012	0.5	<0.005	<0.012	0.0
	σ			0.011		0.000	0.067		0.002	0.084			0.104			0.009
	Total	99.8	100.1	99.7	100.0	100.0	100.0	100.1	99.8	99.2	99.7	99.6	99.5	101.5	100.0	99.8
Compositional variables	**x(cpx)**	0.124			0.111			0.113			0.185			0.128		
	σ	0.004			0.002			0.009			0.005			0.004		
	y(cpx)	0.070			0.062			0.066			0.090			0.089		
	σ	0.006			0.005			0.009			0.011			0.027		

	f(cpx)	0.030			0.033			0.036			0.033			0.050		
	σ	0.006			0.004			0.009			0.013			0.008		
	z(cpx)	0.857			0.856			0.852			0.837			0.862		
	σ	0.009			0.006			0.011			0.021			0.006		
	j(cpx)	0.024			0.029			0.030			0.027			0.035		
	σ	0.001			0.000			0.003			0.002			0.004		
	x(ol)		0.204			0.187			0.186			0.272			0.206	
	σ		0.004			0.007			0.004			0.005			0.004	
	ca(pl)			0.777			0.563			0.481			0.521			0.567
	σ			0.011			0.016			0.025			0.039			0.002
	k(pl)			0.003			0.020			0.019			0.027			0.016
	σ			0.001			0.004			0.005			0.006			0.006

Note: Mineral formula in terms of cations expressed as atoms per formula unit (apfu), with olivine (Ol), clinopyroxene (Cpx), and plagioclase (Pl) were calculated on a basis of 4, 6, and 8 oxygens respectively. Iron was assumed to be all ferrous in olivine and all ferric in plagioclase. Fe^{3+} in clinopyroxene was calculated from stoichiometry following the method of Droop (1987). Uncertainties (σ) are propagated from analytical errors. LLD – lower limit of detection; ND – not determined; σ – standard deviation

Table 3.10 Results of P-T calculations of Group III inclusions

Sample	Lithology	Location	$T\sigma_{fit}$°C	P Mpa	σ_P MPa	σ_{fit}	Depth km
372980	Fsp LHZT	Trill	1050	240	109	1.5	8.7 ± 4.0
4919	Fsp LHZT	Trill	1050	220	190	2.1	8 ± 6.9
4920B	Fsp LHZT	Trill	1120	210	166	1.9	7.7 ± 6.0
4920A	OLGA	Trill	1100	220	183	1.6	8 ± 6.7
358091	Fsp LHZT	Levack	900	300	178	0.7	10.9 ± 6.5

Note: P_o = 4.0 kbar and $T_o = T\sigma_{fit}$ (see discussion by Ziberna et al., 2017) for all calculations. The effect of changing P_o on calculated P is negligible, but the effect of changing T_o on calculated P can be significant, so $T\sigma_{fit}$ has been selected by minimizing σ_{fit} across the temperature interval 700 - 1300°C. Because igneous spinel is not present in our assemblages, we have used the COlP (Cpx - Ol - Pl) calibration, which may overestimate P by ≤ 100 MPa at P < 500 MPa. All P calculations passed the $\chi 2$ test (σ_{fit} < 1.73), except for sample 4920B (within 20% of cut-off value - 1.73). Depth has been calculated assuming a geobarometric gradient of 27.5 MPa/km.

Table S3.1 Composition of olivine and atomic proportions based on 4 oxygens of the mafic-ultramafic inclusions and mafic-ultramafic country rocks

Table S3.2 Composition of orthopyroxene and atomic proportions based on 6 oxygens of the mafic-ultramafic inclusions, ITSM, and mafic-ultramafic country rocks

Table S3.3 Composition of clinopyroxene and atomic proportions based on 6 oxygens of the mafic-ultramafic inclusions, ITSM, and mafic-ultramafic country rocks

Table S3.4 Composition of chromite and atomic proportions based on 4 oxygens of the mafic-ultramafic inclusions and mafic-ultramafic country rocks

Table S3.5 Composition of amphibole and atomic proportions based on 24 (OH, F, Cl, O) of the mafic-ultramafic inclusions and mafic-ultramafic country rocks

Table S3.6 Whole-rock geochemistry of the mafic-ultramafic inclusions and ITSM and mafic-ultramafic country rocks

Table S3.7 Mass balance calculation of the effect of melt infiltration in representative samples of Group III using Microsoft Excel Solver optimization tool

Tables S3.1 – S3.7 are attached in excel files.

CHAPTER 4

GENESIS OF SUBLAYER IN THE SUDBURY IGNEOUS COMPLEX

Yujian Wang, **C. Michael Lesher***, **Peter C. Lightfoot**, **Edward F. Pattison**, and **J. Paul Golightly**

Mineral Exploration Research Centre, Harquail School of Earth Sciences, Goodman School of Mines, Laurentian University, Sudbury P3E 2C6, Canada

*Corresponding Author E-mail: mlesher@laurentian.ca

4.1 Abstract

The Ni-Cu-PGE sulfide mineralization in the 1.85 Ga Sudbury Igneous Complex (SIC) occurs in two discrete environments: 1) mineralization along or near the basal contact, including disseminated to semi-massive mineralization in inclusion-rich Sublayer, semi-massive to fragmental mineralization in underlying anatectic Footwall Breccia (FWBX), and veins and disseminations in underlying pseudotachylitic Sudbury Breccia, and 2) disseminated to semi-massive mineralization in radial and concentric inclusion-bearing quartz diorite (IQD) in offset dikes that extend up to 20 km from the basal contact. Understanding the genesis of Sublayer, FWBX, and IQD is of great economic implications on the ore-formation process of the world's largest accumulation of Ni-Cu-PGE sulfide mineralization. Sublayer, FWBX, and IQD all contain abundant mafic-ultramafic inclusions, some representing anteliths derived from an earlier border phase of the SIC, some representing xenoliths derived from local country rocks, and some representing exotic xenoliths derived from unexposed upper-middle crustal target

rocks. The similar inclusion population indicates a genetic relationship between Sublayer and IQD. Sublayer is characterized by a cumulate noritic matrix, whereas IQD is characterized by a quartz dioritic matrix, which suggests slower cooling in Sublayer and faster cooling in IQD. All of the matrices and most of the inclusions are uniformly enriched in highly incompatible lithophile elements, strongly unradiogenic Nd, and radiogenic Os (except for a few olivine melanorite/melanorite inclusions at Whistle showing unradiogenic Os), reflecting both a strong subduction-related arc and upper continental crustal signature. The overlying Main Mass norite is very homogeneous in terms of Hf isotopes, indicating that the impact melt sheet was well mixed. However, Sublayer, IQD, and overlying basal Main Mass norites vary widely in their Pb-S-(Os) isotopic compositions. The majority of mafic-ultramafic inclusions, except for anteliths, contain no sulfide and exhibit no signature of Ni-Cu-PGE depletion caused by prior sulfide saturation, which indicates that the association between mafic-ultramafic inclusions and Ni-Cu-PGE sulfide mineralization is most likely attributable to their refractory nature and to their similar fluid dynamic behavior rather than a genetic relationship. Anteliths, locally-derived inclusions, and local variations in Pb-S-(Os) isotopes must have been generated in situ, requiring significant degrees of local thermomechanical erosion, whereas exotic inclusions, except for shocked feldspar lherzolite, were derived from mafic-ultramafic protoliths incorporated during impact excavation and/or thermomechanical erosion, and physically transported into their current locations. Thermomechanical erosion played a significant role in the generation of embayments, incorporation of xenoliths and sulfide xenomelts from the country rocks (e.g., EBLI-Nipissing-Huronian), and formation of isotopic heterogeneity in the basal units. Convective and gravity flow likely aided in the horizontal transport of inclusions and sulfide xenomelts into the

embayment when the proto-Sublayer contained less inclusions (<45%), but became less significant when the proto-Sublayer assimilated more inclusions and became more viscous.

Key words: Sudbury, Sublayer, Footwall Breccia, Inclusion-Bearing Quartz Diorite, Ni-Cu-PGE mineralization, mafic-ultramafic inclusions, thermomechanical erosion, convective flow, gravity flow

4.2 Introduction

The Sudbury Structure is one of the oldest (1.8 Ga), largest (up to 250 km diameter), and best exposed terrestrial impact structures (e.g., Grieve and Therriault, 2000), and contains some of the world's largest magmatic Ni-Cu-PGE sulfide deposits (e.g., Naldrett, 2004; Lightfoot, 2016). The Sudbury Structure comprises the Sudbury Igneous Complex (SIC), overlying fall-back breccias, suevites, and basin-fill sediments of the Whitewater Group (e.g., Muir and Peredery, 1984; Rousell, 1984; Ames et al., 2002), and underlying pseudotachylitic, anatectic, and contact-metamorphosed breccias, and it straddles the boundary between the 2.7 – 2.6 Ga Superior Province to the North, East, and West (North Range) and the 2.5 – 2.2 Ga Southern Province to the South (South Range) (Fig. 4.1). The Superior Province in this area consists mainly of felsic-mafic gneisses of the 2.6-2.7 Ga Levack Gneiss Complex (e.g., Krogh et al., 1984), the 2.6 Ga Cartier Granite (Meldrum et al., 1997), and minor mafic-ultramafic rafts/intrusions (e.g., Moore et al., 1993, 1994, 1995). The Southern Province comprises metabasalts, metarhyolites, and metasedimentary rocks of the 2.5-2.2 Ga Huronian Supergroup, associated with 2.5 Ga East Bull Lake suite mafic intrusions, and 2.2 Ga Nipissing suite mafic intrusions.

The SIC comprises a Main Mass, interpreted to be the remnants of an impact melt sheet, an underlying discontinuous inclusion-rich Sublayer, and radial and concentric offset dikes

(Fig. 4.1). The Main Mass is differentiated into a lower noritic unit, a transitional quartz gabbroic unit, and an upper granophyric unit. Sublayer is a discontinuous (0-500m), heterogeneous, fine- to medium-grained, inclusion-rich, noritic to gabbronoritic unit that is localized in embayments, funnels, and troughs along the basal contact of the Main Mass (e.g., Souch et al., 1969; Naldrett et al., 1984; Lightfoot et al., 1997a, b). Sublayer on the North Range is commonly underlain by locally mobilized anatectic Footwall Breccia (FWBX, e.g., Coats and Snajdr, 1984; McCormick et al., 2002), which is also heterogeneous, consisting of abundant inclusions of a wide range of shape, size, and mineralogy within a fine- to medium-grained igneous to subigneous felsic-intermediate matrix. Offset dikes contain an analogous inclusion-rich phase with a quartz dioritic matrix that is referred to as Inclusion Quartz Diorite (IQD). Sublayer, FWBX, and IQD all contain variable amounts of Fe-Ni-Cu sulfides. On the North Range Sublayer grades downwards through FWBX into semi-massive to massive contact ores, whereas on the South Range Sublayer less commonly grades downwards through FWBX but normally grades downwards directly into semi-massive to massive contact ores (e.g., Souch et al., 1969; Naldrett, 1984; Lightfoot, 2016).

The abundant inclusions within the Sublayer, FWBX, and IQD comprise gneissic, metavolcanic, and metasedimentary xenoliths derived from local country rocks (Souch et al., 1969; Grant and Bite, 1984) and a variety of mafic-ultramafic lithologies: harzburgite, phlogopite lherzolite, feldspar lherzolite, wehrlite, olivine clinopyroxenite, orthopyroxenite, olivine melanorite, olivine melagabbronorite, and olivine gabbro on the North Range (Wang et al., Ch 3), and harzburgite, olivine orthopyroxenite, orthopyroxenite, troctolite, and olivine melanorite on the South Range (Scribbins et al., 1984). The inclusions vary

from a few cm (Hewins, 1971) to tens of m in diameter (Naldrett et al., 1972; Wang et al., Ch 3). Locally derived inclusions are typically angular to subangular and mafic-ultramafic inclusions are typically subrounded to rounded, but can have almost any shape (McNutt, 1970). The textures of mafic-ultramafic inclusions vary widely from igneous (e.g., orthocumulate, poikilitic, and interstitial) through shock metamorphic (e.g., shock mosaicism in olivine, planar deformation features in orthopyroxene, and partial isotropization in plagioclase: Wang et al., 2016, 2018) to tectonic metamorphic (e.g., porphyroclastic, granoclastic, hornfelsic, and recrystallized). The contact between inclusions and ITSM is commonly sharp, occasionally with chlorite and carbonate coatings. Feldspar lherzolite inclusions exhibit 5 – 7 mm wide orthopyroxenite reaction zones with ITSM.

The mafic-ultramafic inclusions are interpreted to be of multiple origins (e.g., Vos and Moorhouse, 1965; Souch et al., 1969; Card and Pattison 1973; Rae, 1975; Pattison, 1979; Grant and Bite, 1984; Naldrett et al., 1984; Scribbins et al., 1984; Moore et al., 1993, 1994, 1995; Morrison et al., 1994; Corfu and Lightfoot, 1996; Lightfoot et al., 1997a, b; Farrell 1997; Zhou et al., 1997; Cohen et al., 2000; Wang et al., Ch3):

(1) **Cognate**: Anteliths derived from remnants of unexposed parts of the SIC (Naldrett et al., 1984) or earlier Sublayer cumulates (Lightfoot et al., 1997a, b; Farrell, 1997). Crystallization of any known SIC magma would not produce comparable olivine-orthopyroxene assemblages (Prevec, 2000), which has been interpreted to require contributions from i) mantle-derived magmas (e.g., Lightfoot et al., 1997a, b; Farrell, 1997), ii) unspecified more primitive magmas (Corfu and Lightfoot, 1996; Zhou et al., 1997), and/or iii) melted pre-existing mafic country rocks (Prevec, 2000; Prevec et al., 2000).

(2) **Local**: Xenoliths derived from local country rocks, including Nipissing diabase intrusions (Card and Pattison 1973), East Bull Lake suite intrusions (Pattison, 1979), and ultramafic bodies in the Levack Gneiss (Pattison 1979; Moore et al., 1993, 1994, 1995). However, no systematic comparison of petrography and geochemistry has been conducted for the inclusions and these target rocks.

(3) **Exotic**: Xenoliths derived from unexposed mafic-ultramafic intrusions (e.g., Rae, 1975; Kuo and Crocket, 1979; Scribbins, 1984; Morrison et al., 1994; Cohen et al., 2000; Wang et al., 2018).

There is no consensus on the mechanism(s) of formation of Sublayer, with some suggesting that it represents a mixture of splash-emplaced impact melt and fragments driven up the walls of the crater (Pattison, 1979), and some suggesting that it crystallized from a hybrid melt formed either by mixing between the impact melt and a mantle-derived high-Mg magma (Naldrett and Kullerud, 1967; Naldrett et al., 1984; Zhou et al., 1997) or mixing between the impact melt and a basaltic melt derived by melting mafic footwall rocks (Golightly, 1994; Lightfoot et al., 1997a; Prevec, 2000; Prevec et al., 2000; Prevec and Cawthorn, 2002).

Because Ni-Cu-PGE mineralization is so closely associated with Sublayer, FWBX, and IQD, in particular parts containing mafic-ultramafic inclusions, understanding the formation of Sublayer, FWBX, and IQD, and the origin of the mafic-ultramafic inclusions are critical to understanding the genesis of the Ni-Cu-PGE mineralization in the SIC. The mineralization in many magmatic Ni-Cu-PGE deposits (e.g., Aguablanca: Tornos et al. 2001; Duluth: e.g., Ripley and Alawi, 1986; Noril'sk: e.g., Lightfoot and Zotov, 2007; Platreef: Kinnaird et al., 2005; Voisey's Bay: Li and Naldrett, 2000) is associated with

inclusions, so the results have wider implications and applications. This study builds on work by Wang et al. (2016, 2018) on shock metamorphic features in the mafic-ultramafic inclusions and by Wang et al. (Ch 3) on the mineralogy and geochemistry of the mafic-ultramafic inclusions, and focusses on the genesis of Sublayer and relationship between the Sublayer/mafic-ultramafic inclusions and the Ni-Cu-PGE mineralization.

4.3 Definition of Sublayer

Definitions and classifications of Sublayer, FWBX, and IQD have varied over the years with some workers considering them all to be facies of the same unit and some considering them to be fundamentally different. For example, Hawley (1962), Souch et al. (1969), and Pattison (1979) considered IQD and FWBX to be facies of Sublayer, but Lightfoot et al. (1997c) considered dike-hosted IQD (which has a QD matrix) to be separate from contact-associated Sublayer (which has a noritic matrix) and FWBX (which has an anatectic non-QD, non-noritic matrix). The principal characteristics of basal Main Mass norite, Sublayer, FWBX, and IQD are summarized in Table 4.1.

Sublayer is a mixture of varying proportions of three components:

1) Igneous-textured silicate matrix (ITSM) (0% in massive sulfide, up to 100% in barren inclusion-free Sublayer)
2) Silicate rock inclusions (0-50%, but locally up to 90%: Grant and Bite, 1984)
3) Magmatic Cu-Ni-Fe sulfide (0% in barren Sublayer, up to 100% in massive sulfide)

Sublayer and Main Mass norite share some geochemical similarities, but there are significant differences in major and trace element contents (Lightfoot et al. 1997c; Wang et al., Ch 3). However, given that Sublayer and IQD contain facies with similar populations of inclusions (Lightfoot et al. 1997b), that Sublayer and overlying Norite exhibit ambiguous cross-cutting

relationships indicating more-or-less simultaneous emplacement (Naldrett 1984), and that even where there are unambiguous cross-cutting relationships (e.g., inclusions of QD in IQD), the timing relationships are very tight, we consider Sublayer, Offset IQD, and Breccia Belt IQD to be facies of the same complex and dynamic unit.

The relative ages of Main Mass, Sublayer, and FWBX are complex and controversial. Sublayer only locally contains inclusions of Mafic Norite (Naldrett and Kullerud, 1967; Grant and Bite, 1984; Naldrett et al., 1984). The contact between Sublayer and FWBX is sometimes gradational (Naldrett et al. 1984; McCormick et al. 2002). Gregory (2005) noted that FWBX at McCreedy East grades upwards from (i) intact footwall rocks veined by sulfide, through (ii) angular unrotated clasts in a sulfide matrix, into (iii) subrounded (melted) rotated clasts in a sulfide matrix, into (iv) Sublayer. However, the contact may also be very sharp (e.g., Whistle: Carter et al., 2009; Fig. 4.2). Diapir-like bodies of FWBX locally extend upwards through Sublayer and into the basal Main Mass in the Levack Embayment (see Coats and Snajdr, 1984) and near the Gertrude Mine on the South Range (Fig. 4.3). It appears that Sublayer differs from FWBX mainly in the nature of the matrix (partially melted footwall rocks in FWBX, norite in Sublayer) and proportions of inclusion lithologies (mainly footwall rocks in FWBX, mainly variable proportions of footwall rocks and mafic-ultramafic inclusions in Sublayer).

Key Points:

1) Sublayer, FWBX, and IQD may all be barren, but are normally at least weakly mineralized.
2) All contain a wide variety of locally-derived inclusions.
3) All also contain “exotic” mafic-ultramafic inclusions, especially where mineralized.

4) Sublayer contains cumulus orthopyroxene and plagioclase and exhibits ophitic to locally porphyritic textures, indicating slower crystallization, whereas IQD exhibits finer-grained locally spherulitic and dendritic textures, indicating more rapid crystallization
5) Breccia Belt IQD and FWBX contain sulfide clasts, indicating reworking of previously crystallized sulfides.

4.4 Petrography of Igneous-Textured Sublayer Matrix (ITSM)

Igneous-textured Sublayer matrix (ITSM) is fine- to medium-grained subophitic to locally porphyritic norite, leuconorite, or gabbronorite (Naldrett and Kullerud, 1967). It comprises 30-50% cumulus orthopyroxene and 30-40% cumulus plagioclase laths with variable amounts of clinopyroxene, intercumulus quartz and/or micrographic intergrowths of quartz ± plagioclase ± microcline, biotite ± amphibole, iron oxides, and rare cumulus olivine (Naldrett et al., 1984; Lightfoot, 2016). In many cases pyroxenes are replaced by amphibole-chlorite-biotite-(talc) and plagioclase is locally replaced by sericite.

Major textural variants are described in Table 4.2.

1) Ophitic Sublayer is characterized by a fine-grained subophitic (non-cumulate) texture, abundant unzoned to weakly zoned plagioclase, variable orthopyroxene: clinopyroxene ratios, and variable quantities of interstitial quartz, granophyre, and microcline (Fig. 4.4A). Olivine with thin orthopyroxene rims is sporadically present (Fig. 4.4B; e.g., Whistle, Ella).
2) Cumulus orthopyroxene-rich Sublayer is generally coarser-grained than Ophitic Sublayer and characterized by the presence of abundant prismatic cumulus orthopyroxene (Fig. 4.4C).

3) Porphyritic orthopyroxene-rich Sublayer is similar to cumulus orthopyroxene-rich Sublayer, but is characterized by large prismatic phenocrysts of orthopyroxene (Fig. 4.4D). In some localities these contain abundant blebby exsolution clinopyroxene.

Where detailed petrography has been done (e.g., Whistle and proximal Foy Offset: Pattison 1979), the amount of felsic and interstitial material increases towards the footwall contact, primary (non-xenocrystal) olivine is present only in quartz-free zones adjacent to the upper contact with the main SIC (Fig. 4.4B), and there is an increase in Fe: Mg ratio of both clino- and orthopyroxene towards the footwall contact. These variations suggest that the lower parts of Sublayer have been contaminated by assimilation of underlying rocks.

Sublayer contains highly variable abundances (trace-100%) of Fe-Ni-Cu sulfides (monoclinic and lesser hexagonal pyrrhotite, pentlandite, chalcopyrite, pyrite, and lesser cubanite, bornite, millerite) and a wide variety of minor antimonides, arsenides, bismuthides, tellurides, and native metals (e.g., Cabri and Laflamme, 1976; Naldrett, 1984). Sulfide textures in well-preserved, undeformed sections (e.g., Murray Mine: Souch and Podolsky 1969) vary downwards from disseminated, coarse disseminated (less common in Sublayer than in IQD), through matrix-textured to semi-massive and massive. Sulfide-poor Sublayer is typically richer in pyrrhotite and poorer in chalcopyrite and PGMs than sulfide-rich Sublayer (or IQD or FWBX).

4.5 Distribution of Sublayer

Sublayer is localized within depressions at the base of the Main Mass, some of which are broad and shallow and referred to as embayments (e.g., Levack, Trill), some of which are narrow and deep and referred to as troughs (e.g., Creighton), and some of which are troughs to offset dikes (e.g., Foy, Whistle), but some dike troughs do not contain Sublayer (e.g., Copper Cliff). The

thickness of Sublayer is highly variable and is related to topography along the footwall contact: no Sublayer is present along relatively planar segments of the contact; it is 10-100m thick within shallow embayments (e.g., Little Stobie, Murray), and it may be up to 700m thick within major embayments (e.g., Whistle; Trill).

Table 4.3 summarizes the geological features of major Sublayer-hosting structures on the North and South Ranges. The Whistle embayment is described in detail below as a representative North Range occurrence, and the Little Stobie embayment is described in detail as a representative South Range occurrence.

4.5.1 Whistle Embayment

The Whistle Embayment has been described by Pattison (1979), Grant and Bite (1984), Farrell (1997), Lightfoot et al. (1997a, b), Murphy and Spray (2002), and Carter et al. (2009). It is a trough-shaped depression in the northeast corner of the SIC (Fig. 4.2), which is ~350m wide at the contact with the Main Mass, and extends outwards into Whistle offset dike and possibly correlates with the fault-displaced Parkin offset dike. It is filled with Sublayer that grades upward into Mafic Norite over a distance of less than 1m (Pattison, 1979; Lightfoot, 2016) and is underlain by mobilized FWBX (referred to as “metabreccia” by some authors) of the Whistle dike, which contains discontinuous lenses and pods of quartz diorite (Pattison, 1971; Farrell, 1997; Carter et al., 2009; Lafrance et al., 2014).

Pattison (1979) noted a zonation in the Sublayer norite, with orthopyroxene-rich igneous Sublayer along the SE margin, more siliceous Sublayer along the NW margin, and rare olivine-bearing Sublayer only occurring immediately below Mafic Norite. Grant and Bite (1984) noted an increase in quartz-rich Sublayer as the embayment narrows into the Whistle offset dike. The Sublayer matrix generally contains disseminated sulfides, but massive sulfides occur along the

margins (Farrell, 1997). Sulfides in the Whistle embayment are predominantly pyrrhotite, with granular pentlandite and occasional 1 mm – 1 cm pyrite porphyroblasts (up to 5 modal percent of the total sulfide: Lightfoot et al., 1997b; Lightfoot, 2016), and sulfides tend to be richer in chalcopyrite towards the base of the embayment (Lightfoot et al., 1997a).

The inclusion population comprises: (1) abundant oxide-rich fine-grained diabase (Farrell, 1997); (2) common mafic-ultramafic inclusions (melanorite, olivine melanorite, and highly altered metapyroxenite: Farrell, 1997); (3) rare (<1% of all inclusions) altered anorthosite, gabbro, footwall gneiss, and leucocratic pods (Lightfoot, 2016). No inclusions of dunite, peridotite, harzburgite, or websterite were observed in the Whistle pit (Farrell, 1997). The diabase inclusions are commonly a few centimeters in size (rare up to 1 meter), and tend to have sharp contacts with the Sublayer matrix. Lightfoot (2016) indicated that the diabase inclusions are texturally and mineralogically similar to the 1 – 30 m thick diabase bodies (e.g., Matachewan diabase dikes) exposed in the footwall rocks of the Whistle Mine. The mafic-ultramafic inclusions range in size from five centimeters to several meters. The contacts between the mafic-ultramafic inclusions and ITSM can be sharp and defined by slickensided surfaces to broadly gradational over a few centimeters and defined by a change in grains size and texture (coarse-grained and cumulate-poikilitic texture in the inclusions and medium-grained porphyritic texture in ITSM) (Farrell, 1997). The olivine melanorite and melanorite inclusions commonly contain weakly disseminated (<0.5%) to blebby or patchy (>1%) sulfides (Farrell, 1997). In contrast, pyroxenite inclusions tend to have sharp margins and are broken-up by veins of pyrrhotite (Lightfoot et al., 1997a).

4.5.2 Little Stobie Deposit

The geology of the Little Stobie Mine was described by Davis et al. (1984) from which most of this section is taken. It is located in Blezard Township on the South Range of the SIC, ~ 5 km north of downtown Sudbury. The Little Stobie ore deposit is located in a shallow embayment with a strike length of 670 m and an average thickness of 90 m that projects into the footwall rocks up to 520 m. The contact between the Sublayer and the hanging-wall quartz-rich norite is generally gradational and defined by the increasing abundance of inclusions and sulfides in the Sublayer, whereas the contact between the Sublayer and the footwall is abrupt.

Sublayer norite is fine- to medium-grained and consists on average of 46% lathy plagioclase, 25% prismatic to subophitic clinopyroxene and orthopyroxene, 13% quartz, 9% hornblende, and 7% biotite. Sulfides in the Little Stobie Mine exhibit disseminated, stringer, and massive textures, and mainly comprise pyrrhotite, chalcopyrite, and pentlandite. There are two major orebodies. Number 1 occurred along the contact between the Sublayer and the footwall and extended 610 m along the contact, whereas Number 2 occurred as an appendage almost perpendicular to the Number 1 orebody and protruded 520 m into the footwall.

The inclusion population included predominantly two-pyroxene gabbros, less abundant ultramafic inclusions, minor quartz-rich norites with interstitial sulfide, and locally-derived metavolcanic, metamorphosed basalt and granite inclusions. The two-pyroxene gabbro inclusions ranged from ~2 cm to ~50 m in diameter, and were rounded to sub-rounded in shape. The ultramafic inclusions consisted of harzburgite, olivine orthopyroxenite, orthopyroxenite, olivine melatroctolite, and melanorite, and were small and generally rounded in shape. They were often rimmed by amphibole, talc, chlorite, or biotite. The two-pyroxene gabbro, ultramafic inclusions,

and footwall-derived inclusions were generally barren, but contained rare sulfide fracture fillings. In contrast, the quartz-rich norite inclusions contained interstitial sulfides.

4.6 Geochemical characteristics of Sublayer

ITSM is relatively constant within individual embayments, but varies from embayment to embayment (Lightfoot, 1997a). It normally ranges between 4 and 12% MgO, but an orthopyroxene-porphyritic facies at Creighton ranges up to 17% (Lightfoot et al., 1997a). ITSM on the North Range generally has higher Mg than that on the South Range, except for the orthopyroxene-rich facies at Creighton. In general, Fe increases with increasing Mg and Al-Na-(Ti) and decreases with increasing Mg. Calcium exhibits two overlapping trends: one in which Ca increases with increasing Mg (North and South Ranges) and one in which Ca decreases with increasing Mg (North Range only). These trends suggest that ITSM has accumulated orthopyroxene (North Range only) and/or clinopyroxene (North and South Ranges).

The trace element composition of ITSM in the Whistle trough is systematically different from that of the felsic norite in the Main Mass, e.g., less enrichment of HILE, lower Zr-Nb-Ta-Th-U contents, and flatter HREE patterns (Lightfoot et al., 1997b). The trace element patterns of ITSM at Whistle and McCreedy West on the North Range are mostly similar, whereas the patterns of ITSM at Creighton, Little Stobie, and Crean Hill on the South Range are different from to each other and from those on the North Range (Lightfoot, 2016).

Geochemical and mineral chemical characteristics of ITSM and mafic-ultramafic inclusions are described in detail in Wang et al. (Ch3). Here we summarize the most important features and origins of the mafic-ultramafic inclusions, as listed in Table 4.4.

(1) Anteliths ("cognate xenoliths") comprise Group I igneous-textured olivine melanorite and olivine melagabbronorite inclusions in the Whistle and Levack (Onaping Depth and Dowling) embayments. They similar Nb/U, Zr/Hf, and Nb/Ta ratios and εNd values as ITSM. This suggests that Group I inclusions are most likely anteliths, but as noted by Prevec (2000) and Prevec et al. (2000), the abundance of olivine requires a contribution from a more mafic component. Based on the Os isotopic data, this component may have crystallized from a magma derived by partial melting of older crustal rocks with low Re/Os ratios and unradiogenic Os isotope compositions (Wang et al., Ch3).

(2) Local xenoliths comprise Group IIA shock metamorphosed and recrystallized wehrlite – olivine clinopyroxenite inclusions in the Levack embayment and Group IIB shock metamorphosed olivine melanorite inclusions in the Foy offset dike. Group IIA inclusions have more pronounced negative Th-U and Zr-Hf anomalies, more variable Nb/U ratios, and wider range of subchondritic Zr/Hf ratios and superchondritic Nb/Ta ratios relative to ITSM, but similar trace element characteristics (e.g., negative Th-U, Nb-Ta-(Ti), Sr, and Zr-Hf anomalies) compared to a layered mafic-ultramafic body in the footwall of Levack and Fraser deposits. They likely represent fragments from a local mafic-ultramafic intrusion that was petrogenetically related to the layered mafic-ultramafic intrusion in the footwall of Levack-Fraser mine. Group IIB inclusions are characterized by much lower abundances of trace elements, insignificant HILE enrichment, moderate Nb-Ta depletion, no Th-U, Zr-Hf, or Ti anomalies, and much less REE fractionation relative to ITSM, but have Zr/Y, Zr/Nb, Nb/U, Ta/Yb, and Th/Yb

ratios similar to Group IIA inclusions. Group IIB are most likely also local xenoliths derived from a now-consumed or now-hidden source.

(3) Exotic xenoliths comprise Group III phlogopite/feldspar lherzolite and olivine gabbro inclusions in the Trill, Levack, and Bowell embayments and the Foy offset dike. They define no equivalents in the exposed country rocks. Phlogopite lherzolites are characterized by more significantly negative Th-U and Sr anomalies, greater LREE/HREE fractionation, and significantly lower Nb/U ratios, and feldspar lherzolites are characterized by lower absolute abundances of trace element and lower Nb/U ratios compared to ITSM. Feldspar lherzolites in the Trill embayment exhibit orthopyroxene reaction rims against ITSM, suggesting disequilibrium with the impact melt, and one composite inclusion exhibits igneous layering of feldspar lherzolite and olivine gabbro, suggesting derivation from one or more unexposed layered mafic-ultramafic intrusion(s). The calculated parental magma is similar to continental arc basalt formed by approximately 5% batch melting of garnet peridotite. Ol-Cpx-Pl geobarometry indicates crystallization at low pressure (210 – 240 MPa, equivalent to a depth of 7.7 – 10.9 km: Wang et al., 2018) and relatively high temperatures (1050 – 1120°C), and therefore a relatively shallow excavation depth (Wang et al., 2018). The majority of Group III inclusions appear to be derived from deeper mafic-ultramafic protoliths, except for the shock metamorphosed feldspar lherzolite, which failed to conduct gaobarometry calibration due to shock- and thermal-induced disequilibrium, and is characterized by more enrichment of Ni in olivine (NiO ~ 0.4% vs 0.1 – 0.2%) and very low Gd/Yb_N (1.06 vs 2.20 – 4.75) compare to the igneous feldspar lherzolite in Group III. Although it is difficult to draw any certain conclusion with limited information, it appears that this

shocked metamorphosed feldspar lherzolite may have been derived from shallower and hidden protolith.

The majority of ITSM contains relatively high S (0.2 – 8%) in ITSM exhibits a positive correlation between Ni and S, suggesting that the Ni content is mainly controlled by magmatic sulfide, particularly pentlandite. The mafic-ultramafic inclusions contain few if any sulfides (Ni < 1000 ppm, S < 0.5%; Fig. 4.5) (e.g., Farrell, 1997; Lightfoot et al., 1997b), except for melanorite and olivine melanorite anteliths in the Whistle embayment, which contain disseminated or net-textured Fe-rich sulfides (Ni = 200 – 2000 ppm, S = 0.5 – 3%; Fig. 4.5), and gabbro inclusions in the Little Stobie Mine, which contain fine disseminations and/or fracture fillings of sulfide (Wang et al., Ch 3; Davis, 1984). Naldrett and Kullerud (1967) noted that disseminated sulfides throughout the matrix of the Strathcona Embayment preferentially encircle inclusions, but never occur in appreciable amounts within the inclusions.

4.7 Isotope Geochemistry of Sublayer

The Sm-Nd, Lu-Hf, Pb-Pb, S, and Re-Os isotope geochemistry of Sublayer, Main Mass, and country rocks provide additional constraints on the origin of the inclusions.

4.7.1 Sm-Nd Isotopes

The Sm-Nd isotopic compositions of SIC lithologies, mafic-ultramafic inclusions in Sublayer and IQD have been studied by Faggart et al. (1985), Lightfoot and Naldrett (1989), Dickin et al. (1992, 1996, 1999), Jolly et al. (1992), Prevec et al. (2000), and Prevec and Baadsgaard (2005), and are plotted as $\varepsilon Nd_{1850\ Ma}$ values in Figure 4.6. Excluding several outliers, $\varepsilon Nd_{1850\ Ma}$ values for all SIC lithologies, mafic-ultramafic

inclusions (regardless of inclusion type or locality), and the mafic-ultramafic intrusions in the footwall of the Levack and Fraser deposits range between -11 and -4. Plagioclase-phyric basalt and gabbro inclusions range -9.5 to -8.5 and -6 to -1, Nipissing Diabase ranges -10.5 to -3, Thessalon volcanic rocks range -12 to -6, EBLI intrusions in Falconbridge and Drury Townships range -6 to -1, and two Levack Gneiss samples range -11 to -9. Main Mass lithologies are mainly -10 to -7, ITSM is mainly -10 to -4, and Sublayer/IQD inclusions -8 to -5.

The data confirm a strong continental crustal signature for all components of the SIC (e.g., Faggart et al., 1985; Dickin et al., 1992; Prevec et al., 2000), including all of the mafic-ultramafic inclusions. Only two McCreedy West ITSM samples with near-zero $\varepsilon Nd_{1850\ Ma}$ values provide evidence for a more primitive contaminant (Prevec et al., 2000).

4.7.2 Lu-Hf Isotopes

No Sublayer inclusions have yet been analyzed for Lu-Hf isotopes, but Darling and Moser (2012) and Kenny et al. (2017) showed that offset dikes and Main Mass lithologies on the North and South Ranges vary narrowly between +9 and +12 $\varepsilon Hf_{1850\ Ma}$ and that target rocks vary widely between -40 and +2 $\varepsilon Hf_{1850\ Ma}$. This requires the melt sheet to have been homogenized during impact mixing and/or during subsequent convection. Kenny et al. (2017) attributed the greater homogeneity of the Hf isotopic system to it being much less volatile than Pb (or S: see below) and therefore much less susceptible to modification during post-impact thermomechanical erosion.

4.7.3 Pb-Pb Isotopes

The Pb-Pb isotopic compositions of Sudbury ore sulfides, Main Mass and offset lithologies, and country rocks have been studied by Dickin et al. (1992, 1996), Darling et al. (2010a, 2010b, 2012), and McNamara et al. (2017). On average, North Range Main Mass has a less radiogenic Pb isotope composition with a $\Delta^{207}Pb/^{204}Pb$[1] frequency peak at +325, whereas the South Range Main Mass has a frequency peak at +425 (fig. 10 in McNamara et al., 2017), but there are significant isotopic variations from range to range (-22 to 98 for North Range mines vs -57 to +516 for South Range mines: Dickin et al., 1996) and from embayment to embayment (e.g., -20 to -57 for Frood mine, +168 to +360 for Falconbridge mine), whereas granophyre has a much more homogeneous Pb isotopic composition (+310 to +375: McNamara et al., 2017). The Huronian Supergroup (footwall to the South Range) has a $\Delta^{207}Pb/^{204}Pb$ frequency peak at +550; East Bull Lake Intrusive Suite ranges from 50 to 400 $\Delta^{207}Pb/^{204}Pb$; Nipissing Diabase ranges from +525 to +575 $\Delta^{207}Pb/^{204}Pb$; the Superior Province (footwall to the North Range) has a $\Delta^{207}Pb/^{204}Pb$ frequency peak at +50; Onaping Formation (assimilated by the upper felsic melt) corresponds to the vast majority of the granophyre of the Main Mass. The $\Delta^{207}Pb/^{204}Pb$ of South Range ores occurs between the Pb isotopic compositions of South Range Main Mass and the Nipissing and the East Bull Lake Intrusive Suites (McNamara et al., 2017), whereas the $\Delta^{207}Pb/^{204}Pb$ of North Range ores occurs between the Pb isotopic compositions of North Range Main Mass and East Bull Lake Intrusive Suite (McNamara et al., 2017). North Range mafic norite is less radiogenic than overlying felsic norite but is similar to North Range ores, suggesting that

[1] $\Delta^{207}Pb/^{204}Pb = 1000 * (^{207}Pb/^{204}Pb_{sample} - {}^{207}Pb/^{204}Pb_{Isochron})$. The $^{207}Pb/^{204}Pb_{Isochron}$ is referred to Kramers and Tolstikhin (1997) at 1.85 Ga, which is defined as $0.113 * {}^{206}Pb/^{204}Pb_{sample} + 13.199$.

mafic norite is more closely associated with the Sublayer and sulfide ores than overlying Main Mass.

Dickin et al. (1992, 1996, 1999) attributed larger-scale variations in the Pb isotopic compositions of the ores on the North and South Ranges to heterogeneities in the target rocks and smaller-scale variations to incomplete homogenization of the melt sheet. Darling et al. (2010a, 2010b) suggested that some large-scale variations in target lithologies were preserved in the melt sheet, but that small-scale heterogeneities reflected digestion of local target-rocks, fallback material, and entrained clasts. McNamara et al. (2017) and Kenny et al. (2017) suggested that the melt sheet may have been originally more homogeneous in Pb isotopic composition and that volatilization of Pb during impact made the Pb system more sensitive to incorporation of Pb during subsequent post-impact thermomechanical erosion of isotopically heterogeneous footwall rocks.

4.7.4 S Isotopes

The mass-dependent ^{32}S and ^{34}S isotopic compositions of sulfides in Sudbury ores, Sublayer, Main Mass, and overlying and underlying rocks have been studied by Thode et al. (1962), Schwarcz (1973), Whitehead et al. (1990), Papineau et al. (2007), Ames et al. (2010), Tuba et al. (2014), and Ripley et al. (2015) and are plotted in Figure 4.7. North and East Range ores vary primarily between +2 and +4 ‰ $\delta^{34}S$; South Range ores vary primarily between 0 and +3 ‰. Main Mass norites vary less, but East Range and North Range Main Mass are slightly heavier than South Range and West Range Main Mass. Huronian sulfides range widely between -12.5 and +31.2 ‰, but are mostly within the range from -0.8 to +5.9 ‰.

There are also significant heterogeneities in the basal norite, Sublayer, and Footwall rocks. For example, Crean Hill norite ranges -1.0 to +3‰ $\delta^{34}S$, whereas Crean Hill Sublayer ores range -2.0 to 1.2 ‰ $\delta^{34}S$. Creighton Sublayer ores range +0.8 to +3.6 ‰ $\delta^{34}S$, whereas Creighton footwall ores range -1.0 to +3.9 ‰ $\delta^{34}S$. Garson contact ores range +0.2 to +2.5 $\delta^{34}S$, whereas Garson Ramp ores range +0.2 to +1.4 $\delta^{34}S$. Levack Sublayer ores and Levack footwall ores both range from +0.8 to +4.4 ‰ $\delta^{34}S$, except for a few outliers at -2.1 ‰ and +7.2 ‰ $\delta^{34}S$. There does not appear to be any correlation between S isotope composition and the overall grade or tonnage of sulfide mineralization: high-grade and low-grade deposits have similar ranges in $\delta^{34}S$ (Ripley et al., 2015).

4.7.5 Re-Os Isotopes

The Re-Os isotopic compositions of sulfides in Sublayer, mafic-ultramafic inclusions, and some country have been studied by Walker et al. (1991), Dickin et al. (1992, 1999), Cohen et al. (2000), and Morgan et al. (2002), and are plotted as $\gamma Os_{1850\ Ma}$ values in Figure 4.8. Most of the analyzed contact and proximal footwall ores range between 0 and +750, but Strathcona Deep Copper footwall ores vary between -490 and +1190 $\gamma Os_{1850\ Ma}$. Some Sublayer inclusions fall within this range, but several S-rich gabbro and S-poor melanorite inclusions from Whistle range down to -250. Copper Cliff rhyolite and McKim metasediment in the footwall of the South Range range between +300 and +480, similar to South Range ores. Huronian granitoids and sediments range widely between +1660 and +930. Levack gneiss in the North Range footwall is +330, similar to North Range ores.

The moderately to highly radiogenic $\gamma Os_{1850\ Ma}$ values of the sulfides in Sublayer indicate that the Os was derived largely from old crust, not the mantle or young crust (see Walker et

al., 1991, 1994; Dickin et al., 1992). Small but significant variations in Os isotopic compositions of sulfides from different mines and different parts of the same mines have been attributed to assimilation of local wall rocks with different Os isotopic compositions (Walker et al., 1991, 1994; Cohen et al., 2000) or to fractional crystallization of MSS (Morgan et al., 2002). Rhenium is less compatible in MSS than Os ($D_{Re/Os}^{\frac{\text{MSS}}{\text{sulfide } melt}} \sim 0.5$: Liu and Brenan, 2015), so residual sulfide melts end up with higher Re/Os ratios. Sulfur and Pb isotopic data are not available for the same samples, but some ores have anomalous S (e.g., Crean Hill contact, Levack contact, Levack footwall, Lindsley, Victor 42N: Ripley et al., 2015) and Pb-Pb (e.g., Blezard footwall, Morrison footwall: McNamara et al., 2017) isotopic ratios, which should not change during fractional crystallization, so it seems equally likely that the variations in Re-Os isotopes also result from local contamination.

Returning to the question of the source, Re is less compatible than Os during mantle melting (Walker et al., 1989). Subcontinental lithospheric mantle from which substantial fractions of partial melt have been removed will consequently evolve to negative γOs values (Walker et al., 1989; Carlson and Irving, 1994). As a result, the negative $\gamma Os_{1850\ Ma}$ values of the S-rich mafic and S-poor melanorite inclusions in the Whistle Mine are compatible with a parental magma derived from a Re-depleted peridotitic lithospheric mantle source (see e.g., Ellam et al., 1993; Lambert et al., 1994). These inclusions have unradiogenic Os (negative γOs), which is indicative of a Re-depleted peridotitic mantle source (Marques et al., 2003) or from older crustal rocks with low Re/Os ratios and unradiogenic Os isotopic composition (see Cohen et al., 2000), but also unradiogenic Nd (negative εNd), which is indicative of a crustal source. This isotopic feature is similar to the Ipuera-Medrado chromite deposits in Brazil, which have been interpreted to be formed

from magmas derived from old Re-depleted subcontinental lithospheric mantle (SCLM) that experienced metasomatic enrichment of the incompatible lithophile elements by subduction input (Marques et al., 2003). However, the highly unradiogenic Nd signature argues against a direct contribution from SCLM. Instead, older crustal rocks, e.g., Archean volcanic and subvolcanic rocks in this region, which has been proposed to be derived from a subduction-metasomatized lithospheric mantle (Jolly, 1987; Jolly et al., 1992; Ketchum et al., 2013) must have been sampled during the impact.

4.8 Discussion

The key issues are 1) the relative timing of QD, IQD, FWBX, Sublayer, and Main Mass Norite; 2) the relationship between mafic and ultramafic inclusions and mineralization; and 3) the genesis of Sublayer. Each is discussed below.

4.8.1 Relative Timing of QD, IQD, FWBX, Sublayer, and Main Mass Norite

The relative timing of Sublayer is equivocal, with some workers suggesting that it predates overlying Main Mass norite (e.g., Pattison 1979) and others suggesting that it post-dates Main Mass norite (e.g., Naldrett and Kullerud 1967, Hewins, 1971; Muir, 1981; Dressler, 1982; Grant and Bite, 1984; Naldrett et al., 1984).

The key constraints are:

1) IQD and FWBX contain inclusions of Sudbury Breccia (e.g., Coats and Snajdr, 1984), so they formed after Sudbury Breccia. Sublayer less clearly cuts Sudbury Breccia, which is generally metamorphosed close to the SIC and therefore difficult to

distinguish from Footwall Breccia, but there are probable examples at the Little Stobie Mine (see Davis, 1984) and Whistle (see Carter et al., 2009).

2) The occurrence of inclusion- and sulfide-free QD in the distal parts and along the margins of composite QD-IQD dikes and some embayments, and the similarity of QD to weighted bulk average SIC (Lightfoot et al., 1997a, b) and to average least-altered vitric Onaping (Ames et al., 2002), indicate that QD was the first phase of the SIC to crystallize.

3) IQD contains inclusions of QD, so must have been emplaced after QD.

4) QD, IQD, and some Sublayer have fine-grained non-cumulate matrices (occasionally glassy to aphanitic in the case of QD), whereas most Sublayer contains cumulus orthopyroxene-plagioclase. This indicates differences in cooling rates – faster in the case of QD and IQD, slower in the case of Sublayer – but a common parental magma.

5) Some offset dikes contain Sublayer in their Main Mass-proximal parts (e.g., Foy, Whistle), but many do not (e.g., Copper Cliff, Ministic, Trill, Worthington). Similarly, some offset dikes contain mobilized FWBX in their Main Mass-proximal parts (e.g., Foy, Frood-Stobie, Trill, Whistle), but many do not (e.g., Copper Cliff, Ministic, Worthington).

6) Sublayer transgresses FWBX in the Whistle offset (Carter et al., 2009).

7) Contacts between Sublayer and overlying Main Mass Norite are often sharp and unchilled or unbaked. Outcrop exposures are rare and drill core intersections cannot distinguish between a younger apophysis or an older inclusion.

8) The similarity in the inclusion populations of Sublayer, IQD, and FWBX indicates that they are facies derived from a common precursor. Sublayer contains more ultramafic inclusions than IQD or FWBX. This means that the sources of the non-cognate ultramafic inclusions, which are rarely exposed (e.g., Fraser ultramafic body) and most likely derived from ultramafic bodies exposed in the deeper levels of the crater, must have been eroded after the formation of QD and IQD.

9) The Frood deposit is hosted by intermixed zones of IQD and FWBX with abundant ultramafic inclusions (Zurbrigg, 1957) and therefore appears to be an IQD-FWBX hybrid.

10) Sublayer contains fragments of FWBX (Pattison, 1979), but does not appear to contain fragments of QD, IQD, or SUBX. SUBX, QD, and the matrix to IQD would have been easily melted, leaving a melt that would be easily mixed or assimilated and (in the case of IQD) inclusions that would no different than those in Sublayer.

11) Sublayer and IQD differ mainly in the nature of the matrix and location. The location of IQD in dikes that emanate from the Main Mass suggests that IQD was emplaced prior to formation of Sublayer and cooled more rapidly, forming a QD matrix. Sublayer formed simultaneously or later and cooled more slowly, forming a noritic matrix.

12) FWBX may contain QD-like post-impact “melt pods” but contains no QD or noritic matrix, so it must have acquired the inclusions by incorporating them from footwall rocks during the thermomechanical erosion process or from overlying Sublayer norite. Late-stage FWBX cross-cuts Sublayer and Main Mass norite (e.g., Hwy 144 Bypass).

The timing of formation of the various elements of the SIC implied by these relationships are summarized in Table 4.5, indicating that Sublayer, IQD, and FWBX formed more-or-less contemporaneously over relatively wide time intervals. The greater geochemical heterogeneity, greater angularity of inclusions, and greater amounts of cumulus orthopyroxene-plagioclase in Sublayer relative to IQD are interpreted to reflect different cooling rates and system dynamics. Sublayer cooled more slowly, so was able to assimilate more inclusions, and was initially part of the Main Mass, so was able to accumulate more orthopyroxene and expel more residual silicate melt. In contrast, IQD cooled more rapidly, so was able to assimilate fewer inclusions, and was isolated from the Main Mass, so was able to accumulate less orthopyroxene and expel less residual silicate melt.

4.8.2 Relationship between Mafic-Ultramafic Inclusions and Ni-Cu-PGE Mineralization

Many magmatic Ni-Cu-PGE deposits, particularly those hosted by mafic magmas, contain mafic-ultramafic inclusions (see reviews by Lesher, 2017, 2019b), but only at Sudbury is there a very specific association with mafic and ultramafic inclusions. There are two possible explanations for this:

1) The inclusions and sulfide melts may be derived from the same source (e.g., pre-existing sulfide-bearing mafic-ultramafic rocks). Although EBLI and Nipissing gabbro contain abundant disseminated (e.g., Bullfrog Zone: James et al., 2002) and locally net-textured Fe-Cu-Ni sulfides (e.g., Shakespeare: Sproule et al., 2007), none of the ultramafic inclusions examined in this study or reported by Scribbins (1978), Rae (1975), or Naldrett et al. (1984) contain any sulfides. One explanation for this is that an inclusion containing Fe-sulfides

would begin melting and disaggregating at ~ 900 ºC (Naldrett, 1969), whereas a sulfide-free gabbroic inclusion would begin melting and disaggregating at ~ 1100 ºC (Salvioli-Mariani et al., 2002), and a sulfide-free peridotitic inclusion would begin melting and disaggregating at ~ 1300 ºC (Hirose and Kushiro, 1993; Takahashi et al., 1993). Thus, sulfide-free peridotitic (and dunitic) inclusions or domains of inclusions would be favoured for preservation in the superheated impact melt.

2) The association may be physical, attributable to hydrodynamic equivalence of larger ultramafic inclusions and smaller sulfide blebs. Relative settling velocities (Fig. 4.12: discussed below), indicate that larger but lower density ultramafic inclusions (~ 2.9 g cm^{-3}: Murase and McBirney, 1973) will settle at the same rate as smaller but higher density sulfide droplets (~ 4.2 g cm^{-3}: Dobrovinski et al., 1969; Mungall and Su, 2005). Given the wide range of inclusion sizes and wide ranges in the abundances of the different phases (silicate melt, sulfide melt, and inclusions) in Sublayer, the results broadly agree with the observed median sizes of ultramafic inclusions (~10 cm) and sulfide droplets (2-3 cm). This interpretation is also consistent with i) the association of mineralization with several different types of barren mafic and ultramafic inclusions, some anteliths, some derived from local footwall rocks, and some derived from deeper unexposed lithologies, ii) the absence of Ni depletion in any of the olivines, and iii) no positive correlation between Ni and S in the majority of mafic-ultramafic inclusions, except for olivine melanorites containing disseminated sulfides. It may also explain why Sublayer along the margins of embayments (e.g., western margin of Levack Embayment) contains only very sparse sulfides and very few ultramafic inclusions.

Thus, the association between mafic and ultramafic inclusions and mineralization can be most likely attributed to the refractory nature of the inclusions and to similarly high densities as smaller molten sulfide droplets.

4.8.3 Genesis of Sublayer Mineralization

There are two end-member models for the formation of mineralized Sublayer, which are not mutually exclusive:

1) Exsolution of immiscible sulfide droplets from the cooling impact melt (e.g., Keays and Lightfoot, 2004; Li and Ripley, 2005), settling of sulfides and inclusions to the contact, and migration along the contact into topographic embayments driven by convective currents (e.g., Lightfoot et al. 2001; Keays and Lightfoot, 2004; Zieg and Marsh, 2005) and/or gravity-driven density flow (considered below). In this model the sulfides in the contact-footwall and offset ore systems exsolved from the melt sheet and modified by incorporating S from local country rocks.

2) Devolatilization of Pb (McNamara et al., 2017; Kenny et al., 2017), S (Lesher, 2019a), and other volatile elements (e.g., Hg-Tl-Cd-S-Se-Sn-Te-Zn-Pb-Bi- Sb-Ag-Cu-Au-As: Lesher et al., *in prep.*) during impact, homogenization of the impact melt (Ubide et al., 2017), thermomechanical erosion of footwall rocks by the superheated impact melt (Prevec and Cawthorn, 2002; Gregory, 2005), assimilation of miscible silicate components but only limited amounts of sulfide (see Lesher and Campbell, 1993; Lesher and Burnham, 2001; Lesher, 2017), and generation of immiscible sulfide xenomelts that were upgraded by reaction with the overlying melt sheet (Lesher, 2019a; Lesher et al., *in prep.*). In this model only the sparse sulfides in the lower Main Mass noritic rocks segregated from the overlying melt sheet.

In order to further test these models, we have evaluated the roles of assimilation, thermomechanical erosion, convective currents, and gravity currents in the formation of Sublayer.

4.8.4 Genesis of Sublayer Embayments

The embayments have been interpreted as pre-existing topographic features produced by impact friction and excavation (Morrison, 1984) and/or impact-induced features modified by thermomechanical erosion by superheated impact melt and sulfide liquid (Gregory, 2005).

4.8.4.1 Thermomechanical erosion

The thermal and physical properties of the superheated impact melt at 1700°C would have been similar to a komatiite (Table 4.6), so the rates of erosion should have been broadly similar at very beginning: of the orders of 0.7 – 1.5 m d^{-1} for a consolidated gabbroic substrate, 4.3 – 7.5 m d^{-1} for a consolidated felsic substrate, 5.5 – 23 m d^{-1} for a partly consolidated felsic substrate, and 95 – 130 m d^{-1} for unconsolidated volcanic or sedimentary substrates (Williams et al., 1998, 2001, 2011). However, the rate of erosion of impact melt rapidly decreases with temperature due to the significantly increasing viscosity as the impact melt cools (Table 4.6). The inferred rapid thermomechanical erosion rates suggest that this process should have played a significant role in the generation of inclusions in Sublayer, IQD, and FWBX especially when the melt sheet was superheated.

Mechanical erosion may have been more rapid if molten sulfides were present, as they are very dense and have a very low viscosity (Figs. 4.9 – 4.11), so they are easily able to infiltrate fractures in the footwall rocks, but because the rates of thermomechanical erosion by a superheated magma will be greater than the rates of heat conduction into the footwall rocks (see discussion by Huppert and Sparks, 1985; Williams et al., 1998) and because

sulfide melts solidify at temperatures below the liquidus of the impact melt, it is only during the later stages that sulfides will infiltrate the footwall rocks to form footwall breccia and footwall vein systems (Gregory, 2005).

4.8.4.2 Fluid dynamics

It is important to assess the physical properties and their implications for the fluid dynamic behaviour of the magma before investigating models involving thermomechanical erosion, convective transport, and gravitational flow of the mixture of impact melt, inclusions, and sulfides. In the case being considered here we are interested in the densities and viscosities of mixtures of impact melt, inclusions, and sulfide melt. There are many formulations for effective viscosity (see review by Petford, 2009). For example, assuming spherical particles and hexagonal-closest packing (e.g., Shaw, 1972) effective viscosity increases one order of magnitude with ~ 45% particles, two orders of magnitude with ~ 62% particles, three orders of magnitude with ~ 69% particles, and reaches infinite viscosity at ~ 74% particles (see Lesher, 2017). However, lavas rarely carry more than approximately 55 – 60% phenocrysts (Marsh and Maxey, 1985) and Vetere et al. (2010) determined experimentally that andesitic magmas become effectively rigid as their crystal loads approach 60%. Therefore, we take 60% as the maximum proportion of inclusions required to maintain mobility.

Relative densities (densities of mixtures of impact melt, inclusions, and sulfides divided by the density of pure impact melt) range between 1.0 for inclusion- and sulfide-free melt impact melt to 1.7 for massive Fe-Ni-Cu sulfide melt (Fig. 4.9). Because of the small changes in partial molar volume of particularly the impact melt and inclusions, these variations are unlikely to change significantly with temperature.

The estimated bulk viscosities of pure impact melt at 1 bar and temperature from 1700°C (superheated) to 1180°C (near-liquidus) were estimated using the methods of Giordano et al. (2008), which yield results of 2 Pa s at 1700°C and 507 Pa s at 1180°C. In order to estimate the bulk viscosity of a three-phase mixture of solid inclusions, more-viscous impact melt, and less-viscous sulfide melt, we can use the following equations (adapted from Phan-Thien and Pham, 1997):

if inclusions are smaller than sulfide droplets,

$$\eta 1 = \eta_m[1 - v_c/(1 - v_b)]^{-5/2}(1 - v_b)^{-1} \quad [1]$$

if inclusions and sulfide droplets are of the same size range,

$$\eta 2 = \eta_m(1 - v_c - v_b)^{-(5v_c+2\,v_b)/2(v_c+\,v_b)} \quad [2]$$

and if inclusions are larger than sulfide droplets,

$$\eta 3 = \eta_m[1 - v_b/(1 - v_c)]^{-1}(1 - v_c)^{-5/2} \quad [3]$$

where η = viscosity of the mixture, η_m = viscosity of the melt (in this case impact melt), v_s = volume fraction of the sulfide melt, and v_c = volume fraction of the inclusions.

Relative bulk viscosities (viscosities of mixtures of impact melt, inclusions, and sulfides divided by the viscosity of pure impact melt) at 1 bar and temperature from 1700°C (superheated) to 1180°C (near-liquidus) are shown in Figures 4.10 and 4.11, indicating that the relative viscosities of mixtures of impact melt, inclusions, and sulfides at 1700°C vary from 0.05 to 831 (Fig. 4.10), and at 1180°C vary from 0.0002 to 831 (Fig. 4.11).

The settling velocities of individual spherical inclusions at infinite dilution through the impact melt can be estimated from Stokes' Law:

$$V_{incl} = \frac{2g}{9\eta} \Delta\rho r^2 \quad [4]$$

where (V_{incl}) is settling velocity, $\Delta\rho$ is the density contrast between particle and fluid, g the gravitational acceleration, η is dynamic viscosity, and r is the radius of the particle. The settling velocities of molten sulfide droplets through the impact melt can be estimated using the Hadamard-Rybczinski equation (e.g., Clift et al., 1978):

$$V_{sul} = \frac{gr^2 \triangle\rho}{3\eta} \quad [5]$$

The effects of convective currents will be discussed below, but it is clear that sulfide melt droplets, mafic inclusions, and felsic inclusions carrying sulfides will sink through impact melt, quite rapidly at larger sizes, whereas felsic and mafic inclusions will rise quite rapidly in sulfide liquid and mineralized proto-Sublayer (mixture of 35% QD + 35% sulfide liquid +30% inclusions) (Fig. 4.12) (see also Lesher, 2017).

The settling velocities of sulfide droplets will decrease with increasing inclusion content (see Mungall and Su, 2005), but even a continuous network of silicate inclusions will float in massive sulfide melt and mineralized proto-Sublayer (Fig. 4.12). A typical contact ore segregation profile at Sudbury grades upward from massive sulfide through inclusion-bearing massive sulfide to disseminated sulfide in Sublayer norite (Souch et al., 1969), but many contain only semi-massive ores, suggesting (1) that they were congested suspensions with high effective viscosities, which would inhibit gravitational settling of sulfide droplets and floatation of felsic-mafic inclusions; and/or (2) that inclusions and sulfides continued to be added to Sublayer via assimilation or thermomechanical erosion. The overall low relative viscosities in the mixture of impact melt, inclusions, and sulfide droplets both at

1700°C and 1180°C suggest that the effect of thermomechanical erosion in the formation of embayments and incorporation of the local inclusions is more important.

4.8.5 Localization of Inclusions and Sulfide Liquid into Embayments

Two mechanisms could contribute to the horizontal transport of mixtures of silicate melt with inclusions and sulfide liquid into embayments: convective currents and gravity flow.

4.8.5.1 Convective currents

Zieg and Marsh (2005) suggested the topography of the crater floor "pinned" the upwelling limbs of convection cells over embayments and as convection became laminar, that settling immiscible sulfide droplets were swept up, concentrated, and suspended by the flow in these same upwelling sites above the embayments, which grew until they could no longer be suspended by the flow, producing a steady rain of sulfides into the embayments. Their model did not involve inclusions (which they suggested had melted to form viscous emulsions), which do not coalesce, but presumably inclusions with similar settling velocities would behave similarly. This model is difficult to test, as all physical evidence of convection has been erased, but the physics of the process has been discussed by Marsh and Maxey (1985), Martin and Nokes (1988, 1989), Marsh (1989), Zieg (2001), and Molina et al. (2012).

A quantitative evaluation is difficult because of uncertainties in the compositional structure of the melt sheet: 1) a single layer that fractionally crystallized to form the observed sequence of norite, gabbro, and granophyre (Lightfoot et al., 1997c), 2) segregated layers of impact melt containing mafic inclusions (protonorite) and impact melt containing felsic inclusions (protogranophyre) (Golightly, 1994), or 3) segregated layers of emulsified impact melt and melted mafic inclusions (protonorite) and emulsified impact melt and

melted felsic inclusions (protogranophyre) (Zieg, 2001; Zieg and Marsh, 2005). However, the likelihood that impact melt convected can be evaluated from the Rayleigh number:

$$R_a = \frac{\alpha g \Delta T d^3}{\eta K} \quad [6]$$

where α is thermal expansion coefficient, ρ the density, g the gravity acceleration, ΔT the temperature gradient, d the chamber thickness, K the thermal diffusivity, and η the dynamic viscosity. Using $\alpha = 5 \times 10^{-5}\ °C^{-1}$, $g = 980\ cm\ sec^{-2}$, $\Delta T = 600\ °C$, d = 2500 m, $K = 10^{-2}\ cm^2\ sec^{-1}$ (Zieg, 2001), and $\eta = 20\ g\ cm^{-1}\ sec^{-1}$ (at 1700°C) and $5070\ g\ cm^{-1}\ sec^{-1}$ (at 1180°C), the melt sheet as a whole will have a value of $Ra = 2.3 \times 10^{18}$ at 1700°C and 9.1×10^{15} at 1180°C, which is much greater than the critical Rayleigh number (Ra_c = 1000), indicating that the SIC vigorously convected, at least initially. Using d = 50 - 500 m (Zieg and Marsh, 2005; Lightfoot, 2016) for the thickness of a segregated proto-noritic layer, $Ra = 2.4 \times 10^{11} - 3.7 \times 10^{14}$, still well above the value required for vigorous convection. For a horizontal layer, the critical value of Ra is approximately 1700. The Ra value of the bottom proto-noritic layers is obviously much greater than Ra_c, suggesting that the proto-noritic layer could undergo vigorous laminar convection.

The convective velocity (U_o) is determined by the rate of heat transfer within the magma body (Marsh and Maxey, 1985):

$$U_o = 0.258\ \frac{K}{\mathrm{d}}\ Ra^{1/2} \quad [7]$$

The gradient representing a balance between the settling flux of particles by Stokes's law and the upward suspension of particles by convective flow is inversely proportional to S

(=V_{incl}/U_o). Convective currents play a significant role only if S<1. Figure 4.13 illustrates that sulfide droplets <0.5 cm and felsic-mafic inclusions <5 cm could be entrained and kept in suspension by vigorous convection. Sulfide droplets in a dynamic magma flow tend to break-up to smaller droplets (<0.2 cm: Robertson et al. (2015)), making them easier to transport, but if proximal to a sulfide source they may be larger and more difficult to transport. Similarly, inclusions with diameters >5 cm would be difficult to transport by convection, requiring another mechanism to localize inclusions in the Sublayer and IQD.

4.8.5.2 Gravity currents

Another option for localizing Sublayer in footwall embayments is for the dense mixture of impact melt, sulfide melt, and inclusions to flow under the influence of gravity along the gently sloping floor or locally steep walls of the impact crater into the embayments, much like a submarine debris flow (e.g., Pratson et al., 2000; Parsons et al., 2007; Wu et al., 2015).

The movement of gravity currents is governed by mass, fluid pressure forces, and friction forces (Pratson, 2000). Flow begins when enough mass is accumulated (due to deposition) and/or if fluid pressure forces are increased (e.g., during an earthquake), and stops if the slope is decreased (e.g., at the base of the slope). The fluid pressure and friction at the tail of the flow oppose the mass of the flow and prevent the head from spreading or travelling very far, but the head of the flow may separate from the tail, a process known as runout.

Gravity flow is complex and normally modelled using finite element methods (e.g., Wu et al., 2015), but it is very imprecise because of the wide variations in the physical properties (bulk density, effective viscosity, pore pressure), and environment (slope, topography), which are poorly constrained and which change over time. Because of all of the

uncertainties a fluid dynamic analysis is beyond the scope of this paper, but a comparison of the ranges of density and viscosity relative to QD for the range of proto-Sublayer compositions (0 - 100% sulfide, 0 - 60% inclusions, and 0 - 100% QD) compared to the ranges of density and viscosity relative to seawater for the range of submarine debris flows (Table 4.7), indicates that the relative density of proto-Sublayer is greater and that the relative viscosity is similar when the proportion of inclusions <45%, but that the relative viscosity is greater than the submarine debris flows when inclusions >45% .

The average slope of the continental shelf is 1 – 4 degrees (Lewis, 1971) and the slopes along the floors of most impact craters are less than 6 – 10 degrees (Mikereit et al., 2010), so it can be predicted that the proto-Sublayer would flow like a submarine debris flow only when the melt contained <45% inclusions.

4.8.6 Formation Models for the Sublayer, IQD, and Footwall Breccia

The following model is proposed to account for the formation of the SIC, with emphasis on the formation of Sublayer and IQD, as well as the entrainment of inclusions and genesis of Ni-Cu-PGE sulfide mineralization (Fig. 4.14).

T1 – Impact melting and emplacement of QD: A tremendous amount of energy was transferred into the target rocks during impact, producing a superheated impact melt with an initial temperature of ~1700^{o}C (Ivanov and Deutsch, 1999), which would be ~500°C above the liquidus (Fig. 4.16A). Significant amounts of Pb (McNamara et al., 2017; Kenny et al., 2017) and likely also Hg-Tl-Cd-S-Se-Sn-Te-Zn-Bi and lesser amounts of Sb-Ag-Cu-Au-As (Lesher, 2019a; Lesher et al., *in prep.*) were likely volatilized during impact relative to less volatile chalcophile (Co-Ni-PGE) and lithophile (e.g., Th-Nb-Ta-Hf-Zr-Y-REE) elements (Fig. 4.14A).

The impact excavation stage produced an upward-directed pressure gradient that expelled impact melt entraining xenoliths of shocked and unshocked rocks from the transient crater (Fig. 4.14A), leaving an inclusion-free melt at the base that was injected into impact-induced radial and concentric fractures, forming radial and concentric QD dikes (Fig. 4.16B). The composition of marginal/distal QD was modified by contamination during emplacement, but is close to the composition of the original impact melt (Lightfoot et al., 1997c). Xenoliths that were generated during impact excavation and mobilized under shock waves were preserved as exotic xenoliths due to their refractory nature.

T2 – Isostatic Readjustment and Generation of IQD and Offset Ores

Large transient craters are gravitationally unstable, resulting in uplift of the central parts and rapid collapse, and producing one or more rings separated by relatively flat circular basins (see reviews by Grieve et al., 1977, 1981). This process would have generated abundant clasts that would have cooled the impact melt as they were gradually digested, but additional clasts would have been generated by thermomechanical erosion of the footwall rocks by the superheated impact melt. Most of the footwall rocks contained minor sulfides (Huronian basalts and sediments) and some contained significant amounts of sulfides (e.g., Nipissing Intrusive Suite, East Bull Lake Intrusive Suite), leading to rapid sulfide saturation and formation of xenoliths (most as local xenoliths and some as exotic xenoliths if their protoliths were completed eroded) and sulfide xenomelts, which were injected into the still-hot QD dikes, forming the observed composite QD-IQD dikes and offset ores (Fig. 4.16C) (Lesher, 2012, 2013). Models involving flowage differentiation (e.g., Pilles, 2019) cannot explain the sharp contacts between IQD and QD or the presence of QD inclusions in IQD.

T3 – Formation of Anteliths: The impact melt continued to erode local footwall rocks until it reached the liquidus. Prevec (2000) proposed that a hybrid melt, formed by mixing of impact melt with overlying mafic norite, crystallized an olivine-bearing lithology that was subsequently eroded to form the anteliths, but this requires mafic norite to form over a layer of hybrid liquid. It is more likely that where assimilated footwall rocks were olivine-rich, the contaminated melt crystallized olivine then orthopyroxene then plagioclase, producing a thin layer of olivine melanorite and subsequently disrupted, and forming the protolith of Group I anteliths (Fig. 4.14C-D). Where assimilated footwall rocks were orthopyroxene-rich, the melt crystallized orthopyroxene then plagioclase, forming North Range Mafic Norite. Where the assimilated footwall rocks were mafic to intermediate, the melt crystallized cotectic orthopyroxene-plagioclase, forming South Range Quartz-Rich Norite. The next step is less clear, but Lesher et al. (2015) proposed that a geochemical reversal on the South Range between the Quartz-Rich Norite and overlying South Range Norite was caused by the influx of compositionally different impact melt through a break (rupture) in one or more of the crater rings. This would also explain how the protolith of the Group I anteliths could be eroded and the Pb isotopic difference between NR Mafic Norite and overlying Felsic Norite.

T4 – Formation and Localization of Sublayer: Any mixtures of inclusions (Groups II and III) and sulfide xenomelts that were not extracted into the QD-IQD dikes remained along the basal contact and migrated into topographic lows under the influence of convection currents and/or gravity flow when the melt contained <45% inclusions (Fig. 4.14D). The inclusion- and sulfide-bearing melt emplaced into offset dikes and formed a QD matrix due to rapid cooling, whereas the proto-Sublayer will form a noritic/gabbroic matrix with some orthopyroxene accumulation due to slow cooling.

T5 – Formation of FWBX: FWBX contains no QD or noritic matrix, so must have acquired ultramafic inclusions by incorporating them from Sublayer. When the impact melt was above the liquidus, the rate of thermomechanical erosion would have exceeded the rate of heat conduction into the footwall rocks, continuing to generate Sublayer, but as the melt reached the liquidus the rate of thermomechanical erosion decreased, allowing heat to be conducted into the footwall rocks, forming anatectic footwall breccias and metabreccias (Fig. 4.14D). This explains the many occurrences where FWBX cross-cuts Sublayer and lower Main Mass norites.

4.9 Conclusions

Sublayer, FWBX, and IQD appear to be cogenetic on the basis of similarity of inclusion population, but the greater geochemical heterogeneity, greater angularity of inclusions, and greater amounts cumulus orthopyroxene-plagioclase in Sublayer relative to IQD indicate that Sublayer cooled more slowly and allowed orthopyroxene to accumulate, whereas IQD cooled more rapidly, was able to accumulate less orthopyroxene and expel less residual silicate melt. The significant enrichment of highly incompatible lithophile element, overall moderately-strongly unradiogenic Nd and radiogenic Os isotopic composition of all SIC lithologies, sulfide ores, and most mafic-ultramafic inclusions reflect a strong continental crustal signature. However, there is significant Pb-S-(Os) isotopic heterogeneity in the basal Main Mass norite, Sublayer, and IQD. Mafic-ultramafic inclusions in the Sublayer and IQD include anteliths, local xenoliths, and exotic xenoliths. The majority, except for the anteliths, contain no sulfide and exhibit no signature of Ni-Cu-PGE depletion caused by prior sulfide saturation, which suggest that the association between mafic-ultramafic inclusions and Ni-Cu-PGE sulfide mineralization is most likely attributable to their refractory nature and to their similar fluid dynamic behavior. Anteliths, locally-derived inclusions, significant amounts of sulfide xenomelt, and local

variations in S-Pb-(Os) isotopes must have been generated during thermomechanical erosion of local footwall rocks, whereas the exotic inclusions, except for the shocked feldspar lherzolite, were generated during impact excavation and/or thermomechanical erosion and transported into their current locations. Convective- and/or gravity-driven mass flow contributed to the transportation of the inclusions into the embayment when the impact melt contained inclusions <45%, but became less significant as the impact melt assimilated more inclusions.

References Cited

Ames, D.E., Golightly, J.P., Lightfoot, P.C., and Gibson, H.L., 2002. Vitric compositions in the Onaping Formation and their relationship to the Sudbury Igneous Complex, Sudbury Structure: Economic Geology, v. 97, p. 1541 – 1562.

Ames, D.E., Golightly, J.P., and Zirenberg, R.A., 2010. Trace element and sulfur isotope compositions of Sudbury Ni-Cu-PGE ores in diverse settings. Society of Economic Geologist 2010 Conference, Keystone Resort, Colorado, September 30 - October 9, 2010, Poster E1.

Cabri, L.J., and Laflamme, J.H.G., 1976. The mineralogy of the platinum-group elements from some copper-nickel deposits of the Sudbury area, Ontario. Economic Geology, v. 71, p. 1159 - 1195.

Capes, P.C., 2001. A petrological investigation of the Copper Cliff embayment structure, Sudbury, Canada. Unpublished MSc thesis. University of Toronto, Toronto, Ontario, 162p.

Card, K.D., and Pattison, E.F., 1973. Nipissing Diabase of the Southern Province, Ontario. Geol. Assoc. Can. Spec. Paper 12, p. 7 – 30.

Carlson, R.W., and Irving, A.J., 1994. Depletion and enrichment history of subcontinental lithospheric mantle: Os, Sr, Nd and Pb evidence from xenoliths from Wyoming craton. Earth and Planetary Science Letters, v. 126, p. 457 – 472.

Carter, W.M., Watkinson, D.H., Ames, D.E., and Jones, P.C., 2009. Quartz diorite magmas and Cu-(Ni)-PGE mineralization. Podolsky Deposit. Whistle Offset Structures, Sudbury. Ontario. Geological Survey of Canada, Open File 6134.

Clarke, D.B., 2007. Assimilation of xenocrysts in granitic magmas: Principles, processes, proxies, and problems. The Canadian Mineralogist, v. 45, p. 5 - 30.

Clift, R., Grace, J.R., and Weber, M.E., 1978. Bubbles, Drops, and Particles, Academic Press, New York.

Coats, C.J.A. and Snadjr, P., 1984. Ore deposits of the North Range, Onaping-Levack area, Sudbury. In E.G. Pye, A.J. Naldrett, and P.E. Giblin (eds), The Geology and Ore Deposits of the Sudbury Structure. Ontario Geological Survey Special Volume 1, p. 327 – 346.

Cohen, A.S., Burnham, O.M., Hawkesworth, C.J., and Lightfoot, P.C., 2000. Pre-emplacement Re-Os ages from ultramafic inclusions in the sublayer of the Sudbury Igneous Complex, Ontario. Chemical Geology, v. 165, p. 37 – 46.

Corfu, F., and Lightfoot, P.C., 1996. U-Pb geochronology of the Sublayer environment, Sudbury Igneous Complex, Ontario. Economic Geology, v. 91, p. 1263 – 1269.

Dare, S.A.S., Barnes, S.-J., Prichard, H.M., Fisher, P.C., 2010. The distribution of platinum group elements (PGE) and other chalcophile elements among sulfides from Creighton Ni-Cu-PGE sulfide deposit, Sudbury, Canada, and the origin of palladium in pentlandite. Mineralium Deposita, v. 45, p. 765 – 793.

Darling, J.R., and Moser, D.E., 2012. Impact induced crustal differentiation: New insights from the Sudbury Structure. 43rd Lunar and Planetary Science Conference. p2164.

Darling, J.R., Hawkesworth, C.J., Lightfoot, P.C., Storey, C.D., and Tremblay, E., 2010a. Isotopic heterogeneity in the Sudbury impact melt sheet. Earth and Planetary Science Letters, v. 289. p. 347 – 356.

Darling, J.R., Hawkesworth, C.J., Storey, C.D., and Lightfoot, P.C., 2010b. Shallow impact: Isotopic insights into crustal contributions to the Sudbury impact melt sheet. Geochimica et Cosmochimica Acta, v. 74, p. 5680 – 5696.

Darling, J.R., Storey, C.D., Hawkesworth, C.J., and Lightfoot, P.C., 2012. In situ Pb isotope analysis of Fe-Ni-Cu sulfides by laser ablation multi-collector ICPMS: New insights into ore formation in the Sudbury impact melt sheet. Geochimica and Cosmochimica Acta, v. 99, p. 1 – 17.

Davis, G.C., 1984. Little Stobie Mine: A South Range contact deposit. In Pye, E.G., Naldrett, A.J., and Giblin, P.E., The Geology and Ore Deposits of the Sudbury Structure, Ontario Geological Survey Special Volume 1, p. 361 – 369.

Dessureau, G., 2003. Geochemistry of the mafic and felsic norite in the Whistle embayment: Implications for the crystallization history of the Sudbury Igneous Complex, Sudbury, Ontario. MSc thesis, Laurentian University.

Dickin, A.P., Artan, M.A., and Crocket, J.H., 1996. Isotopic evidence for distinct crustal sources of North and South Range ores, Sudbury Igneous Complex. Geochimica et Cosmochimica Acta, v. 60, p. 1605 – 1613.

Dickin, A.P., Nguyen, T., and Crocket, J.H., 1999. Isotopic evidence for a single impact melting origin of the Sudbury Igneous Complex. In Large Meteorite Impacts and Planetary Evolution II (eds. B.O. Dressler and V.L. Sharpton) Geological Society of American Special Paper 339, p. 361 – 371.

Dickin, A.P., Richardson, J.M., Crocket, J.H., McNutt, R.H., and Peredery, W.V., 1992. Osmium isotope evidence for a crustal origion of platinum group elements in the Sudbury nickel ore, Ontario, Canada. Geochimica et Cosmochimica Acta, v. 56, p. 3531 – 3537.

Dressler, B.O., 1982. Footwall of the Sudbury Igneous Complex, District of Sudbury. In Wood, J., White, O.L., Barlow, R.B., Colvine, A.C. (eds.) Summary of field work, 1982. Ontario Geological Survey Miscellaneous Paper p106. p. 73 – 75.

Dobrovinski, I.E., Esin, O.A., Barmin, L.N., and Chuchmarev, S.K. 1969. Physicochemical properties of sulphide melts. Russian Journal of Physical Chemistry, v. 43, p. 1769 – 1771.

Ellam, R.M., Carlson, R.W., and Shirey, S.B., 1993. Evidence from Re-Os isotopes for plume-lithosphere mixing in Karoo flood basalt genesis. Nature, v. 359, p. 718 – 721.

Faggart, B.E., Basu, A.R., Tatsumoto, M., 1985. Origin of the Sudbury Complex by meteoritic impact - neodymium isotopic evidence. Science, v. 230, p. 436 – 439.

Farrell, K., 1997. Mafic to ultramafic inclusions in the Sublayer of the Sudbury Igneous Complex at Whistle Mine, Sudbury, Ontario, Canada. Master thesis, Laurentian University, Sudbury, Ontario.

Giordano, D., Russell, J.K., Dingwell, D.B., 2008. Viscosity of magmatic liquids: A model. Earth and Planetary Science Letters, v. 271, p. 123 – 134.

Golightly, J.P., 1994. The Sudbury Igneous Complex as an impact melt: evolution and ore genesis. In: Lightfoot, P.C. and Naldrett, A.J., eds., Proceedings of the Sudbury-Norils'k Symposium. Ontario Geologic Survey, v. 5, p. 105 – 117.

Grant, R.W. and Bite, A., 1984. Sudbury quartz diorite offset dikes. In Pye, E.G., Naldrett, A.J., and Giblin, P.E., The Geology and Ore Deposits of the Sudbury Structure, Ontario Geological Survey Special Volume 1, p. 275 – 300.

Gregory, S.K., 2005. Geology, mineralogy and geochemistry of transitional contact/footwall mineralization in the McCreedy East Ni-Cu-PGE deposit, Sudbury Igneous Complex. Unpublished M.Sc. thesis, Laurentian University, Sudbury, Ontario, p. 138.

Grieve, R.A.F., and Therriault, A., 2000, Vredefort, Sudbury, Chicxulub: Three of a Kind?. Annual Review of Earth and Planetary Sciences, v. 28, p. 305 – 333. https://doi.org/10.1146/annurev.earth.28.1.305.

Grieve, R.A.F., Dence, M.R., and Robertson, P.B., 1977. Cratering process: As interpreted from the occurrence of impact melts. In Impact and Explosion Cratering: Planetary and Terrestrial Implications (D.J. Roddy, R.O. Pepin, and R.B. Merrill, eds.) p. 791 – 814. Pergamon, New York.

Grieve, R.A.F., Robertson, P.B., and Dence, M.R., 1981. Constraints on the formation of ring impact structures, based on terrestrial data. In Multi-Ring Basin: Formation and Evolution, Proc. Lunar Planet. Sci. 12A (P.H. Schultz and R.B. Merrill, eds.) p. 37 – 57. Pergamon, New York.

Hawley, J.E., 1962. The Sudbury ores, their mineralogy and origin. Canadian Mineralogist, v. 7, p207.

Hewins, R.H., 1971. The petrology and some marginal mafic rocks along the North Range of the Sudbury Irruptive. PhD Thesis, University of Toronto.

Hirose, K., and Kushiro, I., 1998. The effect of melt segregation on polybaric mantle melting: Estimation from the incremental melting experiments. Phys. Earth Planet. Int., v. 107, p. 111 – 118.

Huppert, H.E., and Sparks, R.S., 1985. Komatiites I: Eruption and flow. Journal of Petrology, v. 26, p. 694 – 725.

Ivanov, B.A. and Deutsch, A., 1999. Sudbury impact event: Cratering mechanics and thermal history. In Dressler, B.O. and Sharpton, V.L., eds., Large Meteorite Impacts and Planetary Evolution II: Boulder, Colorado, Geological Society of America, Special Paper 339.

James, R.S., Jobin-Bevans, S., Easton, R.M., Wood, P., Hrominchuk, J.L., Keays, R.R., Peck, D.C., 2002. Platinum-group element mineralization in Paleoproterozoic basic intrusions in central and northeastern Ontario, Canada. In: Cabri, L.J. ed., Geology, Geochemistry, Mineralogy and Mineral Processing of Platinum Group Elements, CIM Special Publication, v. 54, p. 339 – 366.

Jolly, W.T., 1987. Geology and geochemistry of Huronian rhyolites and low-Ti continental tholeiites from the Thessalon region, central Ontario. Canadian Journal of Earth Sciences, v. 24, p. 1360 – 1385.

Jolly, W.T., Dickin, A.P., and Wu, T.W., 1992. Geochemical stratigraphy of the Huronian continental volcanics at Thessalon, Ontario: contributions of two-stage crustal fusion. Contributions to Mineralogy and Petrology, v. 110, p. 411 – 428.

Keays, R.R. and Lightfoot, P.C., 2004. Formation of Ni-Cu-Platinum Group Element sulfide mineralization in the Sudbury Impact Melt Sheet. Mineralogy and Petrology, v. 82, p. 217 – 258.

Ketchum, K.Y., Heaman, L.M., Bennett, G., and Hughes, D.J., 2013. Age, petrogenesis and tectonic setting of the Thessalon volcanic rocks, Huronian Supergroup, Canada. Precambrian Research, v. 233, p. 144 – 172.

Kinnaird, J.A., Hutchinson, D., Schurmann, L., Nex, P.A.M., de Lange, R., 2005. Petrology and mineralization of the Southern Platree: northern limb of the Bushveld Complex, South Africa. Mineralium Deposita. V. 40, p. 576 – 597.

Kenny, Gavin G., Petrus, Joseph A., Whitehouse, Martin J., Daly, J. Stephen, Kamber, Balz S., 2017. Hf isotope evidence for effective impact melt homogenisation at the Sudbury impact crater, Ontario, Canada. Geochimica et Cosmochimica Acta, v. 215, p. 317 – 336.

Kuo, H.Y., Crocket, J.H., 1979. Rare earth elements in the Sudbury Nickel Irruptive: comparison with layered gabbro and implications for Nickel Irruptive petrogenesis. Economic Geology, v. 79, p. 590 – 605.

Krogh, T.E., Davis, D.W., and Corfu, F., 1984. Precise U-Pb zircon and baddeleyite ages for the Sudbury area. In The geology and ore deposits of the Sudbury Structure, E.G. Pye, A.J. Naldrett and P.E. Gibblin, eds. Ontario Geologic Survey Special Volume 1, p. 431 – 446.

Lafrance, B., Bygnes, L., McDonald, A., 2014. Emplacement of metabreccia along the Whistle offset dike, Sudbury: implications for post-impact modification of the Sudbury impact structure. Canadian Journal of Earth Science, v.51, p. 466 - 484.

Lambert, D.D., Walker, R.J., Morgan, J.W., Shirey, S.B., Calson, R.W., Zientek, M.L., Lipin, B.P., Koski, M.S., and Cooper, R.L., 1994. Re-Os and Sm-Nd isotope geochemistry of the Stillwater Complex, Montana: implications for the petrogenesis of the J-M Reef. Journal of Petrology, v. 35, p. 1717 – 1753.

Lesher, C.M. and Burnham, O.M., 2001. Multicomponent elemental and isotopic mixing in Ni-Cu-(PGE) ores at Kambalda, Western Australia. Canadian Mineralium, v. 39, p. 421 - 446.

Lesher, C.M. and Campbell, I.H., 1993. Geochemical and fluid dynamic modeling of compositional variations in Archean komatiite-hosted nickel sulfide ores in Western Australia. Economic Geology, v. 88, p. 804 – 816.

Lesher CM, 2012, New developments in the genesis of the Sudbury Igneous Complex and associated Ni-Cu-PGE mineralization, in Song X.-Y., Chen, L.-M., and Li, C. (Editors), Extended Abstracts, 12th International Ni-Cu-PGE Symposium, Guiyang, China, 16-21 June, State Key Laboratory, Chinese Academy of Sciences, p. 154 – 157.

Lesher CM, 2013, Catastrophic sulfide saturation and genesis of Ni-Cu-PGE mineralization in the Sudbury Igneous Complex, in Proceedings of the 12th Biennial SGA Meeting, Uppsala, Sweden, 12-15 Aug, Abstract v. 3, p. 1040 – 1043.

Lesher, C.M., 2017. Roles of xenomelts, xenoliths, xenocrysts, xenovolatiles, residues, and skarns in the genesis, transport, and localization of magmatic Fe-Ni-Cu-PGE sulfides and chromite. Ore Geology Reviews, v. 90, p. 465 – 484.

Lesher CM, 2015, Impact melt emplacement, cooling, and crystallization in the Sudbury Igneous Complex, Session P11A: Recent Developments at Sudbury and Other Canadian Impact Structures, AGU-GAC-MAC Joint Assembly, Montréal, QC, 03-07 May.

Lesher, C.M., 2019a. Role of impact devolatilization in the genesis of Ni-Cu-PGE mineralization in the Sudbury Igneous Complex, GAC-MAC Annual Meeting, Québec, QC, Abstract SS-RE03-O07.

Lesher, C.M., 2019b. Up, down, or sideway: emplacement of magmatic Fe-Ni-Cu-PGE sulfide melts in large igneous provinces. Canadian Journal of Earth Sciences, v. 56, p. 756 – 773.

Lewis, K.B., 1971. Slumping on a continental slope inclined at 1° - 4°. Sedimentology, v. 16, p. 97 – 110.

Li, C. and Ripley, E.M., 2005. Empirical equations to predict the sulfur content of mafic magmas at sulfide saturation and applications to magmatic sulfide deposits. Mineralium Deposita, v. 40, p. 218 – 230.

Li, C., Naldrett, A.J., 2000. Melting reactions of gneissic inclusions with enclosing magma at Voisey's Bay, Labrador, Canada: Implications with respect to ore genesis. Economic Geology, v. 95. p. 801 – 814.

Lightfoot, P. C., Zotov, I.A., 2007. Ni-Cu-PGE sulfide deposits at Noril'sk, Russia. Short Course; International Polar Year; Prospectors and Developers Association of Canada. Short Course Notes.

Lightfoot, P.C. and Naldrett, A.J., 1989. Assimilation and crystallization in basic magma chambers: trace element and Nd-isotopic variations in the Kerns sill, Nipissing diabase province, Ontario. Canadian Journal of Earth Science, v. 26, p. 737 – 754.

Lightfoot, P.C., 2016. Nickel sulfide ores and impact melts: Origin of the Sudbury Igneous Complex: Amsterdam, Netherlands, Elsevier, p662.

Lightfoot, P.C., Doherty, W., Farrell, K., Keays, R.R., Moore, M., and Pekeski, D., 1997a. Geochemistry of the main mass, sublayer, offsets, and inclusions from the Sudbury Igneous Complex, Ontario; Ontario Geological Survey, Open File Report, 5959, p231.

Lightfoot, P.C., Keays, R.R., and Doherty, W., 2001. Chemical evolution and origin of Nickel sulfide mineralization in the Sudbury Igneous Complex, Ontario, Canada. Economic Geology, v. 96, p. 1855 – 1875.

Lightfoot, P.C., Keays, R.R., Morrison, G.G., Bite, A., and Farrell, K.P., 1997b. Geologic and geochemical relationships between the contact sublayer, inclusions, and the main mass of the Sudbury Igneous Complex: A case study of the Whistle Mine Embayment: Economic Geology and the Bulletin of the Society of Economic Geologists, v. 92, p. 647 – 673, https:// doi.org /10 .2113/gsecongeo .92 .6 .647.

Lightfoot, P.C., Keays, R.R., Morrison, G.G., Bite, A., and Farrell, K.P., 1997c. Geochemical relationships in the Sudbury Igneous Complex: Origin of the Main Mass and Offset dikes. Economic Geology, v. 92, p. 289 – 307.

Liu, Y., and Brenan, J., 2015. Partitioning of platinum-group elements (PGE) and chalcogens (Se, Te, As, Sb, Bi) between monosulfide-solid solution (MSS), intermediate solid solution (ISS) and sulfide liquid at controlled fO2 - fS2 conditions. Geochimica et Cosmochimica Acta, v. 159, p. 139 – 161.

Marques, J.C., Ferreira Filho, C.F., Carlson, R.W., and Pimentel, M.M., 2003. Re-Os and Sm-Nd isotope and trace element constraints on the origin of the chromite deposit of the Ipueira - Medrado Sill, Bahia, Brazil. Journal of Petrology, v. 44, p. 659 – 678.

Marsh, B., 1989. On convective style and vigor in sheet-like magma. Journal of Petrology, v. 30, p. 479 – 530.

Marsh, B.D. and Maxey, M.R., 1985. On the distribution and separation of crystals in convecting magma. Journal of Volcanology and Geothermal Research, v. 24, p. 95 - 150.

Martin, D., and Nokes, R., 1988. Crystal settling in a vigorously convecting magma chamber. V. 332, p. 534 – 536.

Martin, D., and Nokes, R., 1989. A fluid-dynamical study of crystal settling in convecting magmas. Journal of Petrology, v. 30, p. 1471 – 1500.

McCormick, K.A., Fedorowich, J.S., McDonald, A.M., and James, R.S., A textural, mineralogical, and statistical study of the footwall breccia within the Strathcona Embayment of the Sudbury Structure. Economic Geology, v. 97, p. 125 - 143.

McNamara, G.S., Lesher, C.M., and Kamber, B.S., 2017. New feldspar lead isotope and trace element evidence from the Sudbury Igneous Complex indicate a complex origin of associated Ni-Cu-PGE mineralization involving underlying country rocks. Economic Geology, v. 112, p. 569 – 590.

McNutt, R.H., 1970. A study of the gabbro-peridotite inclusions in the Sudbury ores. A report to the International Nickel Company of Canada Limited.

Meldrum, A., Abdel-Rahman, A-F. M., Martin, R.F., and Wodicka, N., The nature, age and petrogenesis of the Cartier Batholith, northern flank of the Sudbury Structure, Ontario, Canada. Precambrian Research, v. 82, p. 265 – 285.

Mikereit, B., Artemieva, N., and Ugalde, H., 2010. Fracturing, thermal evolution and geophysical signature of the crater floor of a large impact structure: The case of the Sudbury

Structure, Canada. In Gibson, R.L., and Reimold, W.U., eds., Large Meteorite Impacts and Planetary Evolution IV: Geological Society of America Special Paper 465, p. 115 – 131.

Molina, I., Burgisser, A., Oppenheimer, C., 2012. Numerical simulations of convection in crystal-bearing magmas: a case study of the magmatic system at Erebus, Antarctica. Journal of Geophysical Research: Solid Earth, American Geophysical Union, v. 117, p. B07209

Moore, M., Lightfoot, P.C., Keays, R.R, 1993. Project Unit 93-08, Geology and geochemistry of footwall ultramafic rocks, Sudbury Igneous Complex, Fraser Mine, Sudbury, Ontario. In: Baker, C.L., Dressler, B.O., De Souza, H.A.F., Fenwick, K.G., Newsome, J.W., Owsiacki, L. (eds), Summary of field work and other activities 1993. Ontario Geological Survey Miscellaneous Paper 162, p. 85 – 86.

Moore, M., Lightfoot, P.C., Keays, R.R, 1994. Geology and geochemistry of footwall ultramafic rocks, Fraser mine and Levack West mine, Sudbury Igneous Complex, Sudbury, Ontario. In: Summary of Field Work and Other Activities, Ontario Geological Survey, Miscellaneous Paper 163, p. 91 – 94.

Moore, M., Lightfoot, P.C., Keays, R.R, 1995. Geology and geochemistry of footwall ultramafic rocks, Sudbury Igneous Complex, Sudbury, Ontario. In: Summary of Field Work, Other Activities, Ontario Geological Survey, Miscellaneous Paper 164, p. 122 – 123.

Morgan, J.W., Walker, R.J., Horan, M.F., Beary, E.S., and Naldrett, A.J., 2002. 190Pt - 186Os and 187Re - 187Os systematics of the Sudbury Igneous Complex, Ontario. Geochimica et Cosmochimica Acta, v. 66, p. 273 – 290.

Morrison, G.G., Jago, B.C., Little, T.L., 1994. Footwall mineralization of the Sudbury Igneous Complex. In P.C. Lightfoot, A.J. Naldrett, (eds.), Proceedings of the Sudbury-Noril'sk Symposium, Ontario Geological Survey Special Volume 5, p. 57 – 64.

Morris, W.A., 1984. Paleomagnetic constraints on the magmatic, tectonic, and metamorphic history of the Sudbury Basin Region. In E.G. Pye, A.J. Naldrett, and P.E. Giblin (eds.) The Geology and Ore Deposits of the Sudbury Structure, Ontario Geological Survey, Special Volume 1, 603p.

Muir, T.L., 1981. Geology of Capreol area, District of Sudbury: Toronto, Ontario Geological Survey Open File Report 5344, p168.

Muir, T.L., and Peredery, W.V., 1984. The Onaping Formation. In E.G. Pye, A.J. Naldrett, and P.E. Giblin (eds). The Geology and Ore Deposits of the Sudbury Structure Ontario Geological Survey, Special Volume 1, p603.

Mungall, J.E, and Su, S. 2005. Interfacial tension between magmatic sulfide and silicate liquids: Constraints on kinetics of sulfide liquation and sulfide migration through silicate rocks. Earth and Planetary Science Letters, v. 234, p. 135 – 149.

Murase, T. and McBirney, A.R., 1973. Properties of some common igneous rocks and their melts at high temperatures. Geological Society of America Bulletin, v. 84, p. 3563 – 3592.

Murphy, A.J., Spray, J.G., 2002. Geology, mineralization, and emplacement of the Worthington Offset dike: a genetic model for Offset dike mineralization in the Sudbury Igneous Complex. Economic Geology, v. 97, p. 1399 – 1418.

Naldrett, A.J., 2004. Magmatic sulfide deposits: Geology, geochemistry, and exploration. Springer, p727.

Naldrett, A.J., 1969. A portion of the system Fe-S-O between 900 and 1080°C and its application to sulfide ore magmas. Journal of Petrology, v. 10, p. 171 – 201.

Naldrett, A.J., and Kullerud, G., 1967. A study of the Strathcona mine and its bearing on the origin of the Nickel-Copper ores of the Sudbury district, Ontario: Journal of Petrology, v. 8, p. 453 – 531.

Naldrett, A.J., Greenman, L., and Hewins, R.H., 1972. The Main Irruptive and the Sublayer at Sudbury, Ontario. International Geological Congress, 24th, Montreal, Proceedings Section 4, p. 206 – 214.

Naldrett, A.J., Hewins, R.H., Dressler, B.O., Rao, B.V., 1984. The Sublayer of the Sudbury Igneous Complex. In Pye, E.G., Naldrett, A.J., and Giblin, P.E. (eds), The Geology and Ore Deposits of the Sudbury Structure, Ontario Geological Survey Special Volume 1, p. 253 – 274.

Parsons, J.D., Friedrichs, C.T., Traykovski, P.A., Mohrig, D., Imran, J., Syvitski, J.P.M., Parker, G., Puig, P., Buttles, J.L., and Garcia, M.H., 2007. The mechanics of marine sediment gravity flows. Margin Sedimentation, p. 265 - 337. DOI: 10.1002/9781444304398.ch6

Papineau, D., Mozcsis, S.J., and Schmitt, A.K., 2007. Multiple sulfur isotopes from Paleoproterozoic Huronian interglacial sediments and the rise of atmospheric oxygen. Earth and Planetary Science Letters, v. 255. p. 188 – 212.

Pattison, E.F., 1979. The Sudbury Sublayer: Canadian Mineralogist, v. 17, p. 257 – 274.

Petford, N., 2009. Which effective viscosity? Mineralogical Magazine, v. 73, p. 167 – 191.

Pilles, E.A., Osinski, G.R., Grieve, R.A.F., Smith, D., and Bailey, J., 2018. Formation of large-scale impact melt dikes: A case study of the Foy Offset dike at the Sudbury impact structure, Canada. Earth and Planetary Science Letters, v. 495, p. 224 – 233.

Pratson, L.F., Imran, J., Parker, G., Syvitski, J.P.M., and Hutton, E., 2000. Debris flows vs turbidity currents: a modeling comparison of their dynamics and deposits, in Bouma, A.H. and Stone, C.G., eds., Fine-grained turbidite systems, AAPG Memoir 72/SEPM Special Publication 68, p. 57 – 72.

Prevec, S.A. and Baadsgaard, H., 2005. Evolution of Palaeoproterozoic mafic intrusions located within the thermal aureole of the Sudbury Igneous Complex, Canada: Isotopic geochronological and geochemical evidence. Geochimica et Cosmochimica Acta, v. 69, p. 3653 – 3669.

Prevec, S.A. and Cawthorn, R.G., 2002. Thermal evolution and interaction between impact melt sheet and footwall: A genetic model for the contact sublayer of the Sudbury Igneous Complex, Canada. Journal of Geophysical Research, v. 107, p. 1 – 14.

Prevec, S.A., 2000. An examination of model variation mechanisms in the contact sublayer of the Sudbury Igneous Complex, Canada. Mineralogy and Petrology, v. 68, p. 141 – 157.

Prevec, S.A., Lightfoot, P.C., and Keays, R.R., 2000. Evolution of the sublayer of the Sudbury Igneous Complex: geochemical, Sm-Nd isotopic and petrologic evidence. Lithos, v. 51, p. 271 – 292.

Rae, D. R., 1975. Inclusions in the Sublayer from Strathcona Mine, Sudbury, and their significance. Department of Geology, University of Toronto. Degree of Master of Science.

Ripley, E.M., and Alawi, J.A., 1986. Sulfide mineralogy and chemical evolution of the Babbitt Cu-Ni deposit, Duluth Complex, Minnesota. Canadian Mineralogist, v. 24, p. 347 – 368.

Ripley, E.M., Lightfoot, P.C., Stifter, E.C., Underwod, B., Taranovic, V., Dunlop III, and Donoghue, K.A., 2015. Heterogeneity of S isotope compositions recorded in the Sudbury Igneous Complex, Canada: significance to formation of Ni-Cu sulfide ores and the host rocks. Economic Geology, v. 110, p. 1125 – 1135.

Robertson, J.C., Barnes, S.J., and Le Vaillant, M., 2016. Dynamics of magmatic sulphide droplets during transport in silicate melts and implications for magmatic sulphide ore formation. Journal of Petrology, v. 56, p. 2445 – 2472.

Rousell, D.H., 1984. Onwatin and Chelmsford Formations. In E.G. Pye, A.J. Naldrett, and P.E. Giblin (eds) The Geology and Ore Deposits of the Sudbury Structure, Ontario Geological Survey, Special Volume 1, p603.

Salvioli-Mariani, E., Mattioli, M., Renzulli, A., and Serri, G., 2002. Silicate melt inclusions in the cumulate minerals of gabbroic nodules from Stromboli Volcano (Aeolian Islands, Italy): main components of the fluid phase and crystallization temperatures. Mineralogical Magazine, v. 66, p. 969 – 984.

Schwarz, H.P., 1973. Sulfur isotope analysis of some Sudbury ores, Ontario. Canadian Journal of Earth Sciences, v. 10, p. 1444 – 1459.

Scribbins, B.T., 1978. Exotic inclusions from the South Range Sublayer, Sudbury. MSc thesis, University of Toronto.

Scribbins, B.T., Rae, D.R., and Naldrett, A.J., 1984. Mafic and ultramafic inclusions in the Sublayer of the Sudbury Igneous Complex. Canadian Mineralogist, v. 22: p. 67 – 75.

Shaw, H.R., 1972. Viscosities of magmatic silicate liquids: an empirical method of prediction. American Journal of Science, v. 272, p. 870 – 893.

Souch, B.E., Podolsky, T., and Geological Staff of Inco Limited, 1969. The sulfide ores of Sudbury: Their particular relation to a distinctive inclusion-bearing facies of the Nickel Irruptive. Economic Geology Monograph 4, p. 252 – 261.

Sproule, R., Sutcliffe, R., Tracanelli, H., Lesher, C.M., 2007. Paleoproterozoic Ni-Cu-PGE mineralization in the Shakespeare intrusion, Ontario, Canada: a new style of Nipissing gabbro-hosted mineralization. Application of Earth Sciences, IMM trans. B, v. 116, p. 188 – 200.

Takahashi, E., Shimazaki, T., Tsuzaki, Y., and Yoshida, H., 1993. Melting study of a peridotite KLB-1 to 6.5 GPa, and the origin of basaltic magmas, Philos. Trans. R. Soc. London, Ser. A., v. 342, p. 105 – 120.

Thode, H.G., Dunford, H.B., and Shima, M., 1962. Sulfur isotope abundances in rocks of the Sudbury district and their geological significance. Economic Geology, v. 57, p. 565 – 578.

Tornos, F., Casquct, C., Galindo, C., Velasco, F., Canales, A., 2001. A new style of Ni-Cu mineralization related to magmatic breccia pipes in a transgressional magmatic arc, Aguablanca, Spain. Mineralium Deposita, v. 36, 700 – 706

Tuba, G., Molnar, F., Ames, D.E., Pentek, A., Watkinson, D.H., and Jones, P.C., 2014. Multi-stage hydrothermal processes involved in "low-sulfide" Cu(-Ni)-PGE mineralization in the footwall of the Sudbury Igneous Complex (Canada): Amy Lake PGE zone, East Range: Mineralium Deposita, v. 49, p. 7 – 47.

Ubide, T., Guyett, P.C., Kenny, G.G., O'Sullivan, E.M., Ames, D.E., Petrus, J.A., Riggs, N., and Kamber, B.S., 2017. Protracted volcanism after large impacts: Evidence from the Sudbury impact basin. Journal of Geophysical Research: Planets, v. 122, p. 701 – 728.

Vetere, F., Behrens, H., Holtz, F., Vilardo, G., and Ventura, G., 2010. Viscosity of crystal-bearing melts and its implication for magma ascent. Journal of Mineralogical and Petrological Sciences, v. 105, p. 151 – 163.

Vos, M.A. and Moorhouse, W.W., 1965. Quartz-diorite from the North Range, Sudbury (Abstract). Canadian Mineralogist, v. 8, p402.

Walker, R.J., and Morgan, J.W., 1989. Rhenium-osmium isotope systematics of carbonaceous chondrites, Science, v. 243, p. 519 – 522.

Walker, R.J., Morgan, J.W., Hanski, E., and Smolkin, V.F., 1994. The role of the Re-Os isotope system in deciphering the origin of magmatic sulfide ores: A tale of three ores. In Proceedings of the Sudbury-Noril'sk Symposium. (eds. P.C. Lightfoot and S.J. Naldrett). Ontario Geological Survey Special Volume 5, p. 343 – 355.

Walker, R.J., Morgan, J.W., Naldrett, A.J., Li, C., and Fassett, J.D., 1991. Re-Os isotope systematics of Ni-Cu sulfide ores, Sudbury Igneous Complex, Ontario: evidence for a major crustal component. Earth and Planetary Science Letters, v. 105, p. 416 – 429.

Wang, Y., Lesher, C.M., Lightfoot, P.C., Pattison, E.F., and Golightly, J.P., 2016. Shock metamorphic features of olivine, orthopyroxene, and plagioclase in phlogopite-bearing ultramafic-mafic inclusions in Sublayer, Sudbury Igneous Complex, Sudbury, Canada: Abstract 5082 presented at the 35th International Geological Congress, Cape Town, South Africa, 27 August - 4 September.

Wang, Y., Lesher, C.M., Lightfoot, P.C., Pattison, E.F., and Golightly, J.P., 2018. Shock metamorphic features in mafic and ultramafic inclusions in the Sudbury Igneous Complex: Implications for their origin and impact excavation. Geology, v. 46, p. 443 – 446.

Whitehead, R.E.S., Davies, J.F., and Goodfellow, W.D., 1990. Isotopic evidence for hydrothermal discharge into anoxic seawater, Sudbury basin, Ontario, Canada. Chemical Geology (Isotope Geoscience Section), v. 86, p. 49 – 63.

Williams, D.A., Kerr, R.C., and Lesher, C.M., 1998. Emplacement and erosion by Archean komatiite lava flows at Kambalda: Revisited. Journal of Geophysical Research, v. 103, p. 27533 – 27549.

Williams, D.A., Kerr, R.C., and Lesher, C.M., 2011. Mathematical modelling of thermomechanical erosion beneath Proterozoic komatiitic basaltic sinuous rilles in the Cape Smith Belt, New Québec, Canada. Mineralium Deposita. V. 46, p. 943 – 958.

Williams, D.A., Kerr, R.C., Lesher, C.M., Barnes, S.J., 2001. Analytical/numerical modeling of komatiite lava emplacement and thermal erosion at Perseverance, Western Australia. Journal of Volcanology and Geothermal Research, v. 110, p. 27 – 55.

Wu, H., He, N. and Zhang, X., 2015. Numerical model of viscous debris flows with depth-dependent yield strength. Journal of Geoengineering, v. 10, p. 1 – 10.

Zhou, M.-F., Lightfoot, P.C., Keays, R.R., Moore, M.L., and Morrison, G.G., 1997. Petrogenetic significance of chromian spinels from the Sudbury Igneous Complex, Ontario, Canada. Canadian Journal of Earth Science, v. 34: p. 1405 – 1419.

Zieg, M.J. and Marsh, B.D., 2005. The Sudbury Igneous Complex: Viscous emulsion differentiation of a superheated impact melt sheet. Geological Society of America Bulletin, v. 117, p. 1427 – 1450.

Zieg, M.J., 2001. Cooling and crystallization of the Sudbury Igneous Complex. PhD thesis, The Johns Hopkins University.

Zurbrigg, H.F., 1957. The Frood-Stobie mine. Struct. Geol. Can. Ore Dep., v. 2, p. 341 – 350.

Figure Captions

Figure 4.1 Geological map of the Sudbury Igneous Complex, Canada (after Lightfoot, 2016)

Figure 4.2 Geological map of the Whistle Embayment and Whistle Offset dike (after Pattison, 1979)

Figure 4.3 Photograph of footwall breccia along Highway 144 Bypass between the Creighton and Gertrude mines. The breccia intrudes South Range quartz-rich norite (uniform greyish green) and comprises large fragments of Elsie Mountain Formation metabasalt (green and white), small fragments of partially-melted Creighton Granite (white), and coarse Fe-Ni-Cu sulfide blebs (rusty brown). Coin is 28 mm in diameter. Photo by CML.

Figure 4.4 Photomicrographs of igneous-textured Sublayer matrix. A: ophitic-texture ITSM, B: olivine-bearing ITSM, C: prismatic pyroxene ITSM, and D: porphyritic pyroxene ITSM.

Figure 4.5 Plot of whole-rock compositions for mafic-ultramafic inclusions and ITSM. A: Ni (ppm) vs MgO (%) and B: Ni (ppm) vs S (%); Dashed fields in (A) outline the composition of olivine, orthopyroxene, and clinopyroxene in the inclusions.

Figure 4.6 Stacked histogram of $\varepsilon Nd_{1850\ Ma}$ of the compiled Main Mass rock units, ITSM, and mafic-ultramafic inclusions from the North and South Ranges, together with mafic-ultramafic intrusive units and the country rocks of the Sudbury Igneous Complex. Data sources: Faggart et al. (1985), Lightfoot and Naldrett (1989), Dickin et al. (1992, 1996, 1999), Jolly et al. (1992), Prevec et al. (2000), and Prevec and Baadsgaard (2005).

Figure 4.7 Stacked histogram of $\delta^{34}S$ of sulfide ores from multiple deposits and Norite from various locations. Data sources: Thode et al. (1962), Schwarcz (1973), Whitehead et al. (1990), Papineau et al. (2007), Ames et al. (2010), Tuba et al. (2014), and Ripley et al. (2015).

Figure 4.8 Stacked histogram of $\gamma Os_{1850\ Ma}$ of sulfide ores in the basal Main Mass, Sublayer, and IQD, mafic-ultramafic inclusions, and country rocks associated with sulfide mineralization. Data sources: Walker et al. (1991), Dickin et al. (1992, 1999), Cohen et al. (2000), and Morgan et al. (2002).

Figure 4.9 Ternary contour of relative densities of mixtures of silicate melt, sulfide melt, and inclusions.

Figure 4.10 Ternary contour of relative viscosities at 1700°C of mixtures of silicate melt, sulfide melt, and inclusions.

Figure 4.11 Ternary contour of relative viscosities at 1180°C of mixtures of silicate melt, sulfide melt, and inclusions.

Figure 4.12 Maximum settling velocities (estimated using Stokes's law) for sulfide droplets, felsic and mafic inclusions, felsic and mafic inclusions with 10% sulfide melt within pure silicate melt (100% QD), and felsic and mafic inclusions within mineralized Sublayer-melt (35% QD + 35% sulfide melt + 30% inclusions) and within pure sulfide melt. Density of sulfide, felsic inclusion, mafic inclusion, and silicate melt are assumed to be 4.2, 2.6, 2.9, and 2.5 g cm^{-3}, respectively. Viscosity of silicate melt, mineralized Sublayer melt, and sulfide melt are assumed to be 53, 383, and 0.1 Pa s at 1700°C and 10304, 74508, and 0.1 at 1180°C, respectively.

Figure 4.13 Gradients representing settling velocity/convective velocity for sulfide droplets, felsic and mafic inclusions, felsic and mafic inclusions with 10% sulfide melt within pure silicate melt (100% QD) and mineralized Sublayer-melt (35% QD + 35% sulfide melt + 30% inclusions).

Figure 4.14 Geologic model for the formation of the Sublayer, IQD, and FWBX. A: Cross-section diagram through a transient crater, showing the formation of impact crater and movement of impact melt and inclusions. Concentric circles around the original impact point show isobars of peak shock pressure and isotherms of postshock temperatures. (modified from Grieve et al., 1977); B: Digestion of most inclusions by the superheated impact melt, except for some refractory exotic xenoliths and injection of QD into the offset dikes; C: Incorporation of xenoliths and sulfide xenomelts by thermomechanical erosion, sulfide saturation due to assimilation of inclusions and cooling of the melt, crystallization of olivine-orthopyroxene-plagioclase assemblage (forming the protolith of anteliths), and injected of IQD into the still-hot QD dikes; D: crystallization of Sublayer and IQD and formation of FWBX.

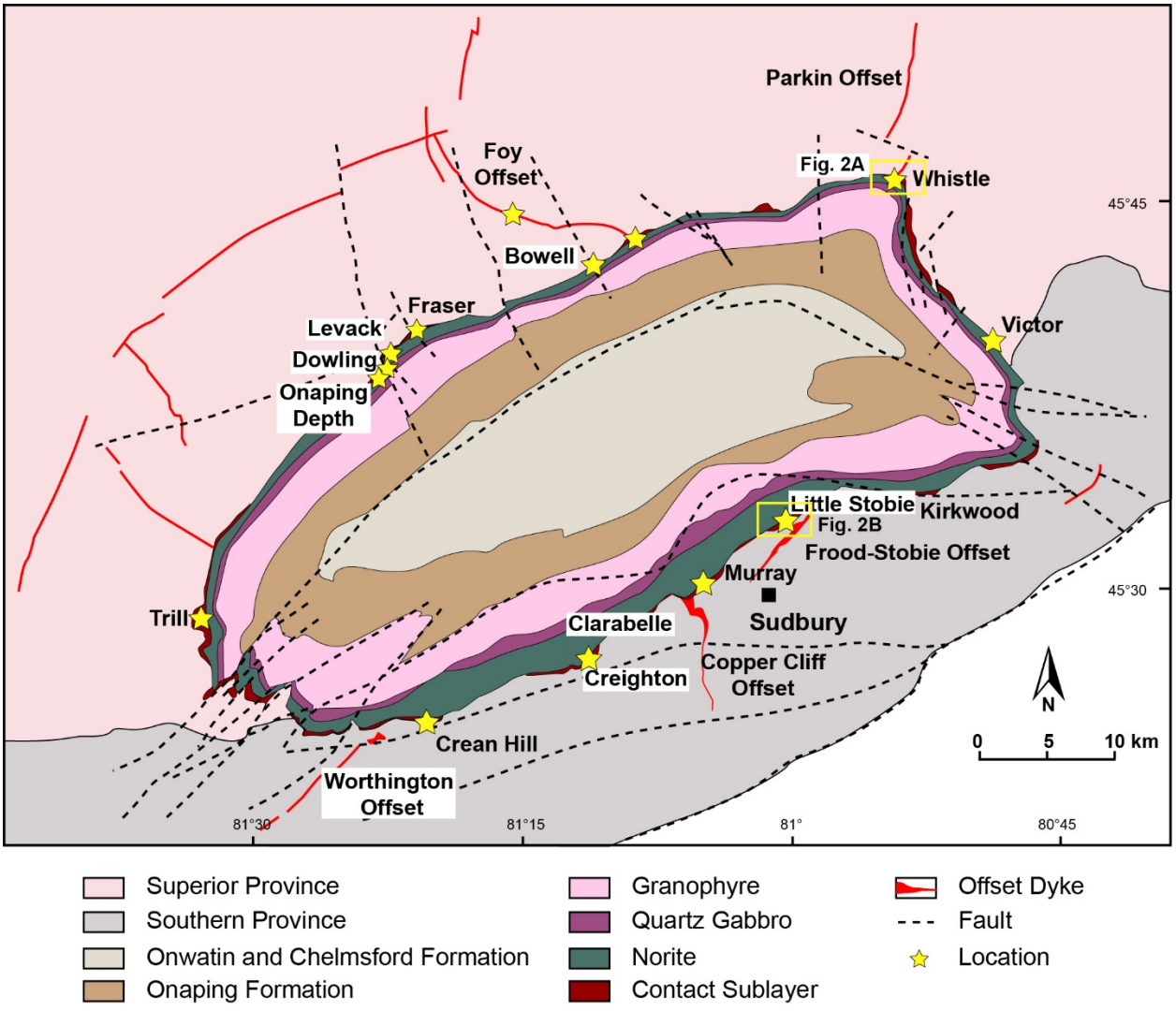

Figure 4.1 Geological map of the Sudbury Igneous Complex, Canada (after Lightfoot, 2016)

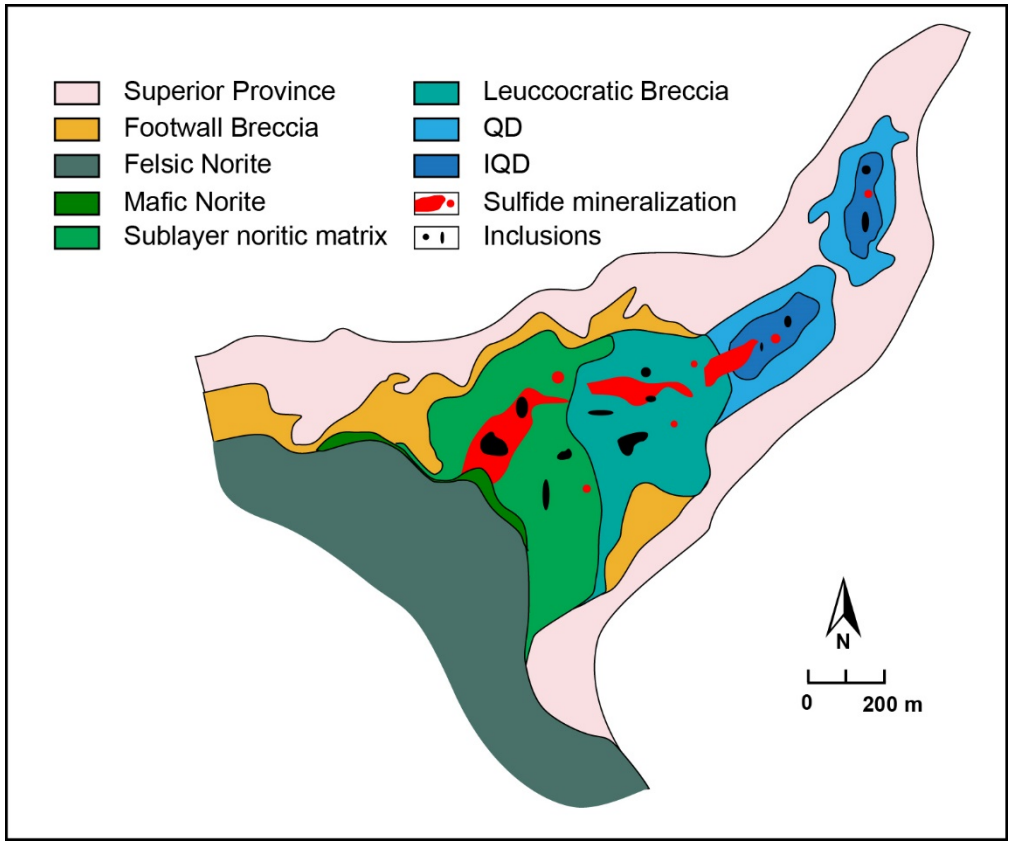

Figure 4.2 Geological map of the Whistle Embayment and Whistle Offset dike (after Pattison, 1979)

Figure 4.3 Photograph of footwall breccia along Highway 144 Bypass between the Creighton and Gertrude mines

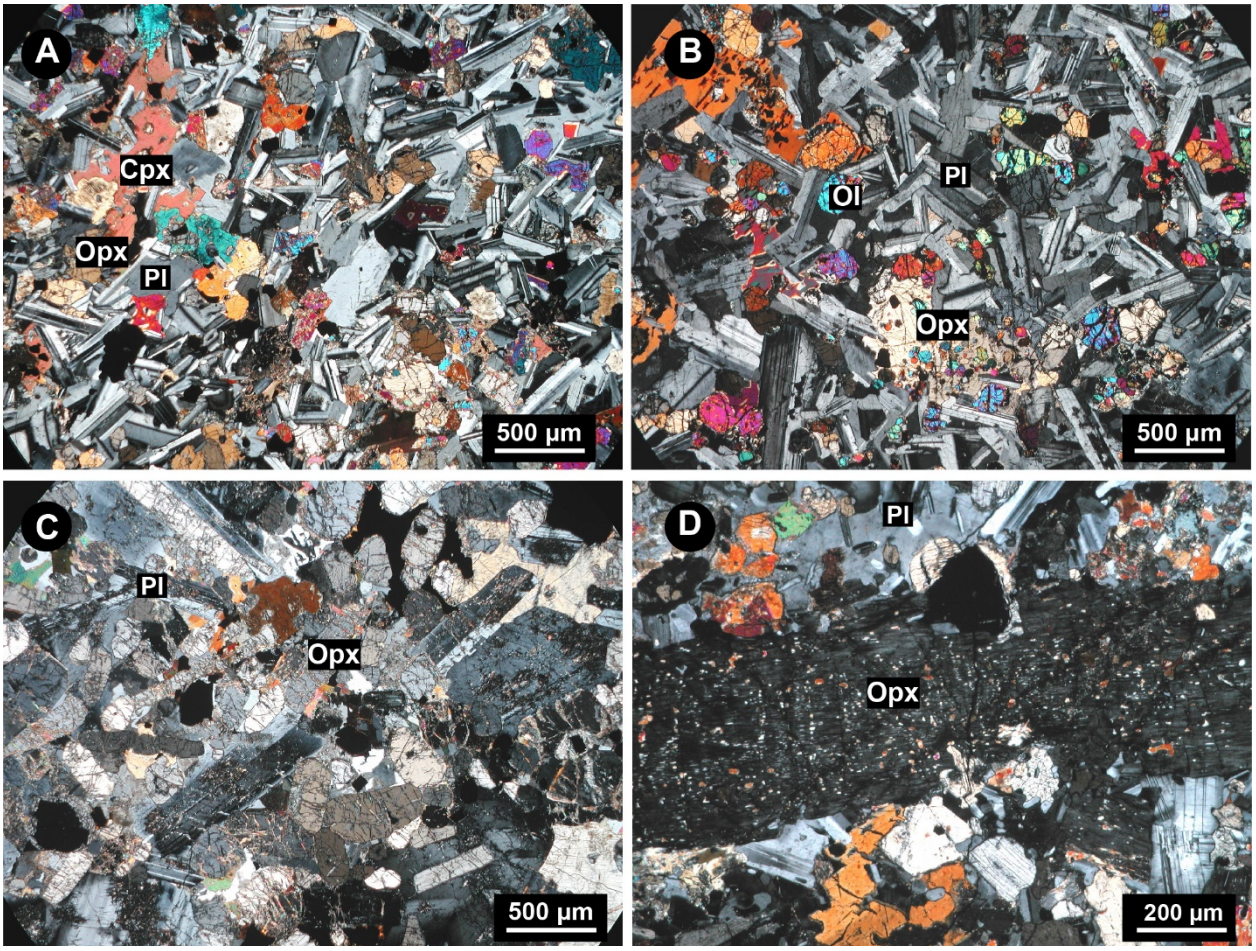

Figure 4.4 Photomicrographs of ITSM

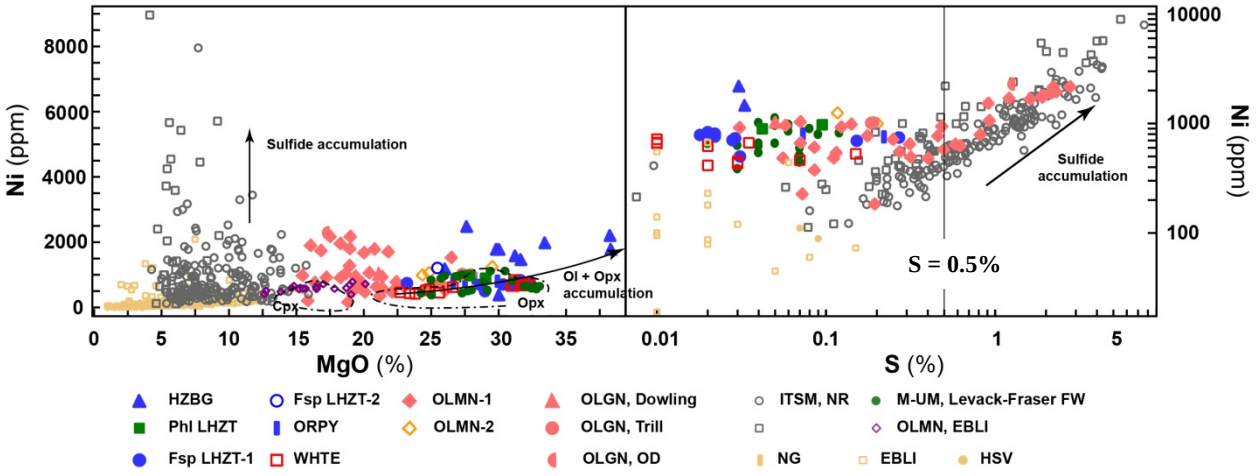

Figure 4.5 Plot of whole-rock compositions for mafic-ultramafic inclusions and ITSM. A: Ni (ppm) vs MgO (%) and B: Ni (ppm) vs S (%)

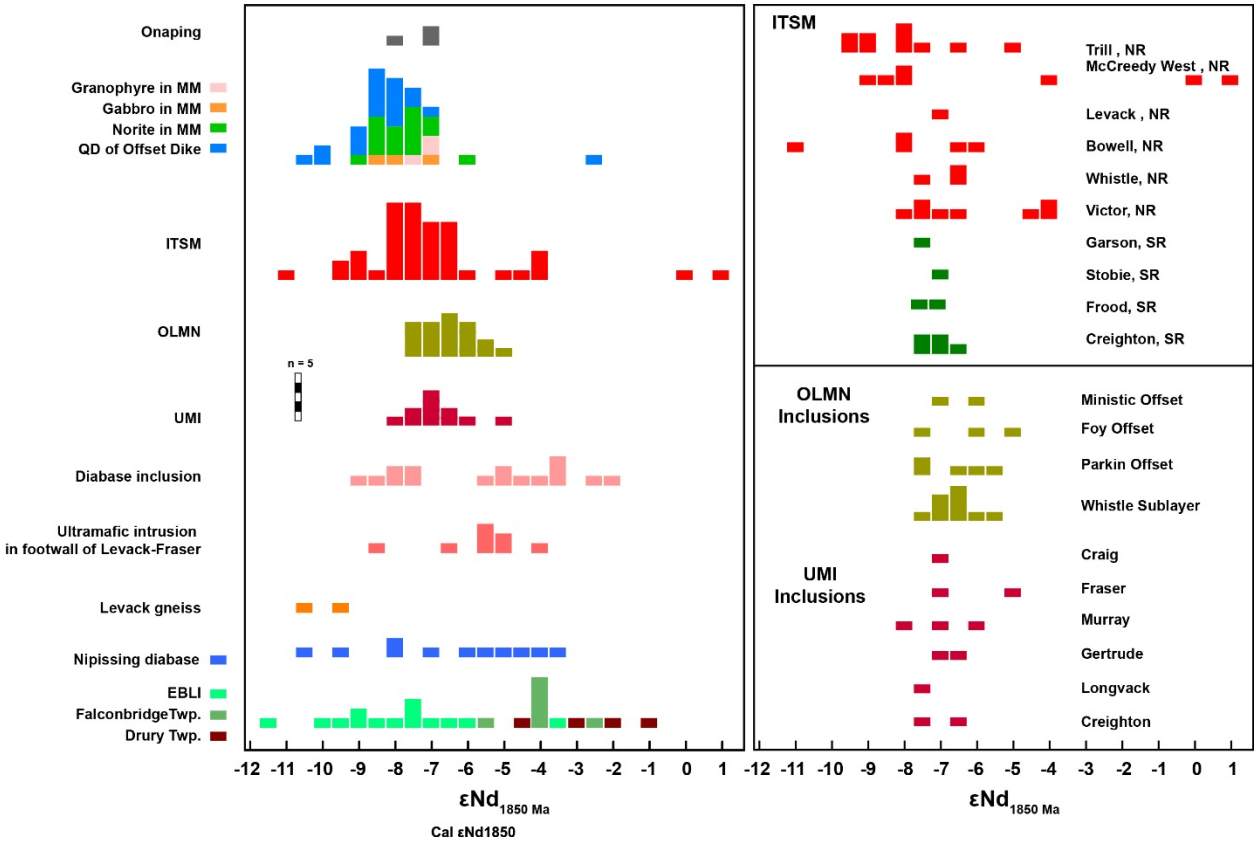

Figure 4.6 Stacked histogram of $\varepsilon Nd_{1850\ Ma}$ of the compiled Main Mass rock units, ITSM, and mafic-ultramafic inclusions from the North and South Ranges, together with mafic-ultramafic intrusive units and the country rocks of the Sudbury Igneous Complex

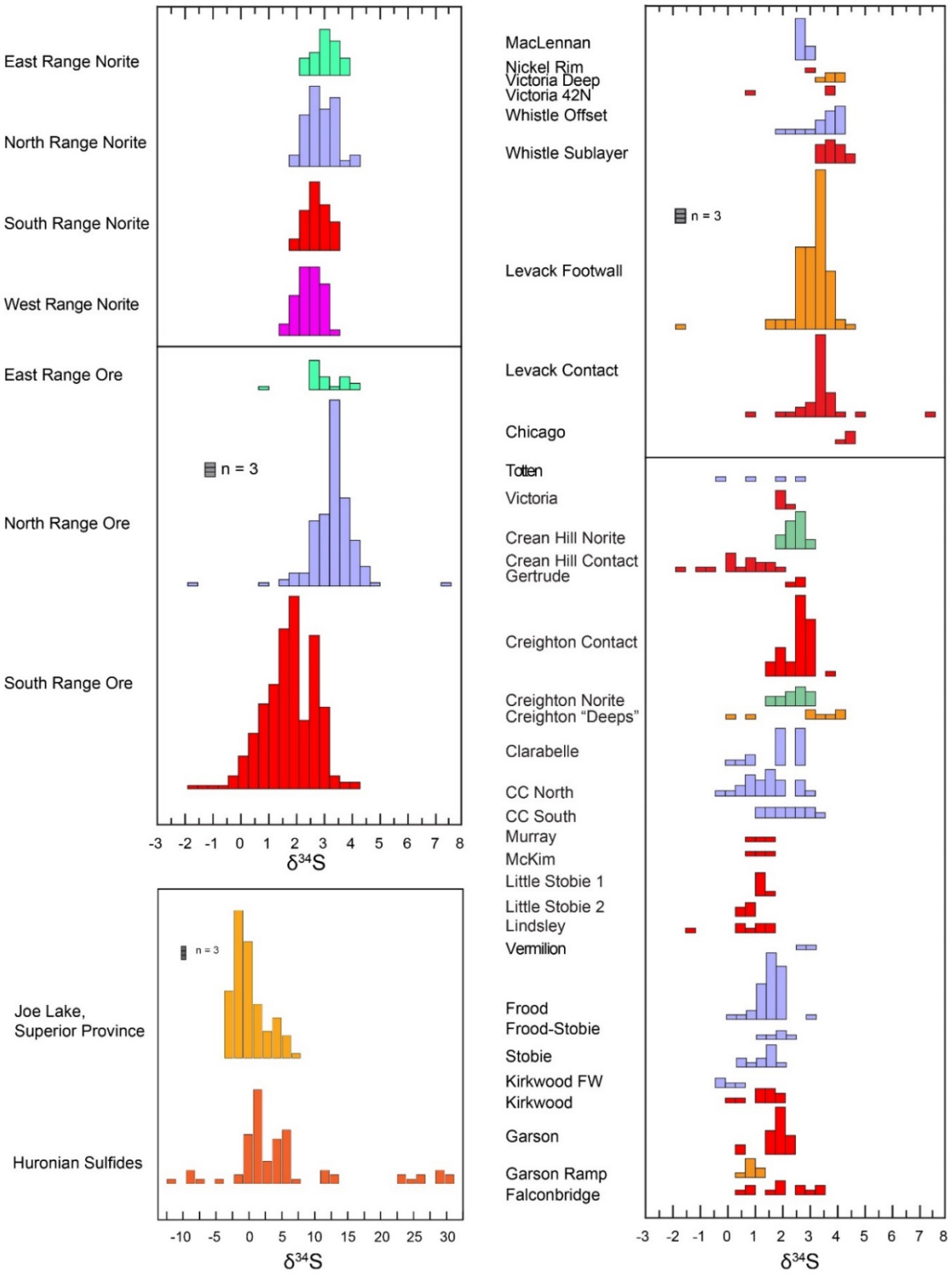

Figure 4.7 Stacked histogram of $\delta^{34}S$ of sulfide ores from multiple deposits and Norite from various locations

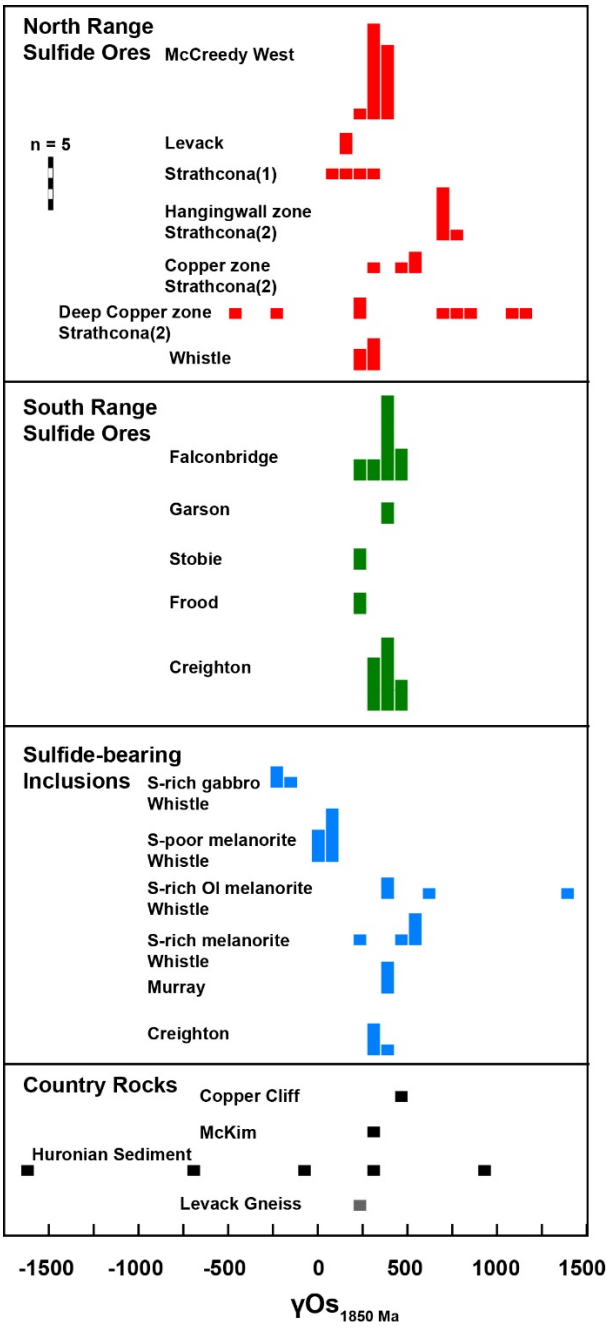

Figure 4.8 Stacked histogram of $\gamma Os_{1850\ Ma}$ of sulfide ores in the basal Main Mass, Sublayer, and IQD, mafic-ultramafic inclusions, and the country rocks associated with sulfide mineralization

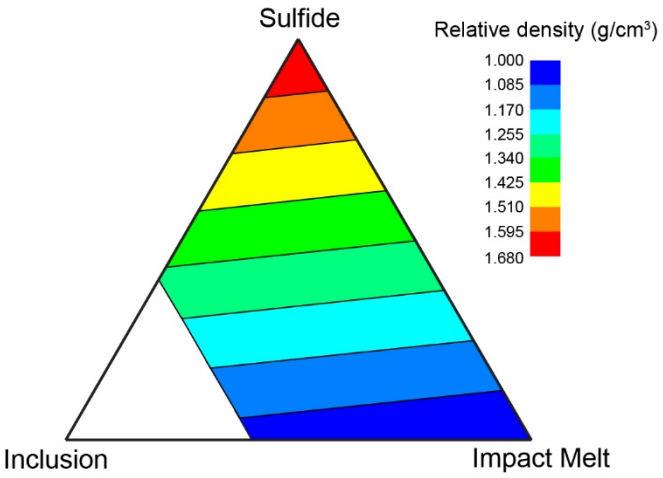

Figure 4.9 Ternary contour of density of mixture with variable proportions of silicate melt, sulfide melt, and inclusions

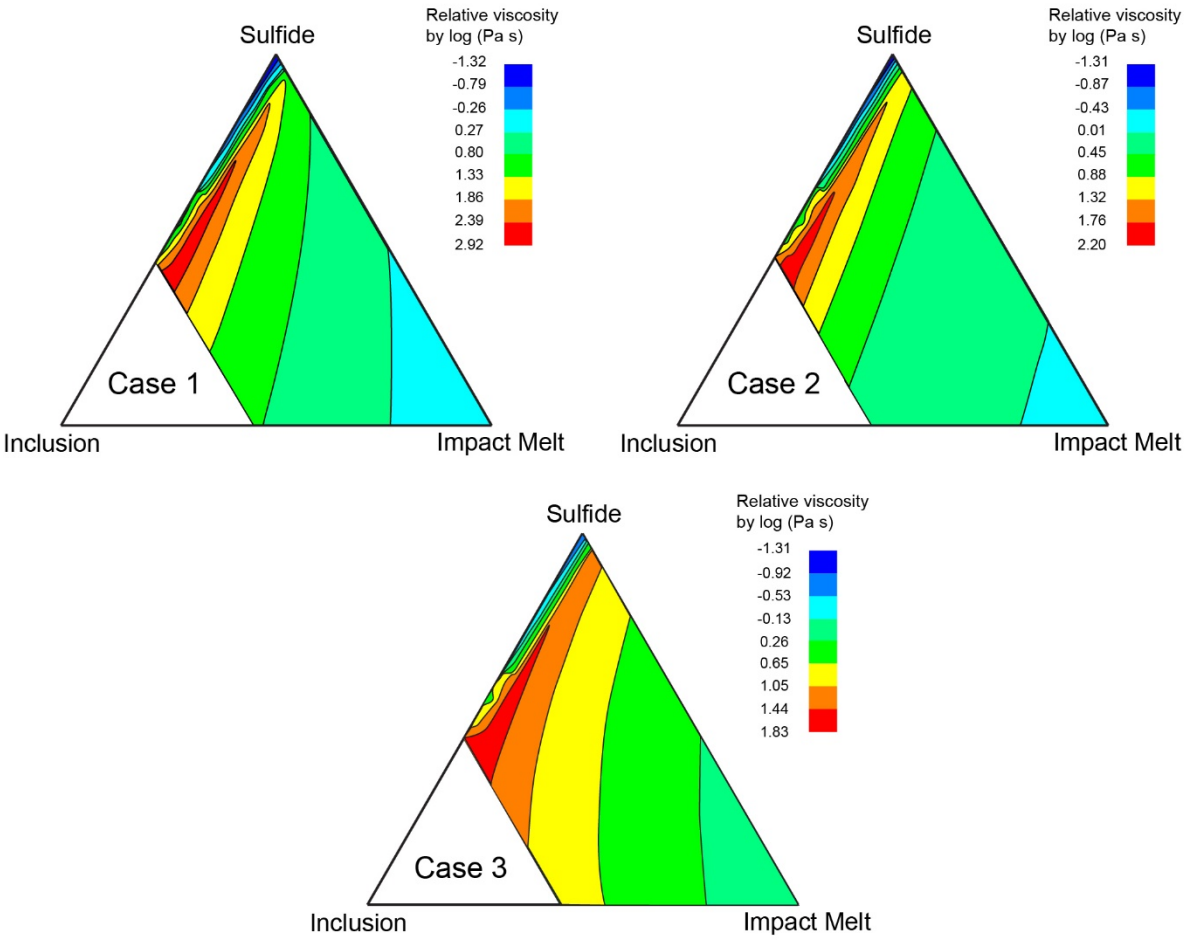

Figure 4.10 Ternary contour of fluid viscosity at 1700°C of mixture with variable proportions of silicate melt, sulfide melt, and inclusions

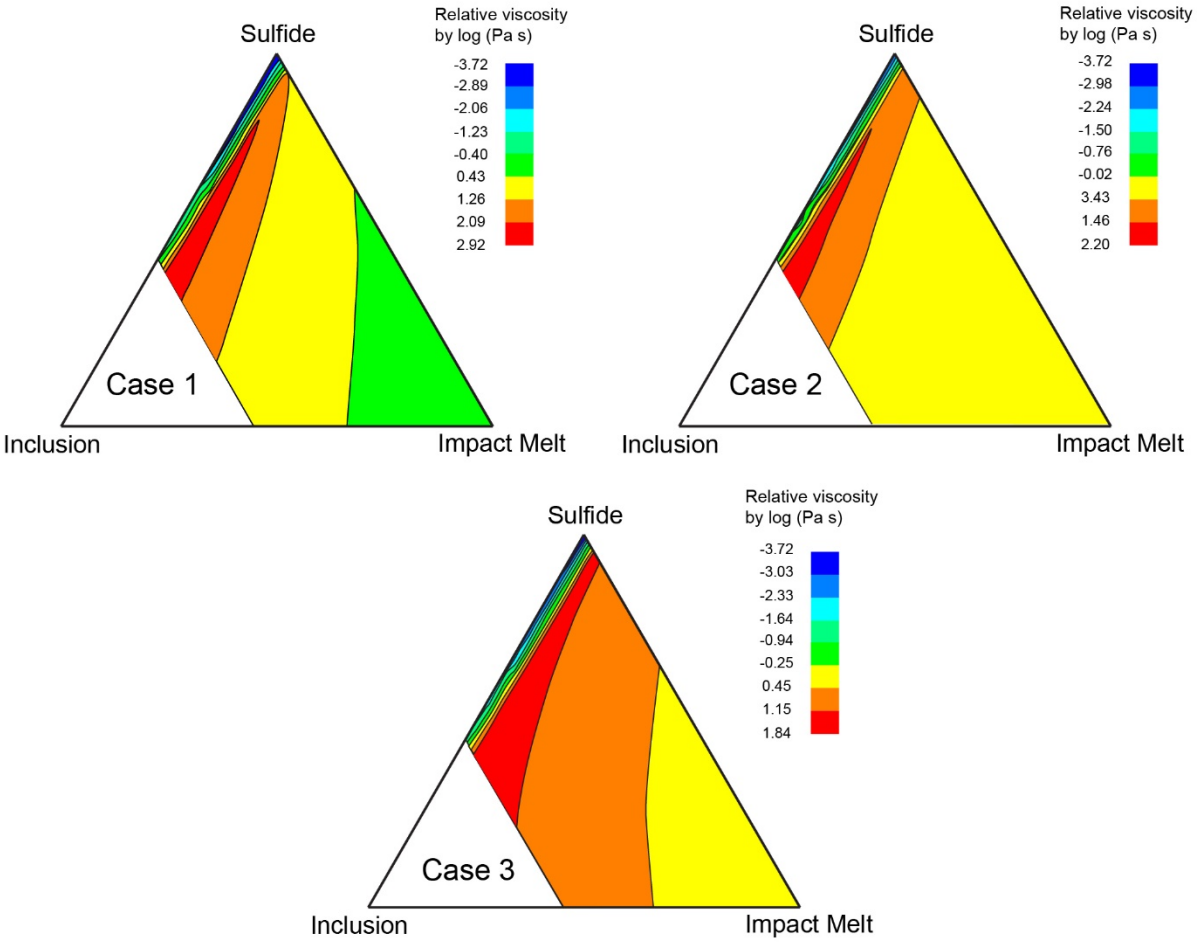

Figure 4.11 Ternary contour of relative viscosities at 1180°C of mixtures of silicate melt, sulfide melt, and inclusions

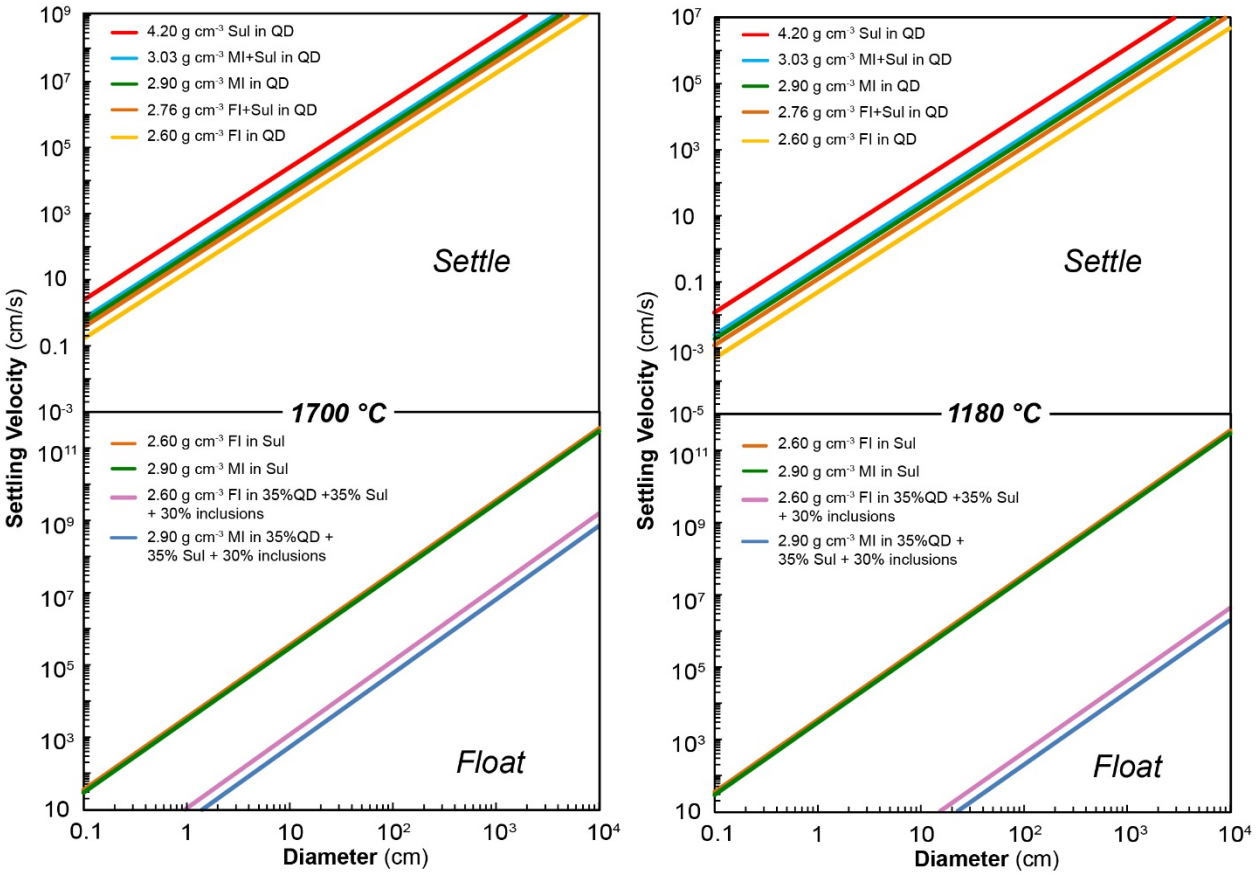

Figure 4.12 Maximum settling velocities (estimated using Stokes's law) for sulfide droplets, felsic and mafic inclusions, felsic and mafic inclusions with 10% sulfide melt within pure silicate melt (100% QD), and felsic and mafic inclusions within mineralized Sublayer-melt (35% QD + 35% sulfide melt + 30% inclusions) and within pure sulfide melt

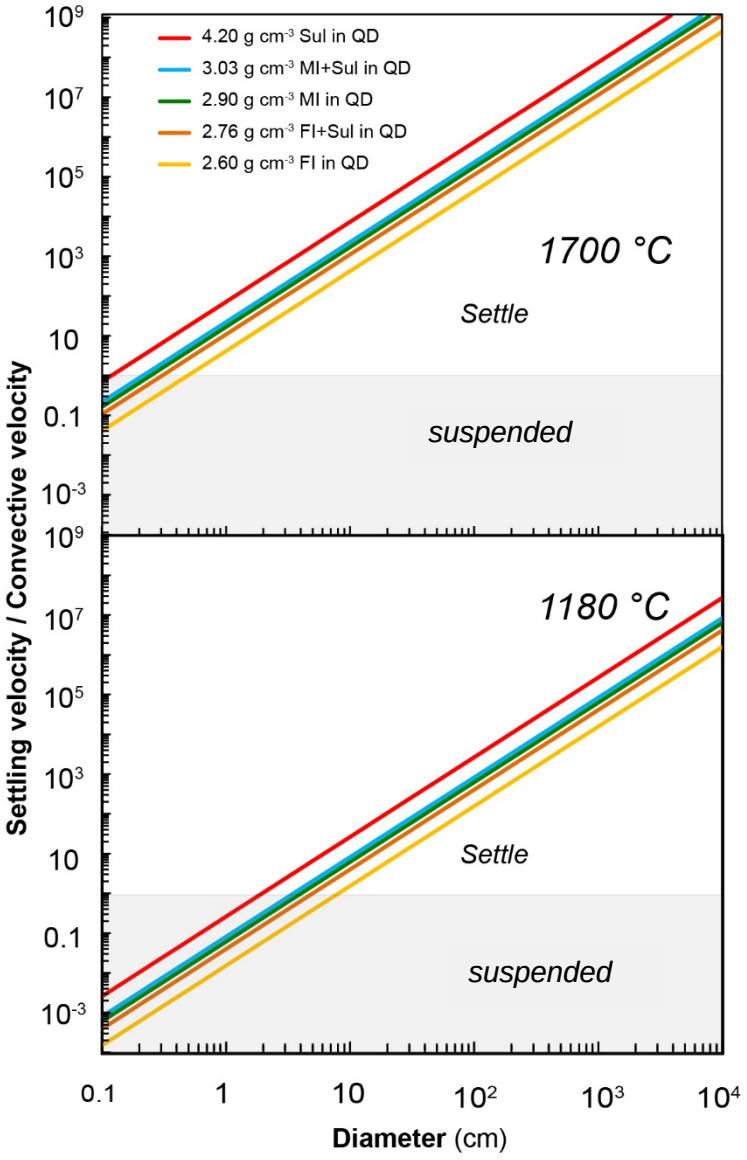

Figure 4.13 Gradients representing settling velocity/convective velocity for sulfide droplets, felsic and mafic inclusions, felsic and mafic inclusions with 10% sulfide melt within pure silicate melt (100% QD) and mineralized Sublayer-melt (35% QD + 35% sulfide melt + 30% inclusions)

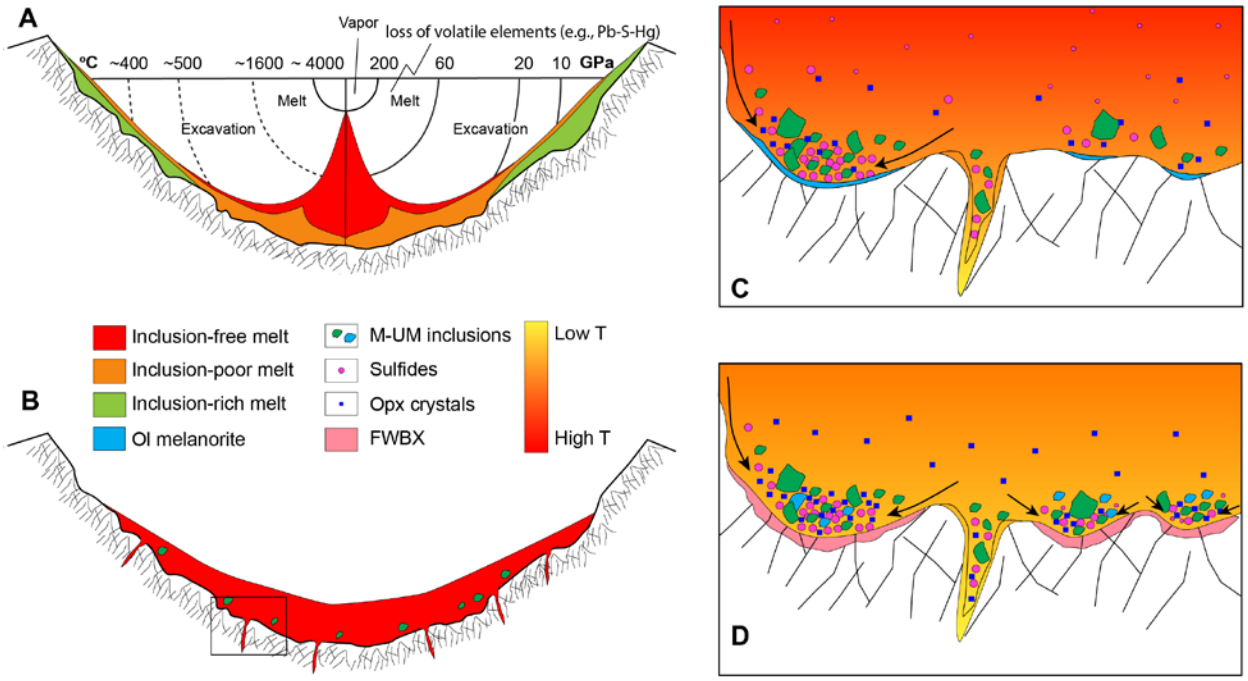

Figure 4.14 Geologic model of formation of the Sublayer, IQD, and FWBX

Table 4.1 Characteristics of basal Main Mass norite, Sublayer, FWBX, and IQD (including South Range Breccia Belt)

	Main Mass Norite	Sublayer	Footwall Breccia	IQD	
Distribution	continuous lower unit of SIC	discontinuous along lower contact of SIC	discontinuous along lower contact of SIC	breccia belt	offset dike
Contacts with Country Rocks	sharp (where Sublayer is absent)	sharp, gradational (where FWBX is present)	gradational	sharp	locally sharp
Matrix					
Nature	igneous	igneous	metamorphic except igneous in melt pods	metamorphic except igneous in melt pods	igneous to metamorphic
Texture	cumulate	ophitic to porphyritic	metamorphic to partially melted	quenched igneous to metamorphic	quenched igneous to metamorphic
Lithology	norite	norite	sulfide and granophyric silicate melts	SUBX except QD in melt pods	QD
Inclusions					
Volcanic-sedimentary	locally abundant	rare	abundant on SR	abundant	rare
Gneissic-granitic	locally abundant	locally abundant	abundant in NR	rare	locally abundant
Gabbroic-anorthositic (Nipissing > EBLI)	locally abundant	abundant	locally abundant	locally abundant	abundant
Opx-bearing ultramafic	locally abundant	present	present	present	present
Ol-bearing ultramafic	not reported	present	present	present	present (altered)
Sulfide clast	not reported	very rare	characteristic	locally abundant	locally abundant
Sudbury breccia	not reported	not reported	present	not reported	rare
Chemistry	SR: QRNR NR: MNOR	highly variable more mafic	highly variable	highly variable ???	much more consistent less mafic
Sulfide Textures	interstitial, blebby	disseminated interstitial, blebby, semi-massive	blebby, fragmental, semi-massive	blebby, fragmental, semi-massive	blebby to semi-massive

Data Sources: Naldrett & Kullerud (1967), Podolsky et al. (1969), Rae (1975), Scribbins (1978), Naldrett et al. (1984), Capes (2002), this study

Table 4.2 Textural facies of igneous-textured Sublayer matrix

	QD-Type Sublayer	Ophitic Sublayer	Cumulus Opx-rich Sublayer	Porphyritic Opx-rich Sublayer
Fabric	none	sometimes	no	none
Texture	intersertal	ophitic	cumulus Opx	porphyritic Opx
Ol	none	rare, embayed to rounded with thin Opx rims	none	none
Opx	fine, prismatic (pseudomorphed by amph)	fine, equant	medium, prismatic	medium-coarse, prismatic
Cpx exsolution	no	no	sometimes	yes
Opx/Cpx Ratio	<<1	variable	>1	>>1
Cumulate	aphanitic to orthocumulate	ophititic to orthocumulate	orthocumulate	orthocumulate
Cloudy Plag	no	no	sometimes	?

Table 4.3 Summary of geological features of major Sublayer-hosting structures on the North Range and South Range

Sublayer	Localities	Morphology	Thickness	Lithology	Mineralization type and scale	Sulfide minerals and texture	Inclusions	References
Creighton	South Range	trough-like depression	up to 150 m		**Contact type Scale:** Large	**Sulfide minerals**: pyrrhotite, pentlandite, and chalcopyrite, minor magnetite; **Texture**: ragged, disseminated and massive	**Local xenoliths:** amphibolite, calcite-tremolite, anorthosite, hornfels **Mafic-ultramafic inclusions:** harzburgite, olivine norite, melanorite, hypersthene melagabbro, augite melanorite,	Pattison, 1979; Lightfoot et al., 1997; Dare et al., 2010
Copper Cliff	South Range	1.6 km wide funnel-shaped embayment, narrows down to 40 m Offset dike		Quartz monogabbronorite to gabbronorite	**Contact-offset type Scale**: Small-Large	**Texture**: blebby and fine disseminated	**Local xenoliths**: amphibolites, metasedimentary rocks, anorthosites and quartzites; **Mafic-ultramafic inclusions**: gabbros, norites, metapyroxenites; **Size:** from < 1 cm up to 20 m in diameter; **Sulfide:** barren	Capes, 2002
Gertrude	South Range	embayment			**Contact type Scale:** Small	**Texture:** heavy disseminated and massive		Lightfoot, 2016
Little Stobie	South Range	embayment, with average width of 90 m	up to 520 m	Fine- to medium-grained gabbronorite	**Contact-footwall type Scale:** Small	**Sulfide minerals:** pyrrhotite, chalcopyrite, and pentlandite; **Texture:** disseminated, stringer, and massive	**Local xenoliths**: footwall amphibolite; **Mafic-ultramafic inclusions**: two-pyroxene gabbro (majorite), harzburgite, olivine orthopyroxenite, orthopyroxenite, olivine melatroctolite, melanorite, hypersthene gabbro, and quartz-rich norite associated with interstitial sulfide; **Size**: from 2 cm to 46 m in diameter; **Sulfide**: barren, except for quartz-rich norite	Davis et al., 1984
Murray	South Range	shallow embayment, close to the flank of the Copper Cliff funnel			**Contact-footwall type Scale:** Large		**Local xenoliths**: no information; **Mafic-ultramafic inclusions:** predominantly Harzburgite, **Size:** from a few millimeters to several hundred feet in diameter;	Scribbins, 1978

Sublayer	Localities	Morphology	Thickness	Lithology	Mineraliza-tion type and scale	Sulfide minerals and texture	Inclusions	References
Frood	South Range	Downward thinning wedge within the Sudbury Breccia Belt			**Contact-footwall type Scale:** Large		**Local xenoliths**: no information; **Mafic-ultramafic inclusions:** predominantly harzburgite, augite melanorite, melanorite, hypersthene gabbro, gabbro;	Scribbins, 1978
Levack-McCreedy	North Range	Trough			**Contact-footwall type Scale:** Large	**Sulfide minerals:** pyrrhotite and pentlandite **Texture:** blebby, disseminated, semi-massive, and massive	**Local xenoliths:** footwall pods, recrystallized wehrlite-olivine clinopyroxenite; **Mafic-ultramafic inclusions:** lherzolite, olivine melagabbronorite, clinopyroxenite, websterite, gabbronorite, gabbro	This study
Strathcona	North Range	Local deep embayment		Fine- to medium-grained gabbronorite	**Contact-footwall type Scale:** Large	**Sulfide minerals:** pyrrhotite and pentlandite **Texture:** blebby and disseminated	**Local xenoliths:** rare footwall pods; **Mafic-ultramafic inclusions (92.8%)**: lherzolite, harzburgite, wehrlite, olivine clinopyroxenite, olivine websterite, websterite, and olivine gabbro; **Size:** from three inches to five feet;	Vos and Moorhouse, 1965; Naldrett and Kullerud, 1967; Souch et al., 1969; Rae, 1975;
Trill	North Range	Trough			**Contact type Scale**: small		**Local xenoliths:** no information; **Mafic-ultramafic inclusions:** lherzolite (predominant), harzburgite, orthopyroxenite (reaction product), olivine gabbro; **Size:** from a few centimeters to a hundred meter **Sulfide:** barren	This study
Coleman	North Range	Local deep embayment			**Contact-footwall type Scale**: Large	**Sulfide minerals:** pyrrhotite and pentlandite **Texture:** blebby and disseminated		Lightfoot, 2016

Sublayer	Localities	Morphology	Thickness	Lithology	Mineralization type and scale	Sulfide minerals and texture	Inclusions	References
Whistle-Norman	East Range	Funnel-shaped depression with approximately 350 wide near the contact with the Main Mass		Zonation: cumulate orthopyrox-ene-rich norite in the core and more siliceous varieties at the rim	**Contact type Scale**: Medium	**Sulfide minerals:** pyrrhotite > pentlandite >> chalcopyrite, minor pyrite **Texture:** disseminated and massive	**Local xenoliths**: predominant diabase, rare anorthosite, gabbro, footwall gneiss, leucocratic pods; **Mafic-ultramafic inclusions**: melanorite, olivine melanorite, and altered metapyroxenite **Size**: diabase are a few centimeters in size (rare up to one meter); mafic and ultramafic inclusions are from five centimeters to several meters **Sulfide**: olivine melanorite and melanorite contain weakly disseminated sulfides.	Pattison, 1979; Grant and Bite, 1984; Farrell, 1997; Lightfoot et al., 1997; Lightfoot, 2016; This study
Victor	East Range	Nickel Rim - Victor trough			**Contact-footwall type Scale**: Large	**Sulfide minerals:** pyrrhotite and pentlandite **Texture:** blebby, disseminated, semi-massive, and massive		Lightfoot, 2016

Table 4.4 Comparison of petrographic and geochemical characteristics between ITSM and mafic-ultramafic inclusions

Unit	Petrography	Major element composition	Trace element composition	Mineral Chemistry		
				Ol	Opx	Cpx
ITSM	Norite - leuconorite rare gabbro - dorite	MgO: 3 - 17% NR; 4 - 11% SR; Positive trends between Mn-Fe and Mg; Negative trends between Al-Na-Ti and Mg; Ca exhibits two overlapping trends: a positive trend for ITSM in both NR and SR and a negative trend for ITSM in NR only.	Strongly HILE enrichment; Pronounced negative Nb-Ta anomalies; Minor negative Zr-Hf and Ti anomalies; Wide ranges of Th-U and Sr concentrations; Nb/U: 5 - 24; Zr/Hf: 30 - 39; Nb/Ta: 6 - 21		Hypersthene; Mg#: 63 - 72; Negative trends between Zr-Cr and Mg#; Flat trends between Ca-Ti and Mg#	Augite; Mg#: 71 - 75
Mafic-Ultramafic Inclusions						
Group I	Olivine melanorite, Olivine gabbronorite	MgO: 15 - 28%; Widely variable Fe-Ca-P; Al deceases with increasing Mg and Na remains low when MgO > 21%, while Al remains high and Nb abruptly elevates when MgO < 21%	Highly HILE enrichment; Pronounced negative Nb-Ta anomalies; Wide ranges of Th-U and Sr concentrations; Nb/U: 4 - 13; Zr/Hf: 34 - 39; Nb/Ta: 15 - 19	Olivine melanorite: Fo: 68 - 73; NiO: 0.12 - 0.20; MnO: 0.28 - 0.45; Olivine gabbronorite in Dowling: Fo: 76 - 78; NiO: 0.40 - 0.50; MnO: 0.26 - 0.31; Olivine gabbronorite in Onaping Depth: Fo: 76 - 78; NiO: 0.22 - 0.28; MnO: 0.27 - 0.33;	Olivine melanorite: Bronzite; Mg#: 75 - 76; Olivine gabbronorite: Bronzite - Hypersthene; Mg#: 78 - 83;	Olivine melanorite: Salite - Augite; Mg#: 79 - 81; Olivine gabbronorite: Mg#: 81 - 84;
Group IIA	Shocked metamorphosed Wehrlite olivine clinopyroxenite	MgO: 23 - 32%; Well-defined arrays between the average composition of clinopyroxene and olivine	Moderate HILE enrichment; Variably negative Nb-Ta and Sr anomalies; Minor negative Ti and Al anomalies; Pronounced negative Th-U and Zr-Hf anomalies; Nb/U: 2 - 36; Zr/Hf: 22 - 34; Nb/Ta: 13 - 26	Fo: 79 - 83; NiO: 0.08 - 0.22; MnO: 0.22 - 0.36; Decoupling between Mn and Fe	Bronzite - Hypersthene; Mg#: 83 - 84;	Diopside - Endiopside; Mg#: 83 - 93;
Group IIB	Shocked metamorphosed Olivine melanorite	MgO: 30% and 25%; Significantly low Ti-P	Minor HILE enrichment; Absence of Th-U, Zr-Hf, and Ti anomalies; Nb/U: 9 - 14; Zr/Hf: 37 - 38; Nb/Ta: 19 - 22	Fo: 83 - 81; NiO: 0.24 - 0.30; MnO: 0.20 - 0.24;	Bronzite; Mg#: 83 - 85;	Diopside - Endiopside; Mg#: 84 - 88;

Group III	Phlogopite lherzolite, feldspar lherzolite, orthopyroxenite, olivine gabbro	MgO: 23 - 32%; No well-defined correlative trends	Moderate HILE enrichment; Pronounced negative Nb-Ta-Ti anomalies; Minor negative Zr-Hf, Th-U, and Sr anomalies; Nb/U: 3 - 10; Zr/Hf: 32 - 42; Nb/Ta: 14 - 23	Lherzolite: Fo: 77 - 83; NiO: 0.09 - 0.19; MnO: 0.21 - 0.37; Shocked feldspar lherzolite: Fo: 82 - 83; NiO: 0.38 - 0.43; MnO: 0.24 - 0.28; Olivine gabbro: Fo: 72 - 73; NiO: 0.12 - 0.15; MnO: 0.37 - 0.39;	Lherzolite: Bronzite - Hypersthene; Mg#: 81 - 85; Orthopyroxenite: Hypersthene; Mg#: 63 - 82;	Lherzolite: Diopside - Endiopside; Mg#: 82 - 92; Olivine gabbro: Salite - Augite; Mg#: 77 - 80;

Table 4.5 Timing of formation of the various elements of the SIC

	Early							**Late**
SUBX (including SRBB)	impact							
Temperature		1700°C	→	→	→	1180	1080	870°C
Thermomechanical Erosion			debris	basal contact	embayments			
QD			dike margins	melt pods in SRBB (e.g., Kirkwood) and metabreccia (e.g., Whistle)	funnel margins		Pele and Cascaden	
Sulfide Ores				exsolution from melt sheet +/- xenomelts from FW rocks	upgrading	MSS1 + residual liquid1	MSS2 + residual liquid2	ISS + residual liquid3
IQD				dike cores				
FWBX				initial formation along contacts???	mobilized into embayments (e.g.,Whistle "Metabreccia")	diapiric into Main Mass (e.g., Hwy 144, Levack)		
SLNR				initial formation along contacts and in primary embayments	mobilized into embayments (e.g., Levack, Trill) and troughs (e.g., Whistle, Foy)			
Crystallization of Main Mass						MFNR-QRNR-Norite	Gabbro	Granophyre
Contact Metamorphic Aureole						narrow →	→	wide

Table 4.6 Comparison of thermal properties of komatiite lava and Sudbury impact melt

	Unit	**Komatiite Lava**	**Sudbury Impact Melt**		
			Impact Melt (100% QD)	**Barren Sublayer** (70% QD + 30% Incl)	**Mineralized Sublayer** (35% QD + 30% Incl + 35% Sulfide melt)
Initial T	°C	≥ 1600	1700		
Liquidus T	°C	1600	1180		
Solidus T	°C	1200	820	~850	
Density	$kg\ m^{-3}$	2800	2500	2560	3155
Specific heat	$J\ kg^{-1}\ °C^{-1}$	730	621		
Bulk viscosity	Pa s	0.13 - 10	1700°C: 2 1180°C: 507	1700°C: 4.9 1180°C: 1237	1700°C: 4.2 - 14.4 1180°C: 1074 - 3666

Table 4.7 Typical values of physical properties of sedimentary debris flow and Proto-Sublayer

	Solid Grain Properties		**Pure Fluid Properties**		**Mixture Properties**			
Property (Unit)	Mass Density (kg/m3)	Mean Diameter (m)	Mass Density (kg/m3)	Kinematic Viscosity (Pa s)	Solid Fraction	Fluid Fraction	**Relative Density** (mixture/fluid)	**Relative Viscosity** (mixture/fluid)
Sedimentary Debris Flow	2500 - 3000	10^{-5} - 10	1000 - 1200	0.001 - 0.1	0.4 - 0.8	0.2 - 0.6	**1.7 - 2.6**	**16 – 50**
Proto-Sublayer	2600 - 4200	10^{-5} - 100	2500	100	0 - 0.6	0.4 - 1.0	**1 - 1.7**	1700°C: **0.05 – 830** 1180°C: **0.0002 – 830**

CHAPTER 5

CONCLUDING STATEMENTS

5.1 Summary of Thesis

The ca. 1.85 Ga Sudbury Igneous Complex (SIC) is the igneous remnant of one of the oldest, largest, and best-preserved impact structures on Earth and contains some of the world's largest magmatic Ni-Cu-PGE sulfide deposits. The majority of the Ni-Cu-PGE mineralization in the SIC is associated with the lowermost, discontinuous, and inclusion-rich Sublayer and Footwall breccia (FWBX) along the basal contact and with inclusion-bearing quartz diorites (IQD) in radial and concentric Offset dikes emanating from the contact between the overlying Main Mass and the footwall rocks. Sublayer and IQD are characterized by the significant abundance of inclusions, including felsic-mafic inclusions that appear to be derived from exposed country rocks and volumetrically important olivine-bearing mafic-ultramafic inclusions that have only rare equivalents in the country rocks and appear to be preferentially associated with mineralization.

The mafic-ultramafic inclusions can be divided into three origins on the basis of petrographic, mineralogical, geochemical, and Sm-Nd and Re-Os isotopic composition:

Anteliths (n = 47) includes olivine melanorite and olivine melagabbronorite inclusions in the Whistle and Levack (Dowling and Onaping Depth) embayments on the North Range. They are characterized by well-preserved igneous textures, including orthocumulate, poikilitic, and interstitial textures. They exhibit similar Zr/Y, Zr/Nb, Nb/U, and Zr/Hf ratios to ITSM and olivine melanorite inclusions in the Whistle embayment have slightly unradiogenic radiogenic $\gamma Os_{1850\ Ma}$ values (-8 to +94), which are indicative derivation from metasomatized subcontinental

mantle or from older crustal rocks with low Re/Os ratios and unradiogenic Os isotope compositions, but unradiogenic $\varepsilon Nd_{1850\ Ma}$ values (-8 to -5), which are indicative of a crustal source. These data suggest that Group I inclusions are anteliths that crystallized from the impact melt that has assimilated of the widespread Huronian volcanic and subvolcanic units in the region, which has been proposed to be derived from subduction-metasomatized lithospheric mantle.

Local xenoliths includes Group IIA (n = 17) wehrlites and olivine clinopyroxenite inclusions in the Levack embayment and Group IIB (n = 2) shock metamorphosed olivine melanorite inclusions in the Foy Offset on the North Range. Group IIA and Group IIB inclusions are characterized by shock mosaicism in olivine, where olivine grains have been deformed into aggregates of small domains having 1 – 5° disorientations, potential planar deformation features in orthopyroxene, which occur as pervasive parallel fractures (1 – 2 μm wide, 3 – 5 μm spaced) and are partially decorated by aligned fluid inclusions, and recrystallized textures. Group IIA inclusions have similar trace element patterns (e.g., negative Th-U, Nb-Ta-(Ti), Sr, and Zr-Hf anomalies) and overlapping Nb/U ratios as a layered mafic-ultramafic intrusion in the footwall of the Levack and Fraser Mines, which together with their limited distribution suggests that Group IIA inclusions are derived from local mafic-ultramafic protoliths that were petrogenetically-related to the above layered mafic-ultramafic intrusion. However, they have low Zr and Zr/Y ratios, variable Zr/Nb ratios, subchondritic Zr/Hf ratios, and superchondritic Nb/Ta ratios, which suggest that they crystallized from a melt derived from a heterogeneous source that had been metasomatized by slab-derived fluids/melts. The petrogenesis of Group IIB inclusions is the least clear because of the strong shock and thermal metamorphism and limited number of samples. They appear to display overlapping Zr/Y, Zr/Nb, and Nb/U variations with and plot on the same

trend as Group IIA inclusions in a plot of Ta/Yb vs Th/Yb, suggesting that they are also local xenoliths derived from a now-consumed or now-hidden source that were petrogenetically related to Group IIA inclusions.

Exotic xenoliths (n = 21) includes phlogopite/feldspar lherzolite inclusions in the Trill, Levack, and Bowell embayments and the Foy Offset dike on the North Range. They are characterized by igneous textures, including orthocumulate, poikilitic, and interstitial textures, tectonic metamorphic textures, including porphyroclastic, granoclastic, hornfelsic, and recrystallized textures, and shock metamorphic texture (sample #373582 only, in which plagioclase is partially isotropic). They have no equivalents in the exposed country rocks. Feldspar lherzolite inclusions in the Trill embayment exhibit orthopyroxene reaction rims against igneous-textured Sublayer matrix (ITSM), suggesting disequilibrium with the impact melt. One composite inclusion exhibits igneous layering of feldspar lherzolite and olivine gabbro, suggesting derivation from an unexposed layered mafic-ultramafic intrusion. The calculated parental magma is similar to continental arc basalt formed by approximately 5% batch melting of garnet peridotite. Ol-Cpx-Pl thermobarometry of several Group III inclusions indicate equilibration at 900^{o}C to 1120^{o}C and 2.1 ± 1.7 kbar to 3.0 ± 1.8 kbar, suggesting emplacement into upper-middle crust (7.7 ± 6.6 to 10.9 ± 6.5 km), prior to being incorporated into the lower parts of the proto-SIC during impact excavation. Shock metamorphosed feldspar lherzolite, for which P-T condition could not be estimated due to shock- and thermal-induced disequilibrium, is characterized by greater enrichment of Ni in olivine (NiO ~ 0.4% vs 0.1 – 0.2%) and very low Gd/Yb_N (1.06 vs 2.20 – 4.75) compare to the igneous feldspar lherzolite in Group III. Although it is difficult to draw any certain conclusion with limited information, it appears that this shocked metamorphosed feldspar

lherzolite may have been derived from shallower and hidden protolith, rather than deeper mafic-ultramafic protoliths for the other inclusions in this group.

Most analyzed inclusions, ITSM, and Main Mass lithologies exhibit enrichment in highly incompatible lithophile elements with negative Nb-Ta-(Ti) anomalies, unradiogenic Nd isotopic, and radiogenic Os isotopic signatures, indicating that the impact sampled rocks formed from upper continental rocks that were originally derived from subduction-metasomatized mantle sources. The widespread Huronian volcanic and subvolcanic rocks are considered to be derived from the subduction-metasomatized lithospheric mantle that likely occurred at 2750 – 2690 Ma beneath the Abitibi-Wawa terrane. Melting of these volcanic and intrusive rocks and underlying Neoarchean Superior Province upper-middle crustal rocks would produce the observed geochemical characteristics.

Sublayer, FWBX, and IQD appear to be cogenetic on the basis of similarity of inclusion population, but the greater geochemical heterogeneity, greater angularity of inclusions, and greater amounts of cumulus orthopyroxene-plagioclase in Sublayer relative to IQD indicate that Sublayer cooled more slowly and allowed orthopyroxene to accumulate, whereas IQD cooled more rapidly, was able to accumulate less orthopyroxene and expel less residual silicate melt. The significant enrichment of highly incompatible lithophile element, over moderately strongly unradiogenic Nd and radiogenic Os isotopic composition of all SIC lithologies, sulfide ores, and most mafic-ultramafic inclusions reflect a strong continental crustal signature. The overlying Main Mass norite is very homogeneous in terms of Hf isotopes, indicating that the impact melt sheet was well mixed. However, Sublayer, IQD, and overlying basal Main Mass norites vary widely in terms of Pb-S-(Os) isotopic compositions. The majority of mafic-ultramafic inclusions, except for anteliths, are barren in sulfide and exhibit no signature of Ni-Cu-PGE depletion

caused by prior sulfide saturation, which suggest that the association between mafic-ultramafic inclusions and Ni-Cu-PGE sulfide mineralization is most likely attributable to their refractory nature and to their similar fluid dynamic behavior. Anteliths, locally-derived inclusions, and local variations in S and Pb isotopes must have been generated in situ, requiring significant degrees of subsequent local thermomechanical erosion, whereas the exotic inclusions, except for the shocked feldspar lherzolite, were derived from mafic-ultramafic protoliths and must have been generated during impact excavation and/or thermomechanical erosion and transported into their current locations. Thermomechanical erosion has played an important role in the generation of embayments, incorporation of local xenoliths, and formation of isotopic heterogeneity in the basal units of SIC. Convective- and/or gravity-driven mass flow contributed to the horizontal transport of the inclusions into the embayment when the impact melt contained inclusions <45%, but became less significant as the impact melt assimilated more inclusions and became more viscous.

5.2 Future Work

The work presented in this thesis mainly focused on olivine-bearing mafic-ultramafic inclusions in available locations mainly on the North Range, because many embayments on the South Range have been mined out and because much of the historical core was lost in a fire in the late 1970s. The greater-than-expected diversity in geochemical composition of the mafic-ultramafic inclusions resulted some challenges in systematically analyzing the trends that might be better defined if more samples had been available. Future work, including more South Range samples from new drilling (e.g., Cryderman area, underground drilling at Creighton and/or Carson), should include more samples to better define the trends.

This study did not include any new isotopic work. Only the Whistle melanorite inclusions have been analyzed for Re-Os and Sm-Nd isotopes, but not on the same samples, and none appear to have been analyzed for S or Pb-Pb isotopes. The target rocks in the Sudbury area had a complex geological history, so future work should include integrated geochemical, S, Pb-Pb, Sm-Nd, and Lu-Hf isotope analyzes on the same inclusions from each group to better constrain their sources.

Although there appears to be no direct genetic association between the mafic-ultramafic inclusions and the Ni-Cu-PGE sulfide mineralization, further work is needed to determine if there are any linkages between inclusion petrology, mineralogy, or geochemistry and the mineral potential of different embayments. This should include documentation on the size and mineral potential of the embayment; the proportions, sizes, lithologies, and geochemistry of inclusion types in Sublayer; and the proportion, texture, mineralogy, and tenor of sulfide to get a better understanding the significance of the inclusions on exploration models.

Although outside the scope of this study, it will be beneficial to quantitatively model thermomechanical erosion, convective transport, and gravity flow to better constrain their relative importance in localizing Sublayer, IQD, FWBX, and mineralization.